UNIVERSITÉ DE STRASBOURG

ÉCOLE DOCTORALE DES SCIENCES CHIMIQUES

INSTITUT CHARLES SADRON

THÈSE présentée par :

Qing CAO

soutenue le : **18 janvier 2017**

pour obtenir le grade de : **Docteur de l'université de Strasbourg**

Discipline/ Spécialité : Chimie/ chimie supramoléculaire

Synthesis and self-assembly of triarylamines modified with nucleobases

Synthèse et auto-assemblage de triarylamines modifiées par des nucléobases

THÈSE dirigée par :

Pr.Giuseppone Nicolas Professeur, université de Strasbourg

RAPPORTEURS :

Dr. Surin Mathieu Chercheur Qualifié F.R.S.-FNRS, Université de Mons

Dr. Ulrich Sébastien Chargé de Recherche CNRS, Institut des Biomolécules Max Mousseron

---

AUTRES MEMBRES DU JURY :

Dr. Lutz Jean-François Directeur de Recherche, Institut Charles Sadron, CNRS

Acknowledgements

Just before 2017 new year, I finished this thesis. Looking back to the 40 months of my PhD research, there are too many words to say and too many people to thank.

All my work was undertaken in the SAMS group in ICS. Firstly, I want to give my acknowledgement to Prof. Nicolas Giuseppone. Thanks for giving me a chance to study and work in his group, where I leant a lot and truly started to understand the scientific research. Always being supportive and encouraging, he showed me not only logical thinking but also how to seize the important points, which I believe will always benefit me.

Besides, I am also strongly thankful to Dr. Emilie Moulin, who guides me so much on experimental skills and detailed data discussion. From my first column to the last thesis modification, Emilie always tried to push me progress and made every effort on leading me to learn and find answers by myself.

To Dr. Gad Fuks, I am also really thankful that he is so kind and patient with my large amounts of TEM and SEM trying. He also gave me many suggestions during my research bottleneck, which inspired me a lot.

Besides, I want to thank all the SAMS group members: Mounir, Odile, Julie, Yunjie, Quan, Justin, Joe, Eric, Adrian, Yves, Artem, Antoine, Valentina, Ting, Simon, Chris, Jean-Remy, Manic, Junjun, Yali, Melodie, Flavio, Damien, some of them keep accompany with me for three years, some shorter; some of them helped me with the experimental section, some of them are my personal friends. However, all the people I met in SAMS group were really nice and always stand by me. They keep on smiling to me and ready to help me, indeed, nearly all of them gave me some different assists and I will keep them in mind always. Special thanks to Junjun, Artem and Chris, who always work with me together during night and weekend.

The work in this thesis could not be completed so quickly without the help of Dr. Michel Rawiso, Guillaume Fleith, Dr. Bruno Vincent and Dr. Emeric Wasielewski, especially for Guillaume and Bruno, who are so gentle and efficient for my X-ray scattering and NMR measurements.

What's more, I also want to thank all the members in ICS. With the friendly atmosphere and people who willing to help, I have a great time during my stay and I would never forgot my French Days.

Importantly, I still need to thank all my Chinese friends in France. They made my life more colorful and interesting beyond the lab and the lunch time with them is my best talking and

laughing hour everyday. They taught me how to play Chinese cards, which I didn't manage for 25 years in China. I will remember those hot-pot parties and travelling routes we spent together.

I also want to give my acknowledgement to my family, who support me to study overseas and being far away from them. They believe in me and respect my decision, which I am rather thankful.

My final and special thanks to friends are going to deliver to Wen. Thanks for being my best friend and partner, thanks for all the meals and thanks for taken care of me. No matter where and how we are in the future, those days will stay and all the tears and smiles are worthy because we grow together.

At last, I want to thank my jury members for having accepted to evaluate my thesis work.

Abstract

Triarylamines are small molecules widely used as charge carriers in the field of organic electronics as they display high hole-transport mobilities. In 2010, our group demonstrated for the first time that chemically-tailored triarylamine amide molecules undergo supramolecular polymerization. For instance, hierarchically organized structures can be reached thanks to the non-covalent co-polymerization of catalytic quantities of triarylammonium radical cations with neutral triarylamine units. In particular, it was shown that chemically-tailored triarylamine compounds can lead to the formation of various morphologies upon light irradiation in chlorinated solvents. On the other hand, the recognition properties of nucleobase residues have been widely used in the last 25 years to trigger self-assembling processes of polymers or small molecules into well-defined supramolecular polymers.

In this thesis, a series of triarylamine amide molecules decorated on their side chains with various nucleobases such as guanine, thymine and cytosine have been synthesized. In a first chapter of results and discussion, we have demonstrated that the triarylamine monomers retain their self-assembling properties in chlorinated solvent upon light irradiation, provided that the nucleobase residue does not affect the non-covalent interactions necessary for the self-assembly of the triarylamine core. In addition, the presence of primary amines on the nucleobase residue was confirmed to prohibit the formation of self-assembled structures, as soon as they are not embedded in hydrogen bonding arrays. Furthermore, the co-self-assembly of triarylamine core and nucleobases were designed and investigated using ions or small molecules (melamine) as template. We then continued to research on templated self-assemblies of our triarylamine-nucleobase molecules in organic solvents, including three sub-projects: (1) morphology construction by templated supramolecular polymerization of triarylamine-monothymine using melamine in various solvents; (2) selective influence of mercury ion on the light responsive properties of triarylamine-monothymine in chloroform and (3) stability and molecular arrangement study on hybrid supramolecular polymers of triarylamine-monoguanine conjugate in absence and in presence of potassium ion. In particular, we have described the first example of supramolecular polymers build from melamine in organic solvents.

Overall, the impact of this work is three-fold: a) it leads to a better understanding of the self-assembly behavior of triarylamine conjugates, b) it influences the design of self-assembling triarylamine structures and c) it offers new approaches for the self-assembly

of triarylamine molecules.

Abbreviations and symbols

Å	ångström
Ac	acetyl
ADA, DAD	acceptor-donor-acceptor, donor-acceptor-donor
AIE	aggregation induced emission
Bn	benzyl
Boc	tert-Butyloxycarbonyl
°C	celsius degree
δ	chemical shift
CD	circular dichroism
CV	cyclic voltammetry
D	diffusion coefficient
DCM	dichloromethane
DIAD	diisopropyl azodicarboxylate
DLS	dynamic light scattering
DMAP	4-dimethylaminopyridine
DMF	dimethylformamide
DMSO	dimethylsulfoxide
DNA	deoxyribonucleic acid
DOSY	diffusion order spectroscopy
eq	equivalent
ESI-MS	mass spectrometry with electrospray ionization
FT/IR	Fourier transform infrared spectroscopy
h	hour
HBC	hexabenzocoronene
HOMO	highest occupied molecular orbital
HPLC	high performance liquid chromatography
J	coupling constant
K_a	association constant
K_d	dissociation constant
L	liter
LC/MS	liquid chromatography coupled to mass spectrometry
LUMO	lowest occupied molecular orbital
λ	emission/absorption wavelength
µL	microliter
µm	micrometer

MAXS	middle angle X-ray scattering
mL	milliliter
μmol	micromole
mmol	millimole
min	minute
MS	mass spectrometry
nm	nanometer
NIR	near infrared
NMR	nuclear magnetic resonance
Ω	ohm
PEG	poly(ethylene glycol)
PNA	peptide nucleic acid
PPh_3	triphenylphosphine
ppm	parts per million
R_f	retardation factor
R_g	gyration radius
R_H	hydrodynamic radius
r.t.	room temperature
s	second
SANS	Small angle neutron scattering
SAXS	small angle X-ray scattering
SEM	scanning electron microscopy
SOMO	singly occupied molecular orbital
T	temperature
TEM	transmission electronic microscopy
TFA	trifluoroacetic acid
THF	tetrahydrofuran
TLC	thin layer chromatography
Ts	tosyl
UPLC	ultra performance liquid chromatography
Upy	ureidopyrimidinone
UV	ultra-violet
Vis	Visible
WAXS	wide angle X-ray scattering

Bibliography

Chapter 1: Generalities on Supramolecular Polymers

Supramolecular chemistry, which was defined by Jean-Marie Lehn as "a highly interdisciplinary field of science covering the chemical, physical, and biological features of chemical species of higher complexity, which are held together and organized by means of intermolecular (noncovalent) binding interactions",[1] has emerged over the last 40 years as an important tool for understanding physical and biological processes but also for building up discrete or hierarchical complex architectures, just to name few possible applications. Since the early 90's, i.e. shortly after the Nobel prize was awarded to Donald J. Cram, Jean-Marie Lehn and Charles J. Pedersen "for their development and use of molecules with structure-specific interactions of high selectivity", supramolecular polymers, which have been defined as "polymeric arrays of monomeric units that are brought together by reversible and highly directional secondary interactions, resulting in polymeric properties in dilute and concentrated solution as well as in the bulk",[2] came out as a potential alternative to traditional covalent polymers, with increased responsiveness and dynamic properties related to non-covalent interactions. Supramolecular polymers can be classified according to different criteria such as i) the physical nature of the supramolecular interactions involved in the polymerization process, ii) the nature of the building blocks used for the polymerization, iii) the thermodynamics of the self-assembly process or even iv) the arrangement of the monomers into A or A-B (one self-complementary or two complementary monomers) type polymers. In this section, we will first focus on non-covalent interactions that are essential for supramolecular polymerization processes. We will then discuss the different mechanisms that govern the formation of supramolecular polymers and finally highlight how such non-covalent polymers can be used as functional materials for various applications.

1. Non-covalent interactions in supramolecular polymers

As stated in the introduction, supramolecular polymers are made of monomers arranged into well-defined structures thanks to intermolecular non-covalent interactions such as hydrogen bonds, π interactions, metal-ligand interactions and so on. These supramolecular interactions, described by Egbert Willem Meijer as, "moderately strong, reversible noncovalent, but lightly directional",[2] encompass a wide range of binding energies from less

[1] Lehn, J. Supramolecular chemistry. Science **260,** 1762–1763 (1993).
[2] Brunsveld, L., Folmer, B. J. B., Meijer, E. W. & Sijbesma, R. P. Supramolecular Polymers. Chem. Rev. **101,** 4071–4098 (2001).

than 5 kJ.mol^{-1} for Van der Waals interactions and up to 200 - 300 kJ.mol^{-1} for ion-ion interactions (**Table 1**).

Table 1| Different types of non-covalent interactions. Reproduced from reference[3].

Interaction	Strength (kJ/mol)	Example
Ion-ion	200-300	Tetrabutylammonium chloride
Ion-dipole	50-200	Sodium-crown ether
Dipole-dipole	5-50	Acetone
Hydrogen bonding	4-120	DNA
Cation-π	5-80	K^+ in benzene
π-π	0-50	Benzene and graphite
Van der Waals	< 5, dependent on surface area	Crystal packing
Hydrophobic	Related to solvent-solvent interaction	Cyclodextrin inclusion complex

Two important features of non-covalent interactions are their reversibility and stimuli-responsiveness compared to covalent bonds, which ensure dynamic and adaptive properties the polymeric structures they are involved in. In general, a single non-covalent interaction is too weak to drive a polymerization process but the combination of several of them results in a higher binding strength, thus leading to stable supramolecular architectures. **Figure 1** shows some examples of four types of supramolecular motifs which have been employed to build supramolecular self-assemblies, namely: (A) directional multiple hydrogen bonding units which strength is related to the number and arrangement of the hydrogen bonds (see next section); (B) highly selective metal-ligand coordination interactions, which association constant depends on the nature of the metal ions; (C) π-π stacking between planar aromatic surface; (D) host-guest interactions based on α-cyclodextrin, 24-crown-8, cucurbit[8]uril, calix[5]arene and pillar[5]arene, which usually involve several types of non-covalent interactions. Other interactions such as hydrophobic, charge-transfer interactions, etc. also play important roles in the formation of supramolecular polymers.

[3] Steed, J. W., Turner, D. R. & Wallace, K. Core concepts in supramolecular chemistry and nanochemistry. (John Wiley & Sons, 2007).

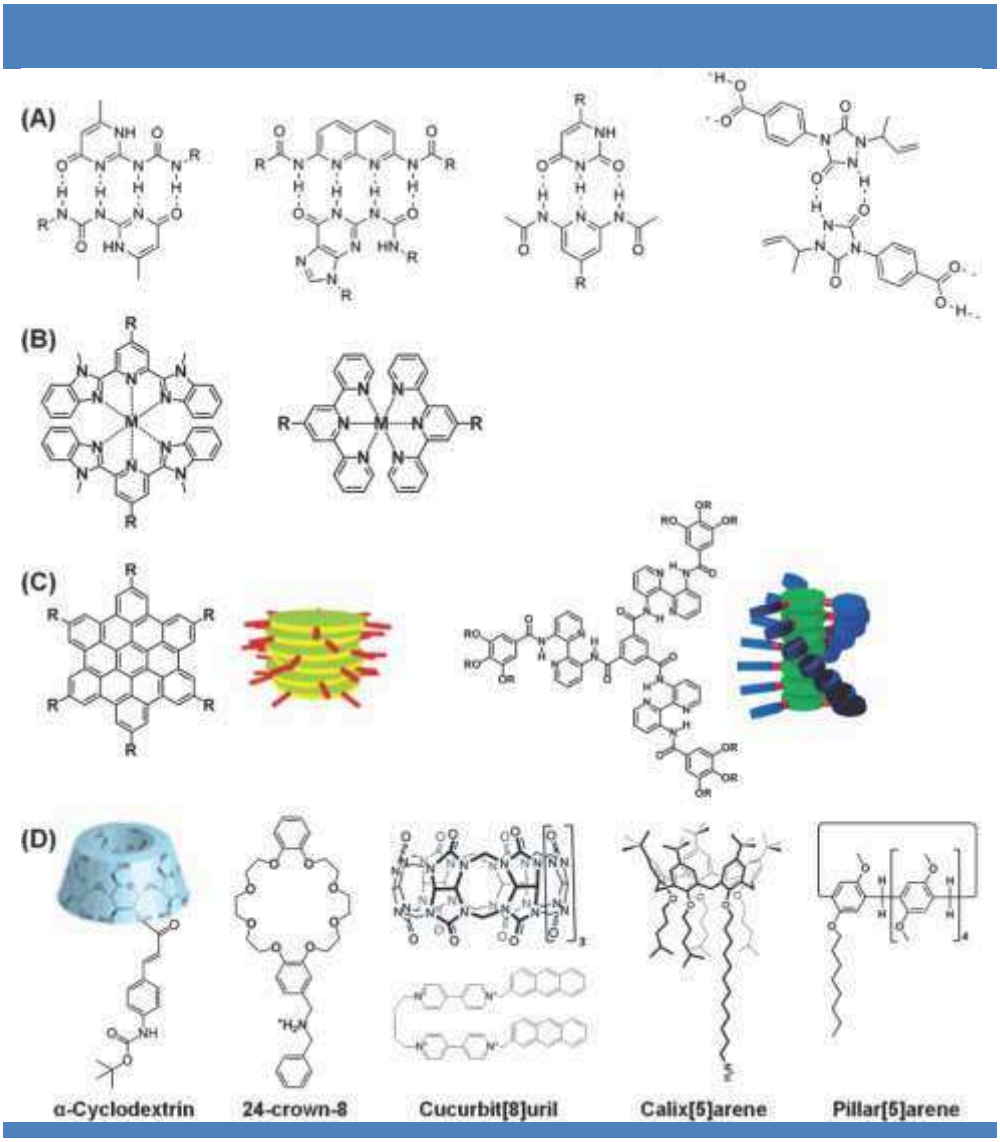

Figure 1 | Different non-covalent interactions for the construction of supramolecular polymers: A) multiple hydrogen bonding, B) metal coordination, C) π-π stacking, D) host-guest interaction. Reproduced from reference[4].

In this manuscript, we will details few supramolecular interactions, namely hydrogen bonding, π-π interactions and metal-ligand interactions, which are predominantly used in this work. We will also highlight to examples which demonstrate the importance of using multiple non-covalent interactions to reach stable supramolecular architectures.

a. Hydrogen bonding

Hydrogen bonding is one of the most widely encountered interaction in nature, such as for DNA pairing and protein folding, and govern the formation of many supramolecular architecture. The hydrogen bond was defined in 2011 by the IUPAC as "an attractive interaction between a hydrogen atom from a molecule or a molecular fragment X–H in which

[4] Dong, R. et al. Functional Supramolecular Polymers for Biomedical Applications. Adv. Mater. **27,** 498–526 (2015).

X is more electronegative than H, and an atom or a group of atoms in the same or a different molecule, in which there is evidence of bond formation".[5] The directionality, diversity, and sensitivity of hydrogen bonds to different environments, such as pH, solvent, and temperature, make them an important tool to build up supramolecular polymers.

In general, the strength of a single hydrogen bond is not high enough to drive the formation of supramolecular polymers. Thus, chemists have developed several hydrogen bonding arrays with association constants that can be as large as 10^{12} M^{-1} (**Figure 2**).

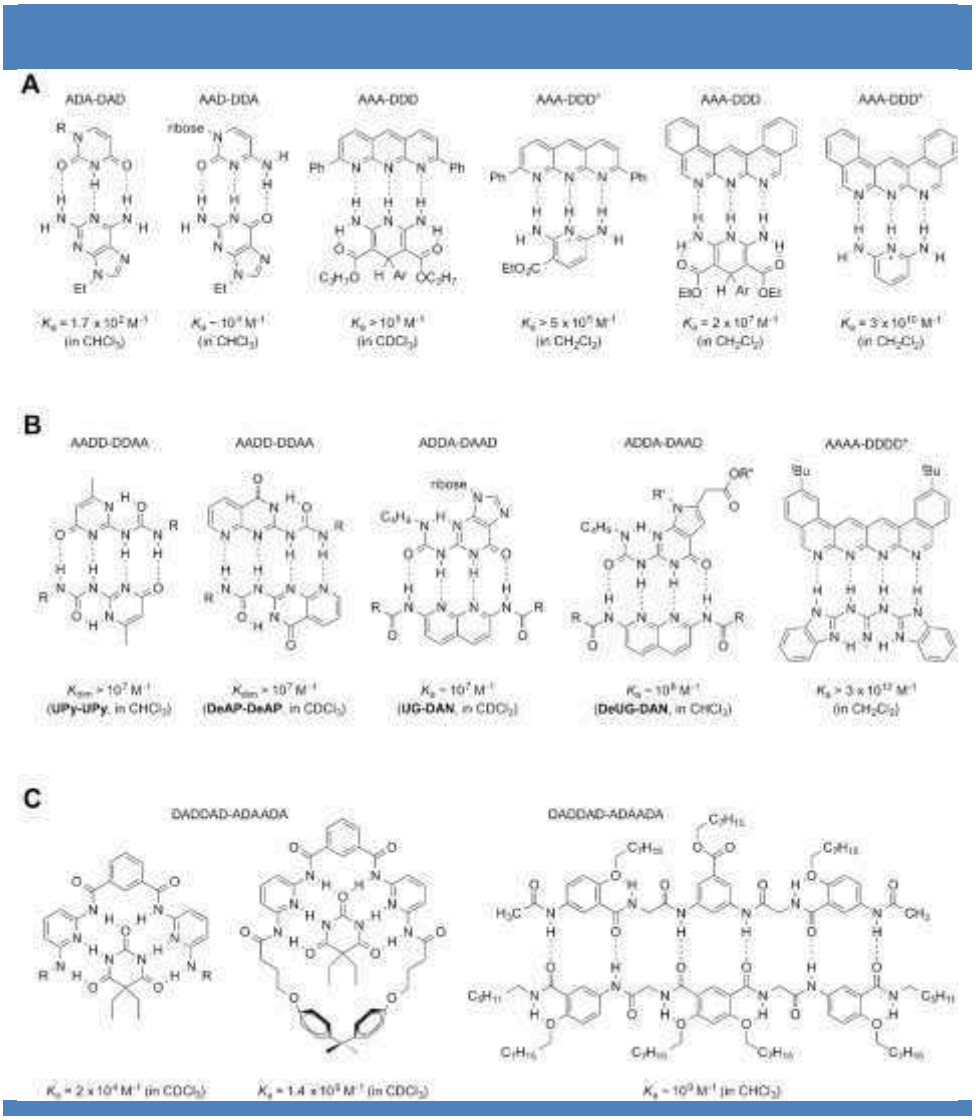

Figure 2 | Hydrogen bonding modules with multiple bonds. (A) Triple, (B) quadruple, and (C) sextuple hydrogen bond motifs. Reproduced from reference [6].

The strength of hydrogen bonding interactions depends not only on the numbers of hydrogen bonds but also the nature of hydrogen bond donor (D) and acceptor (A) atoms involved, and interestingly also on the way that they are arranged. Indeed, attractive and

[5] Arunan, E. et al. Definition of the hydrogen bond (IUPAC Recommendations 2011). Pure Appl. Chem. **83**, 1637-1641 (2011).
[6] Yang, S. K. & Zimmerman, S. C. Hydrogen Bonding Modules for Use in Supramolecular Polymers. Isr. J. Chem. **53,** 511–520 (2013).

repulsive secondary electrostatic interactions between adjacent hydrogen bonds play an important role on the stability of multiple hydrogen bonding modules as reported by Jorgensen and his co-workers in 1990.[7] These secondary effects result in a remarkably higher binding constant for a AAD-DDA system compared to a ADA-DAD system (**Figure 2A**). For instance, two attractive and two repulsive secondary interactions involved in the C-G dimer lead to an increased stabilization compared to the uracil-9H-purine-2,6-diamine dimer, which present four repulsive secondary interactions. Considering the importance of attractive secondary interactions for the stability of triple hydrogen bonding modules, people designed new systems without alternating donor and acceptor groups which led to the development of various AAA-DDD modules[8] with association constant as high as 3×10^{10} M^{-1} in dichloromethane.[9] For instance, the group of Lehn reported the first example of a supramolecular polymer made by hydrogen bonds in 1990, by using triple hydrogen bonding modules such as bifunctional diamidopyridines and bifunctional uracil derivatives.[10] This main-chain supramolecular polymer displayed liquid crystallinity in the solid state, as demonstrated by polarized optical images and X-ray experiments. Interestingly, this property is not expressed by the single monomers, demonstrating that not only supramolecular polymers can achieve functions that their molecularly dissolved building block cannot. Alternatively, following rules similar to the ones developed for triply hydrogen-bonding modules, quadruple and sextuple hydrogen bonding units have also been investigated in order to reach system with high association constant (**Figure 2B-C**).6 To the best of our knowledge, one of the most versatile binding motifs based on quadruple H-bonds and used for linear main chain polymerization is the self-complementary ureidopyrimidinone (UPy) motif (**Figure 3**).[11] This AADD hydrogen bonding module features a strong association constant in a polar solvent ($K_a > 10^7$ M^{-1} in chloroform, $K_a = 6 \times 10^8$ M^{-1} in toluene), which resulted in high degrees of polymerization (DP) in both diluted solutions and bulk materials. Since the discovery of this hydrogen bonding motif the late 90's, this UPy module has been used several times to produce functional supramolecular polymers with adaptive behaviors to environmental conditions (pH, temperature...) and possible applications in optoelectronic

[7] Jorgensen, W. Lnce, D. L. Aromatic-aromatic interactions: free energy profiles for the benzene dimer in water, chloroform, and liquid benzene. J. Am. Chem. Soc. **112,** 4768–4774 (1990).

[8] Murray, T. J. & Zimmerman, S. C. New triply hydrogen bonded complexes with highly variable stabilities. J. Am. Chem. Soc. **114,** 4010–4011 (1992).

[9] Blight, B. A. et al. AAA−DDD Triple Hydrogen Bond Complexes. J. Am. Chem. Soc. **131,** 14116–14122 (2009).

[10] Fouquey, C., Lehn, J.-M. & Levelut, A.-M. Molecular recognition directed self-assembly of supramolecular liquid crystalline polymers from complementary chiral components. Adv. Mater. **2,** 254–257 (1990).

[11] Sijbesma, R. P. et al. Reversible Polymers Formed from Self-Complementary Monomers Using Quadruple Hydrogen Bonding. Science **278,** 1601–1604 (1997).

devices or therapeutic treatments.[12,13]

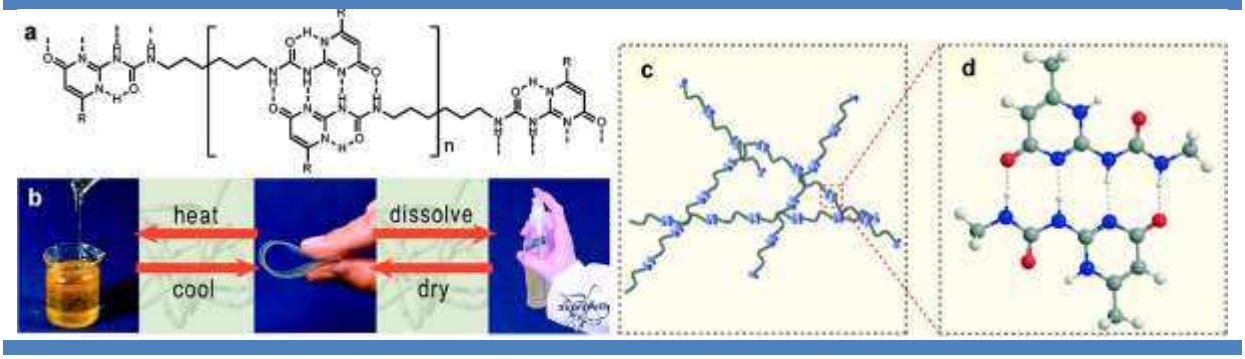

Figure 3 | (a) Chemical structure of a polymer based on two ureidopyrimidinone termini. (b) Adaptive properties of bulk polymers based on Upy. (c) Schematic representation of a polymeric structure based on self-complementary UPy motifs. (d) Molecular model of a self-complementary UPy binding unit. Reproduced from reference [14].

b. π interactions

π interactions can be considered as particular types of electrostatic interactions which involve, on one hand, electron-rich π systems and on the other one, various motifs such as cations, anions or another π system for instance. Accordingly, π interactions can be classified in three main categories: (A) cation-π such as tetramethylammonium and toluene, (B) anion-π such as trifluoro-1,3,5-triazine and chloride anion, and (C) π-π interactions such as, for instance with naphthalene bisimide (NBI)[15] or perylene bisimide (PBI) derivatives.[16] While π-π stacking interactions typically range from 2 to 50 kJ/mol, anion-π and cation-π interactions usually display binding energies in the range of 20-50 kJ/mol and can reach up to 80 kJ/mol (**Table 1**).

Cation-π interactions are ubiquitous in many biological processes,[17] and anion-π interactions have recently emerge as an important tool to transport anions across synthetic membranes.[18] However, π-π stacking interactions, which occur between the π-electrons of one conjugated molecule and the σ-framework of a nearby molecule, remain the most widely used π interactions to build up supramolecular polymers. For instance, Xiao et al. reported the self-assembly and properties of a hexabenzocoronene (HBC) derivative decorated with eight

[12] Abbel, R. et al. White-Light Emitting Hydrogen-Bonded Supramolecular Copolymers Based on π-Conjugated Oligomers. J. Am. Chem. Soc. **131**, 833–843 (2009).
[13] Dankers, P. Y. W. et al. Hierarchical formation of supramolecular transient networks in water: a modular injectable delivery system. Adv. Mater. **24**, 2703–2709 (2012).
[14] Rybtchinski, B. Adaptive Supramolecular Nanomaterials Based on Strong Noncovalent Interactions. ACS Nano **5,** 6791–6818 (2011).
[15] Bhosale, S. V., Jani, C. H. & Langford, S. J. Chemistry of naphthalene diimides. Chem. Soc. Rev. **37**, 331–342 (2008).
[16] Würthner, F. et al. Perylene Bisimide Dye Assemblies as Archetype Functional Supramolecular Materials. Chem. Rev. **116**, 962–1052 (2016).
[17] Ma, J. C. & Dougherty, D. A. The Cation−π Interaction. Chem. Rev. **97**, 1303–1324 (1997).
[18] Jentzsch, A. V. & Matile, S. Anion Transport with Halogen Bonds. Top. Curr. Chem. **358**, 205–239 (2015).

long alkyloxy chains (**Figure 4**).[19] When concentrated in dodecane, this compound self-organized into cables or fibers mainly driven by strong π-stacking interactions, as observed by different microscopy techniques, namely SEM and TEM (**Figure 4B-C**). Using a combination of electron and powder X-ray diffraction, these 1D nanofibers were found to originate from a pseudo-hexagonal arrangement of the HBC derivative with an orthorhombic unit cell of 5.8 nm × 4.5 nm × 0.45 nm (**Figure 4E**). Interestingly, these structures are different from hollow nanotubes obtained by rolling of two dimensional nanosheets made of amphiphilic HBCs.[20] However, the conducting properties measured for these fibers proved to be limited to ~ 10^{-2} cm²/(V.s), which is much lower than what can be expected for such aromatic molecules.

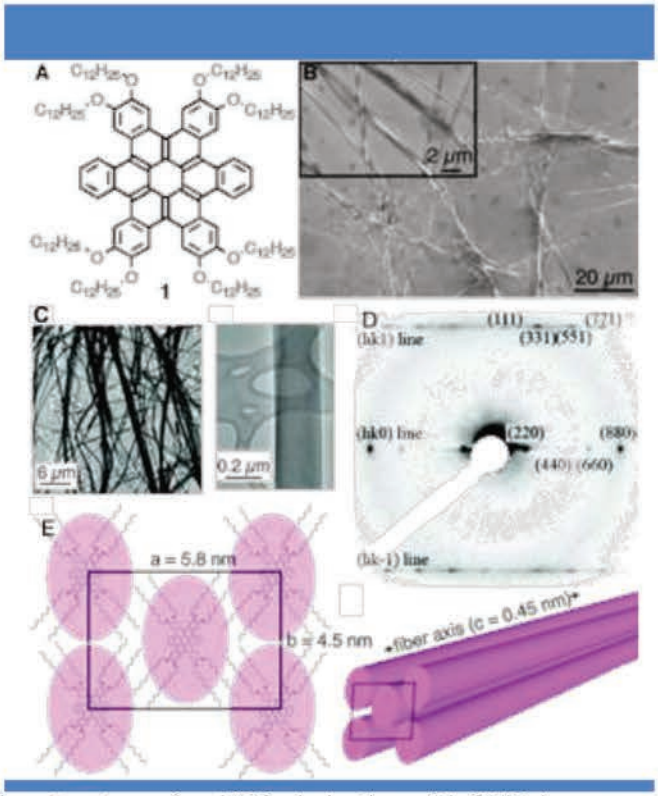

Figure 4 | (A) Molecular structure of a HBC derivative, (B) SEM images and (C) TEM images of self-assembled fibers, (D) Electron diffraction pattern from a single HBC fiber, (E) Rectangular arrangement and packing of the columns into a fiber along the *c*-axis. Reproduced from reference [19].

Several other π-conjugated building blocks such as oligophenylene vinylene, triphenylene,[21] phthalocyanine[22] or porphyrin derivatives[23] among others[24] have been

[19] Xiao, S. et al. Transferring Self-Assembled, Nanoscale Cables into Electrical Devices. J. Am. Chem. Soc. **128,** 10700–10701 (2006).
[20] Hill, J. P. et al. Self-Assembled Hexa-peri-hexabenzocoronene Graphitic Nanotube. Science **304,** 1481–1483 (2004).
[21] Paraschiv, I. et al. H-bond-stabilized triphenylene-based columnar discotic liquid crystals. Chem. Mater. **18,** 968–974 (2006).
[22] Hayashi, H. et al. Segregated donor-acceptor columns in liquid crystals that exhibit highly efficient ambipolar charge transport. J. Am. Chem. Soc. **133,** 10736–10739 (2011).
[23] Sengupta, S. et al. Biosupramolecular Nanowires from Chlorophyll Dyes with Exceptional Charge-Transport Properties. Angew. Chemie Int. Ed. **51,** 6378–6382 (2012).
[24] Zang, L., Che, Y. & Moore, J. S. One-Dimensional Self-Assembly of Planar π-Conjugated Molecules: Adaptable Building Blocks for Organic Nanodevices. Acc. Chem. Res. **41,** 1596–1608 (2008).

explored to produce supramolecular polymers based on π-π stacking interactions. They have found interesting applications in the field of optoelectronic materials such as solar cells, field-effect transistors...[25]

c. Metal–ligand interactions

Metal-ligand coordination interactions usually involve a transition metal center and an organic building block, also known as ligand, which display affinity for the metal center.[26] Typically, metallosupramolecular polymers are built from ditopic monomers with ligands such as phosphines, pyridines, imines, and so on, located as end chains. Three types of interactions can be involved in metal-ligand interactions, i.e. coordinative bonding, ionic/covalent bonding and metal-arene complexation. Furthermore, there are different ways to increase the stability of metal-ligand interactions, either by choosing a mteal ion which has a high binding affinity for the donor atoms of the ligand or by increasing the number of binding sites available for metal coordination. Such strategy has been widely developed and it has led to the development of new organic ligands such as, for instance terpyridine, which presents a binding affinity for zinc that is more than five orders of magnitude higher than pyridine. Importantly, the strength of this binding affinity is one main parameter that influence the degree of polymerization. Owing to the non-covalent nature of these interactions, environmental parameters such as solvent, concentration and temperature may also influence the binding strength of metal-ligand interactions. However, the most versatile way to affect the binding affinity of a ligand is to adjust the metal ion used for coordination.

Recently, our group demonstrated that the polymerization of a terpyridine-terminated pH-switchable interpenetrated rotaxanes is strongly affected by the nature of the metal ion (**Figure 5**).[27] Indeed, when zinc ions were used, polymerization of the rotaxane units proceeded to an average degree of polymerization of 2000 monomers, as demonstrated by light and neutron scattering experiments. Alternatively, when iron metal ions, which present a higher binding strength for terpyridine compared to zinc, were used, the formation of a longer supramolecular main-chain polymer was observed (around 3000 monomers). Importantly, when the system was acidified to induce the extension of the rotaxane unit, the strength of the metal-ligand interaction was found to be crucial for the survival of the single chain supramolecular polymer. Indeed, in the presence of zinc ions, we observed partial

[25] Moulin, E., Busseron, E. & Giuseppone, N. in Supramolecular Materials for Opto-Electronics 1–52 (The Royal Society of Chemistry, 2015).
[26] Winter, A. et al. Synthesis and characterization of metallo-supramolecular polymers. Chem. Soc. Rev. **45,** 5311–5357 (2016).
[27] Du, G., Moulin, E., Jouault, N., Buhler, E. & Giuseppone, N. Muscle-like Supramolecular Polymers: Integrated Motion from Thousands of Molecular Machines. Angew. Chemie Int. Ed. **51,** 12504–12508 (2012).

depolymerization upon addition of protons, which compete with zinc ions for binding to terpyridine ligands. Such behavior was not observed when iron metal ions were used, allowing extension of the supramolecular main chain polymer.

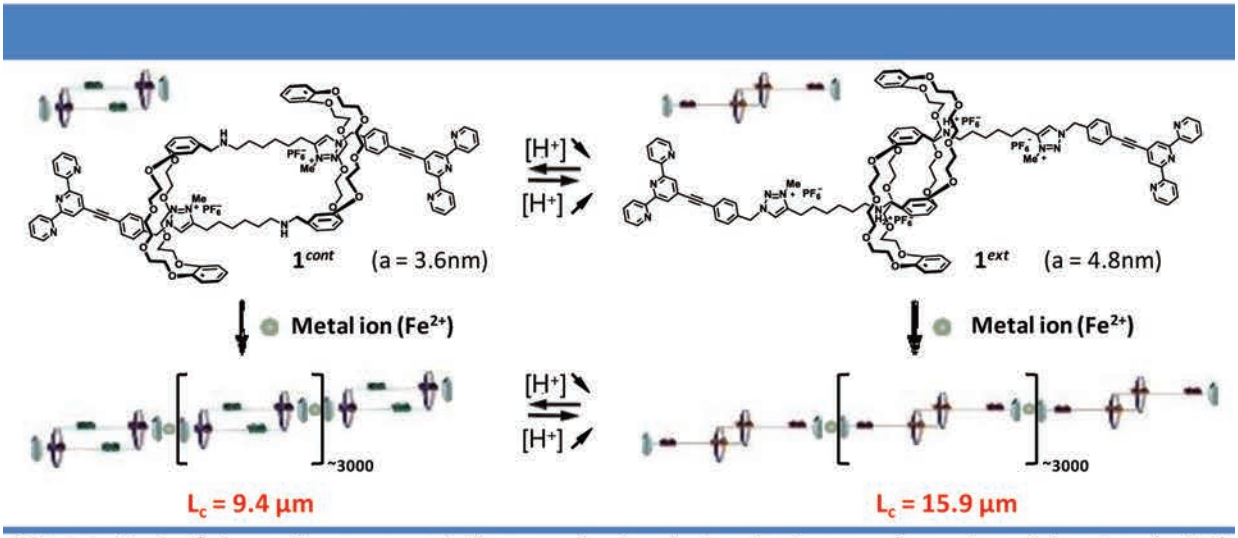

Figure 5 | Schematic representation and chemical structures of a terpyridine-terminated supramolecular polymer made of contractile [c2]daisy chains units. Their collective contraction/extension changes the average size of the polymer chain.

d. Other interactions

As described in **Table 1**, the strongest non-covalent interactions are ion-ion and ion-dipole, which results from the electrostatic attraction of a positively charged species with a negatively charged entity. The strength of such electrostatic interactions can be as high as 200-300 kJ/mol, mostly for ion-ion bonds, which however lack directionality as opposed to most non-covalent interactions described previously. One important asset of non-covalent interactions involving ions is their sensitivity to external conditions, such as pH or solvents, which allows to finely tune the binding strength. Recently, Rodler and coworkers reported how pH can affect the morphology of self-assembled architectures built from a new zwitterionic compound bearing positively charged guanidine and negatively charged carboxyl groups.[28] Using a combination of microscopy, scattering and spectroscopy experiments, the authors demonstrated that, in a narrow pH range, these self-complementary molecules can form ion-pair dimers which further aggregate into hollow vesicles. Interestingly, by adjusting the pH in solution, the self-assembled vesicles could be either opened or closed as a result of different states of the zwitterionic molecule.

Other non-covalent interactions include, for instance, hydrophobic interactions, which occurs when non-polar molecules aggregate in polar solvents such as water and exclude the

[28] Rodler, F. et al. pH-Switchable Vesicles from a Serine-Derived Guanidiniocarbonyl Pyrrole Carboxylate Zwitterion in DMSO. Angew. Chemie Int. Ed. **49,** 8747–8750 (2010).

molecules of solvents, or Van der Waals interactions, which are the weakest non-covalent interactions known to date but play a key role in various supramolecular polymerization processes.

Finally, host-guest complexes, such as the ones depicted on **Figure 1D**, have been widely used to produce main chain supramolecular polymers. The driving force in host-guest interactions is related to the cooperative association of two complementary molecules. As they typically arise from the combination of several non-covalent interactions, host-guest interactions offer the same properties of other non-covalent interactions, such as reversibility, directionality, and responsiveness. Some commonly reported host molecules such as cyclodextrins,[29] calixarenes,[30] and cucurbiturils,[31] are biocompatible and display an amphiphilic character, thus contributing to the formation of self-assemblies both in organic solutions and aqueous media. Furthermore, these macrocyclic hosts display different affinities for small molecules. For instance, Zhao and coworkers reported the formation of a main-chain supramolecular polymer from three ditopic monomers thanks to two orthogonal host-guest interactions.[32] An adamantane-viologen heteroleptic small molecule was mixed with two homoleptic building blocks containing either cyclodextrins and sulfonatocalixarenes as end groups. In water, a 2:1:1 ratio of the monomers resulted in the formation of a linear polymer as imaged by AFM and TEM.

e. Multiple non-covalent interactions

In nature, the most complicated processes are accomplished by more than one non-covalent interactions, such as DNA transcription or protein folding. The combination of several supramolecular forces has thus been widely used by chemists in order to dramatically enhance the stability of supramolecular polymer. In 2008, the group of Elemans reported the supramolecular polymerization of a porphyrin trimer built from a benzene-1,3,5-tricarboxamide (BTA) core, tailored with either long non-chiral or chiral aliphatic chains (**Figure 6A**).[33] This polymerization process was induced by a combination of hydrogen bonding and π-π stacking interactions. Temperature and concentration-dependent NMR, light scattering, CD and UV-vis spectroscopy were used to investigate the self-assembly in solution. Whereas the porphyrin trimer aggregated into long chiral columnar supramolecular polymers

[29] Harada, A. et al. Cyclodextrin-based supramolecular polymers. Chem. Soc. Rev. **38,** 875 (2009).
[30] Guo, D.-S. et al. Calixarene-based supramolecular polymerization in solution. Chem. Soc. Rev. **41,** 5907 (2012).
[31] Liu, Y., Yang, H., Wang, Z. & Zhang, X. Cucurbit[8]uril-Based Supramolecular Polymers. Chem. - An Asian J. **8,** 1626–1632 (2013).
[32] Zhao, H.-X., Guo, D.-S., Wang, L.-H., Qian, H. & Liu, Y. A novel supramolecular ternary polymer with two orthogonal host–guest interactions. Chem. Commun. **48,** 11319 (2012).
[33] van Hameren, R. et al. Supramolecular Porphyrin Polymers in Solution and at the Solid−Liquid Interface. Nano Lett. **8,** 253–259 (2008).

at micromolar concentrations in non-polar solvents as n-hexane and cyclohexane, it remained molecularly dissolving in chloroform. Interestingly, when solutions were drop-casted on mica under argon atmosphere and at room temperature, morphologies different from the ones recorded in solution were observed. This phenomenon was particularly observed for chloroform solutions which lead to the formation of aligned monocolumnar aggregates on a mica surface after spinodal dewetting.

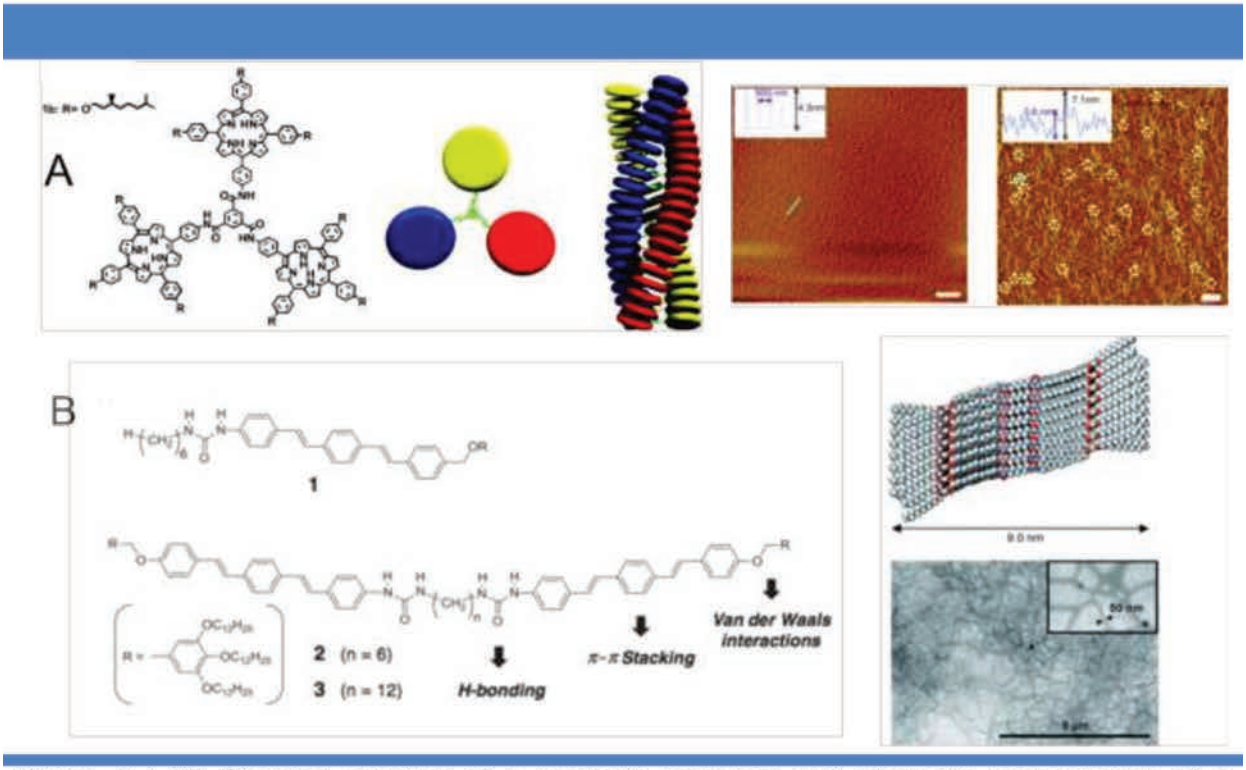

Figure 6 | (A) Chemical structure of a porphyrin monomer and schematic representation of a self-assembled columnar aggregate; (a,b) AFM images of patterns formed after drop-casting a solution of 1b in chloroform (a, scale bar = 1 µm) and n-hexane (b, scale bar = 2 µm). (B) Chemical structures of OPV-functionalized mono- and bisureas (left); part of the molecular-modeled supramolecular polymer of 2 (right, up); STEM image of fibrous aggregates of 2 stained with RuO_4 prepared from a methylcyclohexane dispersion ($c = 3.0 \times 10^{-5}$ M) (right, down). Reproduced from references [33,34,35]

In another example, Yagai et al also found that the number of non-covalent interactions can affect the supramolecular polymerization of the oligo(p-phenylene vinylene) (OPV)-urea hybrids (**Figure 6B**).[35] These molecules offers three possible non-covalent interations, namely hydrogen bonding of the urea moieties, π-π stacking of the OPV units and Van der Waals interactions at the gallic residues. Symmetrical compounds **2** and **3** offer six possible supramolecular interactions compared to compound **1**. Using a combination of scattering and microscopy experiments, compound **2** led to the formation of supramolecular polymers with the highest degree of polymerization as indicated by the presence of micrometric fibers and

[34] Torres, T. & Bottari, G. Organic nanomaterials: synthesis, characterization, and device applications. (John Wiley & Sons, 2013).

[35] Yagai, S. et al. Supramolecular Polymerization and Polymorphs of Oligo(p-phenylene vinylene)-Functionalized Bis- and Monoureas. Chem. - A Eur. J. **14,** 5246–5257 (2008).

larger hydrodynamic radius compared to compounds **1** and **3**, as a result of the cooperativity of the non-covalent interactions.

2. Mechanism of supramolecular polymerization

As stated at the beginning of this chapter, supramolecular polymers arise from molecular units which arrange by "moderately strong, reversible non-covalent, but highly directional" interactions into well-defined polymeric structures. Such supramolecular polymerization processes are highly dependent on thermodynamic factors, such as concentration and temperature, because of the inherent reversible properties of the non-covalent interactions. As commonly accepted, there are three main mechanisms of supramolecular polymerization[36]: isodesmic, ring-chain, and cooperative growth, which is also called nucleation-elongation (**Figure 7**) and we will describe them briefly in this section.

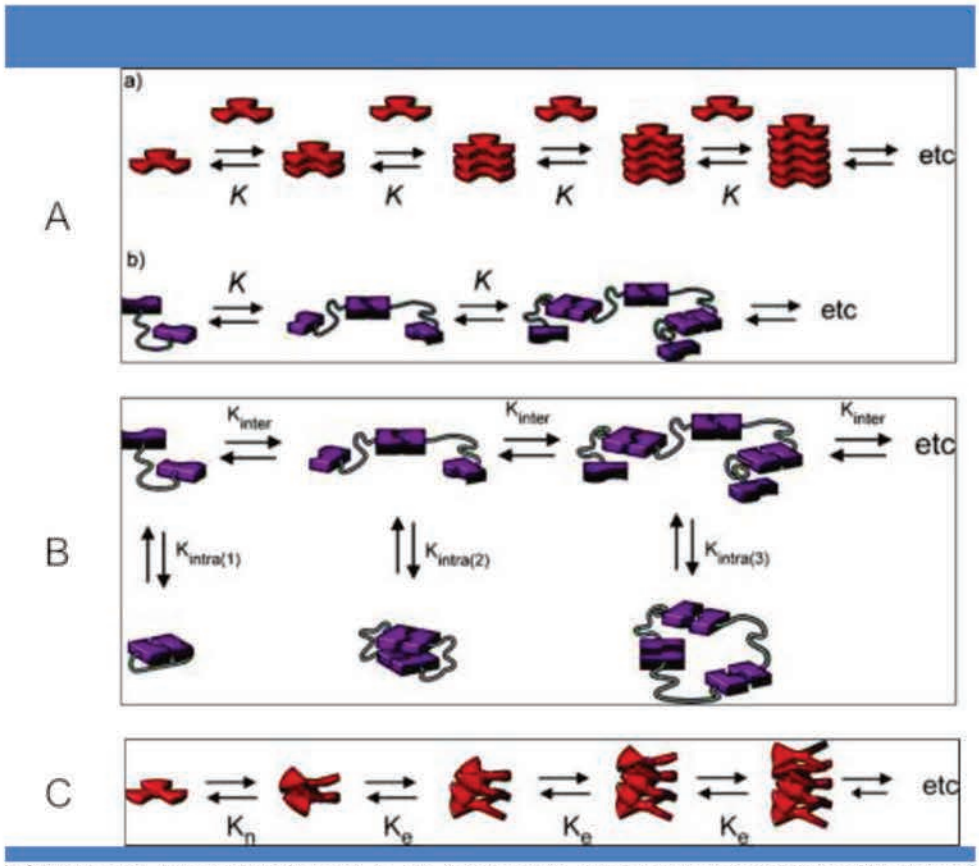

Figure 7 | Schematic representation of A. an isodesmic supramolecular polymerization of a) a rigid discotic molecule into a linear supramolecular polymer and b) a bifunctional monomer in which the two binding groups are connected via a flexible spacer; B. a ring-chain supramolecular polymerization and C. a cooperative ($K_n < K_e$) supramolecular polymerization of a rigid discotic molecule. Reproduced from reference [36].

During the isodesmic polymerization, the binding constant associated with the addition

[36] De Greef, T. F. A. et al. Supramolecular Polymerization. Chem. Rev. **109,** 5687–5754 (2009).

of one monomer at each step of the self-assembly process is identical (**Figure 7A**). This means that the length of the supramolecular polymer chain and the neighboring group effects do not affect the reactivity of the monomers. Therefore, this polymerization process occur at any concentration or temperature but, high concentration and/or low temperature favor the formation of supramolecular polymers with high degree of polymerization.

The second growth process, known as ring-chain, is relevant only for bifunctional monomers (**Figure 7B**). This mechanism features an equilibrium between the formation of main chain supramolecular polymer associated with a binding constant K_{inter} and the presence of cyclic structures of various sizes associated with several binding constant K_{intra}. The degree of polymerization (DP) in such mechanism is determined by the different association constants and the formation of main-chain polymers with high DP occurs only above a critical concentration. Below this concentration, the formation of the cyclic structures is favored.

The third class of supramolecular polymerization known as cooperative growth occurs involves at least two distinct stages: a slow nucleation process and an elongation after formation of the nucleus. Each stage of this mechanism corresponds to an isodesmic polymerization with different association constants, namely one for the nucleation event (K_n) and one for the elongation K_e (**Figure 7C**). By analogy with biological processes such as protein aggregation which occurs following a cooperative mechanism,[37] the formation of polymers according to this mechanism is always delayed as the initial step consists in the formation of a nucleus, which can be shorten or cleared by adding preformed oligomers (seeding). Another main feature of this mechanism compared to the isodesmic one is the presence of the critical concentration and a temperature above which supramolecular polymers are favored over monomers. Ordered supramolecular polymers usually arise from this polymerization mechanism as exemplified for instance by the group of Meijer.[38,39]

Mechanistic studies of the three processes have been developed both experimentally and theoretically.[40,41] Generally, supramolecular polymerization mechanisms are detemined by performing a set of experimental measurements, such as temperature-dependent and concentration-dependent NMR, optical spectroscopies (UV-vis absorbance, fluorescent emission, CD etc.), or even ITC among others. In a recent example, Ogi and coworkers

[37] Frieden, C. Protein aggregation processes: In search of the mechanism. Protein Sci. **16,** 2334–2344 (2007).
[38] Korevaar, P. A. et al. Pathway complexity in supramolecular polymerization. Nature **481,** 492–496 (2012).
[39] Gillissen, M. A. J. et al. Triple Helix Formation in Amphiphilic Discotics: Demystifying Solvent Effects in Supramolecular Self-Assembly. J. Am. Chem. Soc. **136,** 336–343 (2014).
[40] Smulders, M. M. â. J. et al. How to Distinguish Isodesmic from Cooperative Supramolecular Polymerisation. Chem. - A Eur. J. **16,** 362–367 (2010).
[41] Chen, Z. et al. Self-assembled π-stacks of functional dyes in solution: structural and thermodynamic features. Chem. Soc. Rev. **38,** 564–584 (2009).

reported on the self-assembly of a porphyrin derivative decorated with two dodecyl gallate and amide moieties on distal positions, into nanoparticles and fibril aggregates as a result of π-π stacking and hydrogen bonding interactions (**Figure 8**).[42]

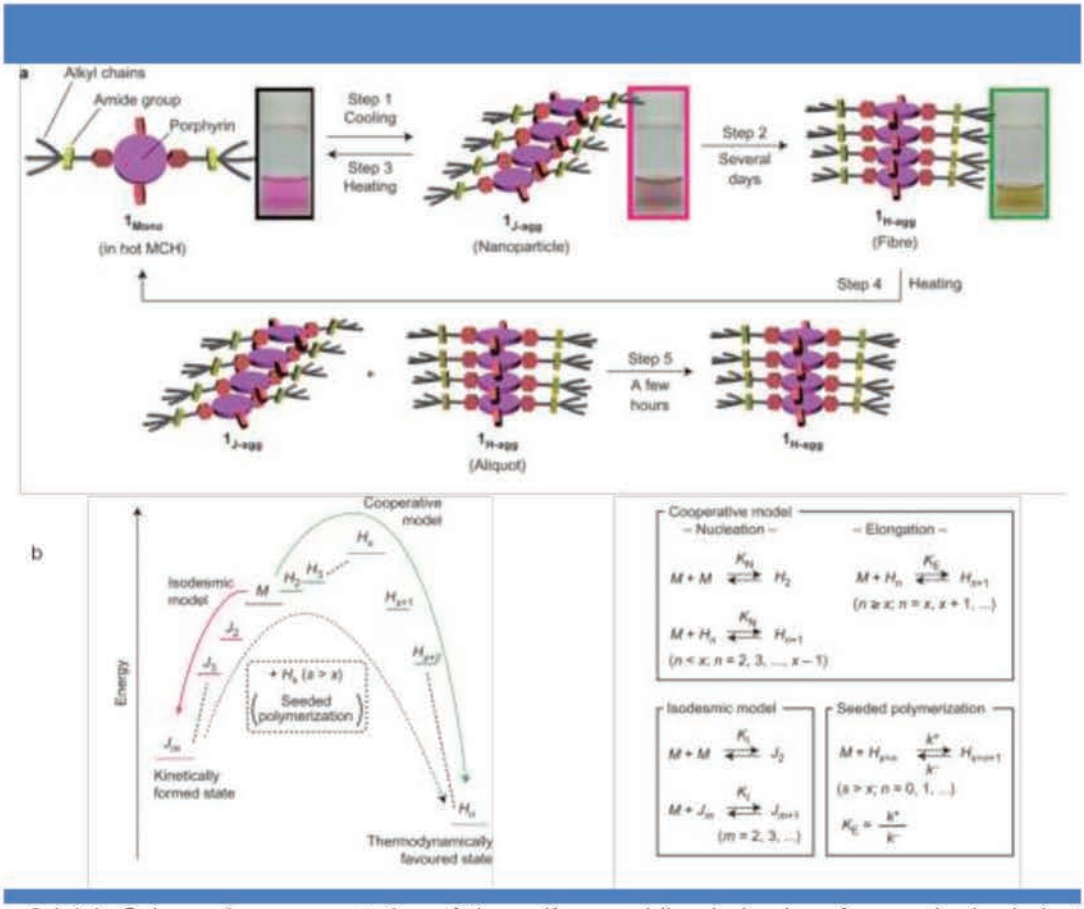

Figure 8 | (a). Schematic representation of the self-assembling behavior of a porphyrin derivative in methylcyclohexane, (b). Energetic landscape representing the pathway complexity in supramolecular polymerization of this prophyrin compound and illustrated on the basis of the thermodynamic parameters determined by van't Hoff plots. Reproduced from reference [42].

Interestingly, using a combination of spectroscopic and imaging experiments, they found out that nanoparticles can evolve into fibrillar aggregates with time and further explored the different self-assembly processes. Absorption spectroscopy was used to demonstrate that nanoparticles results from the J-aggregation of the monomers while fibers arise from their H-aggregation. Temperature-dependant UV-Vis measurements were used to demonstrate that the mechanism of polymerization from monomers 1_{mono} to kinetically trapped $1_{J\text{-}agg}$ is an isodesmic process, while the formation of thermodynamically stabled $1_{H\text{-}agg}$ from 1_{mono} follows the rules of a cooperative model. In this particular example, the nucleation time is long enough so that kinetically formed $1_{J\text{-}agg}$ can be isolated. As shown in **Figure 8** step 5, the addition of a small amount of preformed $1_{H\text{-}agg}$ seed into a $1_{J\text{-}agg}$ solution induces

[42] Ogi, S., Sugiyasu, K., Manna, S., Samitsu, S. & Takeuchi, M. Living supramolecular polymerization realized through a biomimetic approach. Nat. Chem. **6,** 188–195 (2014).

the transformation into pure $1_{H\text{-}agg}$ in only few hours and with a much narrower polydispersity (PDI = 1.1) as imaged by AFM.

Researches focused on supramolecular polymerization mechanisms are of particular importance to better understand self-assembly processes, which should further facilitate the implementation of supramolecular polymers as functional materials.

3. Functional supramolecular polymers

Covalent polymeric materials are commonly encountered in our daily lives, but they offer suffer from problems for recyclability, sensitivity and irreversible damage, just to name few drawbacks. By taking advantage of the tunable, reversible and stimuli-responsive nature of non-covalent interactions, supramolecular polymers have been considered in the last two decades as alternative materials to commonly used polymers with enhanced properties. By fine tuning the aggregation of monomeric units into well-defined architectures such as nanofibers, nanosheets, helices, nanotubes etc., these supramolecular self-assemblies have been developed for different kinds of applications in the field of biomedine (diagnosis and therapeutics), optoeletronics, information storage or even catalysis.[43,44,45]

In this section, we will mainly focus on three possible categories of applications, for which supramolecular polymers have been considered, namely self-healing materials, biomedical applications and organic electronics.

a. Supramolecular polymers as self-healing materials

Self-healing materials which have the ability to repair themselves after external damage is one of the most attractive applications of supramolecular materials. Such properties are inherent to the reversibility and stimuli-responsive nature of the dynamic non-covalent interactions involved in these polymers. **Figure 9A-C** demonstrates the general process of a "self-healing" material built from supramolecular polymers.[46] When a damage occurs in the material thus causing a crack, the reversible and relatively weak non-covalent interactions of the polymer network are broken rather than covalent bonds. Such event leads to the formation of a new interface full of free binding sites. When two pieces of such materials are brought

[43] Aida, T., Meijer, E. W. & Stupp, S. I. Functional Supramolecular Polymers. Science **335,** 813–817 (2012).
[44] Busseron, E., Ruff, Y., Moulin, E. & Giuseppone, N. Supramolecular self-assemblies as functional nanomaterials. Nanoscale **5,** 7098–7140 (2013).
[45] Yang, L., Tan, X., Wang, Z. & Zhang, X. Supramolecular Polymers: Historical Development, Preparation, Characterization, and Functions. Chem. Rev. **115,** 7196–7239 (2015).
[46] Herbst, F., Döhler, D., Michael, P. & Binder, W. H. Self-Healing Polymers via Supramolecular Forces. Macromol. Rapid Commun. **34,** 203–220 (2013).

together, supramolecular interactions can occur, thus healing the damage after recombination of the original non-covalent bonds.

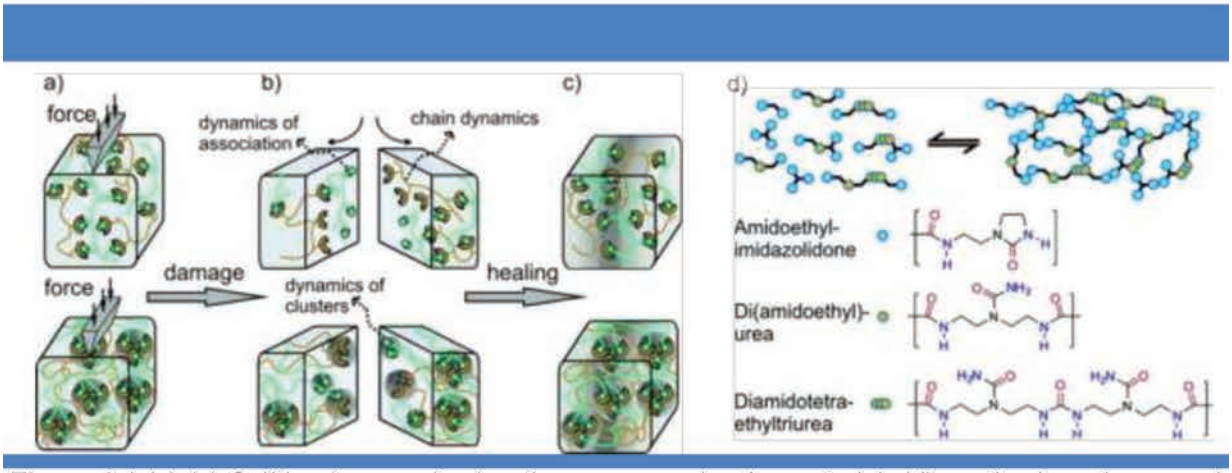

Figure 9 | (a)-(c) Self-healing mechanism for a supramolecular material; (d) synthesis pathway and molecular structure of self-healing rubber. Reproduced from references 46,47.

To build a self-repairing system, there is no need for extremely strong binding motifs, as the healing properties mainly lie on the dynamic and density of the associating interactions. One of the most impressive example which aims at building a self-healing extensible rubber is based on hydrogen bonding interactions, as described by Cordier and coworkers (**Figure 9D**).[47] The supramolecular material relies on three types of urea and amide units, namely amidoethyl-imidazolidone, di(amidoethyl)urea and diamidotetraethyl-triurea, which contain various hydrogen bond acceptor and donor moieties. After association, the presence of numerous hydrogen bonds on the main polymer backbone and also on side-chains along with the high density hydrogen-bonding interactions resulted a supramolecular material with mechanical properties similar to typical covalent rubbers. Since the supramolecular rubber was polymerized by reversible interactions, it was able to self-repair at the cutting interface by just bringing the fractured sites together during some time at room temperature.

In another example, Binder and coworkers designed a self-healing polymer based on poly(isobutylene) decorated with barbituric acid end-groups.[48] Although the self-association constant between barbituric acid groups is not high in solution, polymers aggregated dramatically in the melt state, as evidenced by rheology experiments. Self-healing properties was also monitored at room temperature. Nucleobase pairs, self-complementary ureidopyrimidinone and various hydrogen bonds array systems have also been developed for this kind of applications, Binder suggested that four main kinds of non-covalent interactions

[47] Cordier, P., Tournilhac, F., Soulié-Ziakovic, C. & Leibler, L. Self-healing and thermoreversible rubber from supramolecular assembly. Nature **451,** 977–980 (2008).
[48] Herbst, F. et al. Dynamic supramolecular poly(isobutylene)s for self-healing materials. Polym. Chem. **3,** 3084 (2012).

are involved in the formation of self-healing polymers, namely hydrogen bonding, ionomers, metal bonding and π-π stacking interactions.[46]

b. Supramolecular polymers for biomedical applications

As supramolecular polymers are endowed with advantages such as biodegradation, biocompatibility and responsiveness to bio-stimuli, they have been considered as outstanding candidates for biochemical applications in the field of drug delivery, regenerative medicine, tissue engineering, gene transfection, protein delivery and biomimetic chemistry.[45, 49] Hydrogen bonded supramolecular polymers based, for example, on UPy derivatives, have already been successfully employed for various applications as tissue engineering,[50] protein delivery[51] and intrarenal drug delivery.[52] For instance, Dankers and coworkers reported the synthesis of two kinds of mild and biocompatible hydrogels built from supramolecular polymers with UPy units either within the polymeric backbone or at its terminal groups and their possible use as drug delivery candidates.[52] The gel with UPy within the main-chain polymeric backbone, i.e. bearing more binding sites, was strong, flexible and slow eroding, thus suitable for long-term intrarenal delivery, whilst the gel with UPy as end groups on the polymer chains was weaker, soft and fast eroding, which should be more appropriate for fast delivery of protein drugs to the kidney cortex.

Among all artificial nanomaterials, self-assembled peptide nanofibers are the most widely used structures as they can be easily tuned and designed to signal cells. The group of Stupp developed several peptide amphiphiles (PA) systems which incorporate a hydrophobic alkyl tail, a short peptide sequence with β-sheet propensity, a charged amino acid groups and at the other terminus, bioactive functional epitopes to interact with cell receptors.[53] This series of molecules are known to self-assemble into one dimensional nanostructures, mainly nanofibers with a cylindrical geometry (**Figure 10**), and the nanofibers can be prepared by co-assembly and designed for various biomedicine applications. There are three driving forces for the self-assembly of PAs in water: hydrophobic interactions from alkyl tails and hydrogen bonding between peptide segments act as attractive contributions, while electrostatic repulsive interactions between charged groups lead to opposite contributions. The final

[49] Webber, M. J., Appel, E. A., Meijer, E. W. & Langer, R. Supramolecular biomaterials. Nat Mater **15,** 13–26 (2016).
[50] Dankers, P. Y. W., Harmsen, M. C., Brouwer, L. A., Van Luyn, M. J. A. & Meijer, E. W. A modular and supramolecular approach to bioactive scaffolds for tissue engineering. Nat. Mater. **4,** 568–574 (2005).
[51] Dankers, P. Y. W. et al. Hierarchical Formation of Supramolecular Transient Networks in Water: A Modular Injectable Delivery System. Adv. Mater. **24,** 2703–2709 (2012).
[52] Dankers, P. Y. W. et al. Development and in-vivo characterization of supramolecular hydrogels for intrarenal drug delivery. Biomaterials **33,** 5144–5155 (2012).
[53] Cui, H., Webber, M. J. & Stupp, S. I. Self-assembly of peptide amphiphiles: From molecules to nanostructures to biomaterials. Biopolymers **94,** 1–18 (2010).

aggregation is a result of the combination and balance between these different interactions.

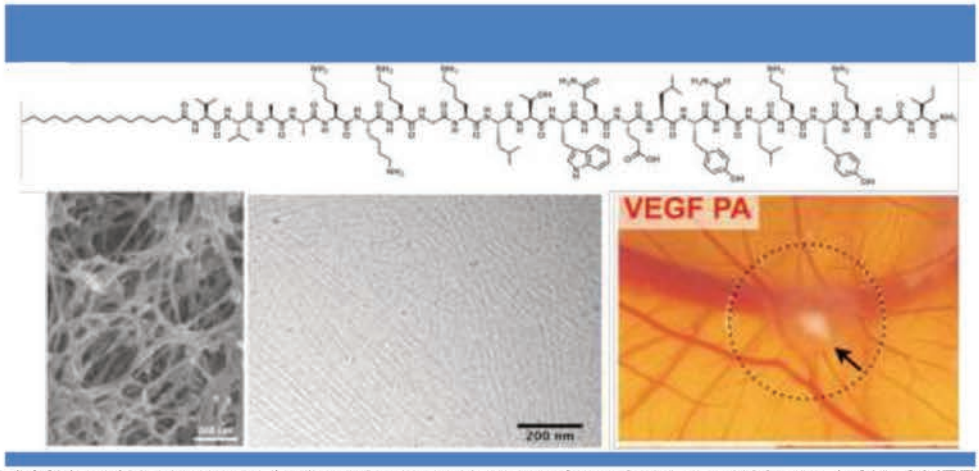

Figure 10 | Molecular structure (up) and nanostructures by microscopy (down, left) of VEFG-mimetic peptide amphiphile and the effect on angiogenesis in a chicken chorioallantoic membrane assay (down, right). Reproduced from reference [54].

Figure 10 represents one example of an artificial peptide amphiphile designed to mimic the activity of VEGF, which is a potent, but time-limited angiogenic factor.[54] The high density of PA nanofibers was verified by TEM and SEM experiments, and they were subsequently found to be recognized by VEGF receptors and promote proangiogenic behavior both in vivo and in vitro.

c. Supramolecular polymers for organic electronics

The field of organic conducting and semiconducting materials developed rapidly because the advantages of low cost, high processability and possibility to reach flexible devices. In particular, supramolecular polymers based on π-conjugated molecules are of particular interest as materials with high directional charge-carrier mobility due to their precisely ordered architectures. Scientists have designed various monomeric structures in order to reach highly organized self-assembled polymers with different properties for applications as field-effect transistors, light-emitting diodes, photovoltaic devices and conductive materials.[55,56] A discussed in a previous section, hexabenzocoronene (HBC) is one of the widely used π-conjugated units for applications in organic electronics.[20,57]

The Aida group, who reported the self-assembly of modified amphiphilic HBC into nanotubes,[20] elaborated several molecules for use as photoconducting materials by connecting trinitrofluorenone (TNF) on one hydrophilic triethylene glycol (TEG) end (**Figure 10**). In one

[54] Webber, M. J. et al. Supramolecular nanostructures that mimic VEGF as a strategy for ischemic tissue repair. Proc. Natl. Acad. Sci. U. S. A. **108,** 13438–43 (2011).
[55] Pisula, W., Feng, X. & Müllen, K. Charge-Carrier Transporting Graphene-Type Molecules †. Chem. Mater. **23,** 554–567 (2011).
[56] Moulin, E., Cid, J.-J. & Giuseppone, N. Advances in supramolecular electronics - from randomly self-assembled nanostructures to addressable self-organized interconnects. Adv. Mater. **25,** 477–487 (2013).
[57] Blau, W. J. & Fleming, A. J. Designer Nanotubes by Molecular Self-Assembly. Science **304,** 1457–1458 (2004).

monomer, HBC played the role of the electron donor moiety and the TNF acted as acceptor, while TEG and C_{12} alkyl chain were used for solubility. TEM and SEM images confirmed the formation of nanotubes. The molecular layer made of trinitrofluorenone moieties is laminated with a graphitic layer of π -stacked HBCs, thus resulting in the formation of coaxial p/n-heterojunction. This supramolecular structure could be used to generate an electrical conductivity upon photoirradiation, with a large on/off ratio of more than 10^4.

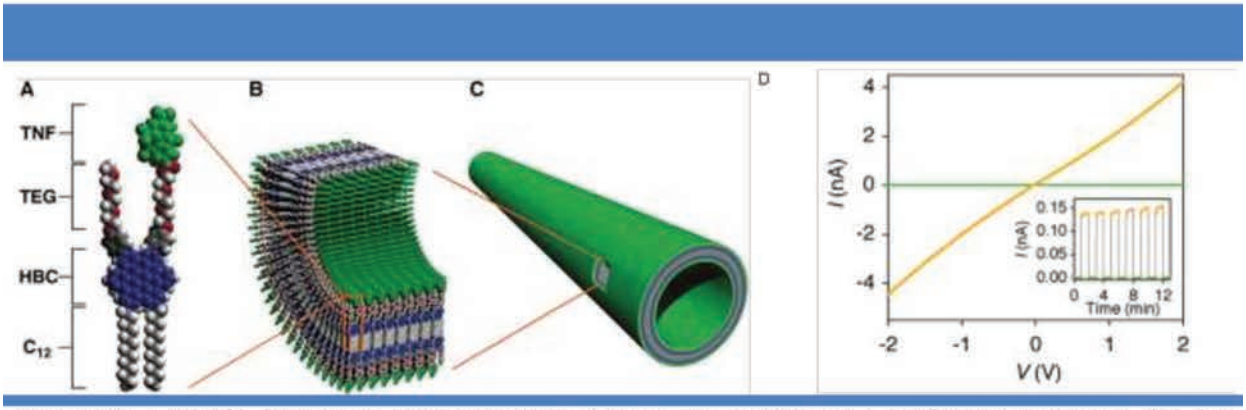

Figure 11 | (A)-(C) Schematic representation of the self-assembly of a HBC-TNF derivative. (D) *I-V* curve recoded at 25 °C for a cast film of the nanotubes. Reproduced from [20].

Several other types of conjugated molecules have been reported to produce supramolecular polymers with potentially interesting conducting properties. In particular, one emerging class of supramolecular polymers with such properties rely on the triarylamine scaffold, which was first discovered in our group.[58] As the majority of the work described in this thesis is related to this family of molecules, we will discuss in more details these chemical structures, their self-assembly behavior and their functionalities in the next chapter.

[58] Moulin, E. et al. The hierarchical self-assembly of charge nanocarriers: a highly cooperative process promoted by visible light. Angew Chem Int Ed Engl **49,** 6974–6978 (2010).

Chapter 2: Triarylamine-based supramolecular polymers

Triarylamine is a functional moiety which has been extensively studied over the last fifty years, mainly because of the easy oxidation of its central nitrogen atom and its ability to transport positive charges via the formation of triarylammonium radical cations. Several star-shaped and dendrimeric triarylamines structures but also side-chain and main-chain triarylamine polymers have been synthesized with the aim to use them in electronic devices such as organic light emitting diodes (OLEDs)[59], organic field-effect transistors (OFETs)[60], organic photovoltaic cell and solar cells[61] and so on.[62] However, to the best of our knowledge, most studies involving triarylamine molecules have been carried out in the bulk, without paying attention to a possible self-organization at the nanoscale.

In this chapter, I will firstly present some examples in which chemical functionalities at the edge of tripodal triarylamine molecules are the driving forces to generate well-defined supramolecular architectures while, in the next sections, we will focus on supramolecular polymers arranged around the triarylamine core from various chemically-designed triarylamine molecules and which display properties inherent to the self-assembly of these triarylamine unit.

1. Self-assemblies based on tripodal triarylamine units

To the best of our knowledge, the first example, which reports the formation of supramolecular architectures incorporating triarylamine units, was described in 2005 and reported the formation of metal-organic frameworks (MOFs) from N,N,N′,N′-tetrakis(4-carboxyphenyl)-1,4-phenylenediamine along with their nitrogen and hydrogen absorption properties.[63] Since this work, several other examples of MOFs incorporating triarylamine units have been reported in the literature.[64,65,66] For instance, the

[59] Shirota, Y. et al. Photo- and electroactive amorphous molecular materials—molecular design, syntheses, reactions, properties, and applications. J. Mater. Chem. **15,** 75–93 (2005).
[60] Song, Y. et al. A cyclic triphenylamine dimer for organic field-effect transistors with high performance. J. Am. Chem. Soc. 128, 15940-15941 (2006).
[61] Ning, Z. et al. Triarylamine: a promising core unit for efficient photovoltaic materials. Chem. Commun. **414,** 5483 (2009).
[62] Thelakkat, M. Star-shaped, dendrimeric and polymeric triarylamines as photoconductors and hole transport materials for electro-optical applications. Macromolecular Materials and Engineering **287,** 442–461 (2002).
[63] Sun, D. et al. Temperature-dependent supramolecular stereoisomerism in porous copper coordination networks based on a designed carboxylate ligand. Chem. Commun. **36,** 5447 (2005).
[64] Venkateswarulu, M., Pramanik, A. & Koner, R. R. Novel metal-organic framework with tunable fluorescence property: supramolecular signaling platform for polynitrophenolics. Dalt. Trans **44,** 6348–6352 (2015).
[65] Hua, C., Baldansuren, A., Tuna, F., Collison, D. & D'Alessandro, D. M. In Situ Spectroelectrochemical Investigations of the Redox-Active Tris[4-(pyridin-4-yl)phenyl]amine Ligand and a Zn(2+) Coordination Framework. Inorg Chem **55,** 7270–7280 (2016).
[66] Wu, P. et al. Photoactive chiral metal-organic frameworks for light-driven asymmetric alpha-alkylation of aldehydes. J Am Chem Soc **134,** 14991–14999 (2012).

groups of He and Duan[66] synthesized MOFs from 4,4',4''-tricarboxyltriphenylamine and $Zn(NO_3)_3 \cdot 6H_2O$ in the presence of a chiral pyrrolidine-2-ylimidazole derivative (**Figure 12B**).

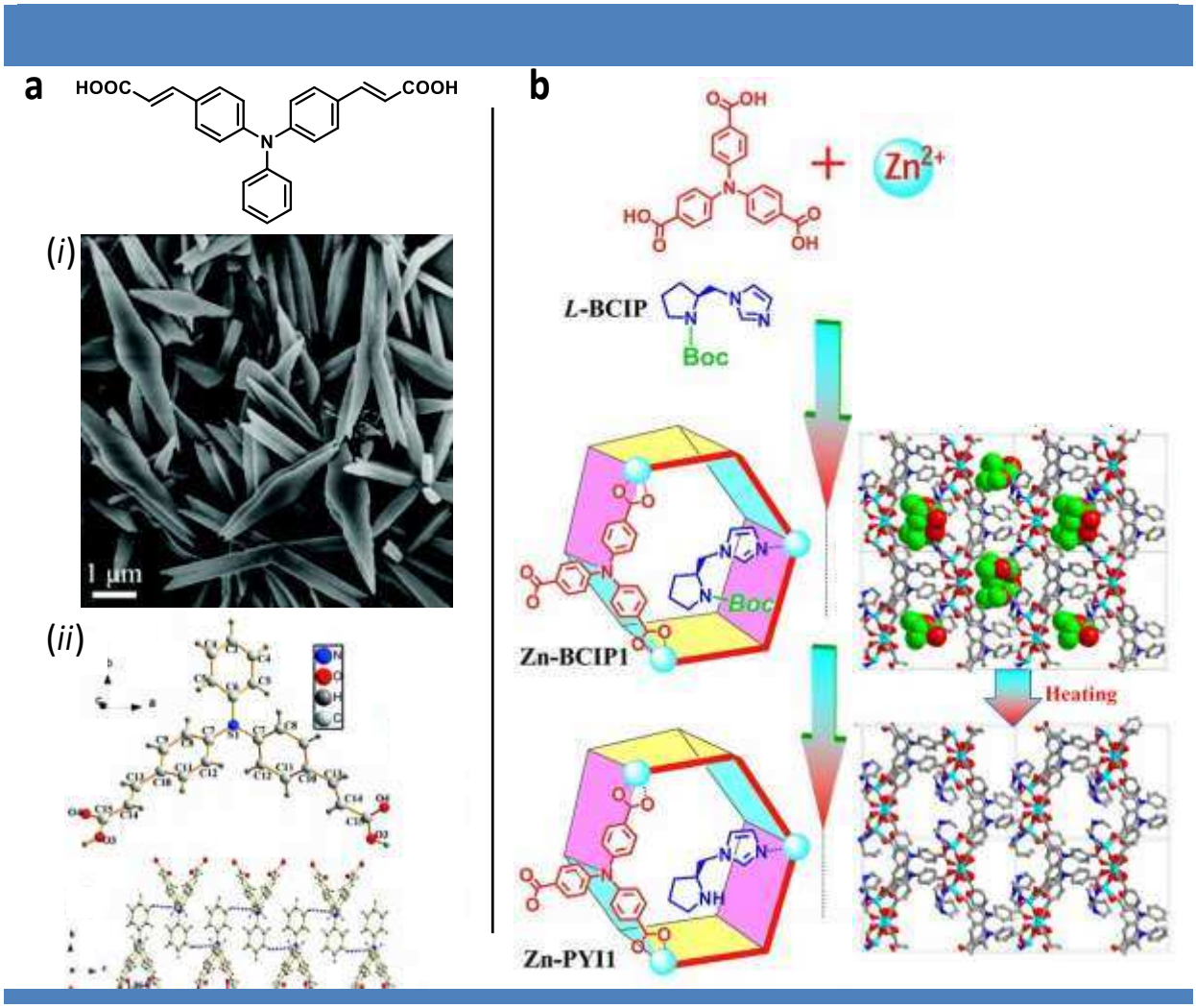

Figure 12 | (a). Chemical structure of A–π–D–π–A type triphenylamine carboxylic acid and its (i) morphologies prepared from THF – H_2O; (ii) Crystal structure and intermolecular interactions with the atom numbering scheme and the two-dimensional architecture was connected by O–H…O(red) hydrogen bonds and C–H…C weak interactions at a distance of 2.865 Å. (b). Schematic representation of the molecular structures (left) of Zn−BCIP1 and deprotected forms Zn−PYI1, showing the photosensitizer, 4,4′,4″-Nitrilotribenzoic Acid (Red or Simply Drawn as Block Red Bars), and the chiral organocatalytic moiety, L-or D-Proline derivatives (Blue) together with crystal structure (right) of the multifunctional framework Zn− BCIP1 showing the packing pattern of these layers (top) and the simulated structure of Zn−PYI1 obtained by thermolytic expulsion of the Boc moieties (bottom), showing the enlargement of the porous MOFs within the channels. The cyan, red, blue, gray, and green balls represent the Zn, O, N, and C atoms and Boc moiety, respectively. Adapted from references [66,67]

Using a combination of spectroscopic analyses and cyclic voltammetry, the authors demonstrated that the MOFs are chiral and electroactive due to the presence of chiral pyrrolidine units and triarylamine moieties, respectively. Ultimately, these MOFs, which have

[67] Kong, L. et al. Effect of solvent, pH and metal ions on the self-assembly process and optical properties of an A–π–D–π–A type triphenylamine carboxylic acid derivative. J. Mater. Chem. C **4,** 2990–3001 (2016).

the capacity to capture small molecules as shown by IR and ^{1}H NMR experiments, were used for the efficient photocatalytic α-alkylation of aliphatic aldehydes with good conversion and significant stereoselectivity. While the triarylamine unit was used as a photoredox station to generate an active radical intermediate necessary for the reaction, the pyrrolidine unit behaved as organocatalyst to produce the enamine necessary to combine with the radical intermediate. This example demonstrates how triarylamine molecules can play a dual role of structuring units and electroactive moieties in supramolecular architectures.

In the absence of metal ions, some triarylamine molecules were also found to self-assemble in various defined architectures such as ropes,[68] nanowires[69] and rhombic-like structures[67] with properties inherent to the triarylamine unit (two-photon absorption, conductivity for example). For instance, Kong and coworkers reported how a triarylamine derivative can be influenced by solvent, pH and metal ions to yield self-assembled nanostructures with different morphologies ranging from fibrillar structures to spherical nanoaggregates (**Figure 12A**).[67] For instance, in a mixture of water and THF, the molecule depicted in **Figure 12A** was found to yield rhombic-type structures (**Figure 12A**(i)) and could be switched upon increasing the pH of the solution into micrometer-long fibers (**Figure 12A**(ii)). Such behavior results from a complex interplay of non-covalent interactions such as for instance, weaker hydrogen-bonding but increased π-π interactions under basic conditions compared to acidic conditions which greatly favor hydrogen-bonding interactions between carboxylic acid residues. Overall, this example demonstrates how chemical functionalities present on the triarylamine scaffold can drive their self-assembly into well-defined supramolecular architectures. In the next sections, we will demonstrate how the triarylamine core itself can drive the formation of supramolecular polymers.

2. Light-triggered triarylamine supramolecular polymers

In 2010, thanks to a combination of physico-chemical and microscopy analyses, our group demonstrated that well-designed triarylamine molecules can self-assemble into fibrillar supramolecular polymers upon light irradiation (Figure 14).[58] As displayed in **Figure 13A**(i), a mono-amide triarylamine tailored with two octyl ether chains on the phenyl moieties, which was synthesized by a modified one-step Ullmann coupling reaction as key step, displays all the expected set of ^{1}H NMR signals after purification by column chromatography. Upon

[68] Lu, C. C. & Su, S. K. Gelation of a highly fluorescent urea-containing triarylamine derivative:N,N,N ′,N ′-tetrakis (p-octadecylureido-phenyl)-p-phenylenediamine in organic solvents. Supramol. Chem. **21,** 547–554 (2009).

[69] Han, J.-M. et al. γ radiation induced self-assembly of fluorescent molecules into nanofibers: a stimuli-responsive sensing. J. Mater. Chem. C **3,** 4345–4351 (2015).

exposure to light in chlorinated solvents, the solution of this molecule changed from yellow to green and the ^{1}H NMR signals corresponding to the aromatic, aliphatic ether and acetamide protons (**Figure 13A**(ii)) disappeared, which could be recovered after heating the solution for 12 hours at 60°C (**Figure 13A(iii)**).

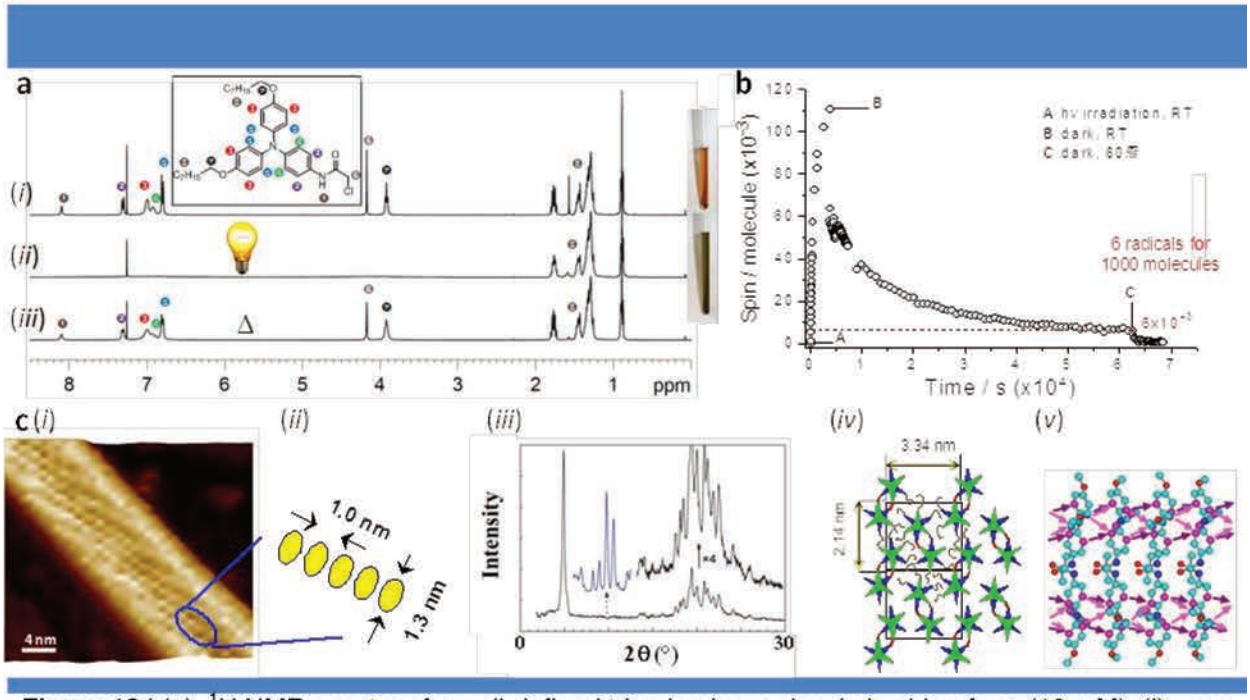

Figure 13 | (a). ^{1}H NMR spectra of a well-defined triarylamine molecule in chloroform (10 mM): (i) upon dissolution in chloroform; (ii) after exposure to visible light; and (iii) after heating overnight at 60 °C. (b). Quantitative EPR data, as a function of time, showing the evolution of the ratio of the triarylammonium radical over neutral: without visible light excitation at RT (point A); upon visible light excitation (A–B); in the absence of light at RT (B–C); and after subsequent heating (60 °C) in the dark (from C; initial concentration = 10 mm). Dotted line: y-axis value of 6×10^{-3}. (c). TAA fibrils in chloroform after 1 h exposition to white light. (i-ii) AFM height image (dry phase) of maize-like structures formed in 1mM solution of TAA1 in chloroform. (iii) The original XRD pattern from 10 mM TAA1 sample (bottom, black) accompanied by its magnification in the WAXS range (top, black) and in the SAXS range (top, blue) registered on the high-flux line. (iv) The proposed internal molecular organization of TAA1 fibrils (in the plane normal to the c-axis) based on the XRD: the lattice cells are shown by rectangles; each crystalline cell consists of 8 molecules and includes two layers (TAA molecules belonging to different layers are shown with green and blue colors, respectively). Amide bonds are shown with red segments, and alkyl side chains with brown curly lines. (v) The simulated all-atomic structure of snowflake double column: the conducting pathways formed between nearest-neighboring carbons (marked with violet color) of adjacent TAA molecules (R_{CC}=0.36-0.37 nm) are marked with violet arrows (hydrogens are not shown). Adapted from references [58,70]

UV-vis-NIR and EPR experiments were then used to understand this phenomenon. While UV-vis-NIR data suggested the formation of radical triarylammonium cations (increased absorbance at 786 nm) upon irradiation for one hour with white light (20 W), EPR studies revealed that the number of radicals increased up to 11% compared to the total number of molecules under the same experimental conditions (**Figure 13B**, from A to B).

[70] Nyrkova, I. et al. Supramolecular Self-Assembly and Radical Kinetics in Conducting Self-Replicating Nanowires. ACS Nano **8,** 10111–10124 (2014).

Moreover, this proportion of radicals was shown to decay smoothly in the dark reaching a stable level of 0.6 % after 16 hours (**Figure 13B**, from B to C), which could be further quenched by heating to 60 °C. Thanks to AFM microscopy, the increased stabilization of these light-triggered radicals localized on the nitrogen atom of triarylamine molecules was attributed to the formation of corn-like structures made of 1D columnar aggregates, with a diameter of 1.3 nm, corresponding to the diameter of a single molecule and a distance between bright spots on the AFM image estimated to 1.0 nm, which could actually correspond to the distance between two non-consecutive molecules pointing in the same direction (**Figure 13C**(i-ii)).

Further X-ray diffraction suggested that the 1D columnar aggregates are arranged according to a monoclinic cell containing 8 molecules (**Figure 13C**(iii-iv)). Within a unit cell, the 8 molecules are organized in "snowflake" dimers in the direction of the columns (**Figure 13C**(iv), one green-colored molecule on top of a blue-colored one) and with 4 molecules hold together by intramolecular hydrogen bonds (**Figure 13C**(iv), red-colored bonds) to fill up the rectangular sublattice perpendicular to the direction of the growing columns. Structural parameters extracted from XRD data are in agreement with the double-columnar arrangement initially suggested by simulation experiments. They also support a dense packing of the molecules within the columns which contributes to the excellent conducting properties of these organic supramolecular polymers (see next section of this chapter) (**Figure 13C**(v)).

Combining UV-vis-NIR and ^{1}H NMR experiments with a theoretical approach allowed us to subsequently elucidate the light-induced self-assembly mechanism of these chemically-designed triarylamine molecules (**Figure 14**).[70] First, the neutral pyramidal triarylamine molecule is excited with light and further reacts with chloroform to generate a stable complex made of a flatten triarylamine radical cation and a chloride anion thanks to electrical dipole interaction (**Figure 14B**). These charge-transfer dipoles further aggregates into supramolecular stacks (**Figure 14C-E**), which can arrange either in a loose chain with chloride anion intercalated between TAA molecules (**Figure 14F**) or in a tight chain, with TAA molecules interacting with each other at a shorter distance of 5 Å and chloride ions put aside (**Figure 14H**). Due to increased π-stacking and van-der-Waals interactions, this tight chain proved to be more energetically favored but, the energy penalty needed to reorganize the chloride ions in this latter state suggests that such transformation from a loose to a tight one can only be achieved for aggregates longer than trimers. Long aggregates of charge-transfer dipoles then preferentially arrange into double columns thanks to lateral hydrogen bonding interactions, thus forming a stable critical nucleus made of six TAA

molecules (**Figure 14I**).

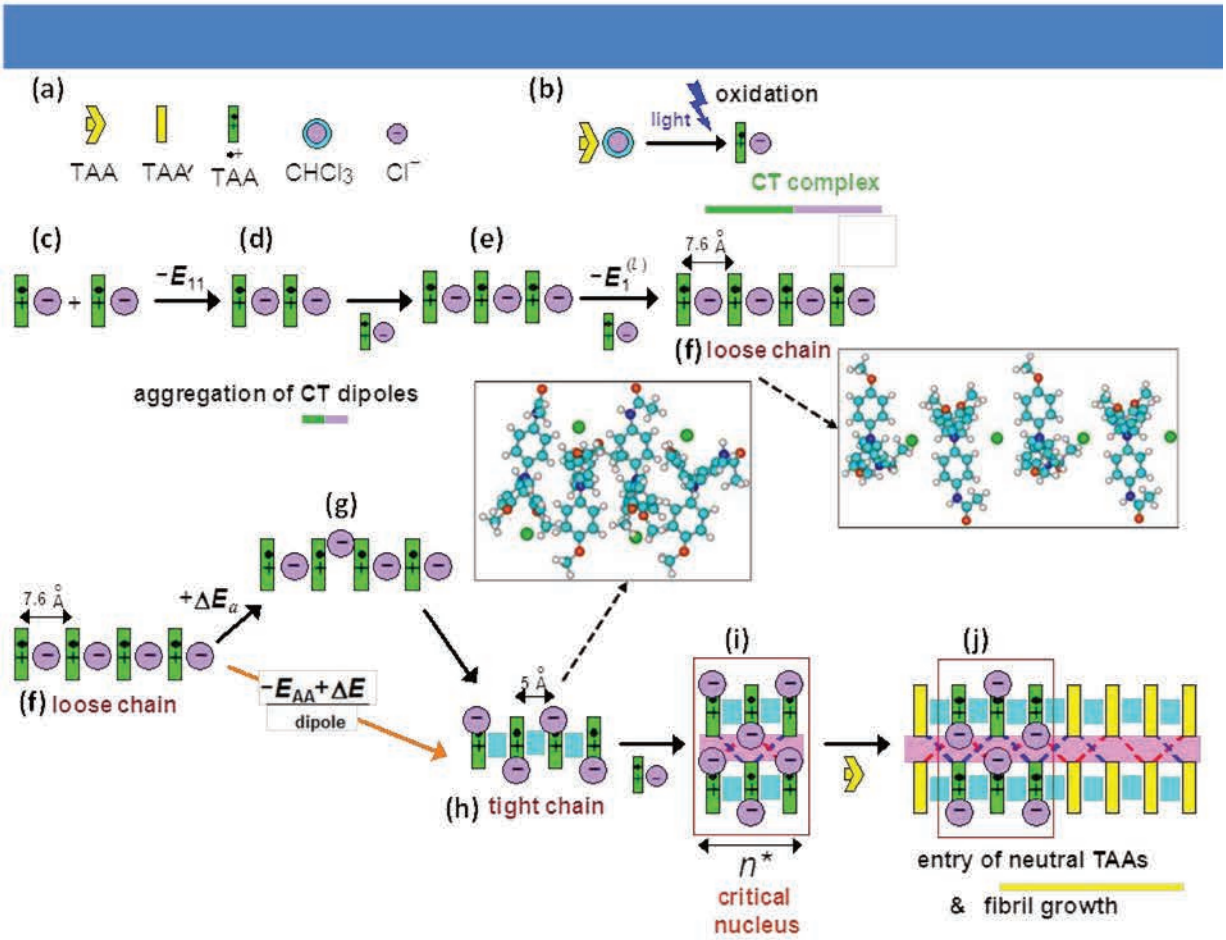

Figure 14 | Light-induced aggregation kinetics in **TAA** solutions. (a) Ion explanation. (b) Light induces oxidation of a neutral TAA molecule producing **TAA**$^{\bullet+}$ radical and Cl^- anion. (c, d) Two free radicals **TAA**$^{\bullet+}$ complexed with the Cl^- counterions attract each other head-to-tail. (e, f) A growing stack of radical dipoles. (f, g, h) Tightening of the stack: chloride ions move sideways (g); aromatic rings of **TAA** molecules benefit from closer contacts, while chloride anions are finally accommodated in the gaps between ether tails of **TAA** molecules (h). (i) Formation of double-columnar nuclei stabilized by H-bonds between the columns. (j) Growth of the structure by attachment of neutral **TAA** molecules. Adapted from reference 70.

Once the nucleation step is completed, neutral triarylamine molecules subsequently pile at the end of the nucleus by π-π and hydrogen bonding interactions, without the need of additional oxidation, thus forming double-columnar fibrillar structures made of "snowflake" packing of TAA molecules (**Figure 14J**).

Our group further demonstrates that this self-assembly mechanism can be used to explain the different light-induced morphologies observed for various mono-amide triarylamines decorated with side chains such as terpyridine,[71] gallic acid residues,[72]

[71] Moulin, E. et al. Light-triggered self-assembly of triarylamine-based nanospheres. Nanoscale **4,** 6748–6751 (2012).

[72] Domoto, Y., Busseron, E., Maaloum, M., Moulin, E. & Giuseppone, N. Control over Nanostructures and Associated Mesomorphic Properties of Doped Self-Assembled Triarylamine Liquid Crystals. Chem. - A Eur. J. **21,** 1938–1948 (2015).

fullerene,[73] benzyl trisamide[74] or even rotaxane units.[75]

3. Applications of light-triggered triarylamine-based supramolecular polymers

Considering the importance of triarylamine molecules in the development of organic electronics and based on molecular modelling suggesting that the dense packing of the TAAs in the self-assembled structure might lead to interesting conducting properties, we examined the electrical conductivity of our supramolecular TAA polymers using a simple device made of two lateral metallic electrodes separated by a distance of 80 ± 20 nm (**Figure 15A**).

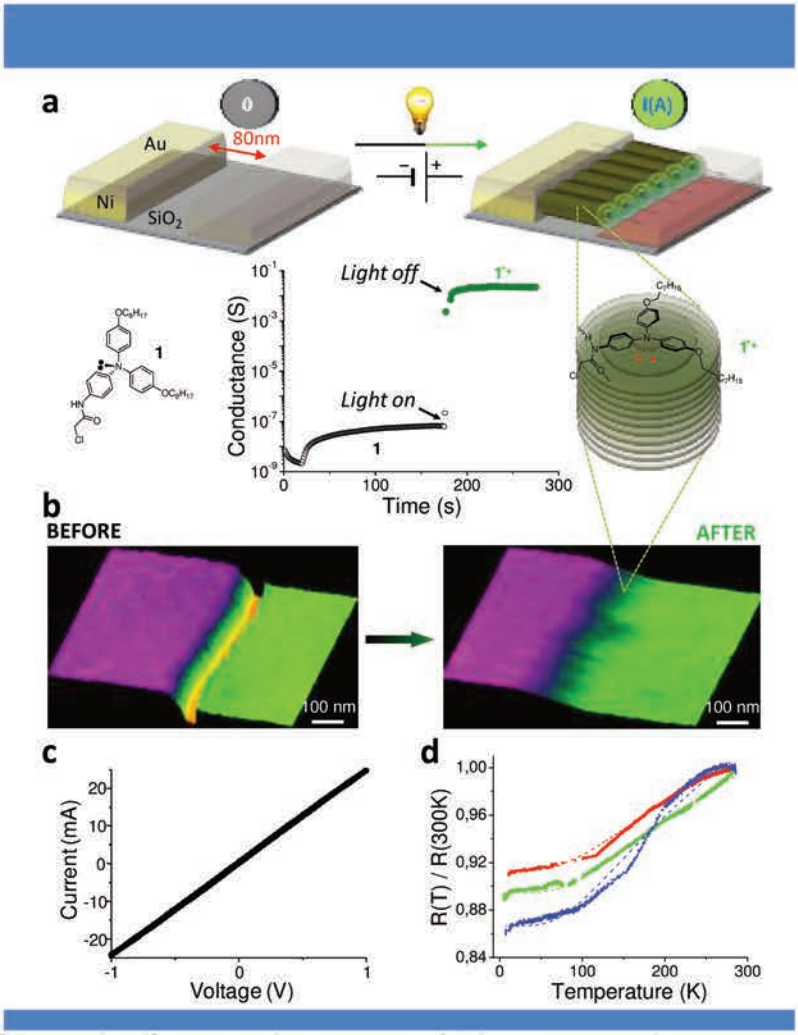

Figure 15 | (a). Triggered self-construction process of **1** in a nanotrench geometry (trench width,100 µm; length, 0.08 µm; ΔV = 0.3 – 0.8 V). Conductance measured for the nanotrench device as a function of time in the dark and then (after 180 s) submitted to white light irradiation (power density, ~10 W.cm^{-2} over 10 s). (b). Left: topography of the opened gap seen by AFM before light irradiation. Right: topography of the closed gap filled with nanowires made of **1** after light irradiation. (c). I/V

[73] Busseron, E. et al. Light-Controlled Morphologies of Self-Assembled Triarylamine-Fullerene Conjugates. ACS Nano 2760–2772 (2015).
[74] Moulin, É. et al. Self-assembly of benzene-tris(bis(p-benzyloxy)triphenylamine)carboxamide. Comptes Rendus Chim. **19,** 117–122 (2016).
[75] Wolf, A. et al. pH and light-controlled self-assembly of bistable [c2] daisy chain rotaxanes. Chem Commun **51,** 4212–4215 (2015).

measurements of the nanotrench after self-assembly of **1**, upon light irradiation and an initially applied voltage of 0.3 V. (d). Resistance of the nanotrench filled with STANWs as a function of temperature and differential conductance measured at low temperature, in vacuum, using an a.c. bridge technique. Adapted from reference [76].

In a typical experiment, the device was set with an electrical current and then, a solution of the triarylamine monoamide in tetrachloroethane was dropped onto the device. Upon light irradiation, the conductivity dramatically increased by 6 orders of magnitude, reaching a value exciding 5 x 10^3 $S.m^{-1}$. Importantly, even when the light was turned off, the conductance remained at the same level. Additional experiments demonstrated that both light irradiation and presence of the electric field are prerequisites to reach highly conducting devices. Furthermore, AFM imaging of these devices before and after light irradiation clearly indicated that the gap was filled by homogeneous nanowires oriented in the direction of the electric field (**Figure 15B**). Considering our different studies on the self-assembled TAA nanowires,[60,70] we believe that the measured high density of hole carriers and the delocalization of the radicals through the stacks might be the explanation for the exceptional conductivity. Such conductivities were independently confirmed by theoretical calculations which suggest that a hole mobility as high as 12 $cm^2.V^{-1}.s^{-1}$ can be achieved using these supramolecular nanowires.[77,78]

Additional I-V measurements at room temperature (**Figure 15C**) and for temperature down to 1.5 K (**Figure 15D**) suggested respectively an ohmic behavior both at atmospheric pressure and under vacuum as well as a metallic character, which is a characteristic that had never been observed before in purely organic supramolecular polymers. To the best of our knowledge, only ballistic carbon nanotubes display better characteristics than our triarylamine nanowires, probably because of a number of ordering defects within the hierarchical bundles of stacked fibrils. Overall, this work represents a first remarkable achievement in order to address precisely supramolecular structures (here, triarylamine nanowires) as organic interconnects in pre-determined positions thanks to the presence of an electrical field. It also opens door to precisely control the formation of nanoscale circuits using a "bottom-up" approach.

Recently, in collaboration with the group of Barboiu, we took advantage of the light-induced in situ self-construction of TAA mono-amide architectures to build functional

[76] Faramarzi, V. et al. Light-triggered self-construction of supramolecular organic nanowires as metallic interconnects. Nat Chem **4,** 485–490 (2012).

[77] Akande, A., Bhattacharya, S., Cathcart, T. & Sanvito, S. First principles study of the structural, electronic, and transport properties of triarylamine-based nanowires. J Chem Phys **140,** 74301 (2014).

[78] Bhattacharya, S., Akande, A. & Sanvito, S. Spin transport properties of triarylamine-based nanowires. Chem Commun **50,** 6626–6629 (2014).

conducting devices with potential applications as bioelectrodes (**Figure 16**).[79] We first synthesized a mesoporous silica-coated gold electrode with hydrophobic pores in two steps (electrochemical formation of a porous silica layer on the electrode and chemical modification of the pores, **Figure 16B**, steps 1 and 2). In a third step, the electrode was immersed in the triarylamine mono-amide solution in chloroform and further white light irradiation triggered their self-assembly within the mesopores, as it was observed by AFM imaging of the device before and after immersion and light irradiation (**Figure 16C-D**).

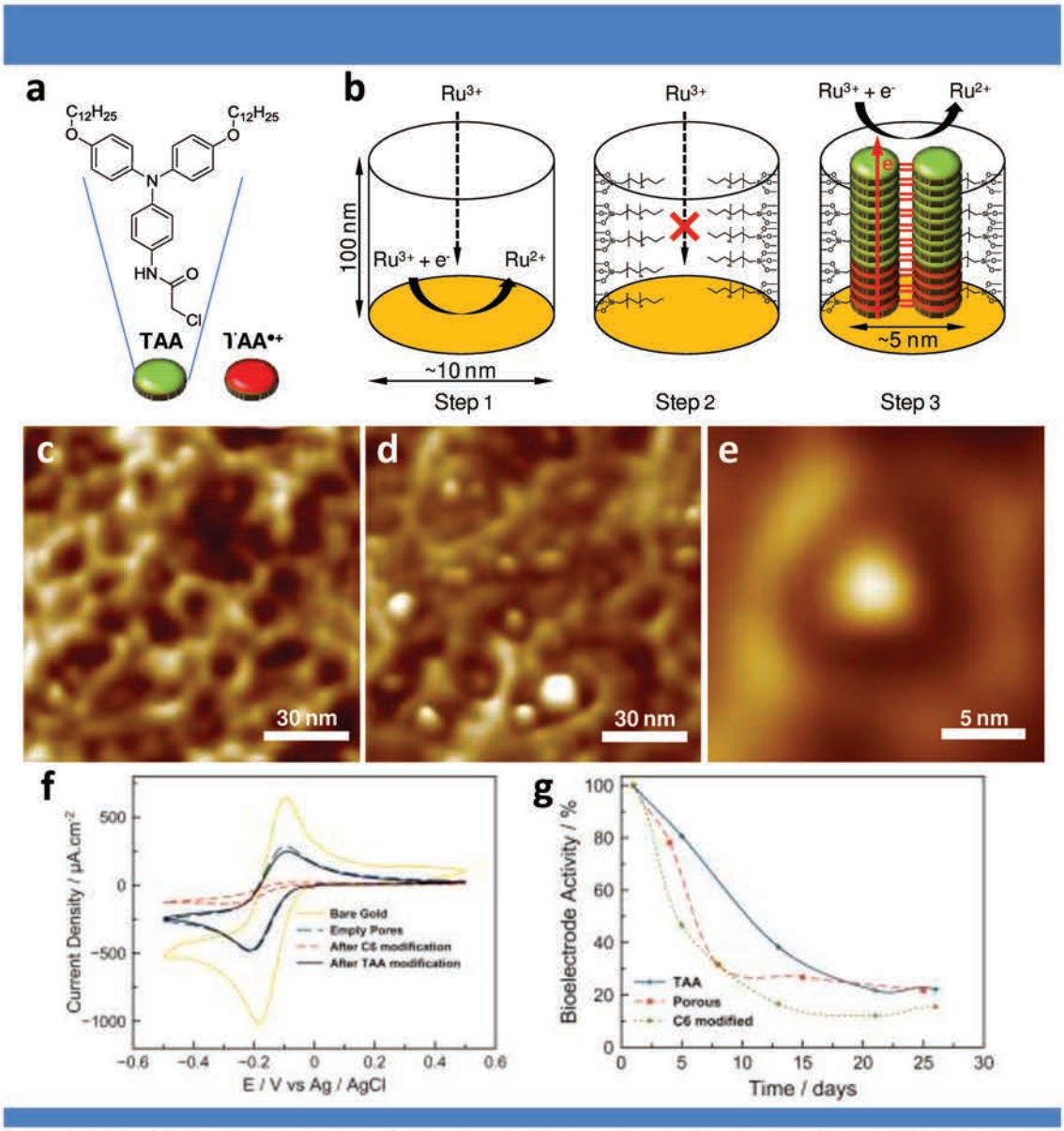

Figure 16 | (a). Molecular structure of the triarylamine mono-amide molecule used in this study. (b). Fabrication of the functional electrodes. It is shown in that each step of the fabrication process (empty pores (1), pores blocked with hydrophobic alkyl chains (2), and TAA doped nanopores (3)) should lead to a specific electrochemical behavior when using a Ru^{3+}/ Ru^{2+} redox probe. (c-d). Typical AFM topography images of the empty mesoporous silica layer (c), and of the corresponding **C12-TAA** doped layer showing several tips of fibrils within nanopores (d). (e). High resolution AFM image of single pore

[79] Licsandru, E.-D. et al. Self-assembly of supramolecular triarylamine nanowires in mesoporous silica and biocompatible electrodes thereof. Nanoscale **8,** 5605–5611 (2016).

after the silica layer was filled with a single self-assembled fibril of **TAA**, in agreement with the size of their section. (f). Cyclic voltammetry curves of $Ru(NH_3)_6^{3+}$ (c = 1 mM , *v* =20 $mV.s^{-1}$ ^{1}, in a 0.1 M aqueous solution of $NaNO_3$) at bare gold electrode (yellow), after mesoporous silica thin film electrodes were prepared by electrogeneration (dashed blue), after hydrophobic modification (dashed red), and after doping with **C12-TAA** (black). (g). Normalized activity evolution of the same biocathodes as a function of time. Adapted from reference 79.

High resolution AFM imaging of a single pore indicated that the diameter of the nanostructures confined inside is less than 5 nm (**Figure 16E**), which is in agreement with the formation of double-columnar structures, as expected for triarylamines mono-amide (see previous section). To further determine the electrical properties of our devices at each step of the fabrication process, we performed cyclic voltammetry experiments using $Ru(NH_3)_6^{3+}$ as a redox probe (**Figure 16F**). When the electrode is covered by a layer of mesoporous silica, its cyclic voltammogram (CV) displays clear oxidation and reduction peaks at potentials identical to the gold electrode, suggesting that the redox probe can access the surface of the electrode by diffusion through the pores. However, after modification of the pores with C_6-alkyl chains, the electrochemical signal becomes very weak, thus indicating that the redox probe cannot access the gold electrode. Finally, in the presence of triarylamine nanowires embedded in the mesopores, the intensity of the redox signals is recovered to the value recorded before hydrophobic modification of the pores. As the hydrophobicity of the device is not modified after immersion in the triarylamine solution, this last experiment suggests that the electron transfer process from the redox probe to the gold electrode occurs mainly through the confinely ordered conductive nanowires.

Finally, inspired by biofuel cells which are able to transfer chemical energy into electrical energy, we evaluate the ability of our hybrid electrodes to drive the electrocatalytic reduction of oxygen using an enzyme (namely a mixture of laccase and a redox mediator (ABTS)) immobilized on their surface (**Figure 16G**). While a biocatalytic activity was recorded for all electrodes, obtained after each fabrication step, the hybrid one displayed an increased stability compared to the others during the first 10 days. Such increased stability was ascribed to the slower release of ABTS as a result of π-π and charge interactions between the mediator and the triarylammonium radical cations. Overall, this work demonstrates the possibility to build functional devices from well-defined supramolecular polymers in a confined environment, widening the possible applications of light-triggered triarylamine supramolecular polymers.

4. Supramolecular polymers based on triarylamines trisamide

In parallel to these various studies on triarylamines mono-amide, we also examined the self-assembling properties of C_3-symmetric triarylamines trisamide (**TATA**), which can be readily synthesized in three steps (aromatic electrophilic substitution, reduction, amidation) from commercially available compounds (**Figure 17a**).[80]

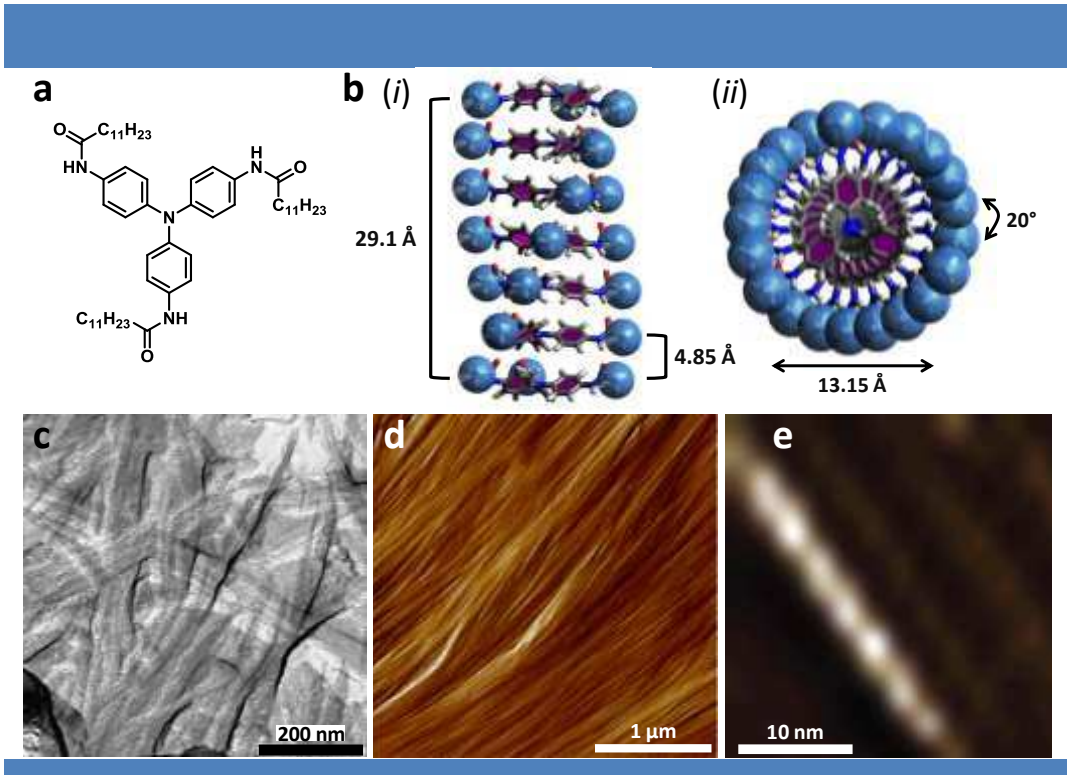

Figure 17 | (a). Chemical formula of **TATA**. (b). Side view (i) and top view (ii) of the proposed stacking structure of **TATA**, as obtained from DFT calculations, and with a longitudinal periodicity of 29.1 Å, a nitrogen−nitrogen. (c). Freeze-fracture TEM image of this **TATA** derivative showing its native form in chloroform. (d, e). AFM imaging of **TATA** at the micrometer scale (d) and at the nanometer scale for a single fiber (e) obtained from a chloroform solution drop cast on mica. Adapted from reference 80.

Due to the presence of three lateral hydrogen bonds, this compound was found to produce micrometer-long mono-columnar helical aggregates in a large variety of solvents and even in the absence of light, as imaged by TEM and AFM (**Figure 17c-e**). This single-columnar helical arrangement was confirmed by a combination of experimental small angle and wide angle X-ray scattering experiments and simulation from density functional theory (DFT), which suggests that the supramolecular structure has a) a width of 13.15 Å corresponding to the diameter of a single molecule, b) a periodicity of 29.1 Å corresponding to the stacking of seven propeller triarylamines, as also observed by AFM, and that c) consecutive triarylamines within this periodical stack are arranged with a 4.85 Å

[80] Armao, J. J. et al. Healable Supramolecular Polymers as Organic Metals. J. Am. Chem. Soc. **136,** 11382–11388 (2014).

nitrogen-nitrogen distance and a 20º dihedral angle between them (**Figure 17b**). Although this compound was found to produce supramolecular structures in the absence of light, we were interested in studying its behavior upon light irradiation in order to determine if innovative properties might emerge from the doped structures. UV-vis-NIR spectra upon light irradiation display the characteristic absorbance at around 800 nm (related to the presence of triarylammonium radical cations located on the nitrogen center) and 400 nm (related to the formation of a self-assembled structure) as already observed for the triarylamine mono-amide compounds (**Figure 18a-b**).

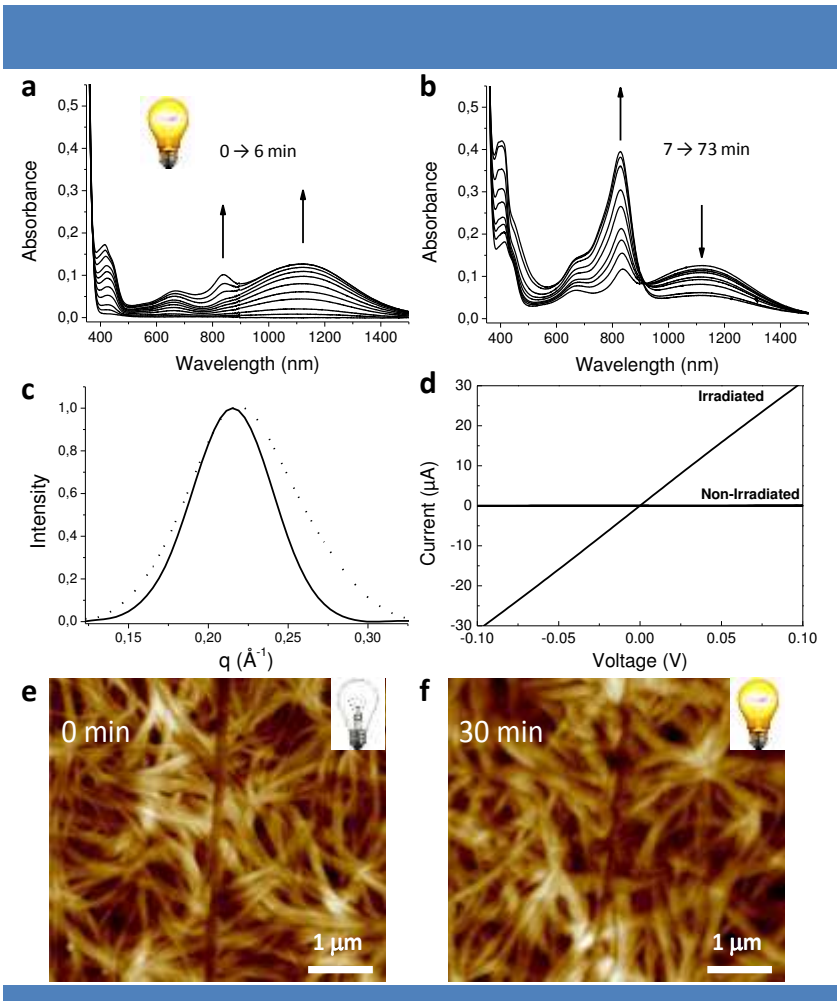

Figure 18 | Effect of light irradiation on TATA self-assemblies. (a, b). Sequential absorbance spectra taken during light irradiation (with a halogen lamp; 10 W.cm^{-2}) of a 0.1 mM solution of **TATA** in $CHCl_3$; (a) first 6 min of light irradiation, (b) from 7 to 73 min of light irradiation. (c). SAXS of nonirradiated (dotted line) and irradiated (full line) thin films demonstrating a 49% increase in the correlation length (calculated as 4π/fwhm). d. I−V curves before and after light-induced fibers formation of **TATA** in a mixed solvent system of 5:3 methanol:toluene +5 vol % tetrachloroethane. (e, f). Effect of light on the self-healing of TATA gel as imaged by AFM. AFM height images of **TATA** obtained from chloroform samples (20 mg/mL) drop cast on mica. Irradiation times under vapors of chloroform (with a halogen lamp; 10 W.cm^{-2}) vary from 0 minutes (e) to 30 minutes (f). Adapted from reference 80.

Additionally, we noticed the presence of a new absorbance band in the NIR at 1100 nm for short irradiation times, which then slightly decayed upon subsequent irradiation. This new

band was found to correspond to the presence of an intermolecular through-space charge transfer between the stacked triarylamine molecules.[81] The fact that the 1100 nm band decays for long irradiation times while the 800 nm band keeps on increasing suggests that radical cations are first quite delocalized within the self-assembled structure and then become more localized on triarylamines with increasing light doping. This explanation is also supported by EPR experiments which show a clear evolution of the nature of the charge transfer with irradiation and the presence of up to 44% of TAA radical cations after more than 70 minutes' irradiation. Interestingly, light irradiation was found to improve the ordering of the fibers, as indicated for instance by a sharpening of the 100 scattering peak observed by SAXS (**Figure 18c**). This improvement of the structure upon light irradiation was confirmed by analyzing several irradiated samples by AFM and further corroborated by the "self-healing" behavior of damaged gels lightened for ~30 minutes in an atmosphere of chloroform (**Figure 18e-f**). Using a series of advanced EPR and UV-vis-NIR experiments, we further demonstrated that the doped fibers displayed charge-transport properties similar to the ones encountered in metallic conjugated covalent polymers. Finally, we probed the electrical properties of the fibers before and after oxidation by light or electrochemically. In both cases, we found that, while single molecules have no electrical properties, undoped supramolecular fibers display a semi-conducting behavior which can be switched to a purely ohmic behavior after oxidation (**Figure 18d**). This work demonstrates how supramolecular polymers can enhance their physical properties due to the inherent dynamics of their non-covalent architectures.

Recently, some other groups have studied fundamental aspects related to these triarylamines trisamide molecules such as, for instance, the formation of chiral helical structures from non-chiral TAA precursors induced by either circularly-polarized light[82] or negligible quantity of TAA decorated with chiral side chains.[83] Finally, owing to the presence of metallic electrons in the self-assembled architectures, we further demonstrated that, by adjusting the molecular structure of these triarylamines trisamide, they can be used as plasmonic interconnects between gold nanoclusters to produce optical nanocircuits[84] and even behave by themselves as supramolecular organic plasmonic waveguides.[85]

Overall, we have highlighted the main achievements performed by our group over the

[81] Heckmann, A. & Lambert, C. Organic Mixed-Valence Compounds: A Playground for Electrons and Holes. Angew. Chemie Int. Ed. **51,** 326–392 (2012).
[82] Kim, J. et al. Induction and control of supramolecular chirality by light in self-assembled helical nanostructures. Nat Commun **6,** 6959 (2015).
[83] Kim, T., Mori, T., Aida, T. & Miyajima, D. Dynamic propeller conformation for the unprecedentedly high degree of chiral amplification of supramolecular helices. Chem. Sci.**7**,6689-6694 (2016).
[84] Armao, J. J. et al. Supramolecular Organic Nanowires as Plasmonic Interconnects. ACS Nano **10,** 2082–2090 (2016).
[85] Haedler, A. T. et al. Long-range energy transport in single supramolecular nanofibres at room temperature. Nature **523,** 196–199 (2015).

last 6 years in the field of triarylamine-based supramolecular polymers, which range from fundamental studies on the self-assembly mechanism to applications mostly related to electronics and plasmonic.

Chapter 3: Supramolecular polymers based on nucleobase pairs

We have seen in the previous chapters that a combination of non-covalent interactions is usually required to reach self-assembled architectures with a controlled morphology. In particular, in the first chapter, we have highlighted the importance of hydrogen bonding arrays to yield recognition motifs with high association constants. Such developments have been indeed inspired by the recognition properties of nucleobases, which are of crucial importance for various biological processes such as RNA/DNA recognition, transcription and so on. In this chapter, we would like to demonstrate how these recognition properties can be used in artificial self-assembling processes to yield well-defined supramolecular polymers. After a general introduction on base pairing, we will show how guanine residues can be used to trigger the self-assembly of discrete molecules and then extend the discussion to other nucleobases.

1. Generalities on nucleobase pairs

Nowadays, it is well understood that the stability of the DNA double helix results from a combination of intermolecular non-covalent interactions (hydrogen bonds, π-π stacking and hydrophobic effects) between four complementary nucleobase pairs: guanine (G) and cytosine (C) on one hand and, thymine (T) and adenine (A) on the other (uracil (U) instead of T in RNA). In DNA, these four nucleobases arrange in a heterocomplementary manner according to the Watson-Crick base-pairing (**Figure 19**). However, owing to the presence of several hydrogen bonding donor (such as N-H) or acceptor (such as C=O) groups on the different faces of the nucleobases, they can form up to 28 dimeric structures involving at least two hydrogen bonding interactions with association constants ranging from ~100 M^{-1} for A-T and up to 10^5 M^{-1} for G-C in chloroform.[86,87] For instance, adenine and thymine residues can arranged in two ways (Watson-Crick or Hoogsteen) involving in both cases two hydrogen bonds, while guanine was found to form stable mismatched Wobble base pairs with thymine by involving two hydrogen bonds of their respective Watson-Crick sides (**Figure 19**). It is noteworthy that all nucleobases can self-recognize by two hydrogen bond interactions to

[86] Sivakova, S. & Rowan, S. J. Nucleobases as supramolecular motifs. Chem. Soc. Rev. **34,** 9–21 (2005).
[87] Sessler, J. L., Lawrence, C. M. & Jayawickramarajah, J. Molecular recognition via base-pairing. Chem. Soc. Rev. **36,** 314–325 (2007).

produce homodimers (A-A, U-U and G-G on **Figure 19**). While A-A display a very weak dimerization constant in chloroform (less than 5 M^{-1}), guanine residues display a high tendency to dimerize with association constants up to 10^4 M^{-1}. The self-complementarity of nucleobases has stimulated the creativity of chemists to create non-natural derivatives inspired by nucleobases and which can self-complementary recognized with increased association constants owing to the higher number of hydrogen bond interactions.[88,89] Furthermore, as all nucleobases display at least two faces accessible for hydrogen-bonding interactions, they can be involved in base-triplets or quadruplets which can be further used to produce supramolecular polymeric arrays.[90]

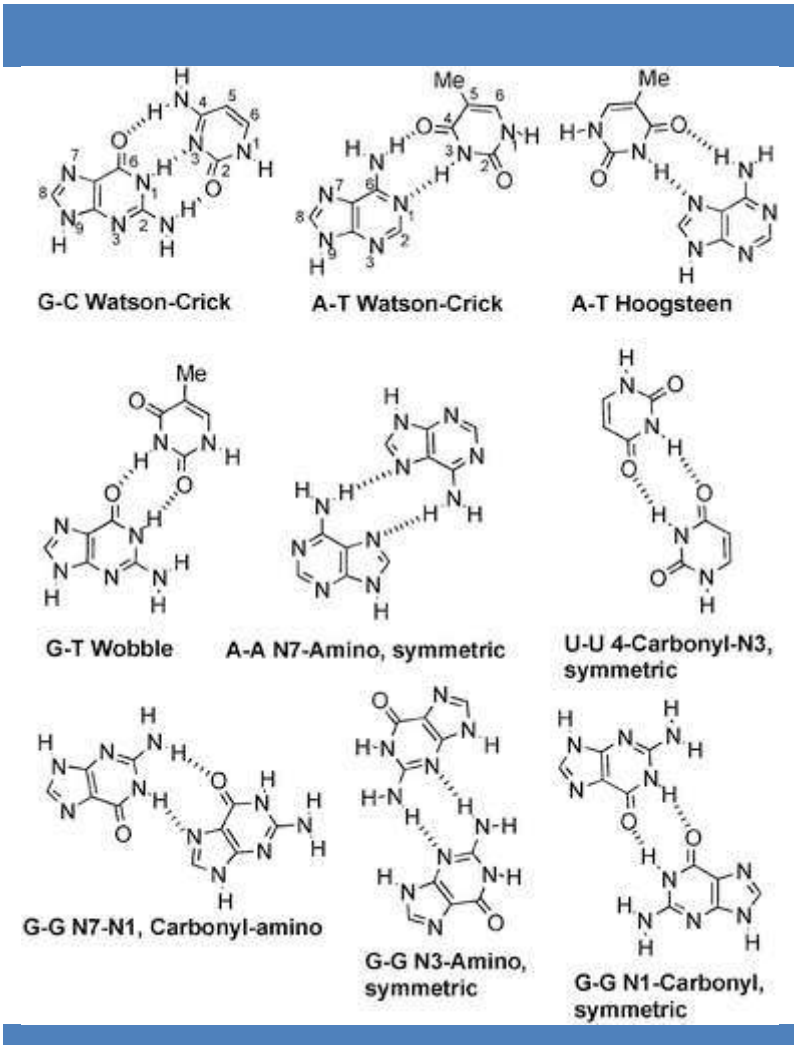

Figure 19 | Illustrations of Watson–Crick, Hoogsteen and wobble base pairs, as well as a series of homodimers assembled through two-point H-bonding interactions. Reproduced from reference 90.

Overall, considering the number of different molecular arrangements accessible by

[88] Beingessner, R. L., Fan, Y. & Fenniri, H. Molecular and supramolecular chemistry of rosette nanotubes. RSC Adv. **6,** 75820–75838 (2016).
[89] Cheng, C.-C. et al. Large-scale production of ureido-cytosine based supramolecular polymers with well-controlled hierarchical nanostructures. RSC Adv. **5,** 76451–76457 (2015).
[90] Fathalla, M., Lawrence, C. M., Zhang, N., Sessler, J. L. & Jayawickramarajah, J. Base-pairing mediated non-covalent polymers. Chem. Soc. Rev. **38,** 1608–1620 (2009).

nucleobases and their derivatives, it is important to be able to properly characterize them. Several spectroscopic techniques such as NMR and IR but also XRD on single crystals or powders have been used to clearly establish the non-covalent interactions involved in the formation of supramolecular polymers. In the following chapters, we will show how their use was crucial to elucidate the structures of supramolecular polymers build from nucleobase derivatives.

2. Supramolecular polymers from guanine and guanosine derivatives

As illustrated on **Figure 19**, guanine offers the possibility to self-recognize due to the presence of three hydrogen bond acceptors A (N and C=O) and three hydrogen bond donor D groups (N-H) on its scaffold.[91,92] For instance, while G-G N1 and G-G N3-Amino homodimers result from the self-complementarity of DA motifs on the Watson-Crick and the minor groove face respectively, G-G N7-N1 homodimer originates from the complementarity of a DD motif on the Hoogsteen face and an AA motif on the Watson-Crick one. Importantly, in these homodimers, some faces remain accessible for further hydrogen bond interactions with other guanine residues thus potentially giving rise to extended polymeric arrays (**Figure 20**). While G-Ribbon I arises only from G-G N7-N1 homodimers, G-Ribbon II originates from a combination of G-G N1 and G-G N3-Amino homodimers and 2D network are obtained via a combination of the three possible dimeric structures (**Figure 20A,C**). Importantly, as described by Gellert and co-workers in 1962,[93] guanine derivatives can also arrange in a tetrameric motif so-called G-quartet via N7-N1 and N2-C=O interactions (**Figure 20B**), which can be further stabilized by metal ions (see the next bibliographical chapter). Considering the poor solubility of guanine in both aqueous and organic solvents, organic chemists have tailored its N9 position with various side chains and further explored its self-assembly in various organic solvents. Hereafter, we have selected three examples which demonstrate that all self-assembled motifs depicted on **Figure 20** are accessible by fine-tuning the structure of guanosine derivatives and/or by adjusting external parameters such as solvent, concentration, etc. which are known to affect non-covalent interactions.

[91] Davis, J. T. & Spada, G. P. Supramolecular architectures generated by self-assembly of guanosine derivatives. Chem. Soc. Rev. **36,** 296–313 (2007).

[92] Lena, S., Masiero, S., Pieraccini, S. & Spada, G. P. Guanosine Hydrogen-Bonded Scaffolds: A New Way to Control the Bottom-Up Realisation of Well-Defined Nanoarchitectures. Chem. - A Eur. J. **15,** 7792–7806 (2009).

[93] Gellert, M., Lipsett, M. N. & Davies, D. R. Helix Formation By Guanylic Acid. Proc. Natl. Acad. Sci. **48,** 2013–2018 (1962).

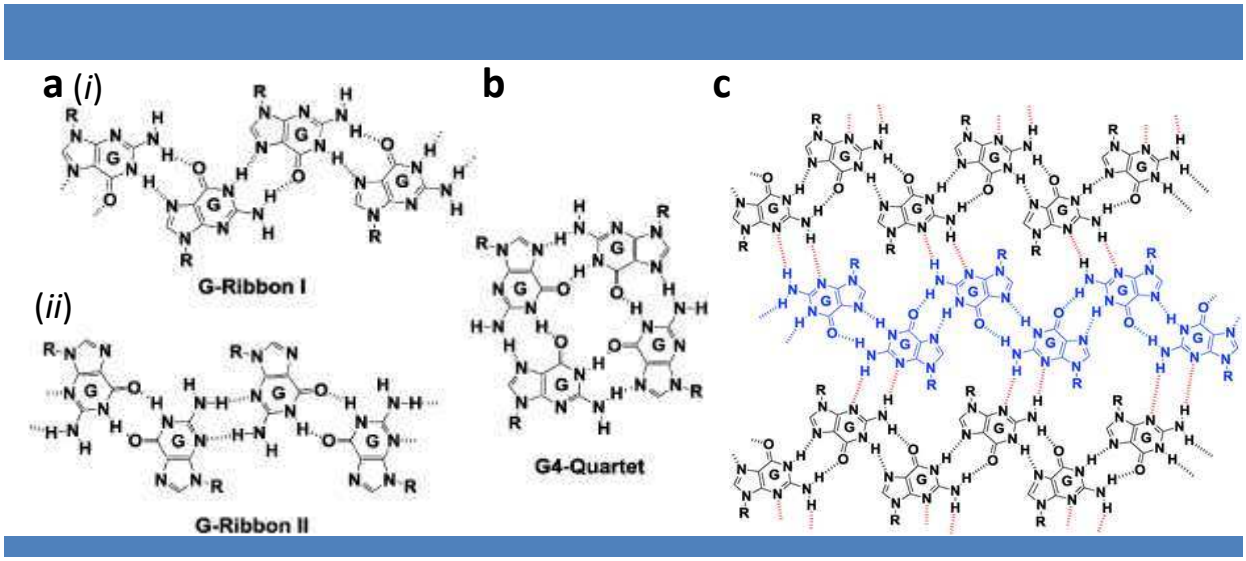

Figure 20 | (a, b). Guanine-containing molecules can form a variety of different self-assembled motifs, including (i) G-ribbon I, (ii) G-ribbon II and (b) the G4-quartet. (c). These ribbons (middle ribbon is blue for differentiation) are stabilized through additional inter-tape hydrogen bonds (shown in red). Reproduced from reference 94.

In the early 2000s, the group of Gottarelli reported that lipophilic guanosine and deoxyguanosine derivatives can give rise to different ribbon-like structures in organic solvents.[95,96,97] Using a series of 1D and 2D NMR experiments, they showed that these molecules self-assemble in chloroform into Ribbon I structures shortly after dissolution, which then evolve towards thermodynamically stable Ribbon II structures. Importantly, in the solid state, X-ray single-crystal diffraction unambiguously demonstrated the presence of a single structure, namely Ribbon I. This kind of structure was also observed at the graphite -1,2,4-trichlorobenzene interface by scanning tunneling microscopy (STM) and in hydrocarbon solvents such as toluene or hexadecane, as demonstrated by IR and XRD experiments. Overall, these studies demonstrated that solvent plays an important role in the self-assembly of guanine derivatives, which can be also affected by the experimental procedures used for the self-organization process. Although most studies on guanine derivatives indicate the formation of ribbon-like structures in the absence of metal ions,[98,99,100] Meng and coworkers reported the synthesis of a guanosine derivative which is able to

[94] Peters, G. M. & Davis, J. T. Supramolecular gels made from nucleobase, nucleoside and nucleotide analogs. Chem Soc Rev **45,** 3188–3206 (2016).

[95] Giorgi, T. et al. Gel‐Like Lyomesophases Formed in Organic Solvents by Self‐Assembled Guanine Ribbons. Chem. Eur. J. **8,** 2143–2152 (2002).

[96] Gottarelli, G. et al. The self-assembly of lipophilic guanosine derivatives in solution and on solid surfaces. Chem. JOURNAL- **6,** 3242–3248 (2000).

[97] Lena, S. et al. Self-Assembly of an Alkylated Guanosine Derivative into Ordered Supramolecular Nanoribbons in Solution and on Solid Surfaces. Chem. - A Eur. J. **13,** 3757–3764 (2007).

[98] Neviani, P. et al. Hierarchical formation of fibrillar and lamellar self-assemblies from guanosine-based motifs. J. Nucleic Acids **2010,** 938536 (2010).

[99] Gao, Y. F., Huang, Y. J., Xu, S. Y., Ouyang, W. J. & Jiang, Y. B. Ordered honeycomb microporous films from self-assembly of alkylated guanosine derivatives. Langmuir **27,** 2958–2964 (2011).

[100] Spada, G. P. et al. Guanosine-based hydrogen-bonded scaffolds: Controlling the assembly of oligothiophenes. Adv. Mater. **20,** 2433–2438 (2008).

reversibly transform from G-quartets to G-ribbons upon increasing the concentration (**Figure 21**).[102] This molecule was found to self-assemble into a gel in acetonitrile at high concentrations (CGC : 25 $mg.mL^{-1}$), which could be reduced down to 20 $mg.mL^{-1}$ upon sonication. NMR and CD measurements confirmed the formation of G4-quartets at low concentration and the transition from G-ribbons to G4-quartets by diluting the sample (**Figure 21C**). Besides, SEM images (**Figure 21D**) and X-ray diffraction (**Figure 21E**) analysis of the xerogel made in acetonitrile suggested that the guanosine derivative self-assembles into Type I G-ribbon structures which further aggregate into a hexagonal columnar structure thanks to intramolecular hydrogen bonding between the amide group close to adamantane and hydrophobic interactions. This example further demonstrates that the presence of competing functional groups on the molecular structure (amide group on the side chain for instance) might influence the self-assembly behavior of guanosine derivatives. Examples of G-quartet without metal templating ions remain however limited to conformationally constrained derivatives.[101]

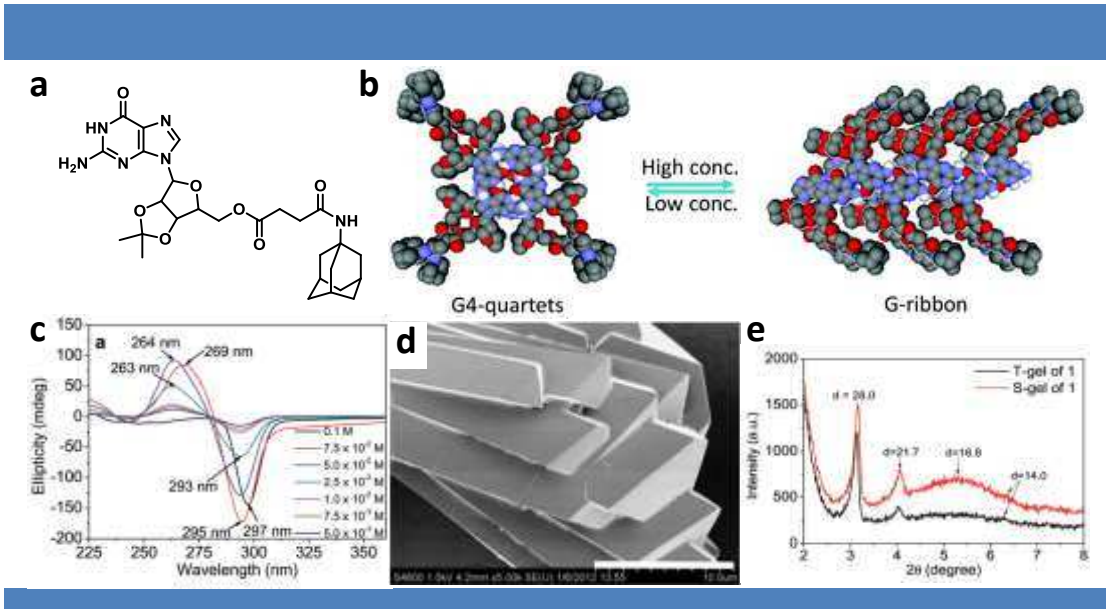

Figure 21 | (a). Chemical structure of guanine derivative compound. (b). The proposed structures of self-assembled G-quartets and G-ribbons. (c). CD spectral changes of the gel formed by 1 in acetonitrile (0.1 M) upon addition of 0, 1/3, 1, 3, 9, 12.3 to 19 equivalent volumes of acetonitrile. (d). SEM images of T-xerogel (scale bar 10 µm). e. Powder X-ray diffraction patterns of xerogel of 1 from CH_3CN at room temperature. Adapted from reference 102.

The group of Araki had an important contribution for the design of self-assembled systems based on alkylsilylated guanosine and deoxyguanosine derivatives, which mostly

[101] Sessler, J. L., Sathiosatham, M., Doerr, K., Lynch, V. & Abboud, K. A. A G-Quartet Formed in the Absence of a Templating Metal Cation: A New 8-(N,N-dimethylaniline)guanosine Derivative. Angew. Chemie **112,** 1356–1359 (2000).

[102] Meng, L., Liu, K., Mo, S., Mao, Y. & Yi, T. From G-quartets to G-ribbon gel by concentration and sonication control. Org. Biomol. Chem. **11,** 1525–1532 (2013).

give rise to network-like structures as depicted in **Figure 20C**.[106,103,104,105] For instance, Yashikawa and coworkers reported that such compounds can lead to the formation of soft supramolecular films in aqueous solution (H_2O – 5 wt% THF) (**Figure 22A-C**).[106] As determined by IR and XRD experiments, these films consist in a 2D hydrogen-bonded network of the guanosine residues self-associated within the layer and the oligoethylene oxide chains exposed to the water environment. When these dried thin films were dissolved in water and further sonicated at 80 °C, differential interference contrast microscopy (DICM) demonstrated the formation of spherical aggregates with a size of several microns (**Figure 22D**). Importantly, when these structures were prepared in the presence of a fluorescent probe such as eosin, fluorescence microscopy indicated the formation of giant vesicles, as eosin could be clearly identified within the spherical aggregates (**Figure 22E**). Finally, AFM experiments revealed the high stability and flexibility of the vesicles, which is inherent to their 2D supramolecular arrangement (**Figure 22F**).

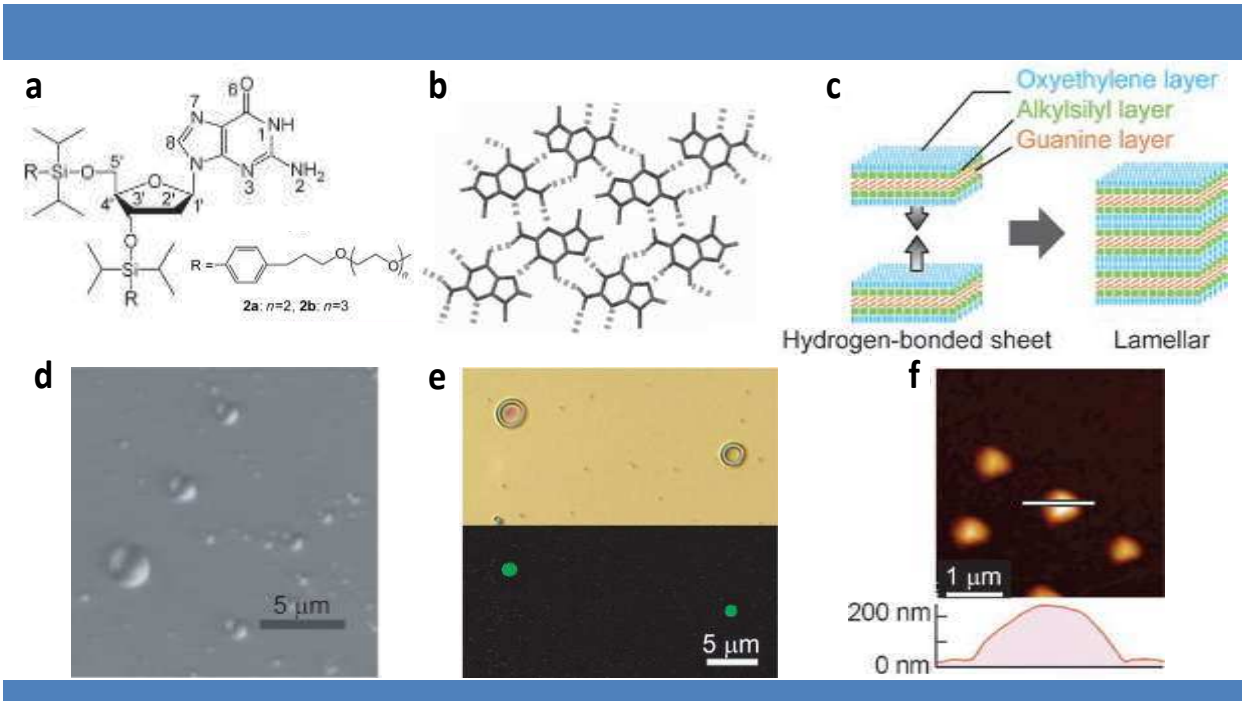

Figure 22 | (a). Structures of the alkylsilylated derivatives of guanosine. (b). Their 2D hydrogen-bonding pattern. (c). The film structure. d-e. The vesicles were prepared by the thin-film method: (d). DIC image, e. microscopy (upper half) and fluorescence (lower half) images of the vesicles containing eosin Y (λ_{abs}= 524 nm, λ_{fl}= 544 nm). f. The AC-mode AFM images of the vesicles prepared by the thin-film method. Height profiles along the lines within the images are shown under each image. Vesicles under ambient conditions observed with the default setting (maximum applied force: 2.3 nN). Adapted from reference 106.

[103] Araki, K. et al. Design, fabrication, and properties of macroscale supramolecular fibers consisted of fully hydrogen-bonded pseudo-polymer chains. Chem. Commun. **278,** 1826–1827 (2001).

[104] Yoshikawa, I., Li, J., Sakata, Y. & Araki, K. Design and Fabrication of a Flexible and Self-Supporting Supramolecular Film by Hierarchical Control of the Interaction between Hydrogen-Bonded Sheet Assemblies. Angew. Chemie Int. Ed. **43,** 100–103 (2004).

[105] Yoshikawa, I., Yanagi, S., Yamaji, Y. & Araki, K. Nucleoside-based organogelators: gelation by the G–G base pair formation of alkylsilylated guanosine derivatives. Tetrahedron **63,** 7474–7481 (2007).

[106] Yoshikawa, I., Sawayama, J. & Araki, K. Highly Stable Giant Supramolecular Vesicles Composed of 2D Hydrogen-Bonded Sheet

To conclude this section, we would like to mention that some discrete supramolecular architecture have been synthesized from a combination of guanine and cytosine derivatives.[86] However, although the G-C interaction is relatively strong, these examples remain limited and to the best of our knowledge, they have not yet been used to form polymeric structures.[94]

3. Supramolecular polymers from other nucleobases

Although guanine has been widely used as recognition unit to build supramolecular polymers, probably because of the variety of accessible polymeric arrays, examples involving other nucleobases such as adenine, uracil and thymine have also been developed in the last 25 years. For instance, as early as in 1990, the group of Lehn reported the first supramolecular polymer that takes advantage of the recognition properties of nucleobases, namely uracil, which was found to effectively associate with diacetamidopyridine (DAP).[10] Tartaric acid was decorated at both ends with either U or DAP motifs and the association of both monomers in various organic solvents resulted in the formation of a main-chain supramolecular polymer, as determined by ^{1}H NMR experiments and further confirmed by optical and electron microscopy studies.

As suggested in the first part of this chapter, there are two ways to produce self-assembled systems from nucleobase units: either by self-recognition (also named homotopic and exemplified in the previous section on guanine derivatives) or by hetero-complementarity between two different units (also called heterotopic such as for instance A-T). In this part, we would like to highlight some selected examples of self-assembled systems which are built according to these two strategies, focusing first on architectures built from small molecules or covalent polymers bearing self-recognition motifs as end groups[107,108] and then either on the assembly of heterotelechelic monomers (A-B molecules with A and B being self-complementary)[109,110] or the 1:1 co-assembly of homotelechelic A-A with B-B monomers.[111,112]

Structures of Guanosine Derivatives. Angew. Chemie Int. Ed. **47,** 1038–1041 (2008).

[107] Cortese, J., Soulié-Ziakovic, C., Cloitre, M., Tencé-Girault, S. & Leibler, L. Order–Disorder Transition in Supramolecular Polymers. J. Am. Chem. Soc. **133,** 19672–19675 (2011).

[108] Nuthanakanti, A. et al. Hierarchical self-assembly of switchable nucleolipid supramolecular gels based on environmentally-sensitive fluorescent nucleoside analogs. Nanoscale **8,** 3607–3619 (2016).

[109] Shimizu, T., Iwaura, R., Masuda, M., Hanada, T. & Yase, K. Internucleobase-Interaction-Directed Self-Assembly of Nanofibers from Homo- and Heteroditopic 1, ω -Nucleobase Bolaamphiphiles. J. Am. Chem. Soc. **123,** 5947–5955 (2001)

[110] Berger, O. et al. Light-emitting self-assembled peptide nucleic acids exhibit both stacking interactions and Watson–Crick base pairing. Nat. Nanotechnol. **10,** 353–360 (2015).

[111] Sivakova, S., Wu, J., Campo, C. J., Mather, P. T. & Rowan, S. J. Liquid-Crystalline Supramolecular Polymers Formed through Complementary Nucleobase-Pair Interactions. Chem. – A Eur. J. **12,** 446–456 (2006).

[112] Wang, D. et al. Supramolecularly engineered phospholipids constructed by nucleobase molecular recognition: upgraded generation of

Considering native nucleobases and as illustrated in **Figure 19**, adenine offers the possibility to self-recognize by its three faces, all of them presenting a donor-acceptor motif. The group of Sleiman took advantage of this ability to report the (co-)self-assembly of a series of nucleobase peptide amphiphiles (NPAs) incorporating an adenine residue as side chain modification of a dipeptide backbone (**Figure 23A**).[113] While **PEG-A** did not produce any self-assembled structure in water or buffer, **Hex-A** gave rise to the formation of micrometer-long fibrillar aggregates in similar solutions. Owing to the amphiphilic nature of **Hex-A**, the core of these rod-like structures is built thanks to a combination of hydrogen bonding interactions between the dipeptide unit and hydrophobic interactions of the alkyl side chain, with the adenine moiety pointing out of the self-assembled structure (**Figure 23B**) Importantly, the presence of adenine moieties at the edge of the rod-like structures further induced the alignment of the fibrillar aggregates by intermolecular hydrogen bonds over several micrometers as imaged by AFM and TEM experiments (**Figure 23C-D**).

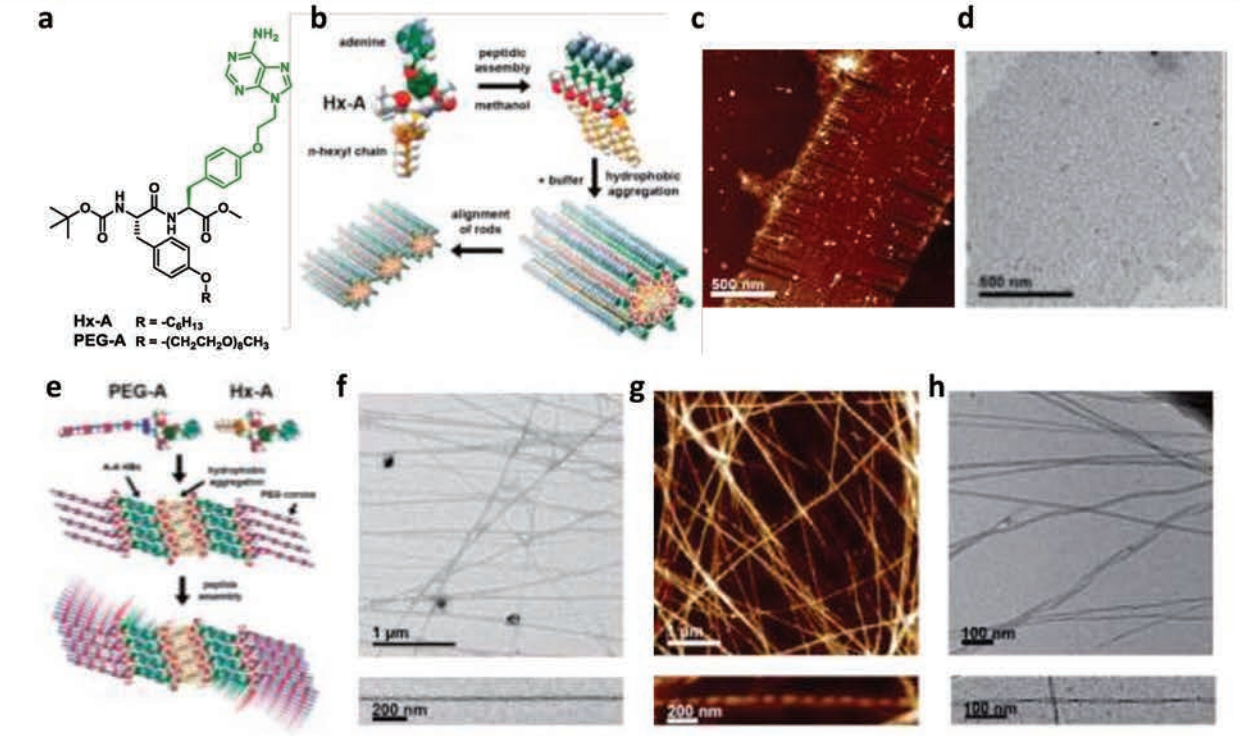

Figure 23 | (a). Chemical structure of **Hex-A** and **PEG-A**. (b-d). Self-assembly of **Hex-A**. (b) Overview of hierarchical self-assembly to yield aligned nanorods; (c) AFM images illustrating hierarchy of fiber aggregation in 9 : 1 TAEMg : methanol; (d) TEM images of the same features. e-h. Self-assembly of **PEG-A**, on its own and in combination with **Hex-A.** (e) Proposed self-assembly scheme of 1 : 1 **PEG-A** : **Hex-A**; (f) TEM image of helical fibres in the gel, with magnification of a single example; (g) AFM image of helical fibers in the gel, with magnification of a single example; (h) Cryo-EM image of helical gel fibers, with magnification of a single example. Adapted from reference 113.

phospholipids for drug delivery. Chem. Sci. **6,** 3775–3787 (2015).

[113] Serpell, C. J. et al. Nucleobase peptide amphiphiles. Mater. Horizons **1,** 348–354 (2014).

Interestingly, when **PEG-A** and **Hex-A** were mixed in a 1:1 ratio in aqueous solutions, the formation of a hydrogel occurred at a concentration as low as 0.5 wt%. TEM, AFM and cryo-EM imaging demonstrated the formation of left-handed helical ribbons with a thickness of around 27 nm and a helical pitch of ~110 nm (**Figure 23F-H**). Considering that similar CD spectra were recorded for both **Hex-A** and its 1:1 mixture with **PEG-A**, the structure proposed for these helical ribbons consists in a core made of **Hex-A** arranged similarly as in **Figure 23b** with its adenine residues hydrogen-bonded to the ones of **PEG-A**, which is also arranged in β-sheet structures (**Figure 23E**).

In addition to the self-complementarity of native nucleobases which has only been used few times (except for guanine) to produce supramolecular polymers, chemists have designed several new motifs inspired by nucleobases and which can self-associate. For instance, the group of Fenniri took advantage of a purely synthetic heterocyclic motif which presents the Watson-Crick hydrogen-bonding pattern of cytosine on one side and the Watson-Crick hydrogen-bonding pattern of guanine on the other one to produce nanorosettes architectures of well-defined dimensions.[88] Alternatively, the group of Cheng has reported the self-assembly of poly(propylene oxide) (PPO) chains decorated with self-complementary ureido-cytosine end-chain groups.[89] In toluene, these polymers were found to self-assemble into different morphologies depending on the concentration. Spherical aggregates and lamellar microstructures were observed by TEM at respectively low and high concentrations. These differences can be explained by the favored formation of ring-chain polymers at concentrations as low as 0.03 $g.mL^{-1}$ while linear oligomers are preferentially formed above 0.2 $g.mL^{-1}$.

Alternatively, supramolecular polymers and/or self-assembled structures could be produced using hetero-complementary base pairs. For instance, using similar PPO oligomeric chains, the group of Leibler took advantage of the hetero-complementarity of thymine and diaminotriazine units as end groups to study how the polarity of the solvent affect their self-assembly (**Figure 24A**).[114] Similar behaviors were observed for both the supramolecular polymerization of heterotelechelic oligomers and the co-self-assembly of homotelechelic oligomers. Here, we would like to stress that, for main-chain supramolecular polymerization, the stoichiometry used for each homotelechelic monomer is particularly important to reach a polymer with a high degree of polymerization as a slight excess of one monomer will act as a chain stopper. To sum up, in DMSO, where hydrogen bonds are suppressed, no

[114] Cortese, J., Soulie-Ziakovic, C. & Leibler, L. Binding and supramolecular organization of homo- and heterotelechelic oligomers in solutions. Polym. Chem. **5,** 116–125 (2014).

supramolecular polymers were formed and the non-polar nature of the PPO backbone favored the formation of micelles with thymine and diaminotriazine residues solvated by DMSO at their surfaces. Based on specific viscosity measurements and subsequent analyses, an isodesmic mechanism was found to take place in chloroform, which suggested the preferential formation of linear main-chain oligomers mainly driven by hydrogen bonding interactions, the PPO chain being well-soluble in this solvent (**Figure 24b,d**). Finally, in toluene, specific viscosity measurements were only satisfactorily fitted with a colloidal model suggesting that the core of the aggregates is made of a columnar arrangement of thymine and diaminotriazine units favored by both hydrogen bonds and π-π stacking interactions, which is further surrounded by the PPO chains which are also fully soluble in toluene (**Figure 24c,d**).

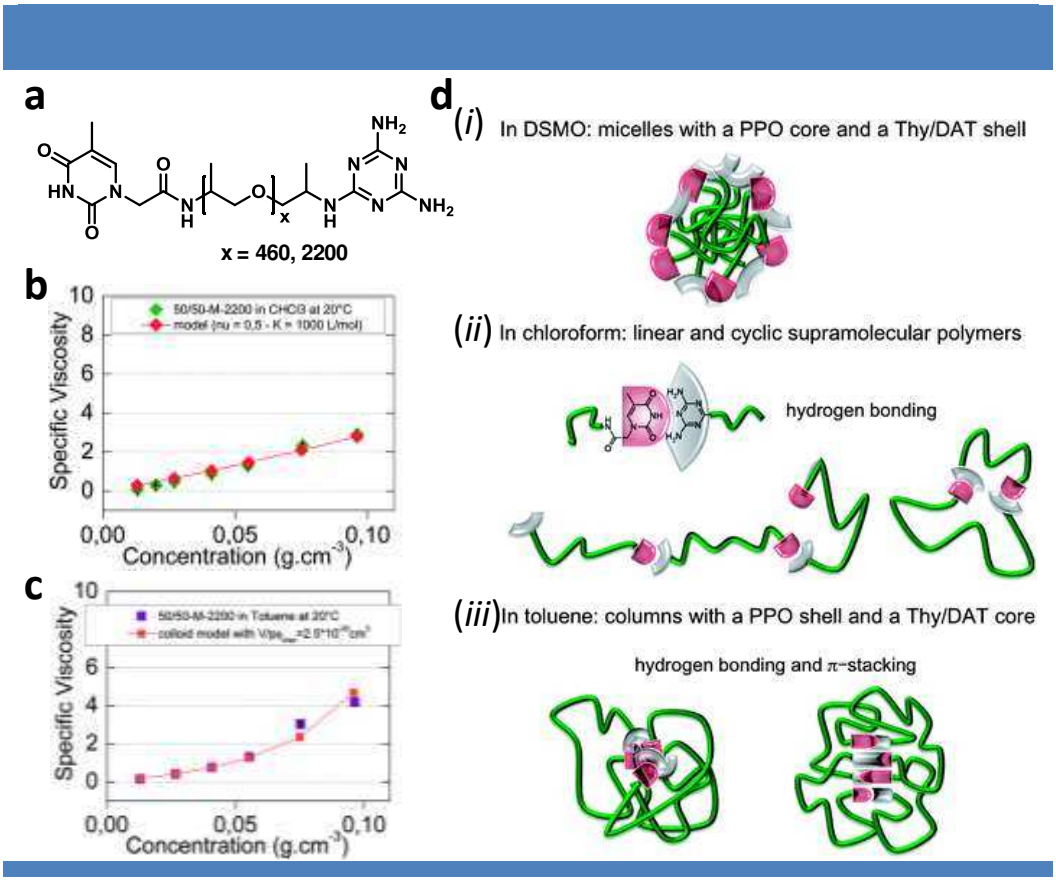

Figure 24 | (a). Chemical structures of the heterotelechelic oligomers, Thy-PPO-X-DAT. b-c. Concentration-dependent specific viscosity of 50/50-M-2200 (50: 50 mixtures of Thy-PPO-2200-Thy and DAT-PPO-2200-DAT) at 20 °C in chloroform: (b). Viscosity model for an isodesmic supramolecular polymerization into linear chains with an association constant of 1000 $L.mol^{-1}$; (c). Viscosity model for colloidal supramolecular polymers. (d). Heterotelechelic oligomer Thy-PPO-2200-DAT solution mesoscopic organization: (i) in DMSO, (ii) in chloroform, (iii) in toluene. Reproduced from reference 114.

However, examples reporting on the supramolecular recognition of heteroditopic monomers are limited, probably due to the difficult and lengthy synthesis of such molecules. Thus, various research groups have focused on the 1:1 co-assembly of homoleptic ditopic

monomers based either on natural nucleobases or their synthetic analogues to access self-assembled architectures in a well-controlled manner.[115] For instance, the group of Barboiu reported that alkylsiloxane small molecules decorated with either adenine or uracil units can self-organize into two different structures in solution depending on the hydrogen bond interactions involved (Hoogsteen and/or Watson-Crick).[116] Importantly, when this preorganized mixture was frozen thanks to a sol-gel transcription process of the siloxane units, only one preferred structure resulting from Watson-Crick interactions between adenine residues and Hoogsteen ones between adenine and uracil residues could be recorded by X-ray powder diffraction. Such observation was found to be in agreement with the preferential Hoogsteen binding of a 1:1 mixture of alkyladenine and alkylthymine molecules. This example highlights how to build hybrid materials in a templated manner thanks to nucleobase recognition properties. Recently, the groups of Surin and Bonifazi reported the supramolecular polymerization of ditopic small molecules decorated either with two uracil units or two diacetamidopyridine units as end groups (**Figure 25**).[117] By varying the polarity of the solvents used for the polymerization process, they demonstrated that these supramolecular copolymers can lead to the formation of very distinct morphologies with particular optical properties. For instance, while in chloroform micrometer-long rigid rod-like structures made of bundles of nanometric fibers (~6 nm) were observed by TEM (**Figure 25B-C**), softer helical morphologies with a diameter of 5-10 nm were recorded in a 95:5 mixture of cyclohexane/THF (**Figure 25D-E**). In the latter conditions, fluorescence experiments on a 1:1 mixture of compounds **(R)-1** and **2** indicated the formation of J-aggregates of the aromatic cores and hydrogen-bonded structures. Furthermore, molecular modelling suggested that the presence of a chiral precursor leads to the formation of a single helix with a preferred handedness which further self-interdigitated into a double helical structure. This mechanism was found to be in agreement with SAXS, TEM and SEM experiments which show the evolution from chiral tape-like aggregates which finally dimerize into nanofibers. For the self-assembly in chloroform, the formation of aggregated fibrillar structures was ascribed to hydrophobic effects and extensive van der Waals interactions between the C12 alkyl chains.

[115] Marangoni, T. & Bonifazi, D. Nano- and microstructuration of supramolecular materials driven by H-bonded uracil·2,6-diamidopyridine complexes. Nanoscale **5,** 8837–8851 (2013).
[116] Arnal-Hérault, C. et al. Constitutional Self-Organization of Adenine–Uracil-Derived Hybrid Materials. Chem. – A Eur. J. **13,** 6792–6800 (2007).
[117] Đorđević, L. et al. Solvent Molding of Organic Morphologies Made of Supramolecular Chiral Polymers. J. Am. Chem. Soc. **137,** 8150–8160 (2015).

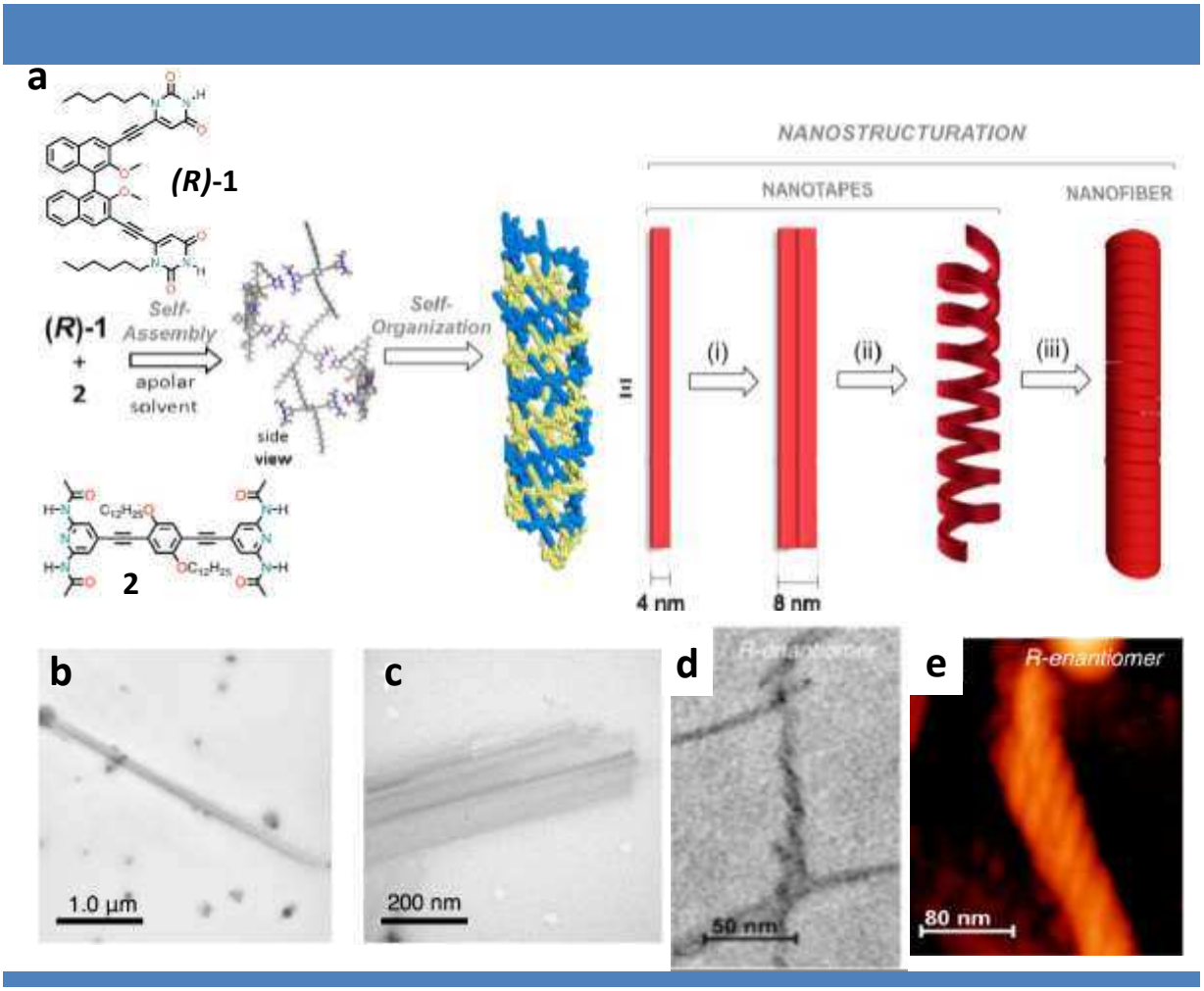

Figure 25 | (a). Molecular structure and proposed simulated model for self-organized nanofibers (one helix in blue, the other in yellow, ~15-nm-long fiber as obtained through several MM simulations cycles of the superstructure): at first, the self-assembly occurs through H-bonding between the complementary modules in a helix-type arrangement, which is right-handed for [**(R)-1·2**]n, followed by a self-interdigitation of the single helices yielding double helix nanofibers. As observed by SAXS analysis in solution and AFM images on surfaces, it is envisaged that the individual nanofibers are organized into the final superhelical nanofibers by a possible three-step mechanism based on the formation of a tape structure (i) that will eventually twist into a single helical tape (ii) and finally dimerize into the final nanofibers structure (iii) observed by TEM and AFM. b-d. TEM images the morphologies obtained from (b-c) a drop-casted $CHCl_3$ solution of [**(R)-1·2**] (c = 1.3 × 10^{-3} M) and (d) a drop-casted cyclohexane/THF (95 : 5, v/v) solution of [**(R)-1·2**] (c = 1.7 × 10^{-3} M) on a carbon-coated grid. (e). Tapping mode-AFM image of a drop-casted cyclohexane/THF (95 : 5, v/v) solution of [**(R)-1·2**] (c = 1.7 × 10^{-3} M) on a carbon-coated on a mica surface. Adapted from reference 117.

Overall, in this chapter, we have shown that nucleobases can effectively drive the self-assembly of monomers in a controlled manner. However, their role is usually limited to a binding motif and molecular design is an important parameter to consider for yielding functional self-assembled systems. In the next chapter, we will try to highlight how these nucleobases can be used as functional units, particularly for recognition processes of metal ions, small molecules or even DNA oligo/polymer.

Chapter 4: Templated self-assemblies involving nucleobase units

We have seen in the previous chapter that molecules decorated with nucleobases can either self-recognize or co-assemble with complementary hydrogen-bonded motifs to form supramolecular architectures of various morphologies. However, it is also well-known that nucleobases have high and selective affinities for metal ions,[118,119,120] which have been exploited to produce functional materials.[121,122,123] Alternatively, small molecules presenting several faces for hydrogen bonding interactions can drive the self-assembly of nucleobase residues into various architectures whose morphologies is determined by the ratio of the different monomers involved.[124] Furthermore, owing to their molecular design, small molecules incorporating nucleobase recognition units are good candidates to combine with DNA strands in order to produce programmable hybrid supramolecular assemblies of well-defined dimensions, which could further be used in a variety of applications ranging from catalysis to optoelectronic materials.[125,126]

In this chapter, we will discuss first the ion-templated self-assembly of guanine and thymine derivatives, and then show how small molecules can also assist their organization thanks to well-defined arrays of hydrogen bonding interactions. Finally, we will highlight some recent examples showing how small molecules incorporating nucleobase residues can be co-assemble with DNA strands to produce bio-hybrid supramolecular architectures.

1. Ion-templated self-assemblies

Since the early 1960s, several studies have emphasized the importance of

[118] Lippert, B. & Sanz Miguel, P. J. The Renaissance of Metal–Pyrimidine Nucleobase Coordination Chemistry. Acc. Chem. Res. **49,** 1537–1545 (2016).
[119] Tanaka, Y. et al. Structures, physicochemical properties, and applications of T–Hg II –T, C–Ag I –C, and other metallo-base-pairs. Chem. Commun. **51,** 17343–17360 (2015).
[120] Abet, V. & Rodriguez, R. Guanosine and isoguanosine derivatives for supramolecular devices. New J. Chem. **38,** 5122–5128 (2014).
[121] Dash, J. & Saha, P. Functional architectures derived from guanine quartets. Org. Biomol. Chem. **14,** 2157–2163 (2016).
[122] Scharf, P. & Müller, J. Nucleic Acids With Metal-Mediated Base Pairs and Their Applications. Chempluschem **78,** 20–34 (2013).
[123] Chen, G., Guo, Z., Zeng, G. & Tang, L. Fluorescent and colorimetric sensors for environmental mercury detection. Analyst **140,** 5400–5443 (2015).
[124] Roy, B., Bairi, P. & Nandi, A. K. Supramolecular assembly of melamine and its derivatives: nanostructures to functional materials. RSC Adv. **4,** 1708–1734 (2014).
[125] Catherall, T., Huskisson, D., McAdams, S. & Vijayaraghavan, A. Self-assembly of one dimensional DNA-templated structures. J. Mater. Chem. C **2,** 6895 (2014).
[126] Surin, M. From nucleobase to DNA templates for precision supramolecular assemblies and synthetic polymers. Polym. Chem. **7,** 4137–4150 (2016).

metal-nucleobase interactions in DNA in order to control biological processes[127] but also more recently using small molecules or nanomaterials such as nanoparticles,[128] carbon dots,[129] graphene oxide[130] decorated with pyrimidine or purine residues in order to produce functional materials. On one hand, pyrimidine bases such as thymine, uracil and cytosine have been found to interact strongly with transition metal ions such as mercury, silver, platinum, palladium…[131] In particular, the selectivity of thymine and cytosine for respectively mercury and silver have been elucidated using a series of physico-chemical techniques such as NMR and FTIR spectroscopy, X-ray diffraction, or even calorimetry (ITC for instance).[119] On the other hand, in water or aqueous solutions, G-quartets have, to the best of our knowledge, only been isolated in the presence of various metal ions such as potassium, sodium, cesium, etc., but several studies have demonstrated that metal-templated structures can also be isolated in organic solvents.[92] In this bibliography section, we will only focus our discussion first on the self-assembly of metal-templated G-quartets and then highlight the potential of native thymine units and some related structures for binding mercury.

a. Self-assembly of metal-templated G-quartets

For the sake of clarity, it is important to define first the difference between G-quartet and G-quadruplex. While G-quartet corresponds to the macrocyclic arrangement of four guanine residues through a combination of Watson-Crick and Hoogsteen hydrogen-bond interactions, their subsequent oligomerization into columnar stacks via several non-covalent interactions (hydrogen-bonds, π-π stacking and cation-dipole interactions) leads to the formation of G-quadruplexes, which could be described as a supramolecular polymer of G-quartets. Considering the extensive literature on G-quartet and G-quadruplex both using biologically relevant molecules and artificial ones, we will only focus on examples which describe the self-organization of G-quartets into G-quadruplexes.

In aqueous environments, several monovalent and divalent cations, such as for instance Ag^+, NH_4^+, Sr^{2+}, have been shown to trigger the formation of G-quartet, leading in most cases to the formation of micrometer-long fibrillary aggregates which further entangle to form

[127] Rhodes, D. & Lipps, H. J. G-quadruplexes and their regulatory roles in biology. Nucleic Acids Res. **43,** 8627–8637 (2015).
[128] Lee, J. S., Han, M. S. & Mirkin, C. A. Colorimetric detection of mercuric ion (Hg^{2+}) in aqueous media using DNA-functionalized gold nanoparticles. Angew Chem Int Ed Engl **46,** 4093–4096 (2007).
[129] Xu, H. et al. Highly selective and sensitive fluorescence probe based on thymine-modified carbon dots for Hg^{2+} and l -cysteine detection. RSC Adv. **5,** 89121–89127 (2015).
[130] Liu, L. et al. Enhancing the Hg(II) Removal Efficiency from Real Wastewater by Novel Thymine-Grafted Reduced Graphene Oxide Complexes. Ind. Eng. Chem. Res. **55,** 6845–6853 (2016).
[131] Lippert, B. & Sanz Miguel, P. J. The Renaissance of Metal-Pyrimidine Nucleobase Coordination Chemistry. Acc. Chem. Res. **49,** 1537–1545 (2016).

hydrogels.[132,133,134] For instance, Ishihara and Kimura described the self-assembly in water of a tetra-β-peptidic macrocycle tailored with a lateral guanine residue (**Figure 26**).[135] The peptidic macrocycle was designed to self-assemble into nanotubular aggregates via intermolecular hydrogen-bonding interactions. However, in water and in the absence of potassium ions, only fuzzy aggregates were imaged by TEM. Nevertheless, when KCl was added to this macrocyclic molecule in water, CD experiments showed the appearance of a positive Cotton effect in the amide region, suggesting the formation of G-quartet into G-quadruplexes, which further drives the self-assembly of peptidic nanotubes. Such hierarchical organization of the macrocyclic molecules were confirmed by TEM imaging, which showed the presence of well-defined nanotubular structures with lengths up to 10 µm and widths estimated to 4.8 nm (corresponding to the diameter of a tetrameric arrangement of the single molecules) by electron diffraction (**Figure 26B-D**). This example demonstrates how preorganization at the molecular scale is important to reach hierarchical supramolecular structures at the microscopic scale.

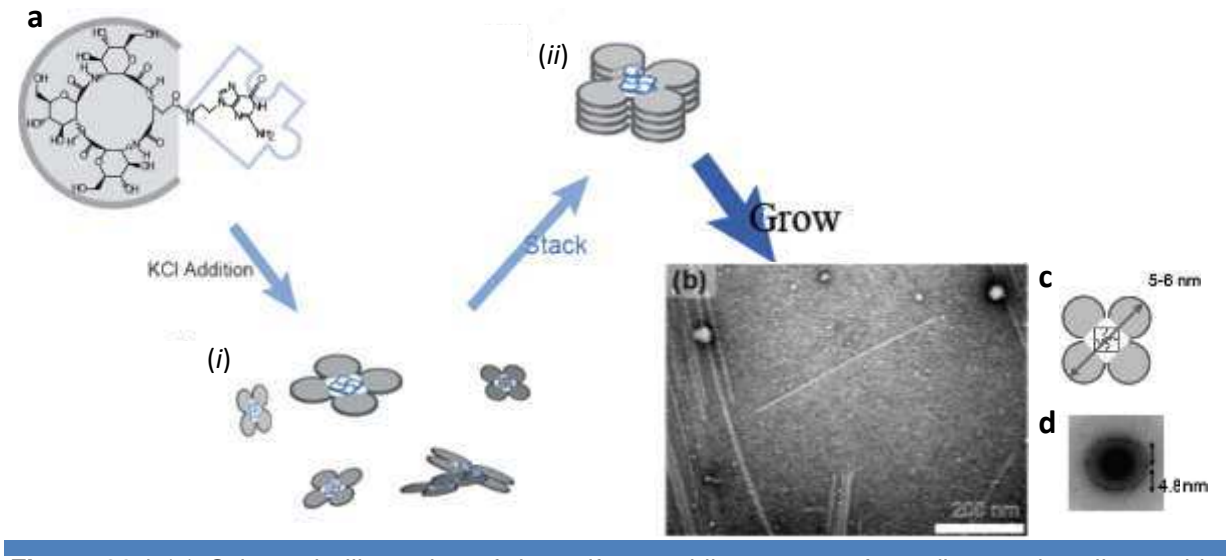

Figure 26 | (a) Schematic illustration of the self-assembling process from dispersed cyclic peptide guanine molecule to (i) quadruplication *via* G-quartet, (ii) seed formation of a quadruple peptide-nanotube bundle, and (b) nanofibrous assembly as shown by TEM image in the presence of potassium ions. (c) Schematic illustration of the diameter of a quadruple peptide-nanotube bundle. (d) Electron diffraction pattern obtained from the aligned fibrous assembly. Adapted from reference 135.

[132] Hu, D., Ren, J. & Qu, X. Metal-mediated fabrication of new functional G-quartet-based supramolecular nanostructure and potential application as controlled drug release system. Chem. Sci. **2,** 1356 (2011).
[133] Dash, J., Patil, A. J., Das, R. N., Dowdall, F. L. & Mann, S. Supramolecular hydrogels derived from silver ion-mediated self-assembly of 5′-guanosine monophosphate. Soft Matter **7,** 8120 (2011).
[134] Adhikari, B., Shah, A. & Kraatz, H.-B. Self-assembly of guanosine and deoxy-guanosine into hydrogels: monovalent cation guided modulation of gelation, morphology and self-healing properties. J. Mater. Chem. B **2,** 4802 (2014).
[135] Ishihara, Y. & Kimura, S. Four-peptide-nanotube bundle formation by self-assembling of cyclic tetra-beta-peptide using G-quartet motif. Biopolymers **100,** 141–147 (2013).

Furthermore, the group of Davis, who had a strong contribution to the field,[94] demonstrated that small aromatic molecules can be used to enhance the stability of these hydrogels by enabling the polymerization of G-quartets into long supramolecular polymers, leading to increased rheological and healing properties.[136] Such G-quartet-based hydrogels have found numerous applications such as drug release,[137] ion-channels,[138] or even light-harvesting antenna.[139]

However, examples related to the formation of G-quadruplex architectures in organic solvents are more limited, mainly focusing on the design of lipophilic guanosine derivatives.[140,141,142,143] In 2009, the group of Meijer reported a very fundamental study which demonstrated the influence of molecular design, solvent polarity and cation-anion distances in the formation of G-quadruplexes of well-defined dimensions.[144] Overall, they showed that large G-quadruplexes are favored by (a) high solvent polarity (except for solvents competing for hydrogen bond interactions), due to a more efficient solvatation of the dissociated anion; (b) least coordinating anions such as iodine, picrate or hexafluorophosphate ions; and (c) small anion-cation distances as it reduces the ion-pair separation energy. By playing with these different criteria and using a simple guanosine-2',3'-acetonide, they showed that micrometer-long fibers can be formed in acetone using KPF_6 as metal ion salt. The group of Barboiu has taken advantage of the self-assembling properties of guanine derivatives in organic solvents to design hybrid materials based on G-quartet structures.[145,146,147] For instance, they designed a guaninesiloxane derivative G_{Si} and studied its self-assembling properties in acetone in the presence and the absence of potassium ions (**Figure 27**).[145]

[136] Peters, G. M., Skala, L. P. & Davis, J. T. A Molecular Chaperone for G4-Quartet Hydrogels. J Am Chem Soc **138,** 134–139 (2016).
[137] Plank, T. N. & Davis, J. T. A G 4 ·K + hydrogel that self-destruct s. Chem. Commun. **52,** 5037–5040 (2016).
[138] Kumar, Y. P., Das, R. N., Schütte, O. M., Steinem, C. & Dash, J. Bis-triazolyl diguanosine derivatives as synthetic transmembrane ion channels. Nat. Protoc. **11,** 1039–56 (2016).
[139] Pu, F., Wu, L., Ran, X., Ren, J. & Qu, X. G-quartet-based nanostructure for mimicking light-harvesting antenna. Angew Chem Int Ed Engl **54,** 892–896 (2015).
[140] Forman, S. L., Fettinger, J. C., Pieraccini, S., Gottarelli, G. & Davis, J. T. Toward artificial ion channels: a lipophilic G-quadruplex. J. Am. Chem. Soc. **122,** 4060–4067 (2000).
[141] Shi, X. et al. Lipophilic G-Quadruplexes Are Self-Assembled Ion Pair Receptors, and the Bound Anion Modulates the Kinetic Stability of These Complexes. J. Am. Chem. Soc. **125,** 10830–10841 (2003).
[142] Ma, L., Iezzi, M., Kaucher, M. S., Lam, Y.-F. & Davis, J. T. Cation Exchange in Lipophilic G-Quadruplexes: Not All Ion Binding Sites Are Equal. J. Am. Chem. Soc. **128,** 15269–15277 (2006).
[143] Gonnelli, A. et al. Small-angle X-ray scattering study of self-assembling lipophilic guanines in organic solvents: G-quadruplex formation and cation effects in cyclohexane. J Phys Chem B **117,** 1095–1103 (2013).
[144] González-Rodríguez, D. et al. G-quadruplex self-assembly regulated by Coulombic interactions. Nat. Chem. **1,** 151–155 (2009).
[145] Arnal-Hérault, C., Banu, A., Barboiu, M., Michau, M. & van der Lee, A. Amplification and Transcription of the Dynamic Supramolecular Chirality of the Guanine Quadruplex. Angew. Chemie Int. Ed. **46,** 4268–4272 (2007).
[146] Mihai, S. et al. Supramolecular self-organization in constitutional hybrid materials. New J. Chem. **33,** 2335–2343 (2009).
[147] Mihai, S., Le Duc, Y., Cot, D. & Barboiu, M. Sol–gel selection of hybrid G-quadruplex architectures from dynamic supramolecular guanosine libraries. J. Mater. Chem. **20,** 9443 (2010).

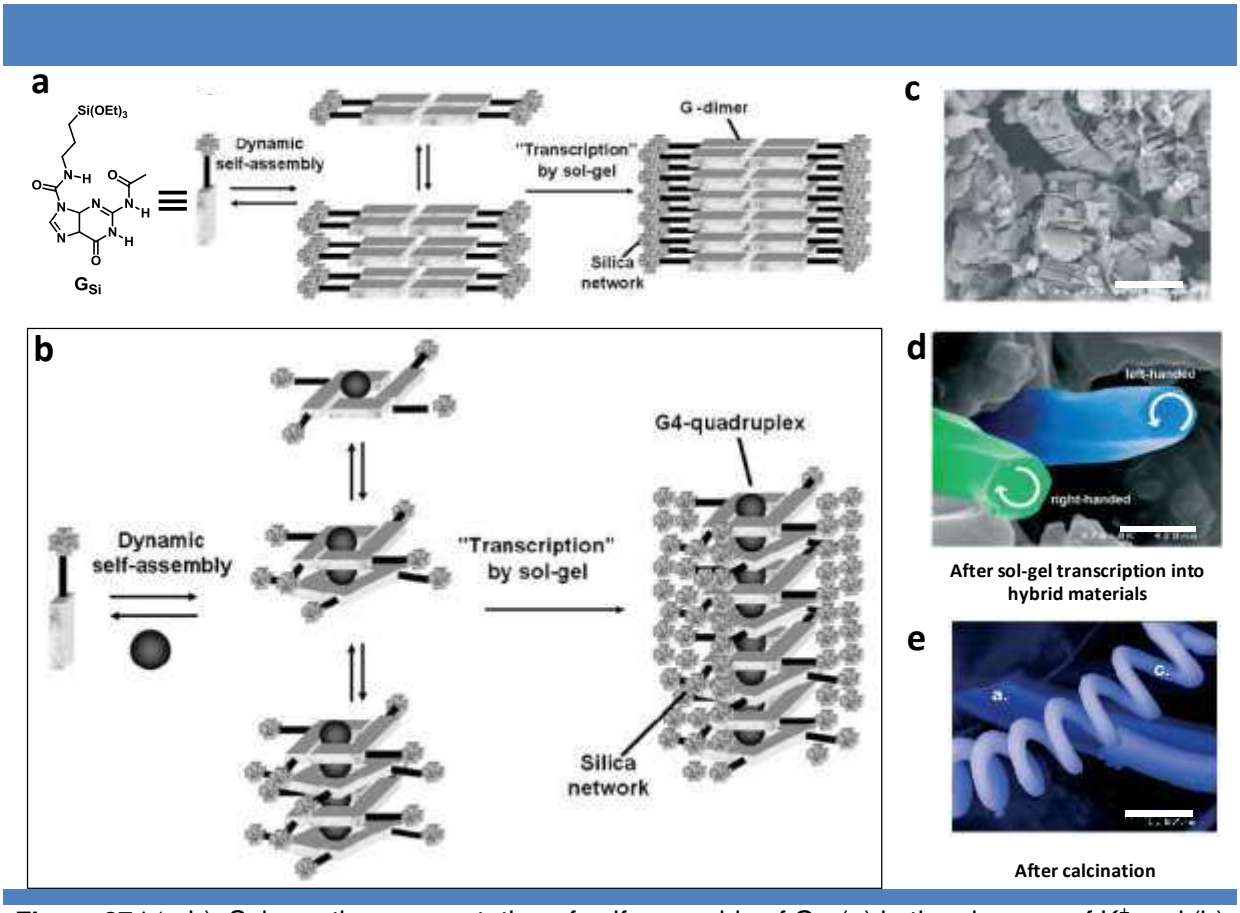

Figure 27 | (a-b). Schematic representation of self-assembly of G_{Si} (a) in the absence of K^+ and (b) in the presence of K^+. (c-e). SEM images of (c) the G-dimer hybrid in the absence of K^+ after calcination (scale bar: 2 µm); (d) G-quadruplex hexagonal nanorods resulting from sol-gel transcription in the presence of K^+ (scale bar: 429 nm); (e) silica nanofibers and microsprings after calcination (scale bar: 1.67 µm). Adapted from reference 145.

FTIR and ^{29}Si magic angle spinning (MAS) NMR were first used to demonstrate the formation of the G-quartet in the presence of potassium triflate. Interestingly, in the absence of metal ion, XRD analysis evidenced the formation of hydrogen-bonded dimers, which further aggregate into parallel ribbons. After sol-gel process at the siloxane units in order to freeze the self-assembled architecture and calcination of the resulting material, SEM imaging confirmed the formation of platelet-like structures (**Figure 27C**). On the other hand, XRD analysis of G_{Si} in the presence of K^+ suggested that G-quartets are formed and arranged into G-quadruplexes by π-π stacking interactions. Subsequent sol-gel process led to the formation of hexagonal rod-like structures of both handednesses, as imaged by SEM (**Figure 27D**). Finally, upon calcination of the hybrid material, several morphologies ranging from nanofibers and nanobundles to microsprings were observed (**Figure 27E**) and were reminiscent of the chiral arrangement of the G-quartet at the nanoscopic scale. This example evidencs how the addition of a metal template can affect the self-assembly of guanine derivatives and lead to the formation of chiral well-defined aggregates from achiral monomers,

thanks to a second level of organization in G-quadruplexes.

b. Self-assemblies from metallo-thymine derivatives

As mentioned in the introduction of this section, pyrimidine units have been shown to form duplexes with various transition metals. In particular, as determined by thermal denaturation UV absorbance and ITC experiments, thymine demonstrates a high specificity for mercury involving highly ionic N(thymine)-Hg bonds as demonstrated by ^{15}N NMR and Raman spectroscopies.[119,131] Thus, considering toxicity issues associated with mercury and their related impact on human health, thymine derivatives have been considered as potential candidates for sensing and Hg^{2+}-trapping.[123,148,149,150] For instance, the groups of Tian and Xu recently reported the synthesis of a distyrylanthracene (DSA) derivative decorated with two thymine residues as side chains, which present aggregation-induced emission properties in acetonitrile with increasing amounts of water (**Figure 28A**).[151]

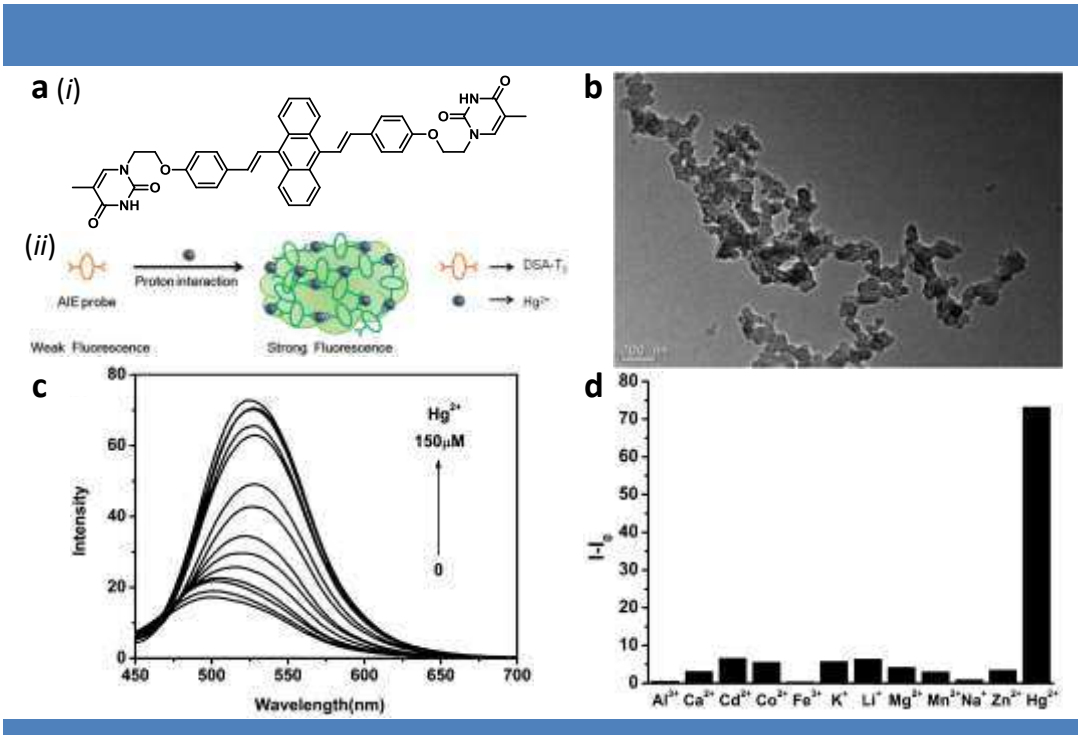

Figure 28 | a. *(i)* Molecular structure of the distyrylanthracene (DSA-T_2) derivative and *(ii)* design rationale for the Hg^{2+} chemosensor. b. TEM image of DSA-T_2 (1.16×10^{-5} M) in CH_3CN-H_2O (3 : 2, v/v) after addition of $Hg(NO_3)_2$ (1×10^{-4} M). c. Fluorescence spectra of DSA-T_2 (1.16×10^{-5} M) in CH_3CN-H_2O (3 : 2, v/v) with increasing amounts of Hg^{2+}, λ_{ex} = 420 nm. d. Normalized fluorescence intersity (I_{521nm}) of DSA-T_2 (1.16×10^{-5} M) in CH_3CN-H_2O (3 : 2, v/v) in the presence of different metal ions (7×10^{-5} M). Reproduced from reference 151.

[148] Liu, X., Qi, C., Bing, T., Cheng, X. & Shangguan, D. Highly Selective Phthalocyanine–Thymine Conjugate Sensor for Hg2+ Based on Target Induced Aggregation. Anal. Chem. **81,** 3699–3704 (2009).

[149] Luo, X. et al. Novel thymine-functionalized MIL-101 prepared by post-synthesis and enhanced removal of Hg2+ from water. J. Hazard. Mater. **306,** 313–322 (2016).

[150] Kim, H. N., Ren, W. X., Kim, J. S. & Yoon, J. Fluorescent and colorimetric sensors for detection of lead, cadmium, and mercury ions. Chem. Soc. Rev. **41,** 3210–3244 (2012).

[151] Ma, K., Li, X., Xu, B. & Tian, W. A sensitive and selective 'turn-on' fluorescent probe for Hg^{2+} based on thymine-Hg^{2+}-thymine complex with an aggregation-induced emission feature. Anal. Methods **6,** 2338–2342 (2014).

While at 60% water only few molecules aggregated in the absence of mercury ions, the addition of increasing amounts of mercury nitrate led to a bathochromic increase of the fluorescence similar to the one observed for high contents of water (**Figure 28C**). This observation indicates that DSA molecules aggregate upon binding to mercury, which is also evidenced by TEM images as shown by the formation of spherical aggregates with sizes of ~20-30 nm (**Figure 28B**). Interestingly, this chemosensor was found to be selective to mercury as no fluorescence increase was monitored upon addition of various metal ions (**Figure 28D**). This example demonstrates the selectivity of thymine residues for mercury thanks to a well-defined imino proton-metal exchange mechanism.[119] Moreover, the group of Jiang has shown that vesicles incorporating thymine residues at their surface can be used to selectively sense mercury by naked-eye detection at around 0.1 µM.[152]

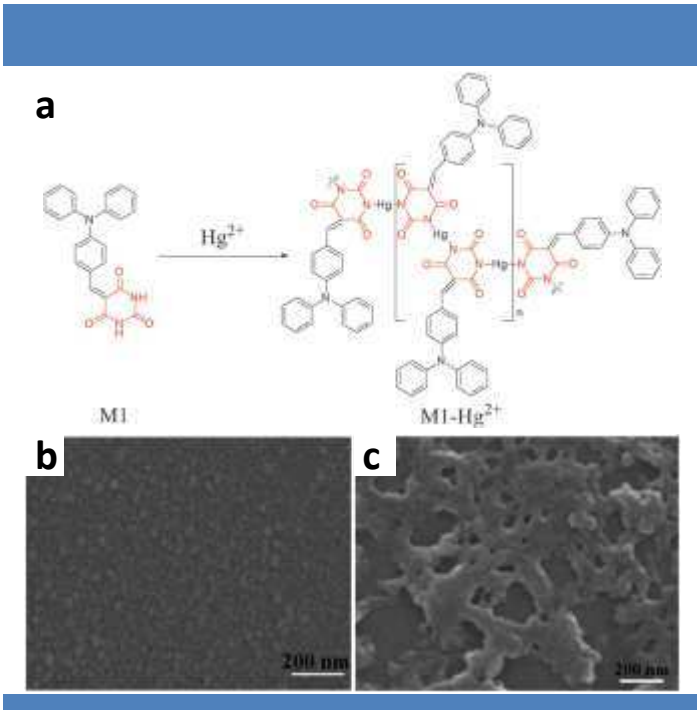

Figure 29 | a. Molecular structure of triarylamine-barbituric acid derivative M1 and its proposed aggregation with mercury. b-c. SEM images of M1 (5×10^{-5} M) in THF-water (3 : 7, v/v) (b) before and (c) after the addition of Hg^{2+} (1×10^{-4} M). Reproduced from reference 155.

Alternatively, barbituric acid residues, which present two imide faces reminiscent of thymine, have also been considered as potential candidates for mercury binding.[153,154,155] For instance, the groups of Shi[155] and Wang[153] independently reported the mercury sensing

[152] Ma, X., Sheng, Z. & Jiang, L. Sensitive naked-eye detection of Hg(2+) based on the aggregation and filtration of thymine functionalized vesicles caused by selective interaction between thymine and Hg(2+). Analyst **139,** 3365–3368 (2014).

[153] Wang, J., Zhang, L., Qi, Q., Li, S. & Jiang, Y. Specific ratiometric fluorescent sensing of Hg^{2+}via the formation of mercury(ii) barbiturate coordination polymers. Anal. Methods **5,** 608–611 (2013).

[154] Wang, E. et al. Twisted intramolecular charge transfer, aggregation-induced emission, supramolecular self-assembly and the optical waveguide of barbituric acid-functionalized tetraphenylethene. J. Mater. Chem. C **2,** 1801–1807 (2014).

[155] Shi, W. et al. Barbituric acid–triphenylamine adduct as an AIEE-type molecule and optical probe for mercury(ii). New J. Chem. **40,** 7814–7820 (2016).

properties of a barbituric acid moiety decorated with either a triarylamine or an anthracene unit respectively, owing to their aggregation-induced emission properties. Using a combination of optical spectroscopies (UV-Vis, Fluorescence, FTIR), Shi and coworkers demonstrated that compound **M1** selectively binds to mercury even in the presence of competing metal ions in aqueous solutions (THF/water 3:7), potentially leading to a network due to the presence of two imide faces on barbituric acid (**Figure 29A**). Finally, SEM imaging of solutions of **M1** before and after addition of mercury acetate confirmed the formation of such network-like structures, as also evidenced by DLS experiments (**Figure 29B-C**). This example demonstrates how molecules with imide faces can be used as selective recognition motifs for mercury and how their combination with optically-active synthons can lead to the formation of sensors.

2. Small molecule-templated self-assemblies

Besides ions, small molecules presenting several hydrogen bonding faces such as melamine (M), barbituric acid (BA) or cyanuric acid (CA), could be used to trigger the self-assembly of molecules or polymers decorated with nucleobase derivatives. Melamine, also known as 1,3,5-triazine-2,4,6-triamine, displays nine H-bonding sites arranged along three edges in a A-D-A array, which is thus complementary to thymine and uracil residues, and offers the possibility of secondary interactions by π-π stacking of its aromatic core. Cyanuric and barbituric acids, on the other hand, offers three or two D-A-D arrays respectively, which could be ideally matched to the minor groove face of guanine or, via 2 intermolecular interactions with adenine and cytosine Watson-Crick faces. The group of Whitesides pioneered studies on the self-assembly of melamine and cyanuric acid in the solid state, leading to the formation of various supramolecular architectures such as linear or crinkled tapes and cyclic hexameric rosette motifs, which can be precisely achieved by tuning the chemical structures of native M and CA.[155,156,157] Indeed, one main problem associated with M, BA and CA molecules is their poor solubility in common organic solvents, thus fostering their studies at surfaces[158] or interfaces.[159] Nevertheless, over the last decades,

[156] Zerkowski, J. A., Seto, C. T. & Whitesides, G. M. Solid-state structures of rosette and crinkled tape motifs derived from the cyanuric acid melamine lattice. J. Am. Chem. Soc. **114,** 5473–5475 (1992).

[157] Zerkowski, J. A., MacDonald, J. C., Seto, C. T., Wierda, D. A. & Whitesides, G. M. Design of Organic Structures in the Solid State: Molecular Tapes Based on the Network of Hydrogen Bonds Present in the Cyanuric Acid.cntdot.Melamine Complex. J. Am. Chem. Soc. **116,** 2382–2391 (1994).

[158] Slater, A. G. et al. Thymine functionalised porphyrins, synthesis and heteromolecular surface-based self-assembly. Chem. Sci. **6,** 1562–1569 (2015).

[159] Xin, Y., Kong, X., Zhang, X., Lv, Z. & Du, X. Self-Assembly and Molecular Recognition of Adenine- and Thymine-Functionalized Nucleolipids in the Mixed Monolayers and Thymine-Functionalized Nucleolipids on Aqueous Melamine at the Air–Water Interface.

chemists have developed a variety of M, BA or CA analogues, which retain their hydrogen bonding properties but present enhanced solubility. These molecules have been shown to produce various self-assembled morphologies going from discrete supramolecular architectures to nanotubes or even extended networks and potentially leading to the formation of functional supramolecular materials such as sensors.[124] For instance, the group of Tang demonstrated how tetraphenylethene decorated with a barbituric residue can generate supramolecular polymers of different morphologies (nanospheres to nanorods) in the presence or the absence of melamine.[154] Interestingly, the self-assembled microrods obtained only with melamine were found to display interesting optical waveguiding properties.

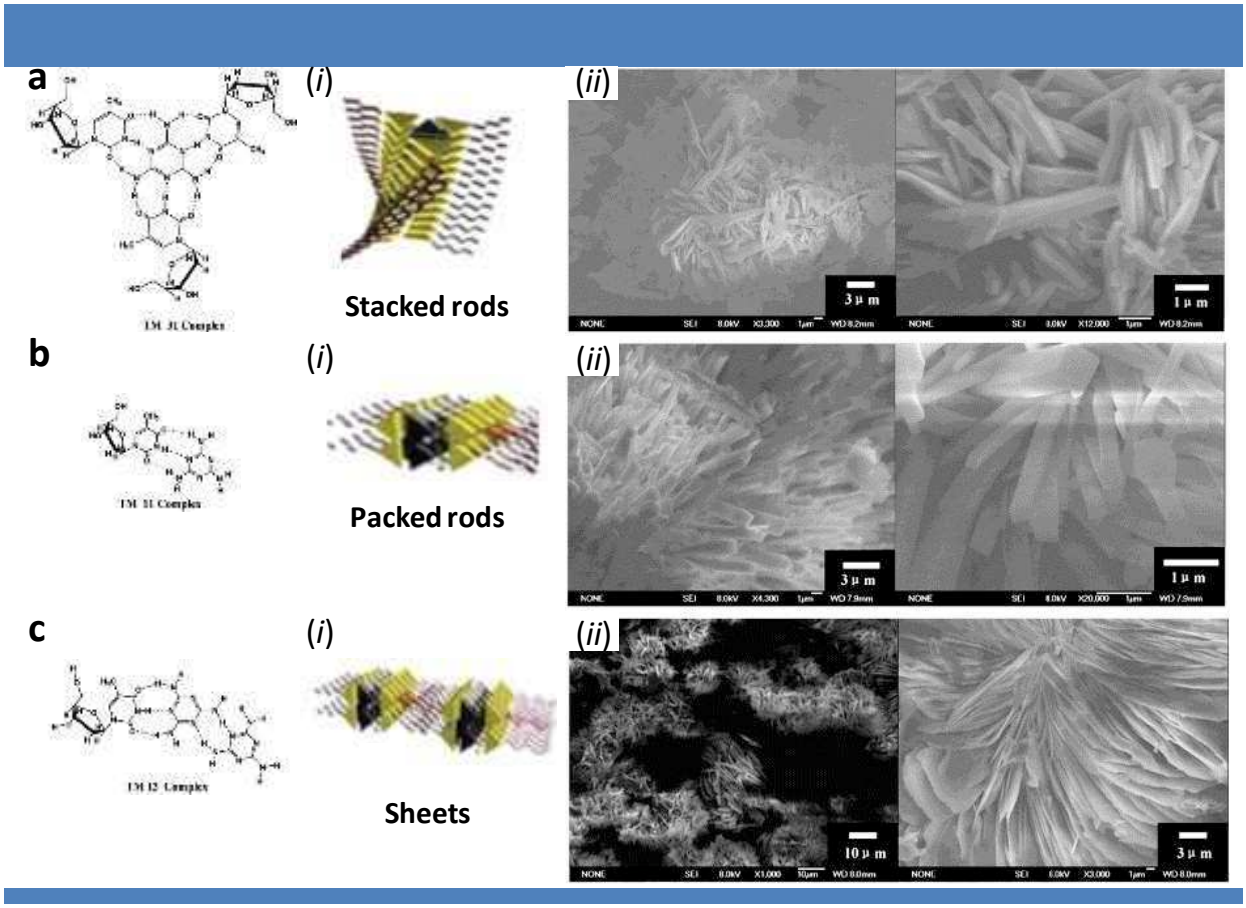

Figure 30 | Schematic illustration of the self-assembly of thymidine-melamine complexes obtained for different ratio of thymidine and melamine monomers: (a) 3:1, (b) 1:1 and (c) 1:2 with *(i)* their proposed self-assembly patterns and *(ii)* SEM images of the corresponding xerogels. Adapted from reference 160.

Besides molecular design, the ratio between melamine and the nucleobase derivative is an important parameter to control the observed aggregation patterns, as melamine also has the possibility to self-recognize by two hydrogen bonding interactions. For instance, Yu and coworkers reported how the stoichiometry of thymidine (T) and melamine (M) mixtures can

Langmuir **28,** 11153–11163 (2012).

affect the morphology of their corresponding aggregates in water while keeping the macroscopic xerogel properties (**Figure 30**).[160] For instance, when melamine was mixed with 3 equivalents of thymidine (TM 31 complex), FTIR experiments indicated that all N-H bonds from the melamine unit were engaged in hydrogen bond interactions with T. Owing to the π-π stacking ability of M, this TM 31 complex was shown to form short rods with lengths up to 4 µm (**Figure 30A**). For the 1:1 complex (TM 11), FTIR suggested the presence of non-hydrogen bonded N-H for the melamine (small sharp peaks at 3400-3450 cm^{-1}) but SEM images showed similar structures to TM 31 complex albeit with larger widths (up to 800 nm) but shorter lengths (max. 2 µm, **Figure 30B**). Finally, when the xerogel was prepared from an excess of melamine (2 equivalents for one of T), thin sheet-like structures over micrometric distances were recorded by SEM, as a result of hydrogen-bonding network between the melamine residues (**Figure 30C**). This example highlights how stoichiometry is an important parameter to control morphology in multicomponent supramolecular polymers.

Similarly, using a self-assembling peptide decorated on a lysine residue with cyanuric acid which presents potentially two imide faces for melamine binding, the groups of Chen and Yang demonstrated how the quantity of melamine can affect the morphologies of the self-assembled structures (**Figure 31**).[161] While the Nap-FFYGK-CA peptide was found to form fibrillar structures with a diameter of ~25 nm in the absence of melamine in different aqueous media (buffer, milk, urine) (**Figure 31a**), the addition of increasing amount of this aromatic molecule did not disrupt the self-assembled fibrils but led to an increase of their diameters along with the appearance of cross-linking points (**Figure 31b-c**). Interestingly, in the three aforementioned medium, addition of melamine to the peptidic molecule led to the formation of gels, which robustness was found to be dependent on the melamine content, i.e. higher storage and loss modulus for 2 equivalents of melamine. Such SEM and rheological observations are consistent with the formation of fibers hold mainly by hydrogen bond interactions for low melamine contents and with additional π-π stacking for higher melamine contents (**Figure 31**). Overall, this example highlights how supramolecular polymers can be used as sensors to detect melamine at relatively low concentrations (20 ppm). However, to the best of our knowledge, there are no examples of such polymers which can achieve the high sensing properties of nanomaterials such as gold nanoparticles decorated with thymine residues or polyT DNA strands (ppb range).[162,163,164]

[160] Yu, Z. et al. Morphology-tuning by changing the composition of a binary hydrogel comprising thymidine and melamine. Mater. Sci. Eng. C **31,** 880–884 (2011).
[161] Zhang, J. et al. Visualized detection of melamine in milk by supramolecular hydrogelations. Chem Commun **50,** 12873–12876 (2014).
[162] Qi, W. J., Wu, D., Ling, J. & Huang, C. Z. Visual and light scattering spectrometric detections of melamine with polythymine-stabilized

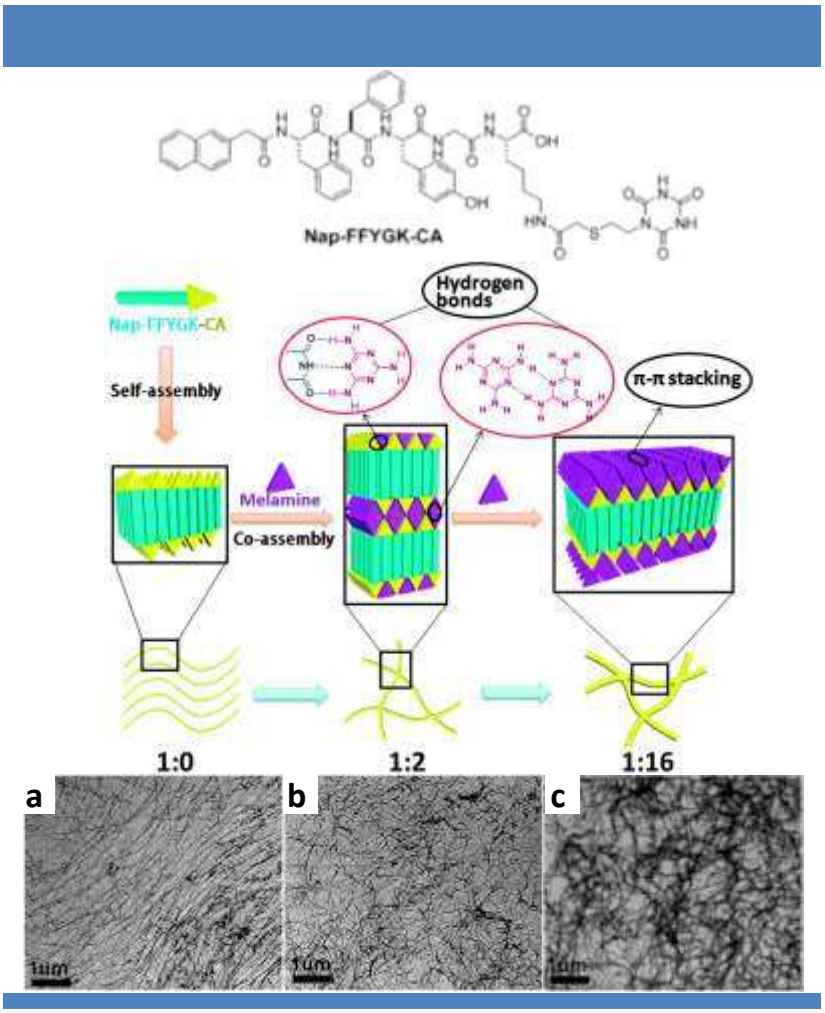

Figure 31 | Molecular structure of Nap-FFYGK-CA and possible molecular arrangements in self-assembled nanofibers of Nap-FFYGK-CA and in gels with different amounts of melamine. a-c. TEM images of (a) solution of Nap-FFYGK-CA and gels made of Nap-FFYGK-CA (a) with 2 equivalents and (c) 16 equivalents of melamine. Adapted from reference 161.

3. DNA-templated self-assemblies

Besides ions and small molecules, DNA macromolecules can be used to trigger the self-assembly of molecules or polymers decorated with nucleobase derivatives. A DNA strand consists of a polymeric phosphate backbone decorated on its side chains with nucleobase residues. Furthermore, DNA displays excellent recognition properties at its nucleobase sites, making this macromolecule a powerful tool to construct 2D or 3D architectures by self-assembly at the nanoscale,[165] as exemplified by the DNA origami technology.[166] Furthermore, the presence of negatively charged phosphate anions and of nucleobases with

gold nanoparticles through specific triple hydrogen-bonding recognition. Chem. Commun. (Cambridge, United Kingdom) **46,** 4893 (2010).

[163] Du, J., Wang, Z., Peng, X. & Fan, J. In Situ Colorimetric Recognition of Melamine Based on Thymine Derivative-Functionalized Gold Nanoparticle. Ind. Eng. Chem. Res. **54,** 12011–12016 (2015).

[164] Li, Y., Xu, J. & Sun, C. Chemical sensors and biosensors for the detection of melamine. RSC Adv. **5,** 1125–1147 (2015).

[165] Jones, M. R., Seeman, N. C. & Mirkin, C. A. Programmable materials and the nature of the DNA bond. Science **347,** 1260901–1-1260901–11 (2015).

[166] Rothemund, P. W. K. Folding DNA to create nanoscale shapes and patterns. Nature **440,** 297–302 (2006).

hydrogen bonding abilities on the DNA backbone have led to the development of various templated strategies involving either positively charged small molecules or small molecules decorated with nucleobases.[126] In the following sections, we will describe some selected examples related to these two templating approaches.

a. DNA-templated self-assemblies without specific recognition

DNA/RNA-templated organizations driven by electrostatic interactions are observed in biological systems, such as for the formation of the Tobacco Mosaic Virus. Inspired by these complex architectures, self-assembled structures involving electrostatic interactions between the negatively charged phosphodiester backbone and small molecules functionalized with positively charged units such as guanidinum[167, 168] or spermine[169] groups have been developed. For instance, the groups of Surin and Ulrich[168] studied the interaction of three guanidinium centered compounds with single strand DNA using a combination of optical spectroscopies (UV-Vis, fluorescence, circular dichroism) and mass spectrometry (**Figure 32**).

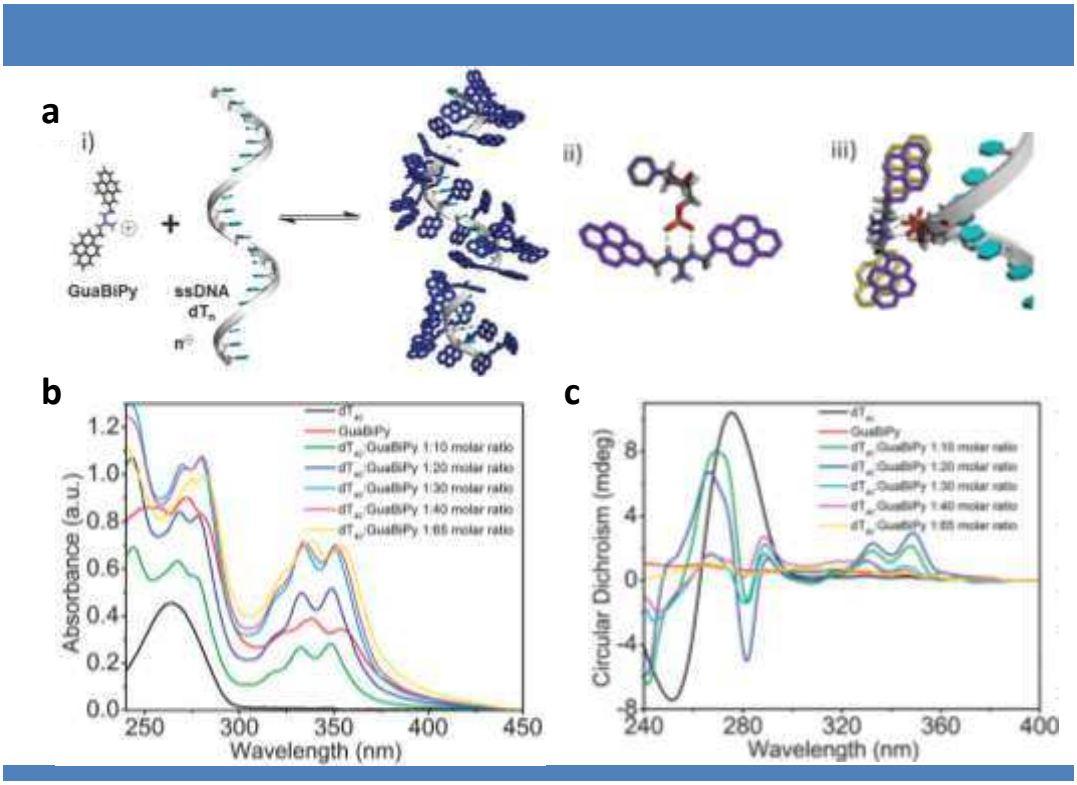

Figure 32 | (a). (i) Schematic representation of DNA-templated self-assembly with GuaBiPy, and the different types of intermolecular interactions: (ii) guanidinium–phosphodiester salt bridge and (iii) π-stacking with the pyrene moieties of two adjacent GuaBiPy. (b). UV-vis and (c). CD titration of dT_{40} : GuaBiPy at various molar ratio. Reproduced from reference 168.

[167] Kocsis, I., Rotaru, A., Legrand, Y.-M., Grosu, I. & Barboiu, M. Supramolecular rulers enabling selective detection of pure short ssDNA via chiral self-assembly. Chem. Commun. **52,** 386–389 (2016).

[168] Paolantoni, D. et al. Probing the importance of π-stacking interactions in DNA-templated self-assembly of bisfunctionalized guanidinium compounds. Chem. Commun. **50,** 14257–14260 (2014).

[169] Sargsyan, G., Leonard, B. M., Kubelka, J. & Balaz, M. Supramolecular ssDNA Templated Porphyrin and Metalloporphyrin Nanoassemblies with Tunable Helicity. Chem. - A Eur. J. **20,** 1878–1892 (2014).

For the guanidinium decorated on both sides with a pyrene unit (GuaBiPy), a strong interaction with a ss-DNA made of 40 thymine units (dT_{40}) was observed by UV-Vis titration, as illustrated by the presence of new absorption bands in the 300-400 nm region for dT40-GuaBiPy mixture (**Figure 32b**), and CD experiments which indicated the formation of an helical assembly of the GuaBiPy units (**Figure 32c**). Furthermore, fluorescence experiments showed the appearance of a band at ~470 nm which is a clear signature of the formation of excimers due to π-π stacking interactions of the lateral pyrene units. Overall, these experiments indicated that positively-charged guanidinium compounds have a strong affinity for the negatively-charged DNA backbone and the resulting assembly is further stabilized by π-π interactions of the aromatic moieties.

Interestingly, electrostatic interactions have also been used to trigger the formation of covalent polymers such as polyaniline[170,171] and polythiophene[172], using the DNA strand as template. Although this strategy allows to fabricate DNA nanostructures with interesting properties, this methodology lacks selectivity (that is without discrimination between different chains of nucleobases in the same sample), which might limits its applications.

b. DNA-templated self-assemblies with specific nucleobase recognition

Alternatively, small molecules decorated with nucleobase residues could be used to produce highly ordered nanostructures due to the enhanced recognition properties of nucleobases. Polynucleobases have been used to template the self-assembly of stacks of aromatic chromophores[173,174] and a cooperative effect between the length of the template and the stability of the assembly was observed, as longer templates led to more stable assemblies.[175] In this section, we would like to highlight some selected examples of NDA-tempated nanostructures based on nucleobase recognition and demonstrate that such methology can give rise to well-defined architectures with interesting properties. For instance, the group of Shimizu[176,177,178] reported the co-self-assembly of a oligo(p-phenylene vinylene)

[170] Wang, Z.-G., Liu, Q. & Ding, B. Shape-Controlled Nanofabrication of Conducting Polymer on Planar DNA Templates. Chem. Mater. **26,** 3364–3367 (2014).
[171] Lu, C.-H. et al. Hemin–G-quadruplex-crosslinked poly-N-isopropylacrylamide hydrogel: a catalytic matrix for the deposition of conductive polyaniline. Chem. Sci. **6,** 6659–6664 (2015).
[172] Rubio-Magnieto, J. et al. Chirality in DNA-pi-conjugated polymer supramolecular structures: insights into the self-assembly. Chem Commun **49,** 5483–5485 (2013).
[173] Janssen, P. G. A., Vandenbergh, J., van Dongen, J. L. J., Meijer, E. W. & Schenning, A. P. H. J. ssDNA Templated Self-Assembly of Chromophores. J. Am. Chem. Soc. **129,** 6078–6079 (2007).
[174] Ruiz-Carretero, A. et al. Directing energy transfer in discrete one-dimensional oligonucleotide-templated assemblies. Chem. Commun. (Camb). **47,** 884–886 (2011).
[175] Janssen, P. G. A. et al. Insights into Templated Supramolecular Polymerization: Binding of Naphthalene Derivatives to ssDNA Templates of Different Lengths. J. Am. Chem. Soc. **131,** 1222–1231 (2009).
[176] Iwaura, R. et al. Molecular-Level Helical Stack of a Nucleotide-Appended Oligo(p-phenylenevinylene) Directed by Supramolecular Self-Assembly with a Complementary Oligonucleotide as a Template. J. Am. Chem. Soc. **128,** 13298–13304 (2006).

(OPV) decorated at both ends with thymidylic acid residues and a complementary oligoadenylic acid backbone dA_{20}, which is known to form right-handed helices in neutral water solutions (**Figure 33a**).[176] Thanks to AFM imaging, they showed that the 1:1 mixture of both compounds generates long micrometric fibers with a right-handed helical pitch of around 60 nm and a fiber height of 6.4 nm (**Figure 33b**). Further UV-Vis and CD experiments as a function of concentration and temperature confirmed the right-handed helical arrangement of the OPV molecules in the low millimolar range and suggested that the transition from helical aggregated to non-helical ones occurs in a non-cooperative manner, which is different from what is actually observed for DNA molecules, respectively (**Figure 33b**). All these experiments suggested that the OPV molecules are inserted between two oligomeric dA_{20} backbones and that the helical pitch corresponds to the pilling of around 170 OPV molecules.

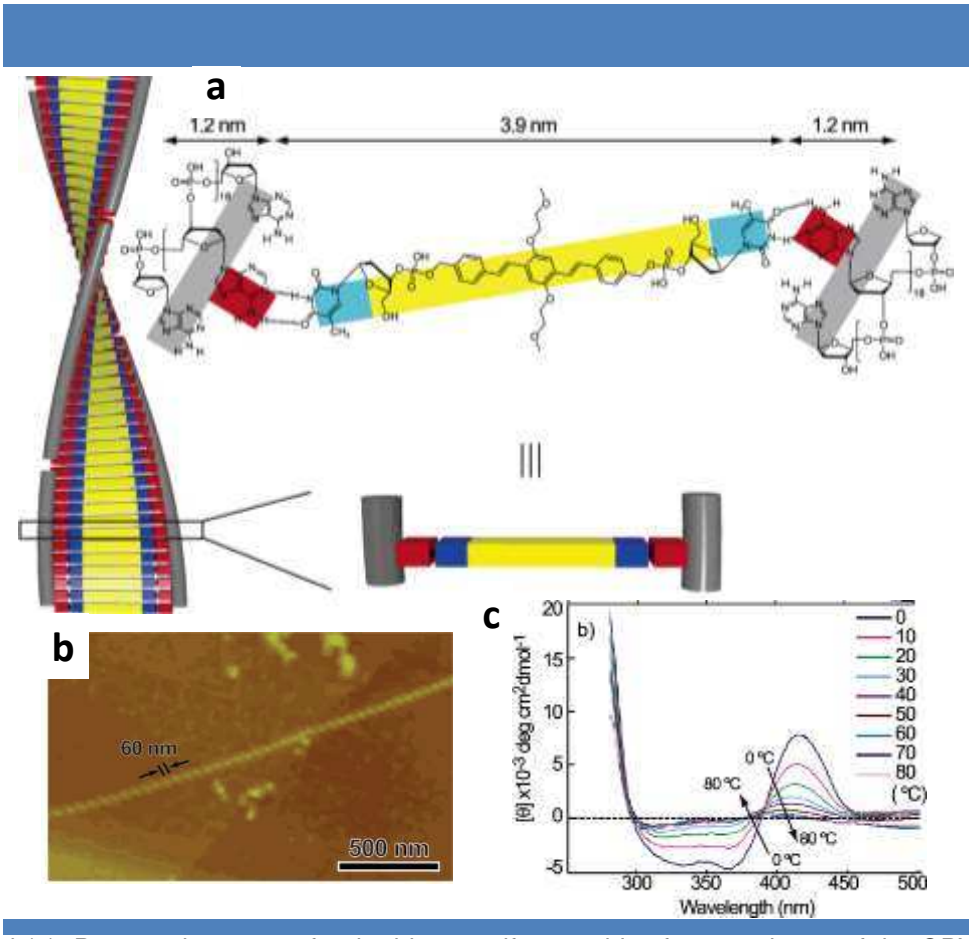

Figure 33 | (a). Proposed structure for the binary self-assembly of a 1:1 mixture of the OPV molecule and dA_{20}. (b). AFM images for the binary self-assembly of a 1:1 mixture of the OPV molecule and dA_{20}. (c). Temperature-dependent CD spectra of the binary self-assembly of a 1:1 mixture of the OPV molecule and dA_{20} in buffer solutions. Reproduced from reference 176.

[177] Iwaura, R. et al. Oligonucleotide-Templated Self-Assembly of Nucleotide Bolaamphiphiles: DNA-Like Nanofibers Edged by a Double-Helical Arrangement of A–T Base Pairs. Angew. Chemie Int. Ed. **42,** 1009–1012 (2003).

[178] Iwaura, R., Kikkawa, Y., Ohnishi-Kameyama, M. & Shimizu, T. Effects of oligoDNA template length and sequence on binary self-assembly of a nucleotide bolaamphiphile. Org. Biomol. Chem. **5,** 3450–3455 (2007).

In another example, the group of Balaz[169] reported the templated self-assembly of a porphyrin derivative decorated with a 2,6-diaminopurine and a ss-DNA made of 40 thymine units (dT_{40}) (**Figure 34a**).

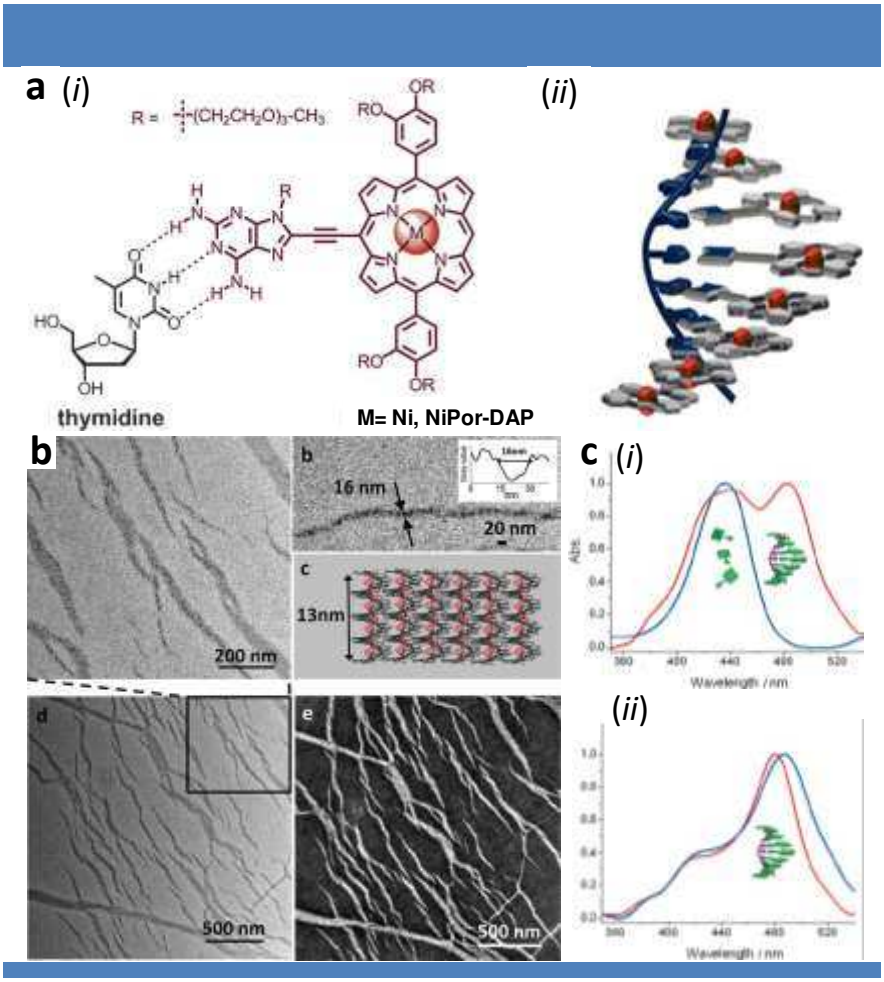

Figure 34 | (a). (i) Molecular structure and hydrogen bonding between porphyrin–diaminopurine conjugate NiPor-DAP and thymidine; (ii) Representation of the right-handed DNA-templated multiporphyrin nanoassembly. (b). TEM images of right-handed fibrils of NiPor-DAP:dT40 nanoassemblies in bright field and dark field modes, grey scale cross-section of the nanowire (inset) and model representation of the NiPor-DAP:dT_{40} nanoassembly and its side-to-side self-assembly into a nanowire (dT_{40} in red and NiPor-DAP in black). (c). UV-vis spectra of NiPor-DAP:dT40 nanoassemblies before (red) and after (blue) dialysis at 20 °C (red) and 85 °C (blue). Reproduced from reference 169.

Extensive UV-vis, fluorescence and CD experiments evidenced the formation of helical supramolecular polymers both in the presence or the absence of nickel ions within the porphyrin core (**Figure 34c**). Interestingly, the annealing rate was found to favor the formation of helices with a single handedness and these structures displayed stabilities for pH ranging from 3 to 12 while being also stable up to 80°C. Further TEM studies of the co-self-assembly of porphyrins with dT_{40} indicated the formation of 1D nanowires of micrometric lengths and with a width of around 16 nm (**Figure 34b**). Such width is consistent with the helical arrangement of the porphyrin units around the DNA backbone which further

aggregates by side-to-side interactions of the triethylene glycol chains. It is noteworthy that the presence of nickel ions could evidence the presence of the porphyrin units with the nanofibers in the dark-field imaging mode.

Overall, these examples demonstrate that small molecules decorated with nucleobase moieties can be used to form well-defined DNA-tempated nanostructures.[179] Importantly, the size of the nanostructure is usually governed with the length of the DNA bakcbone, demonstrating the excellent cooperativity between the different self-assembling processes. Finally, it is important to note that such templated strategies can be used to produce functional materials with properties inherent to the templated self-assembly of the monomeric units.[180]

In conclusion, we have highlighted some selected examples of supramolecular polymers produced by templating strategies involving small molecules decorated with nucleobase residues, which ultimately can lead to the formation of functional materials. Considering the functional properties of triarylamine units, the results presented hereafter in this manuscript are related to the design of new molecular units composed of a triarylamine core and nucleobases side chains and the study of their self-assembling properties under various environmental conditions such as light irradiation, presence of metal ions or even small molecules.

[179] (a) Janssen, P. G. A., Brankaert, N. J. M., Vila, X. & Schenning, A. P. H. J. ssDNA templated assembly of oligonucleotides and bivalent naphthalene guests. Soft Matter **6,** 1494 (2010). (b) Surin, M. et al. Supramolecular Organization of ssDNA-Templated π-Conjugated Oligomers via Hydrogen Bonding. Adv. Mater. (Weinheim, Ger. **21,** 1126–1130 (2009). (c) Janssen, P. G. A., Ruiz-Carretero, A., González-Rodríguez, D., Meijer, E. W. & Schenning, A. P. H. J. pH-Switchable Helicity of DNA-Templated Assemblies. Angew. Chemie Int. Ed. **48,** 8103–8106 (2009). (d) Lin, J. et al. On the mechanism of dynamic polymerization via recycled ss-DNA templated assembly of non-natural bases. Chem. Sci. **3,** 2732 (2012).

[180] Stevens, A. L. et al. Energy Transfer in Single-Stranded DNA-Templated Stacks of Naphthalene Chromophores. J. Phys. Chem. C **115,** 10550–10560 (2011).

Results

Chapter 5: Light-triggered self-assembly of triarylamine-nucleobase conjugates

1. Objectives and targeted molecules

We have seen in the previous chapters that, on one hand, triarylamine molecules can produce supramolecular polymers presenting various architectures depending on their molecular design.[58,71,72,73,75] These nanostructures can either be formed directly in non-polar solvents or triggered by an external stimulus such as light or oxidation.[58,70,80] On the other hand, several groups have demonstrated that nucleobases can drive the self-assembly of small molecules into well-defined supramolecular polymers (Chapters 3 and 4). We were wondering if the triarylamine scaffold could be decorated with nucleobase units to access nanostructures that are driven by both building blocks.

We thus designed a series of triarylamine molecules incorporating either one or three identical nucleobases on their extremities, as we know that triarylamines trisamide can self-assemble without an external stimulus into mono-columnar aggregates while mono-substituted triarylamines give rise to bundles of fibers upon oxidation (**Figure 35**).

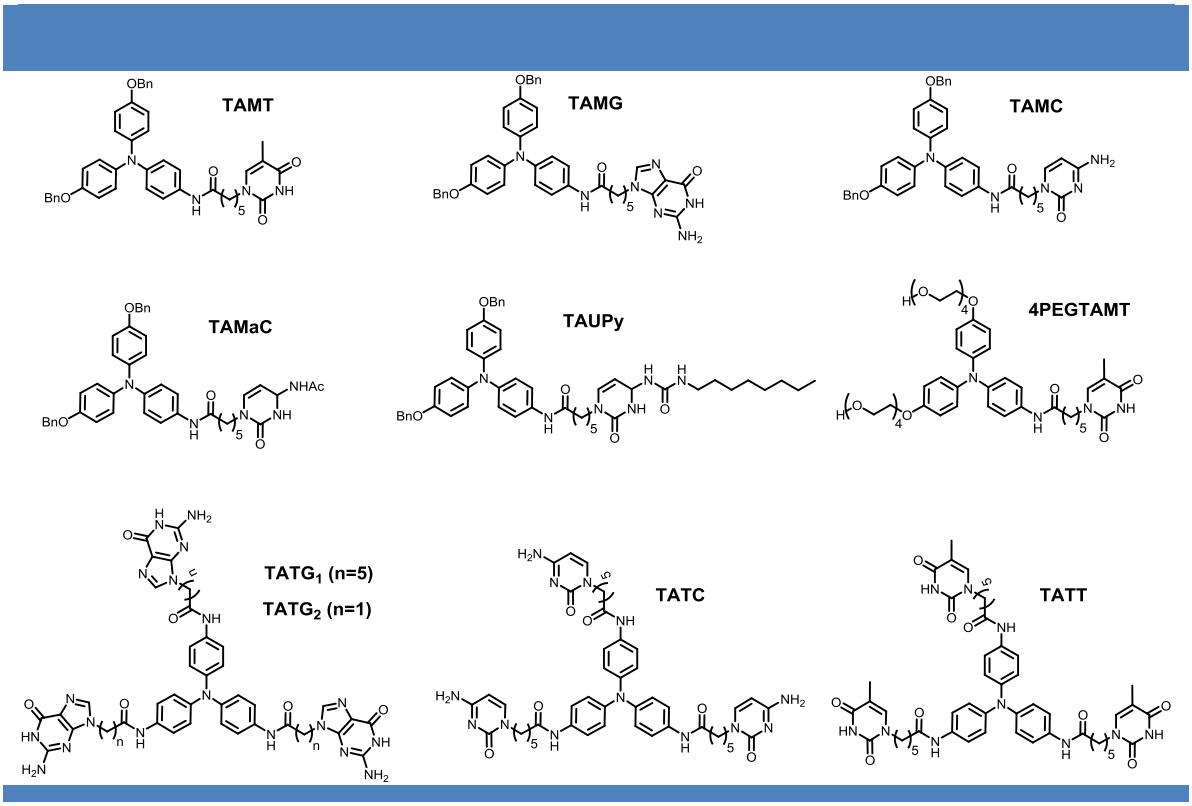

Figure 35| Molecular structures of all triarylamine-nucleobase conjugates synthesized for this work.

Our study aims at demonstrating that nucleobases do not alter the self-assembling propensity of triarylamine molecules while being a secondary building block for further polymerization into ordered architectures. In this chapter, we will first report on the synthesis of all triarylamine-nucleobase conjugates depicted in **Figure 35** and characterize their self-assembling properties upon light irradiation using a series of physico-chemical analyses.

2. Synthesis of targeted molecules

Synthetic routes that were designed to access all molecules displayed on **Figure 35** are highly convergent as they rely on two key intermediates **TAMBr (11)** and **TATBr (3)**, which are triarylamines molecules with either one or three brominated side chains, respectively. Methylene carbons bearing a bromine atom can then serve as anchoring points to introduce various nucleobases.

The synthesis of mono-substituted triarylamines is reported on **Scheme 1**. Compound **10** was obtained in one step from commercially available building blocks using a modified Ullmann coupling reaction as key process.[58] The nitro group was then reduced using tin chloride into the corresponding amine without affecting the benzyl protecting groups and the aromatic amine derivative was further reacted with 6-bromohexanoyl chloride to yield common intermediate **TAMBr** (**11**) in excellent yield.

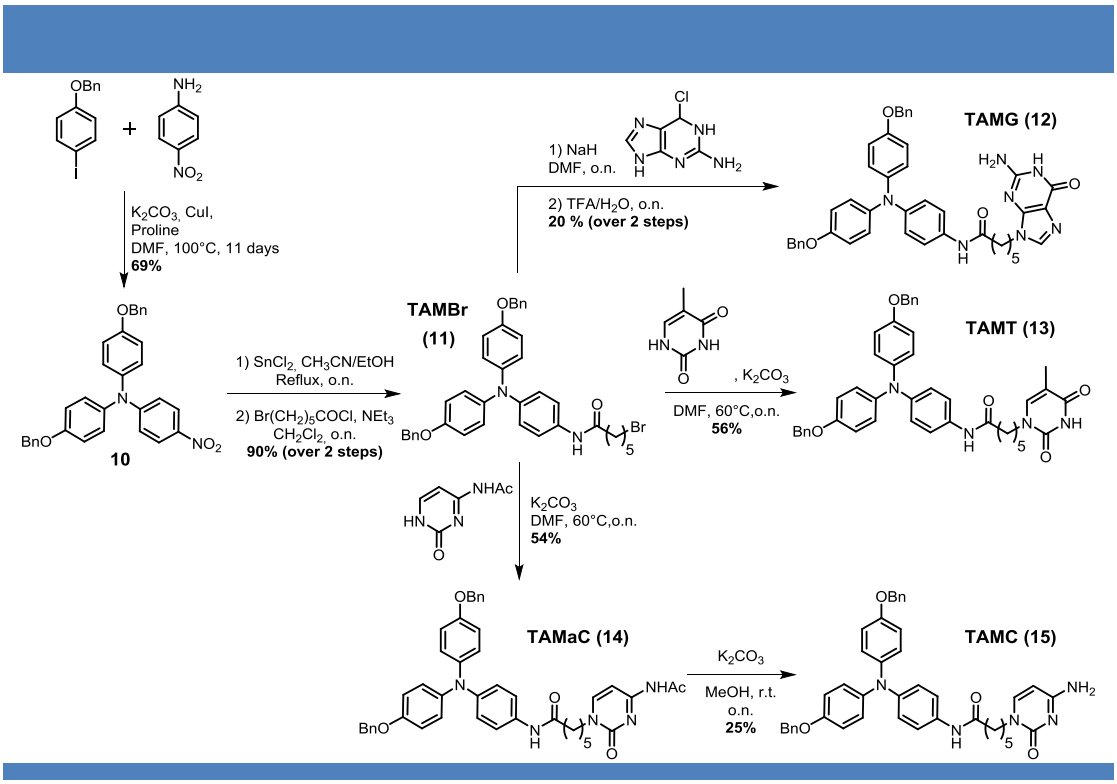

Scheme 1 | Synthesis of MonoTriaryalmine-nucleobase conjugates **TAMG (12)**, **TAMT (13)**, **TAMaC (14)** and **TAMC (15)**.

Guanine **(12)**, thymine **(13)** and cytosine **(15)** derivatives were then obtained in one or two step from **TAMBr** by substitution of the primary bromide with the respective nucleobase, following procedures reported in the literature.[181,182,183] For instance, compound **TAMG (12)** was synthesized in two steps from compound **(11)** and commercially available 2-amino-6-chloropurine after sequential nucleophilic substitution and deprotection of the carbonyl using trifluoroacetic acid. Similarly, compound **TAMC** (**15**) was obtained after nucleophilic substitution with commercially available N4-acetylcytosine and removal of the acetate with potassium carbonate.

One interesting asset of these structures is their potentially easy modification either at the nucleobases or at the phenolic groups (**Scheme 2**). Indeed, nucleobases presenting a primary amine group such as cytosine or guanine can be modified with isocyanate to produce hydrogen bonding arrays such as ureidopyrimidinones (UPy). Such motifs have self-recognition properties with binding constants much higher than self-complementary nucleobases in non polar solvents. In this work, we synthesized ureidopyrimidinone derivative **TAUPy (16)** in one step from the cytosine derivative **(15)** and commercially available octyl isocyanate in decent yield after purification by reverse-phase preparative HPLC.

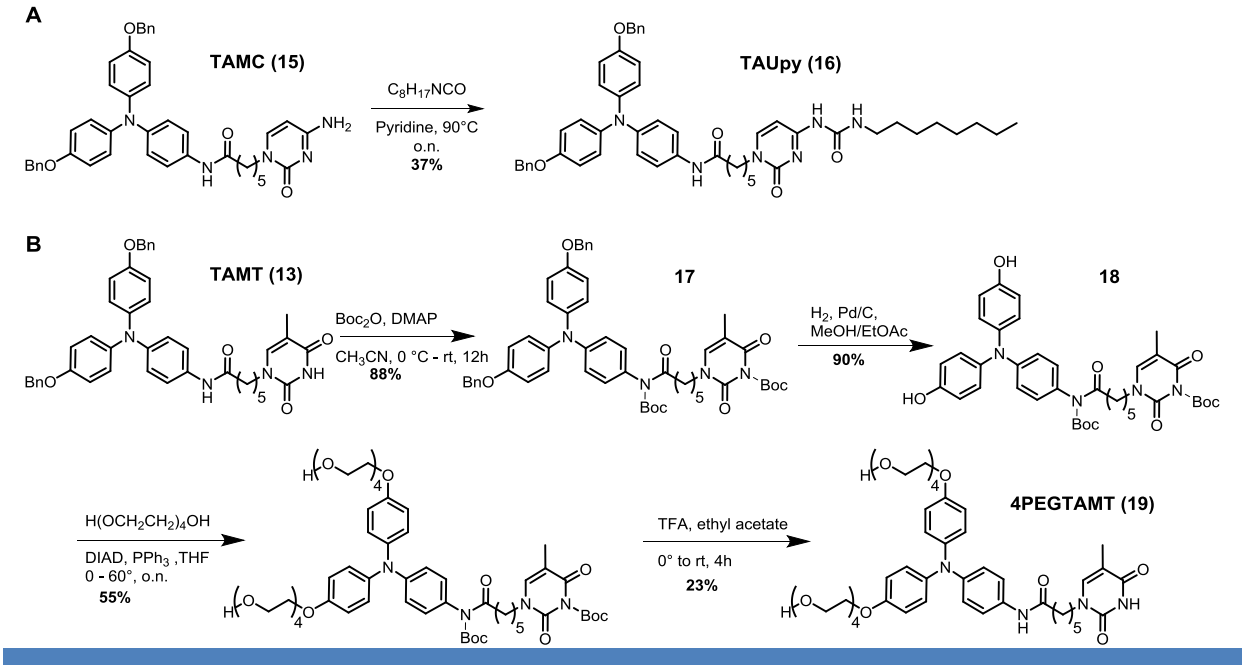

Scheme 2 | Synthesis of A) monotriaryalmine-ureidopyrimidinone derivative **TAUPy (16)** and B)

[181] Kramer, R. A., Bleicher, K. H. & Wennemers, H. Design and Synthesis of Nucleoproline Amino Acids for the Straightforward Preparation of Chiral and Conformationally Constrained Nucleopeptides. Helv. Chim. Acta **95,** 2621–2634 (2012).

[182] Greco, E. et al. Cytosine modules in quadruple hydrogen bonded arrays. New J. Chem. **34,** 2634 (2010).

[183] Tan, H. et al. Biological self-assembly of injectable hydrogel as cell scaffold via specific nucleobase pairing. Chem. Commun. **48,** 10289 (2012).

tetraethyleneglycol-monotriaryalmine-thymine conjugate **4PEGTAMT (19)**.

Alternatively, phenol groups can be deprotected by hydrogenolysis and further modified with any side chain presenting well-defined properties such as hydrophilic ethylene glycol units. We first attempted to directly enter tetraethylene glycol chains on the benzyl-deprotected **TAMT** molecule. However, either Mitsunobu reaction or nucleophilic substitution resulted in the concomitant alkylation of the phenol units and the imide moiety. Therefore, we first protected the imide and amide moieties of **TAMT** with Boc groups and then proceeded to the hydrogenolysis of the benzyl groups. Subsequent Mitsunobu reactions between the resulting free phenol units and commercially available tetraethylene glycol followed by deprotection of the imide and amide units using trifluoroacetic acid afforded compound **4PEGTAMT** (**19**) in 23 % yield after purification by reverse phase HPLC.

Following similar synthetic procedures, triarylamines trisamide molecules decorated with one nucleobase on each side chain were synthesized. Compound **1** was obtained from an aromatic nucleophilic substitution reaction between of p-phenylenediamine and p-fluoronitrobenzene in basic conditions (**Scheme 3**).[80]

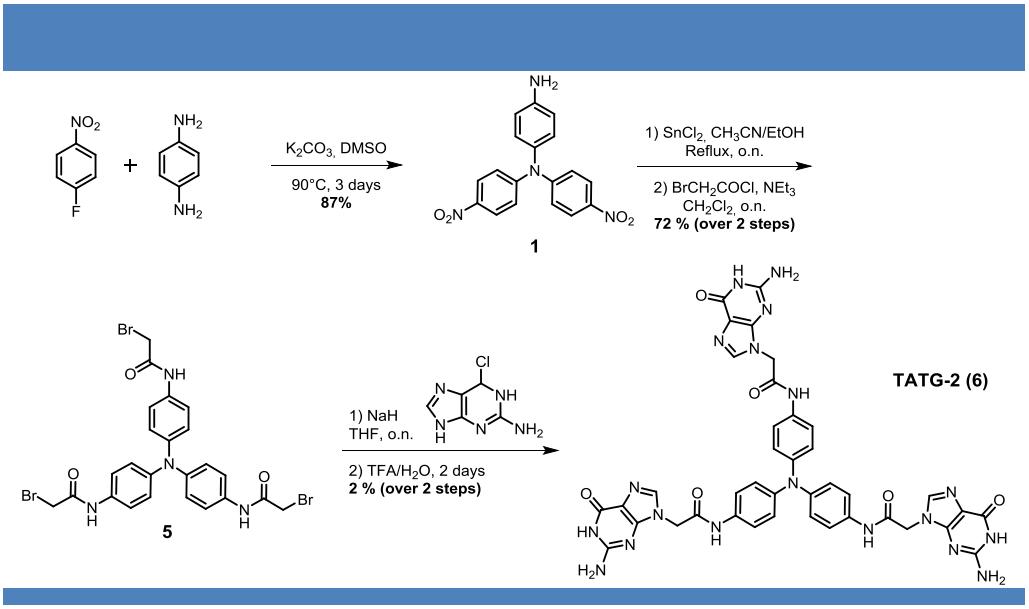

Scheme 3 | Synthesis of TrisTriaryalmine-nucleobase conjugates **TATG-2 (6)**.

After reduction of the nitro groups into the corresponding amines using tin chloride, amidation using bromoacetyl chloride provided compound **5** as a potential intermediate to access various nucleobases derivatives. Further nucleophilic substitution with 2-amino-6-chloropurine and deprotection using trifluoroacetic acid afforded compound **6** in very low yield. Indeed, one main problem associated with **TATG-2** was its solubility in all solvents (non-polar, polar, aqueous solutions). Thus, we decided to use a longer spacer

between the triarylamine core and the nucleobase in order to improve the solubility in organic solvents (**Scheme 3**). Following a sequence identical to the one used to reach compound **5**, common intermediate **TATBr** (**3**) was obtained in two steps and good yields from compound **1** and commercially available 6-bromohexanoyl chloride.

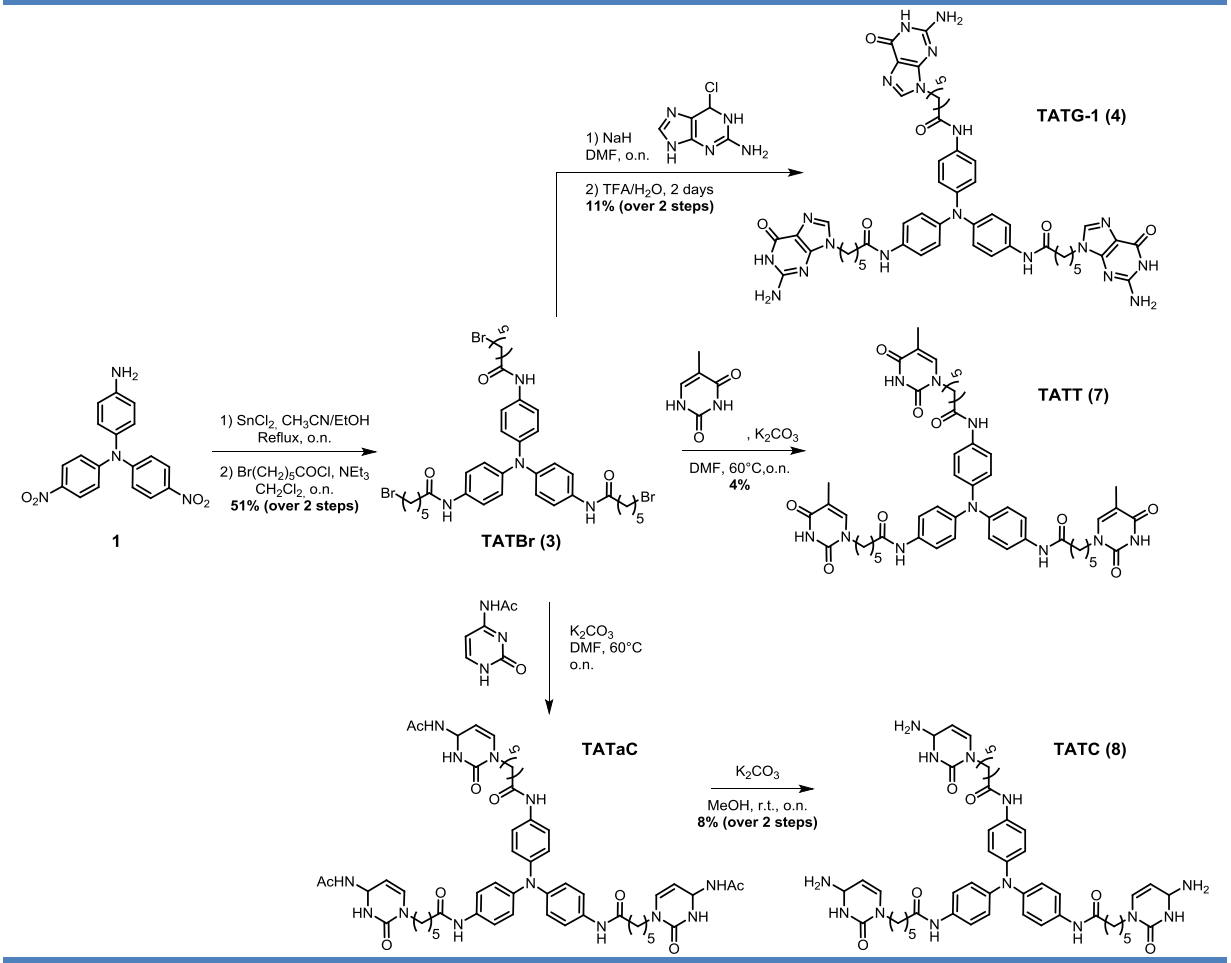

Scheme 4 | Synthesis of TrisTriarylamine-nucleobase conjugates **TATG-1 (4)**, **TATT (7)** and **TATC (8).**

All guanine **(4)**, thymine **(7)** and cytosine **(8)** derivatives were obtained from this intermediate following identical procedures to the ones developed for the mono derivatives, albeit in lower yields after reverse-phase preparative HPLC. We found out that these low yields might come from the poor solubility of these triarylamines trisamide derivatives in common organic solvents. For instance, the guanine derivative **TATG-1** was found to be only soluble in dimethylsulfoxide while **TATT** was soluble in methanol or even in a toluene/methanol (5:3) mixture. Thus, further studies on the self-assembling properties of tris-triarylamine-nucleobase conjugates were conducted only on the thymine **TATT** derivative.

3. Characterizations of the light-triggered self-assemblies

Considering the experience of our group with the characterization of triarylamine self-assemblies, we performed systematic studies on the aforementioned compounds to elucidate their possible self-assembling properties upon light irradiation.

a. ^{1}H NMR spectroscopy

^{1}H NMR spectroscopy is the most convenient experiment to study the self-assembly of our triarylamine derivatives. The ^{1}H NMR spectra of all mono-triarylamine derivatives (**12**, **13**, **14**, **15**, **16**, **19**) displayed all the expected set of signals in chloroform just after purification. Interestingly, after exposure to white light (20 W halogen lamp) for 30 minutes, all solutions except for the cytosine derivative **15** turned green and their ^{1}H NMR spectrum dramatically changed (**Figure 36** and **Figures S1-S3**).

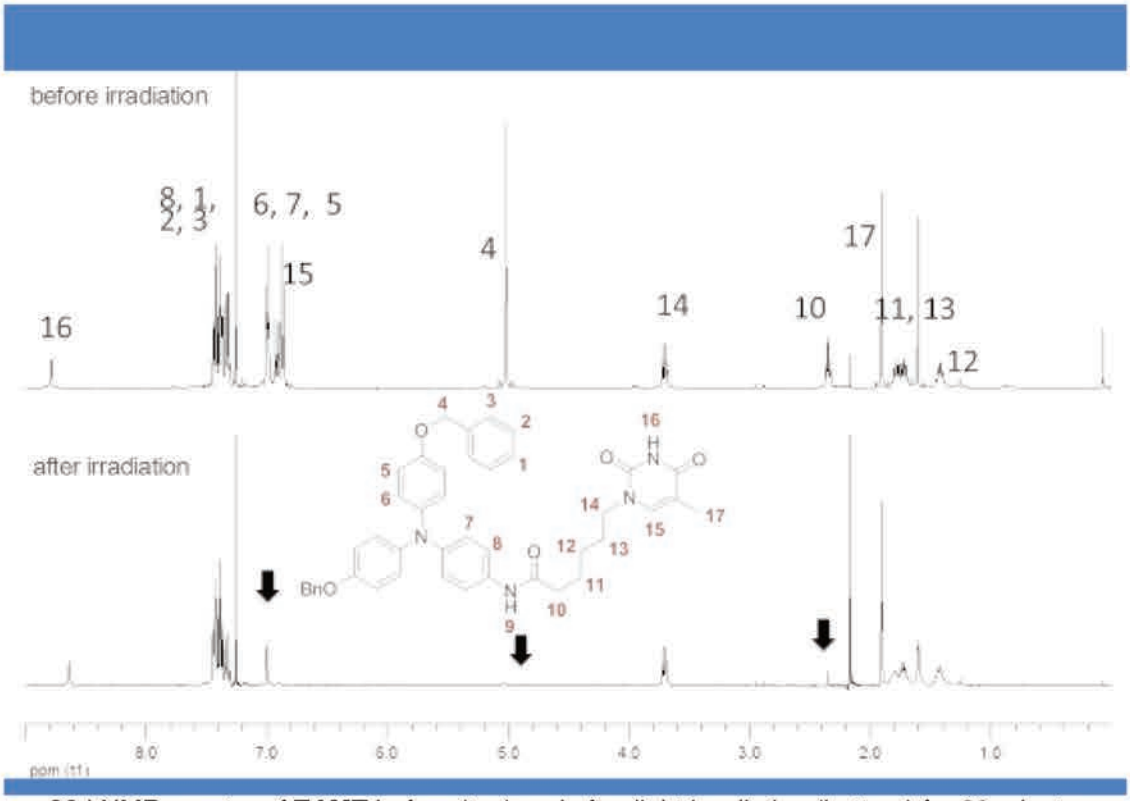

Figure 36 | NMR spectra of **TAMT** before (top) and after light irradiation (bottom) for 30 minutes.

For instance, for the mono-thymine derivative **13**, all ^{1}H NMR signals corresponding to the protons of the triarylamine core (**5-8**) and to the nearest methylene protons (**4**, **10**) disappeared after white light irradiation (**Figure 36**). This phenomenon along with the color change are in agreement with observations made on other triarylamine compounds,[58] suggesting that nucleobases do not influence the formation of triarylammonium radical cations and that the triarylamine core is involved in aggregated structures.

We also probed the ability of the triarylamine-tristhymine derivative **7** to self-assemble in a 5:3 mixture of toluene and methanol containing 5 vol% of chloroform, necessary to induce the formation of radical cations (**Figure 37**).

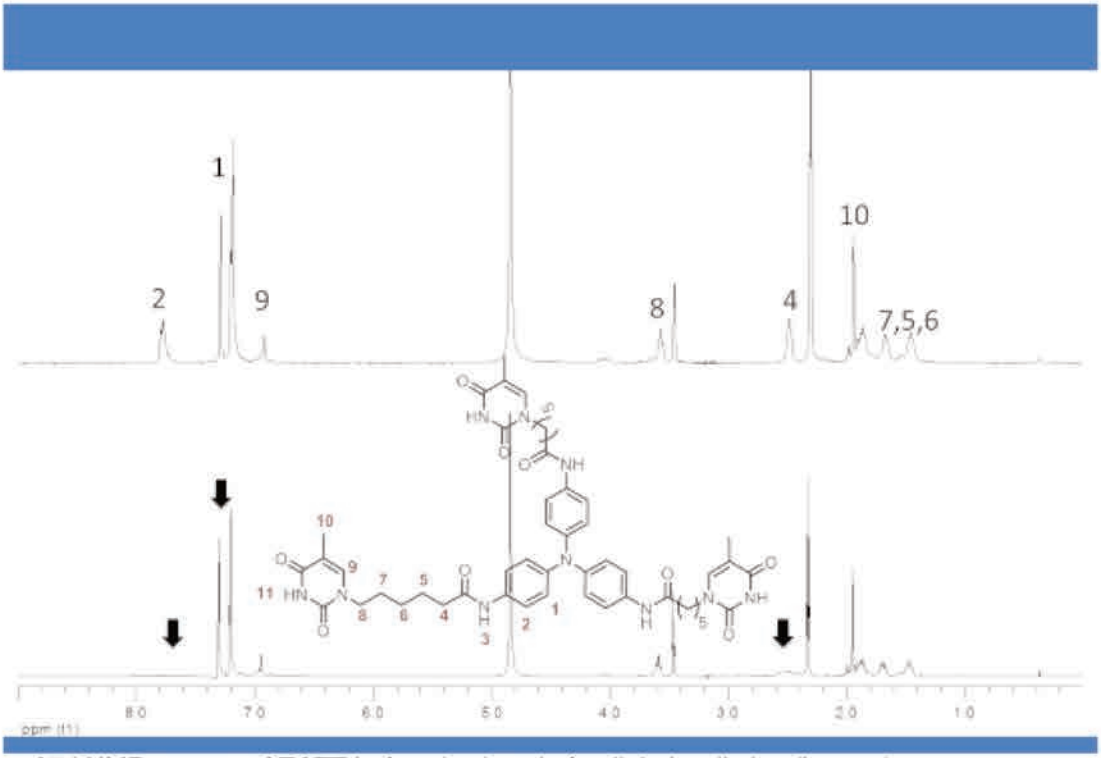

Figure 37 | NMR spectra of **TATT** before (top) and after light irradiation (bottom).

Similarly to what was recorded for the previous mono-triarylamine derivatives and to tris-triarylamine already described by our group,[80] we observed the disappearance of the protons of the triarylamine core (**1,2**) and to the nearest methylene proton (**4**) upon white light irradiation for 30 minutes. These experiments indicate that the presence of guanine or thymine units on the triarylamine core does not affect their self-assembling properties while cytosine completely prohibits this phenomenon.

b. UV-vis-NIR spectroscopy

As we know that the green color of the light-irradiated solution is associated with the presence of triarylammonium radical cations, which present a clear NIR signature at around 800 nm, we probe the light-induced process by UV-Vis-NIR spectroscopy.[58,70] Typically, one triarylamine compound was dissolved at a 0.1 mM concentration in pure deuterated chloroform. UV-Vis-NIR absorption spectra were recorded upon increasing irradiation times using a 20 W halogen power lamp.

As shown on **Figure 38A**, a new absorption band at 805 nm appeared upon light irradiation, which indicates the production of localized triarylammonium radical cations. The

intensity of this band increased with irradiation time until reaching a maximum after irradiating for 40 minutes. Interestingly, this maximum absorption after 40 minutes irradiation is associated with a maximum of absorption of the band at 400 nm, which is related to the self-assembly of triarylamine molecules (**Figure 38B**).

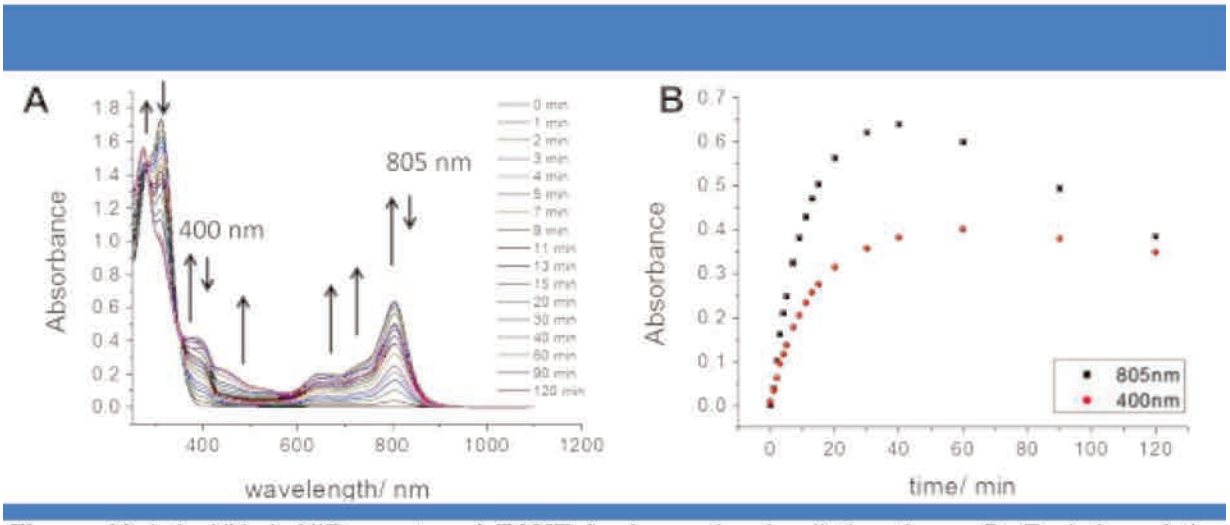

Figure 38 | A. UV-vis-NIR spectra of **TAMT** for increasing irradiation times. B. Evolution of the absorbance at 805 nm (black) and at 400 nm (red) as a function of irradiation time (c = 0.1 mM in chloroform).

Further increased irradiation times led to the decrease of this 805 nm band, while the band at 400 nm remained stable. These observations suggest that, after 40 minutes irradiation, all triarylamine molecules are self-assembled and that further doping with light lead to a reduction of the radical at the extremities of the fibers as already observed with other triarylamine derivatives.[73] Further studies by electron paramagnetic resonance spectroscopy should demonstrate that we reach a maximum of radicals after 40 minutes of irradiation. Similar behaviors were recorded for the acetylcytosine (**14**) and the ureidopyrimidinone (**16**) derivatives albeit with slower kinetics (~ 100 minutes for **16** and no maximum reached for **14** after 120 minutes irradiation), suggesting that longer aggregates might be formed for these derivatives compared to **TAMT** (**Figures S4-S5**). Interestingly, while the overall behavior of the UV-Vis-NIR spectra of **TAMG** upon light irradiation was almost identical to the one of **TAMT**, we observed two main differences: a) a blue shift of the absorbance from 789 nm for short irradiation times to 777 nm for longer ones, and b) the presence of two regimes in the kinetics of irradiation with a crossover of the two regimes at ~ 100 minutes at both 400 and 777 nm (**Figure 39**). We believe that the presence of two regimes in the light irradiation kinetic might be due to two different aggregation processes such as the self-assembly of the triarylamine core and the formation of G-ribbons or G-quartets which affect the packing of the triarylamine units.

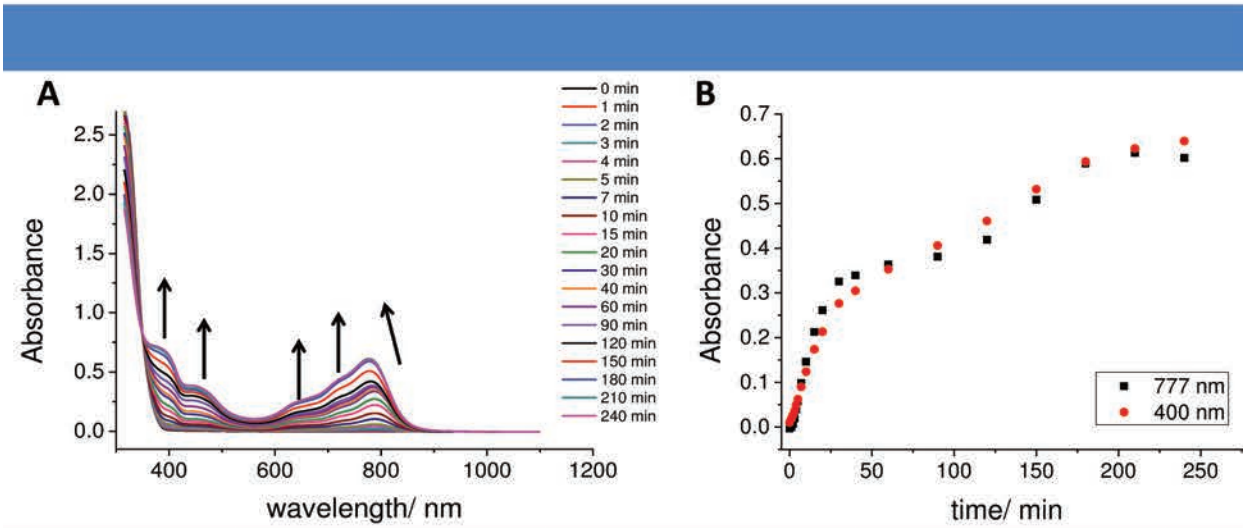

Figure 39 | A. UV-vis-NIR spectra of **TAMG** for increasing irradiation times. B. Evolution of the absorbance at 777 nm (black) and at 400 nm (red) as a function of irradiation time (c = 0.1 mM in chloroform).

Similarly to the ^{1}H NMR experiment, the UV-Vis-NIR kinetic study of **TATT** upon light irradiation was recorded in a 5:3 mixture of toluene/methanol containing 10 vol% of chloroform (**Figure 40**).

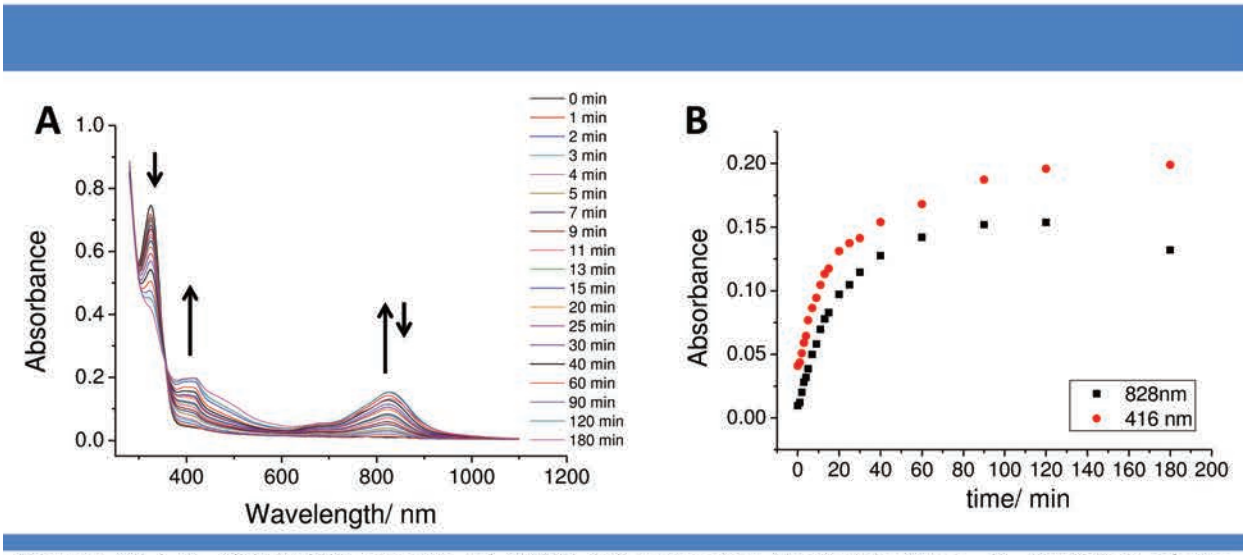

Figure 40 | A. UV-vis-NIR spectra of **TATT** for increasing irradiation times. B. Evolution of the absorbance at 828 nm (black) and at 416 nm (red) as a function of irradiation time (c = 0.1 mM in a 5:3 mixture of toluene/methanol with 10 vol% chloroform).

Compared to the mono-triarylamine thymine derivative (**13**), compound **7** displayed a slower kinetic (maximum of absorption reached after 120 minutes instead of 40 minutes), suggesting the formation of longer aggregates. However, we should mention that the NIR absorption behavior of this triarylamine trisamide compound is different from the one recorded previously by our group as no intermolecular charge-transfer band at around 1100 nm is recorded for **TATT**.[80] This observation might suggest that the presence of thymine

residues on the tris-triarylamine core affect the molecular arrangement of the triarylamine units in the self-assembled structure.

c. Fluorescence spectroscopy

Considering that the absorbance at 400 nm corresponds to the triarylamine self-assembly, we then probed the emission of the self-assembled structures by fluorescence spectroscopy ($\lambda_{excitation}$ = 400 nm). For the monotriarylamine-thymine derivative **13,** we observed the appearance of a broad structure-less band at ~ 546 nm, which intensity increases with increasing irradiation times (**Figure 41**).

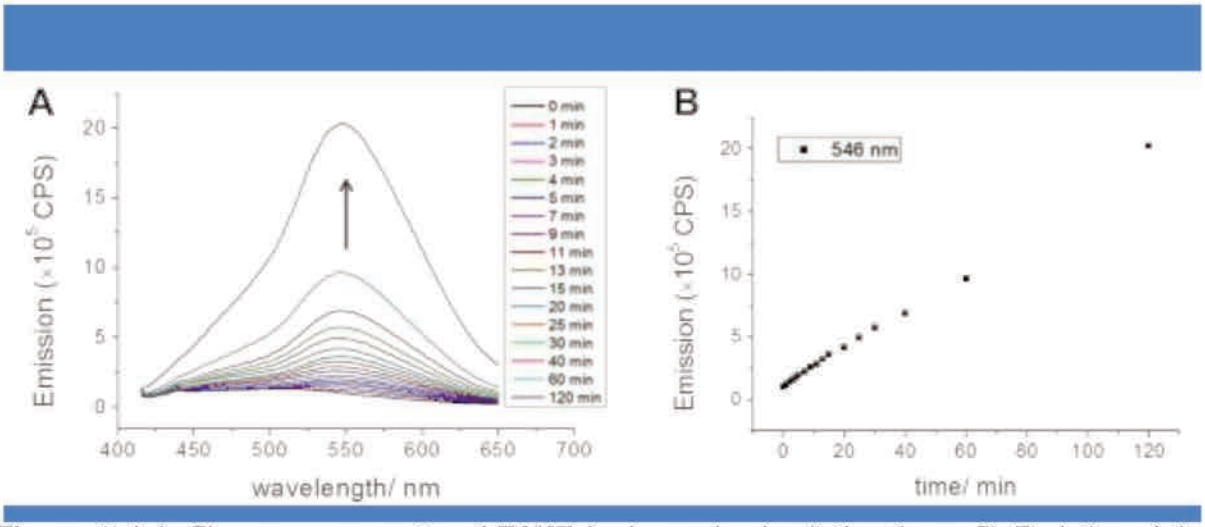

Figure 41 | A. Fluorescence spectra of **TAMT** for increasing irradiation times. B. Evolution of the emission intensity at 546 nm (black) as a function of irradiation time (c = 0.1 mM in chloroform, $\lambda_{exc.}$ = 400 nm).

These measurements indicate an aggregation induced emission (AIE) phenomenon as already observed in similar triarylamine self-assemblies,[72,73] and which might be due to restriction of intramolecular rotations of the triarylamine units in aggregates.[184,185] A similar behavior was recorded for the guanine (**12**) and ureidopyrimidinone (**16**) derivatives with an increased emission intensity at 539 and 537 nm, respectively (**Figure 41A** and **Figure S5B**). The presence of a shoulder emission band at around 460-470 nm for both molecules might suggest the presence of remaining free triarylamine molecules or small oligomers. For the monoacetylcytosine derivative (**14**), a lag time of around 20 minutes was observed before the emission intensity at 536 nm started to increase and the one at ~ 450 nm decreased to its minimum intensity (**Figure S4B**). This observation suggests that the formation of large aggregates is not favored for **TAMaC**, which is in agreement with the longer kinetics

[184] Ning, Z. et al. Aggregation-induced Emission (AIE)-active Starburst Triarylamine Fluorophores as Potential Non-doped Red Emitters for Organic Light-emitting Diodes and Cl2 Gas Chemodosimeter. Adv. Funct. Mater. **17,** 3799–3807 (2007).

[185] He, Q. et al. A Hole-Transporting Material with Controllable Morphology Containing Binaphthyl and Triphenylamine Chromophores. Adv. Funct. Mater. **16,** 1343–1348 (2006).

recorded by UV-Vis-NIR absorption spectroscopy. Finally, we studied the fluorescence kinetic of **TATT** upon light irradiation in a 5:3 mixture of toluene/methanol with 10 vol% of chloroform (**Figure 41**).

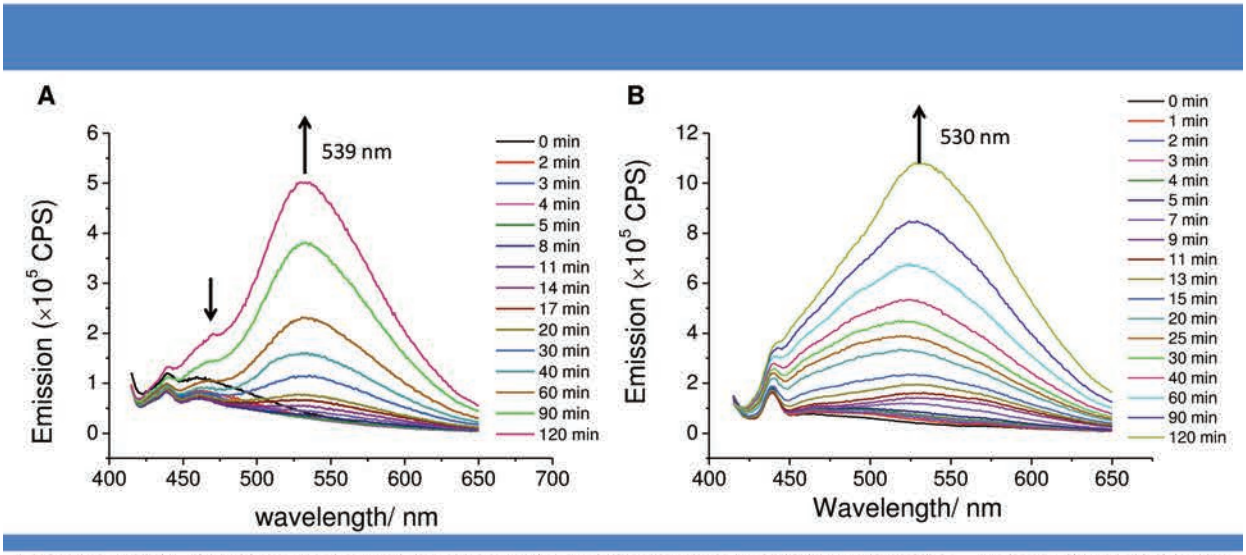

Figure 42 | A. Fluorescence spectra of **TAMG** for increasing irradiation times (c = 0.1 mM in chloroform, $\lambda_{exc.}$ = 400 nm). B. Fluorescence spectra of **TATT** for increasing irradiation times (c = 0.1 mM in a 5:3 mixture of toluene/methanol with 10 vol% chloroform, $\lambda_{exc.}$ = 400 nm).

The behavior recorded for this tris-triarylamine molecule is very similar to the one recorded for compounds **12**, **13** and **15**, but is very different from the ones recorded for supramolecular polymers made of tris-triarylamine molecules, which display and aggregation-induced quenching behavior.[80] This observation is in agreement with UV-Vis-NIR experiments which suggest that **TATT** molecules do not self-assemble in monocolumnar aggregates as "classical" triarylamine trismaide molecules do.

d. Additional experiments

We then tried to probe the morphologies of the various supramolecular polymers made of **7**, **12**, **13**, **14** and **16** by transmission electron and/or atomic force microscopy. However, we could never observe any well-defined structures in the solvents used for light-induced kinetic measurements. For the tris-triarylamine molecule **TATT** decorated with thymine residues, we manage to record the formation of spherical aggregates in a chloroform/toluene/methanol mixture (50/45/5 vol%), which size becomes larger and less polydisperse after light irradiation for 90 minutes (**Figure 43**). This observation was confirmed by dynamic light scattering experiments which indicate a mean diameter of 526 nm (± 250 nm) before irradiation and of 717 nm (± 154 nm) after light irradiation. Further experiments will have to be conducted in order to better understand the molecular arrangements of the triarylamine units in these spherical aggregates.

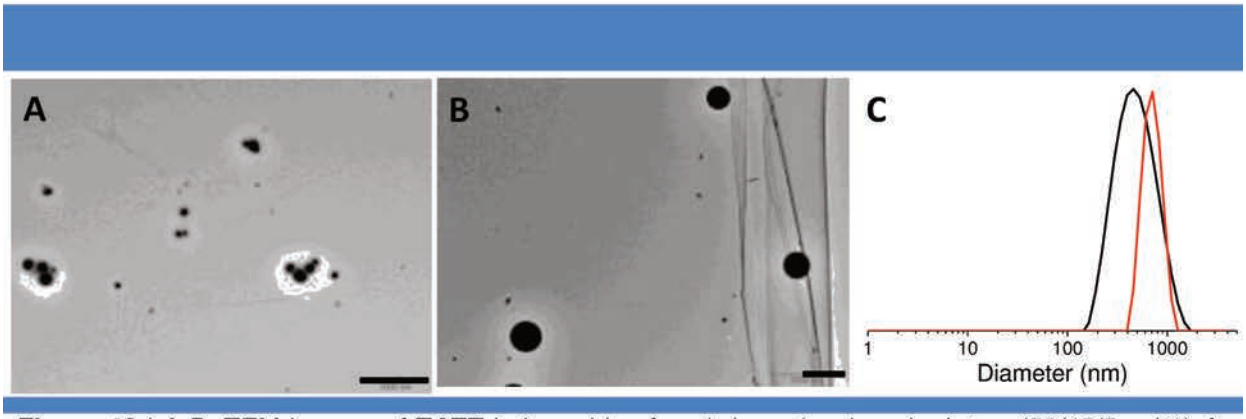

Figure 43 | A-B. TEM images of **TATT** in in a chloroform/toluene/methanol mixture (50/45/5 vol%) A. before irradiation (c = 1 mM, scale bar: 1 µm) and B. after irradiation (c = 0.1 mM, scale bar: 1 µm); C. Distributions of hydrodynamic diameters observed for **TATT** before (black) and after (red) light irradiation for 90 minutes.

For the monotriarylamine-thymine derivative **13**, complementary small angle and wide angle X-ray scattering (SAXS and WAXS) experiments were performed in order to elucidate the molecular arrangement of the molecules. These analyses were performed on powders obtained by drying a 10 mM solution of **TAMT** in chloroform before and after light irradiation for one hour (**Figure 44**).

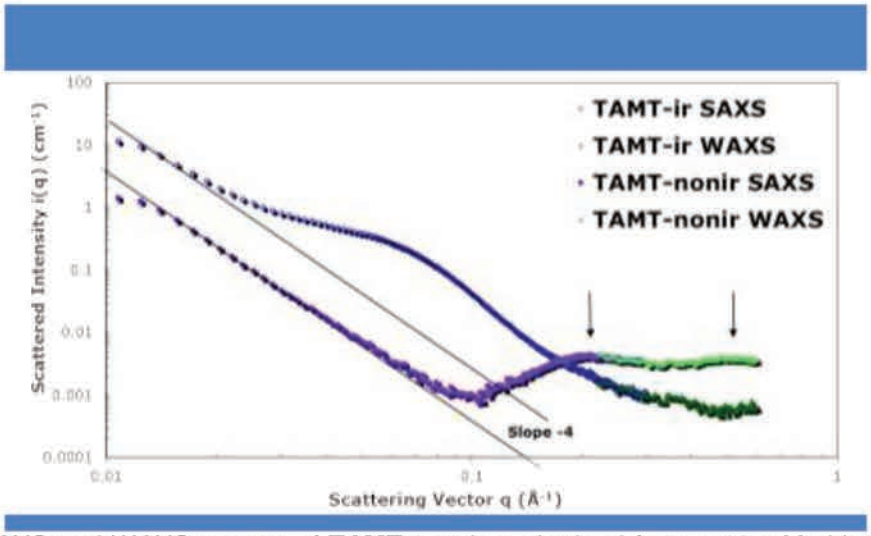

Figure 44 | SAXS and WAXS spectra of **TAMT** powders obtained from a 10 mM chloroform solution before and after light irradiation for 1 hour.

However, one main problem associated with the use of powders is the presence of air-solid interfaces characterized by a q^{-4} slope at low q (below 0.1 $Å^{-1}$) which preclude any analysis of the data in this q range. For the non-irradiated sample, two broad Bragg peaks located at ~ 0.2 $Å^{-1}$ and 0.5 $Å^{-1}$ were observed, which corresponds to distances of ~ 31.4 Å and 12.6 Å, respectively according to Bragg's equation. Based on molecular modelling performed on simple triarylamine molecules,[70] we can assume that these distances can correspond to dimeric structures either produced by intermolecular self-recognition of two

thymine residues or by intermolecular hydrogen bonding of the amide moieties. Further experiments such as infrared spectroscopy should be performed in order to discriminate between both arrangements. Surprisingly, these two broad Bragg peaks were not present on the light-irradiated powder but might be masked by the concentration fluctuation observed at around 0.07 $Å^{-1}$, which corresponds to an ordered self-assembly as large as 9.0 nm. Furthermore, the higher scattered intensity for the irradiated sample observed for q values below 0.1 $Å^{-1}$ indicated a higher electron density, which might be related to the presence of larger aggregates. Although these scattering experiments remain preliminary and deserve a more detailed analysis, they suggests that larger ordered nanostructures are formed by **TAMT** after irradiation.

4. Discussion

This series of spectroscopic experiments evidenced the formation of supramolecular polymers for monotriarylamine molecules decorated with guanine (**12**), thymine (**13**), acetylcytosine (**14**) and ureidopyrimidinone (**16**) moieties and triarylamine triasmide presenting thymine residues as end chain groups. However, so far, it proved difficult to elucidate the molecular arrangement and supramolecular morphologies of the aggregates by scattering and microscopy experiments.

For the TrisTriarylamine-thymine molecule, spectroscopic data suggest a different molecular arrangement of the triarylamine core compared to the triarylamines trisamide already reported by our group,[80] which arrange in mono-columnar aggregates. Optical spectroscopic behaviors suggest an arrangement similar to the one encountered in monotriarylamine derivatives, i.e. formation of intermolecular hydrogen bonds between neighboring molecules and arrangement of the triarylamine core in a snowflake pattern.[70] Such arrangement would be reminiscent of the one observed in highly order triarylamine trisamide crystals.[186]

Finally, one important result of this chapter is related to the propensity of cytosine to prohibit the disappearance of ^{1}H NMR signals upon light irradiation. Compared to other nucleobase residues, cytosine features a primary amine, which cannot be involved in a strong hydrogen bonding network, as opposed to guanine which can be engaged in G-ribbons or G-quartet (see chapter 3). We believe that the presence of this primary amine prohibit the formation of radical cations necessary to induce the formation of self-assembled structures. In

[186] Armao, J. J., Rabu, P., Moulin, E. & Giuseppone, N. Long-Range Energy Transport via Plasmonic Propagation in a Supramolecular Organic Waveguide. Nano Lett. **16,** 2800–2805 (2016).

order to probe this hypothesis, we performed two control experiments. First, we recorded the FT-IR spectra of **TAMG** before and after irradiation (**Figure 45**).

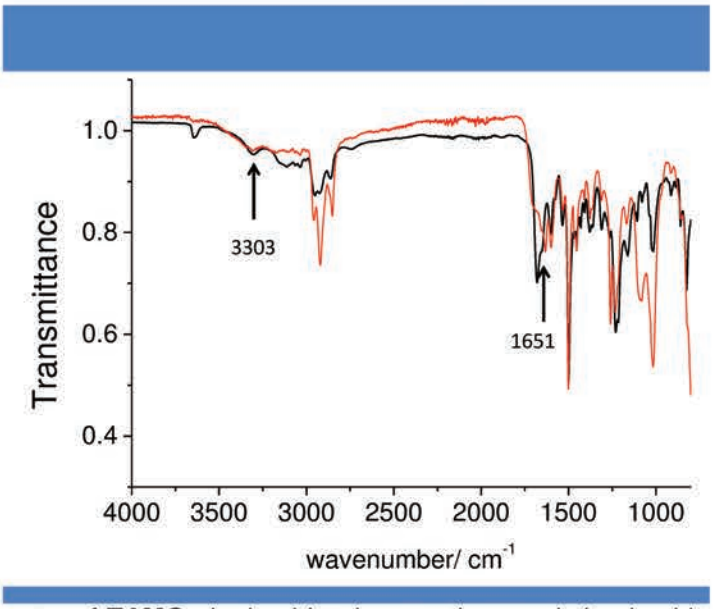

Figure 45 | FT-IR spectra of **TAMG** obtained by drop-casting a solution in chloroform before (black) and after light irradiation for 1 hour (red).

The absence of free NH stretching band at 3495 cm^{-1} along with the presence of a should peak at 1651 cm^{-1}, possibly attributed the in-plane C=O deformation peak, suggest that guanine residues are involved in hydrogen bond network and thus do not desactivate the light-induced process. Second, we studied the light-responsiveness of a 1:1 mixture of **TAMG** and **TAMC** in chloroform (**Figure 46**).

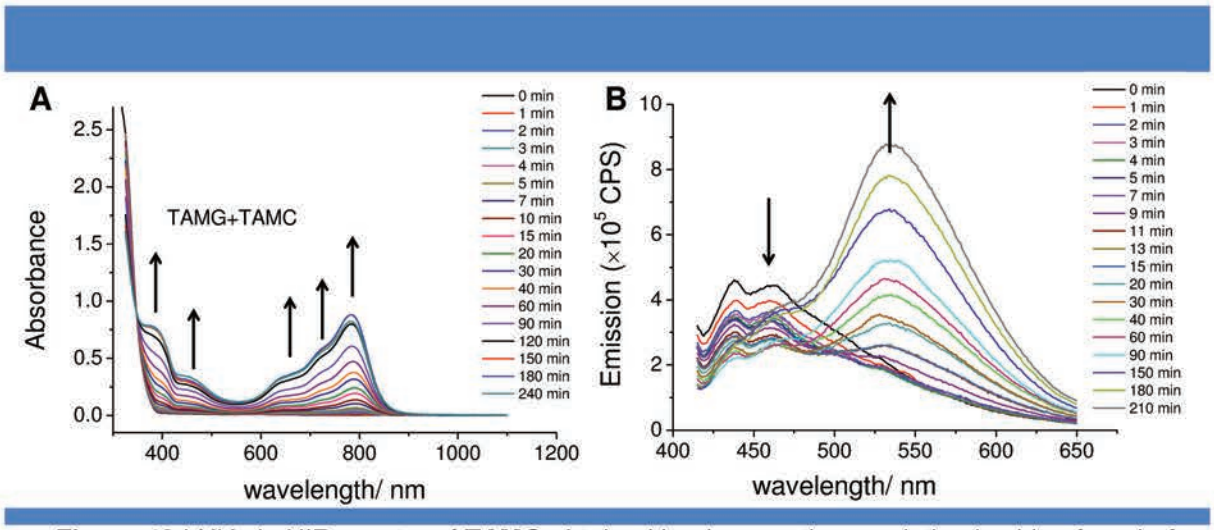

Figure 46 | UV-vis-NIR spectra of **TAMG** obtained by drop-casting a solution in chloroform before and after light irradiation for 1 hour.

Comparison of the ^{1}H NMR spectra of this complex before and after light irradiation indicate the complete disappearance of the proton signals corresponding to the triarylamine core and to the nearest methylene protons, thus suggesting that TAMC and TAMG are

oxidized upon light irradiation. This behavior was further confirmed by UV-Vis-NIR and fluorescence experiments on a solution of this 1:1 complex in chloroform (**Figure 38**). The spectroscopic behavior of this complex is very similar to the one recorded for other triarylamine molecules in this chapter. It consists in an increase of the absorption intensities at 782 and 400 nm and of the emission intensity at 534 nm and in a decrease of the emission intensity at around 450 nm, which is typically related to the presence of molecularly dissolved triarylamine molecules. Furthermore, we found that this 1:1 **TAMG/TAMC** complex give rise to the formation of sheet-like structures with various aspect ratio after light irradiation, while we have not been able to image the formation of any structure for **TAMG** supramolecular polymers (**Figure 47**).

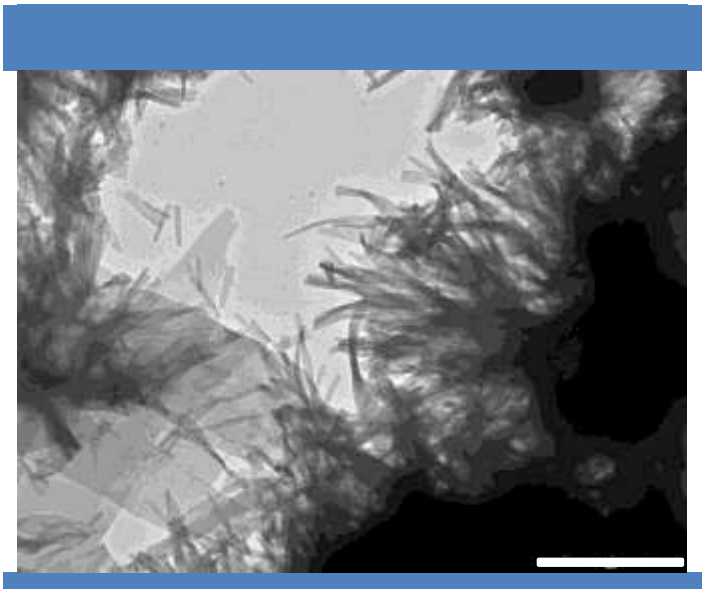

Figure 47 | TEM image of the 1:1 **TAMG/TAMC** complex in chloroform solution upon light irradiation for one hour (Scale bar: 1 µm).

Although this study on the **TAMG/TAMC** complex deserves more experiments, in particular, regarding the possible molecular arrangement of the triarylamine units which lead to these well-organized structures, it clearly demonstrates that the monotriarylamine-cytosine conjugate has to be involved in a hydrogen bonding network in order to give rise to the formation of supramolecular polymers. At large, these results suggest that the presence of any primary amine on the triarylamine structure either on its core or as side chain will preclude any self-assembly process by prohibiting the light or chemically induced oxidation of the triarylamine core.

Overall, in this chapter, we have described the synthesis of ten different triarylamine-nucleobase conjugates and studied their light-induced self-assembling properties

in chloroform. Although some of these molecules could not be studied due to solubility issues, we have shown that the presence of nucleobases close to the triarylamine core does not affect its self-assembling properties upon light irradiation, provided that primary amines are embedded in hydrogen bonding network. This work leads to a better understanding of the self-assembly behavior of triarylamine conjugates and will influence the design of self-assembling triarylamine structures.

Chapter 6: Templated self-assembly of triarylamine-nucleobase conjugates

1. Objectives

In the bibliography section, we have highlighted that nucleobases, in particular thymine and guanine, have high and selective affinities for metal ions and small molecules. Most of these studies have been reported in water or aqueous mixtures and give rise to the formation of self-assembled structures upon addition of a chemical stimulus. Furthermore, in the previous chapter, we have shown that nucleobase residues do not affect the propensity of triarylamine molecules upon light irradiation, although we have currently not been able to determine precisely the structures and/or the molecular arrangement of the corresponding supramolecular polymers. Furthermore, we have ultimately demonstrated that binary complexes such as **TAMG/TAMC** can self-assemble into well-defined objected in chloroform after light irradiation.

In this chapter, we would like to determine if the addition of an external chemical probe could affect the ability of the triarylamine to self-assemble into well-defined morphologies. Considering the limitations in terms of solubility of some triarylamine-nucleobase conjugates, we have thus studied the influence of the addition of a mercury salt or melamine on the self-assembly of the monotriarylamine-thymine (**TAMT**) conjugate and the propensity of the monotriarylamine-guanine (**TAMG**) conjugate to produce G-quartet in the presence of potassium ions. Importantly, all these studies were performed in organic solvents of various polarities as they might affect the formation of the self-organized structures. We believe that the use of light as an additional trigger might not be a prerequisite to produce organized nanostructures and that the combination of a chemical probe with the choice of a proper solvent could be sufficient to induce the formation of well-defined supramolecular polymers.

2. Melamine-templated self-assembly of TAMT

Melamine is a small molecule which present three possible hydrogen bonding faces arranged in a DAD pattern, which is complementary to the ADA hydrogen bonding face present on the thymine residue. Thus, we have studied the influence of the addition of melamine on the self-assembly of **TAMT**. Indeed, based on molecular modeling, we believe

that the formation of a 3:1 complex between thymine units and melamine respectively, will induce the formation of a relatively planar core with the ability to further stack into columnar structures by a combination of hydrogen bonding and π-π stacking interactions (**Figure 48**). The minimized structure suggests that triarylamine units should be located on the surrounding and should preserve its self-assembling properties.

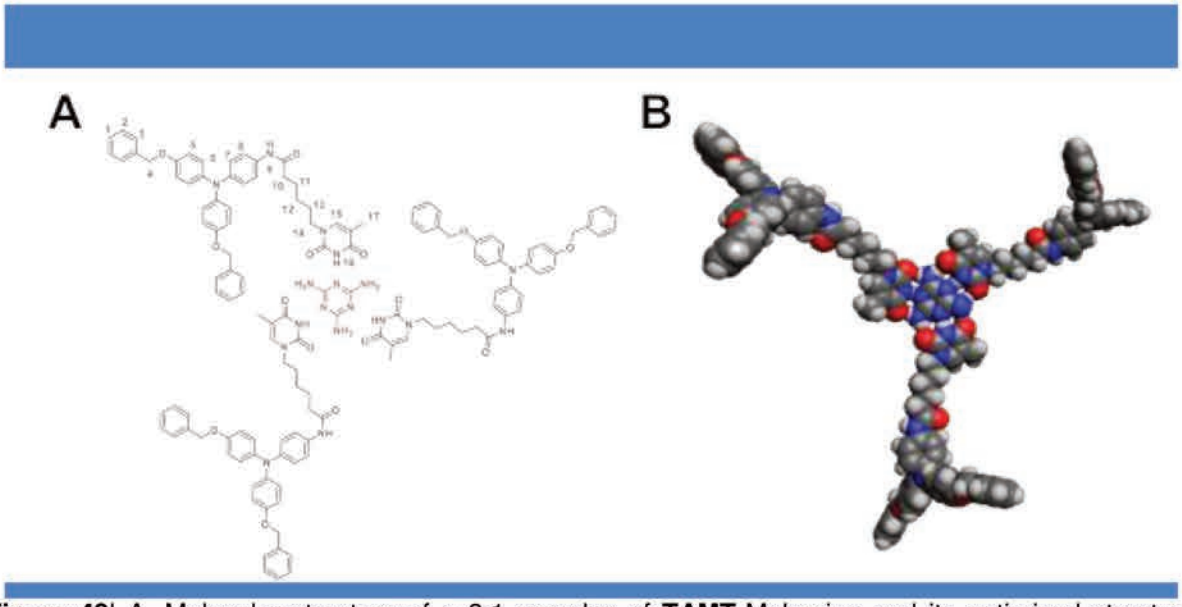

Figure 48| A. Molecular structure of a 3.1 complex of **TAMT**-Melamine and its optimized structure using Avogadro with MMFF94 force field.

In this section, we will first describe the synthesis and characterization of the 3:1 **TAMT**/melamine complex and then study its self-assembly in various solvents.

a. Synthesis and characterization of the melamine-TAMT complex

Since melamine is poorly soluble in organic solvents (only slightly soluble in hot methanol), we tried to induce the formation of the **TAMT**-Melamine complex by heating a solution of both compounds in either acetone or chloroform under microwave irradiation.[187] The formation of the complex was followed by ^{1}H NMR spectroscopy until the integration of the melamine chemical shift (6.16 ppm in d_6-acetone, **Figure 49**) became stable. In order to improve the synthesis of the complex, we varied independently several parameters such as the heating temperature, the time of the reaction, the initial concentration of **TAMT** and the oxygen content of the solution. Overall, we found that the synthesis of the complex was more efficient in acetone compared to chloroform after heating at 90 °C for 1 hour, with an initial concentration of **TAMT** as high as 14 mM, while the oxygen content did not influence the synthesis.

[187] Kappe, C. O. Controlled Microwave Heating in Modern Organic Synthesis. Angew. Chemie Int. Ed. **43,** 6250–6284 (2004).

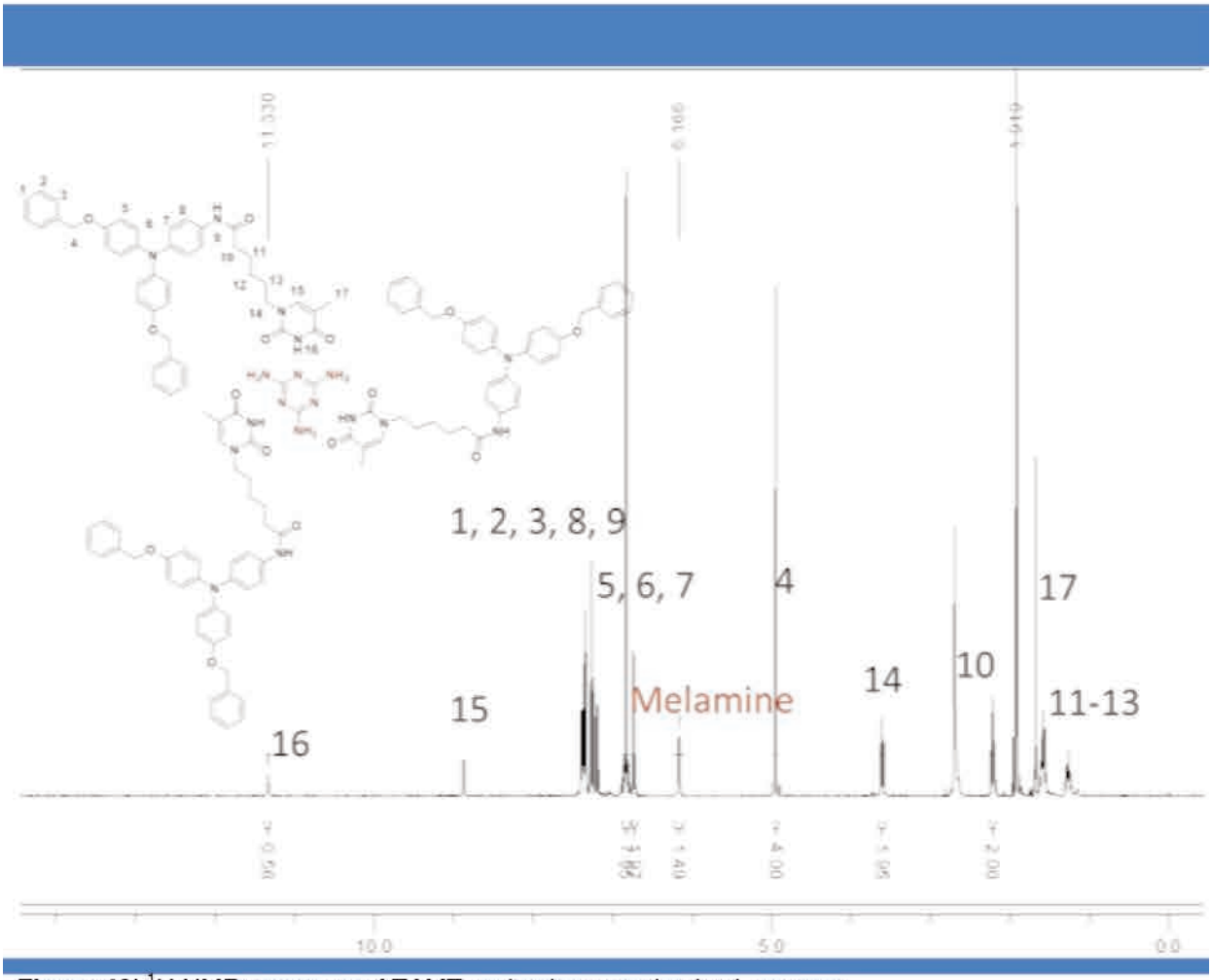

Figure 49| ^{1}H NMR spectrum of TAMT-melamine complex in d_6-acetone.

We then studied the stability of this complex in chloroform. For that, a solution of the complex in acetone was evaporated under reduced pressure and the resulting solid residue was taken back in deuterated chloroform. We found that the complex was stable under these conditions as the integration of the melamine signal compared to the imide proton of the thymine was in agreement with the formation of a 3:1 complex (**Figure S6**). Furthermore, we also found that the complex was stable for up to 17 days in chloroform as no decrease of the integration ratio was observed (**Figure S7**).

After we confirmed the stability of the complex in chloroform, the influence of the ratio **TAMT**/melamine under the previously optimized conditions was investigated by DOSY NMR experiments in d_6-acetone. In particular, we probed if the use of a precise 3:1 ratio compared to the formation of the complex using an excess of melamine (1:1 ratio) would affect the size of the complex, as it is known that the use of an excess of melamine might affect the morphology of supramolecular polymers.[160,161] As illustrated on **Figure 50**, we found that, in both cases, all NMR signals appeared at the same diffusion coefficient and as a

single set suggesting that the association between **TAMT** and melamine is complete and that only one complex is present in solution. Moreover, the complex was found to diffuse less than pure **TAMT**, which is in agreement with a larger hydrodynamic radius of the complex compared to the monomer.

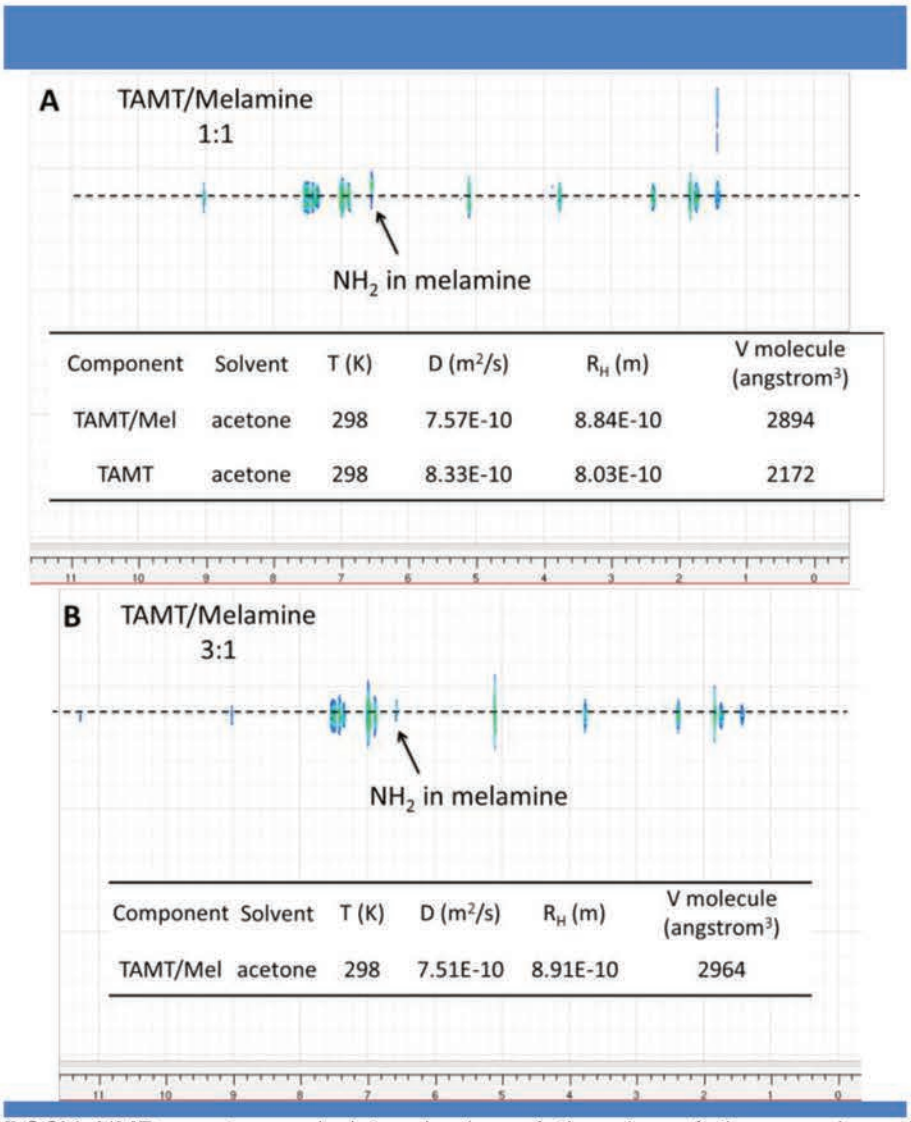

Figure 50| DOSY NMR spectra and determination of the size of the complex with an initial **TAMT**/Melamine ratio of (A) 1:1 and (B) 3:1 in d_6-acetone.

SANS experiments were then carried out in acetone in order to confirm the size of the complex (**Figure 51**). The scattering spectrum shows the presence of a Guinier regime in the medium q range, suggesting a finite size of the complex. Guinier analysis of this signal allowed us to determine a radius of gyration (R_g) of 7.2 Å for the complex in acetone. We then calculated the ρ ratio (R_g/R_H) from DOSY and SANS experiments as it can provide information on the morphology of the complex. We calculated that this shape factor is 0.81, i.e. be smaller than 1, and thus suggesting that the complex form a relatively hard sphere.

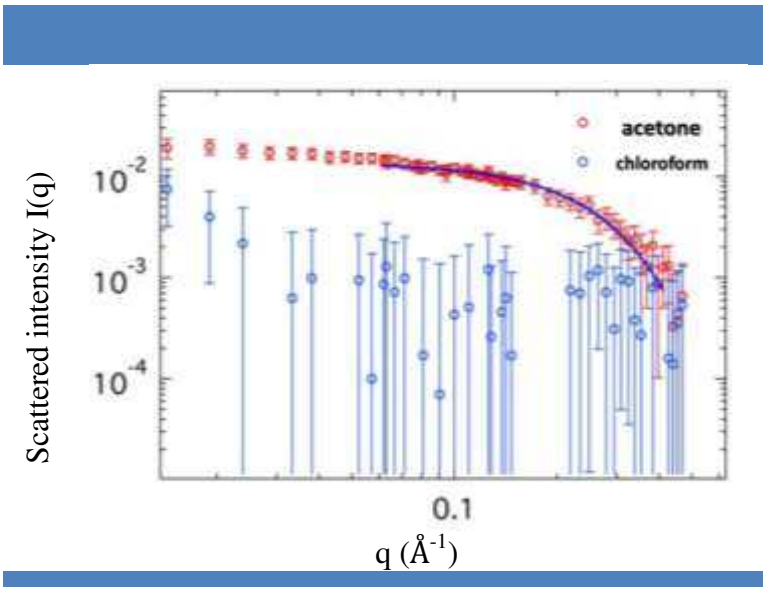

Figure 51| SANS scattering spectra of a **TAMT**-melamine complex in acetone (red) and in chloroform after light irradiation (blue) ([complex] = 12 mM).

Overall, using a combination of NMR and SANS experiments, we have confirmed the formation of a 3:1 **TAMT**/melamine complex in acetone. We will know focus on its possible self-assembly in various solvents.

b. Characterization of the light-triggered self-assembly of the melamine-TAMT complex

We have shown in the previous section that the **TAMT**/melamine complex remain stable in chloroform after several days and we thus probed its light-triggered self-assembly in this solvent. We proceeded with the same systematic study as the one performed in the previous chapter.

First, ^{1}H NMR spectroscopy at room temperature showed the typical behavior observed for the self-assembly of triarylamine compounds upon light irradiation, i.e. disappearance of the ^{1}H NMR signals corresponding to the triarylamine core and to the benzylic protons (large blue arrows, **Figure 52**). Interestingly, we could also observe that the ^{1}H NMR signals corresponding to the alkene proton of the thymine (H15, chemical shift at around 7.0 ppm) and to the melamine (NH_2) are not affected by the light-induced process, thus suggesting that they are not enforced in a strong self-assembled structure.

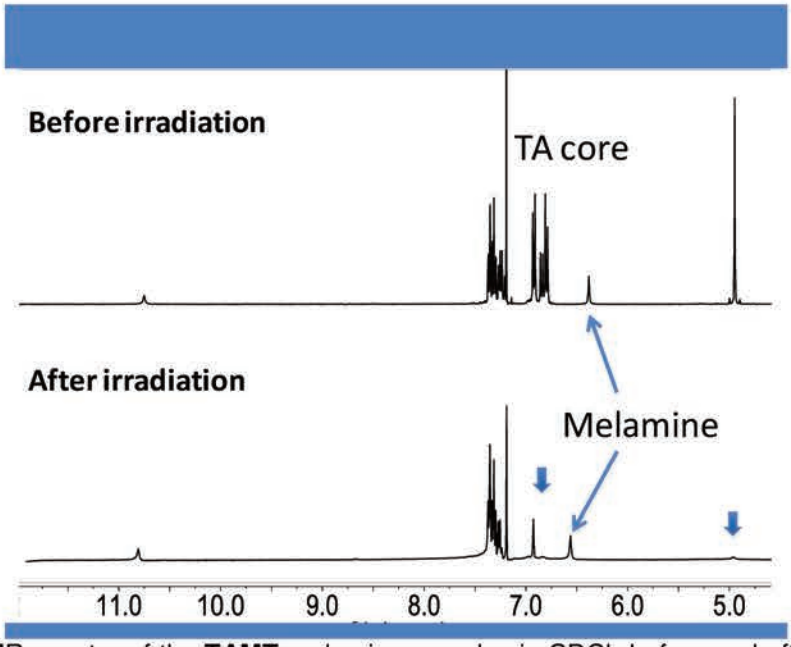

Figure 52| ^{1}H NMR spectra of the **TAMT**-melamine complex in $CDCl_3$ before and after irradiation with white light.

Similarly to single triarylamine-nucleobase conjugates, we then performed a kinetic study on the **TAMT**-melamine complex at 0.1 mM in chloroform by UV-vis-NIR spectroscopy upon light irradiation (Figure 53).

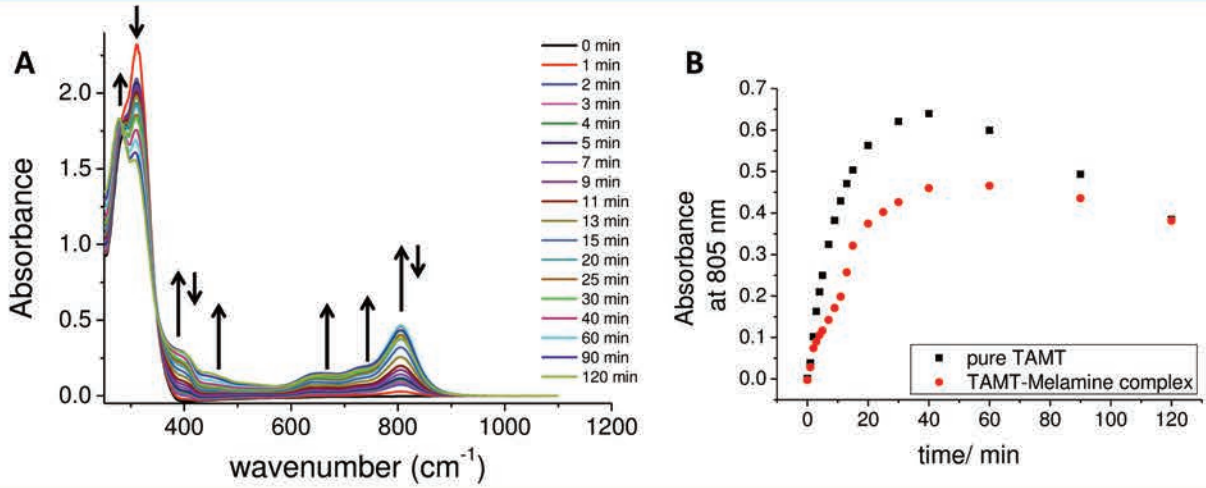

Figure 53| A. UV-VIS-NIR spectra of a **TAMT**-melamine complex upon seuqential light irradiation (0.1 mM in chloroform). B. Evolution of the absorbance at 805 nm for pure **TAMT** (black) and a **TAMT**-melamine complex (red) as a function of irradiation time (c = 0.1 mM in chloroform).

As shown on Figure 53**B**, a new absorption band at 805 nm appeared upon light irradiation, which indicates the production of localized triarylammonium radical cations. The intensity of this band increased with irradiation time until reaching a maximum after irradiating for 40 minutes. Interestingly, this maximum absorption after 40 minutes irradiation is associated with a maximum of absorption of the band at 382 nm, which is related to the

self-assembly of triarylamine molecules. Further increased irradiation times led to a small decrease of the 805 nm band, while the band at 382 nm remained stable. These observations suggest that, after 40 minutes irradiation, all triarylamine molecules are self-assembled and that further doping with light lead to a reduction of the radical at the extremities of the fibers as already observed with other triarylamine derivatives.[73] Compared with the kinetic experiments recorded for pure **TAMT** in chloroform, we observe that the complex does not affect the propensity of the triarylamine moiety to self-assemble. Although the kinetics seem very similar for both **TAMT** and its complex with melamine, we can see that the recombination of radicals is less pronounced in the complex suggesting that the complex give rise to longer aggregates compared to the molecule alone.

We thus probed the morphology of the supramolecular polymers formed by the **TAMT**/melamine complex by TEM microscopy (**Figure 54**).

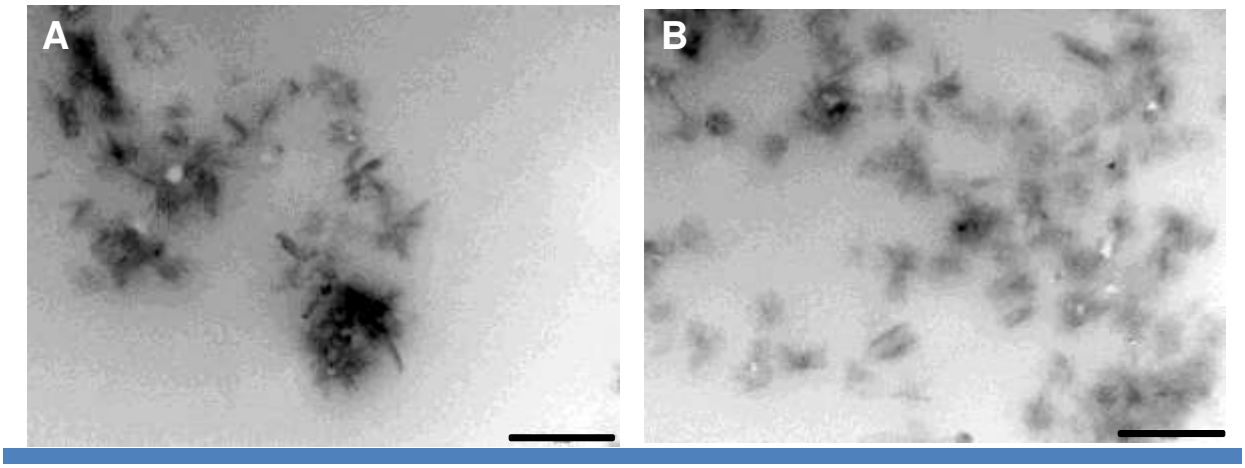

Figure 54| TEM images of the **TAMT**-melamine complex after light irradiation for 1 hour (10 mM solution in chloroform, Scale bar: 1µm)

Although images are not very clear due to the presence of organic matter at their surface, we could observe clusters of short fibers with lengths comprised between 200 and 400 nm. The formation of these dense structures is in agreement with the SANS experiments recorded on the complex after light irradiation in chloroform (**Figure 52**, blue points). Indeed, in this case, we only observe a scattering intensity which corresponds to the scattering intensity of the solvent. Such behavior has already been observed for several triarylamine self-assemblies and indicates that the complex form dense and large aggregates which size is not observed in the q range provided by SANS.

Overall, using a set of ^{1}H NMR, UV-Vis-NIR and TEM experiments, we have shown that the 3:1 **TAMT**/melamine complex form well-defined fibrillar aggregates in chloroform

upon light irradiation. Further experiments will be dedicated to the understanding of the molecular arrangement of this complex within the self-assembled structures.

c. Morphological studies of the melamine-TAMT complex in various solvents

Finally, we also probe the possible self-assembly of the **TAMT**/melamine complex in solvents of various polarities. Indeed, in an attempt to crystallize the fibers observed upon light irradiation for one hour in chloroform, we added methanol (around 1:1 ratio with chloroform) as a poor solvent to force the crystallization. After diffusion of the methanol layer into chloroform and further slow evaporation for around one month, we observed the formation of millimetric porous spheres with a quite uniformed radius (**Figure 55**).

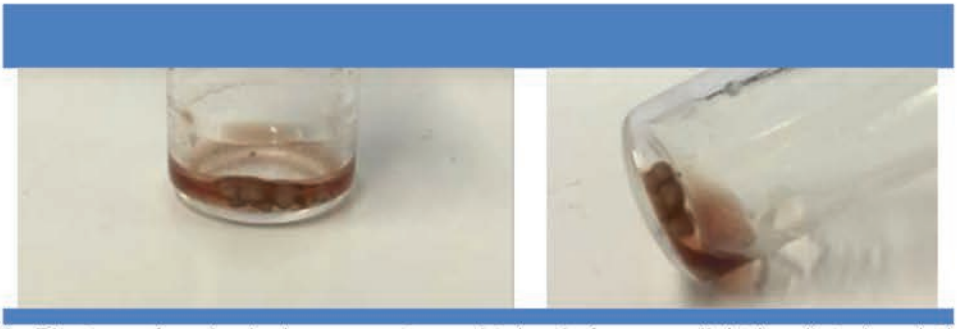

Figure 55| Photos of spherical aggregates obtained from a light-irradiated solution of the **TAMT**-melamine complex after slow diffusion of methanol for one month.

These surprisingly large macroscopic aggregates were further imaged by SEM and analyzed by X-ray scattering in order to investigate their internal structure (**Figures 56 and 57**). SEM imaging interestingly showed the presence of two morphologies: rigid crystalline rods indicated as **a** on **Figure 56** and flexible fibers surrounding the rods indicated as **b** on **Figure 56**. Having determined the micrometric internal structure of the macroscopic spheres, we then turned to X-ray scattering experiments in order to understand the possible molecular arrangement of the complex within the different morphologies (**Figure 57** and **Table 2**). Complementary small angle, middle angle and wide angle X-ray scattering experiments were performed on powders of the spheres, which showed the presence of several sharp diffraction peaks suggesting a high crystallinity within the spherical aggregates (**Figure 57**). Characteristic distances corresponding to these sharp peaks were calculated according to the Braggs equation (see experimental part). Two series of distances were observed for these spherical aggregates which is in agreement with the two different morphologies observed by SEM (**Table 2**).

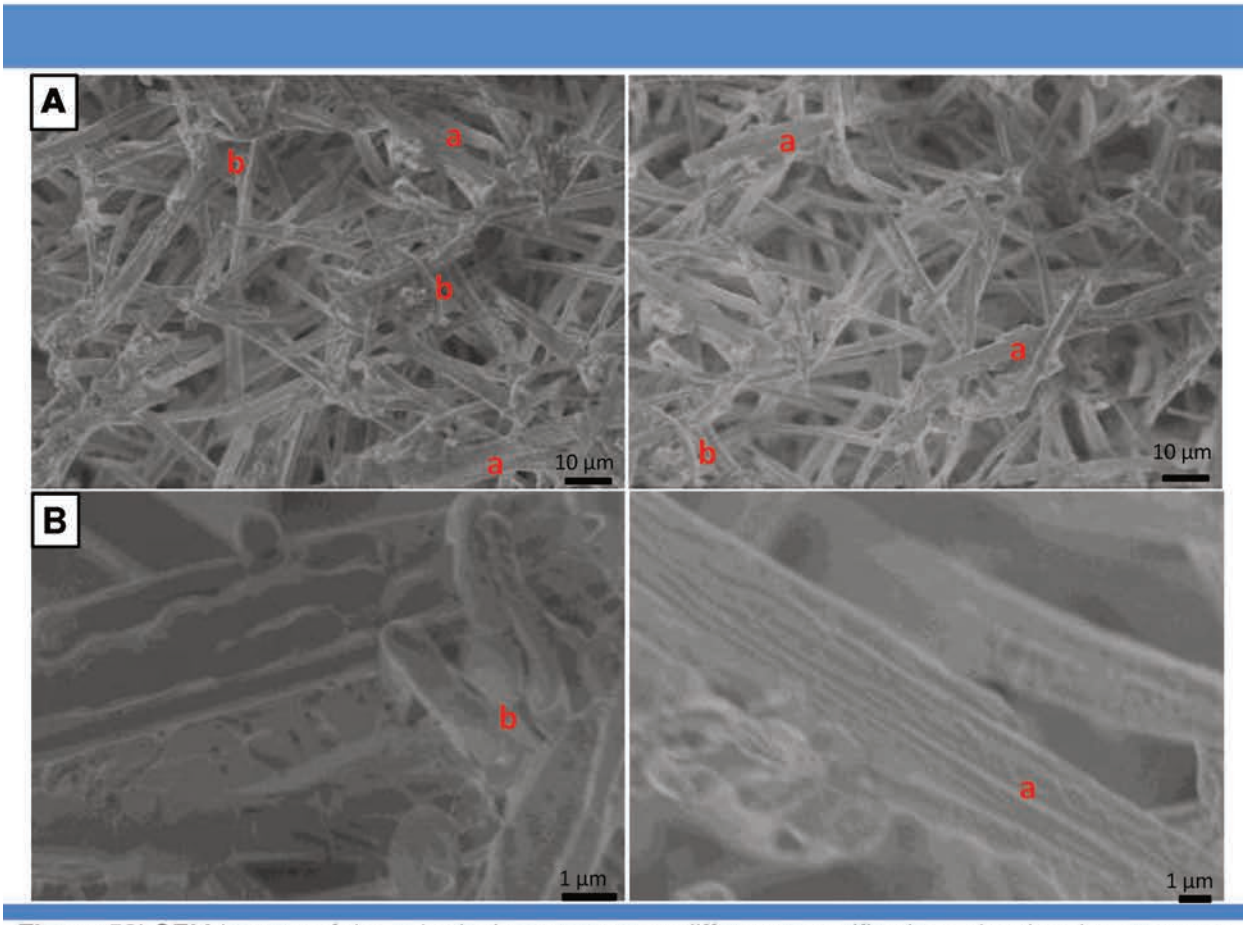

Figure 56| SEM images of the spherical aggregates at different magnifications showing the presence of rigid crystalline rods (**a**) and flexibl fibers (**b**).

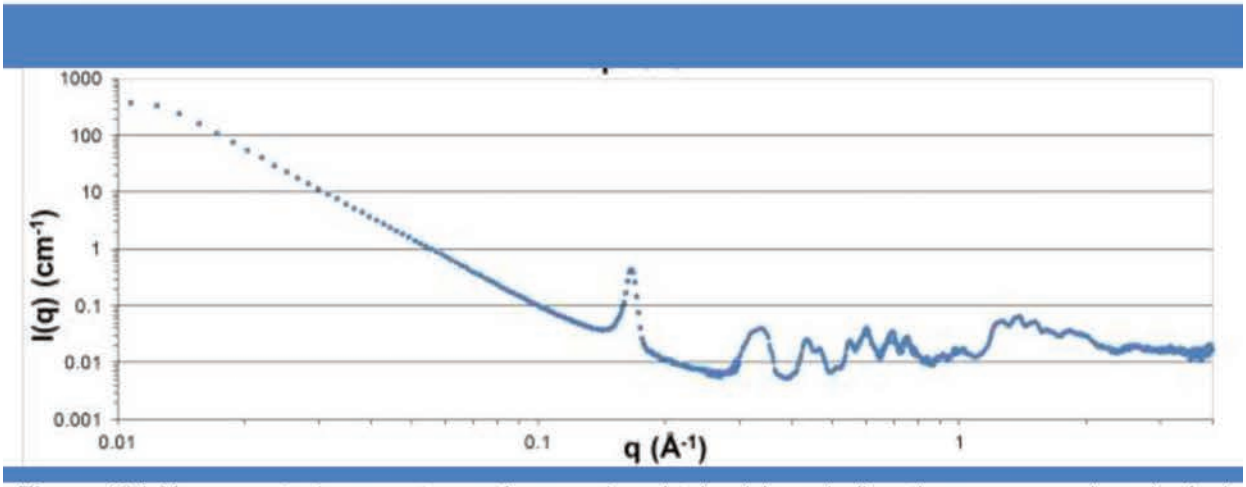

Figure 57| X-ray scattering spectrum of a powder obtained by grinding the macroscopic spherical aggregates.

A first set of diffraction peaks corresponding to a periodical pattern (1, 1/2, 1/3…) was attributed to the formation of a lamellar-like molecular arrangement, while a second set of typical diffraction peaks in the ratio of $1:1/\sqrt{3}:1/2:1/\sqrt{7}\ldots$ for d spacing suggest the formation of a 2D hexagonal lattice.[72]

Table 2| Scattering peaks and corresponding distances observed by X-ray scattering experiments on the spherical aggregates.

Scattering angle ($Å^{-1}$)	Distance (Å)	lamellar	Hexagonal
0.1667	37.6	1	
0.3206	19.59	1/2	
0.3441	18.25		1
0.5083	12.35		$1/\sqrt{3}$
0.6042	10.39	1/3	
0.6957	9.03		1/2
0.9133	6.88		$1/\sqrt{7}$

By analogy with some of our previous work on liquid crystalline phases,[72] we believe that the rigid crystalline rods observed by SEM arise from the lamellar-like molecular arrangement while the flexible twisted fibers arise from a 2D hexagonal arrangement of the complex.

Finally, since three triarylamines are involved in the **TAMT**-melamine complex, we also probe the possible self-assembly of the **TAMT**-melamine complex in toluene as we know that triarylamine trisamide molecules can lead to the formation of fibrillar aggregates in this solvent (unpublished results). The **TAMT**-melamine complex was dissolved in toluene at a concentration of 28 mM and left standing overnight at room temperature, leading to the formation of an organic opaque gel (**Figure 58**).

Figure 58| Photo of the gel formed by the **TAMT**-melamine complex in toluene (28 mM).

In toluene, ^{1}H NMR experiments on the complex and on pure **TAMT** showed a broadening and shift of the signals corresponding to the protons of the thymine residue (H14, H15 and H16) and of the melamine (NH_2) (**Figure 59**). These observations suggest that the thymine/melamine complex is probably responsible for the self-assembly in toluene while the triarylamine core has only a minor influence.

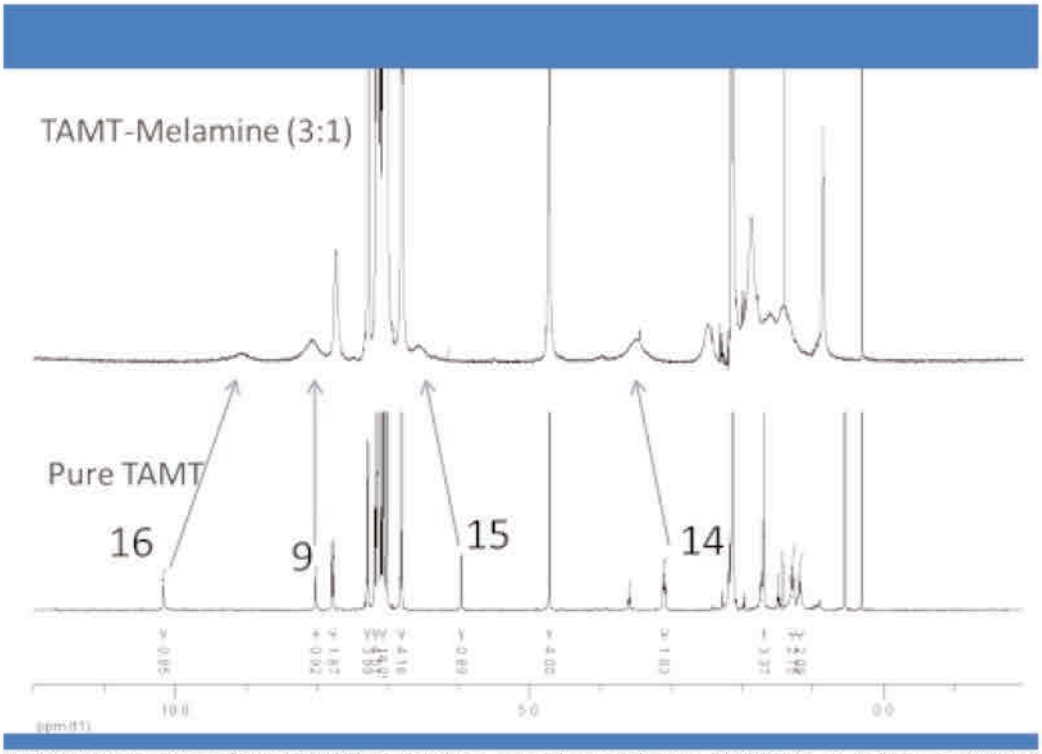

Figure 59| NMR spectra of the **TAMT**-melamine complex and pure **TAMT** in d_8-toluene at 20mM.

For concentration slighly lower than the critical gelation concentration in toluene, we observed that the clear solution slowly turned into a colloidal suspension upon stirring. As the **TAMT**-melamine complex was fully soluble before stirring, we believe that the colloidal suspension results from its aggregation over several length scales. This suspension was then studied by SEM in order to confirm the elucidate the morphology of the aggregates formed in toluene (**Figure 60**). Long and well-oriented nanofibers with a width of around 50-100 nm can be detected, which are reminiscent of the nanowires formed from the triarylamine trisamide compound reported by our group previously.[80]

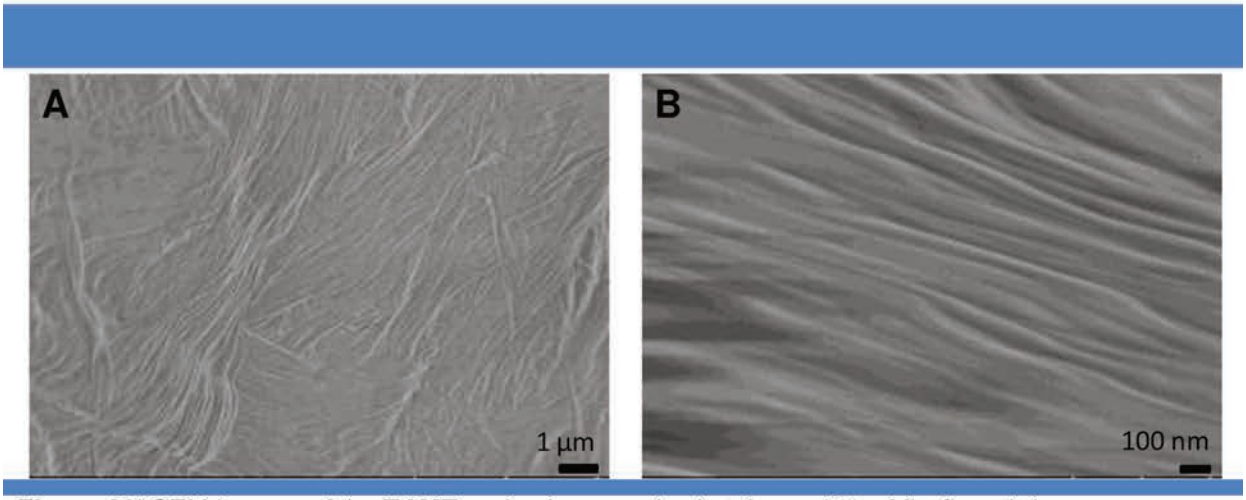

Figure 60| SEM images of the **TAMT**-melamine complex in toluene (23 mM) after stirring.

In order to get a better understand of the morphology of these, TEM images were recorded on toluene solutions at concentrations lower than the gelation concentration (**Figure 61**).

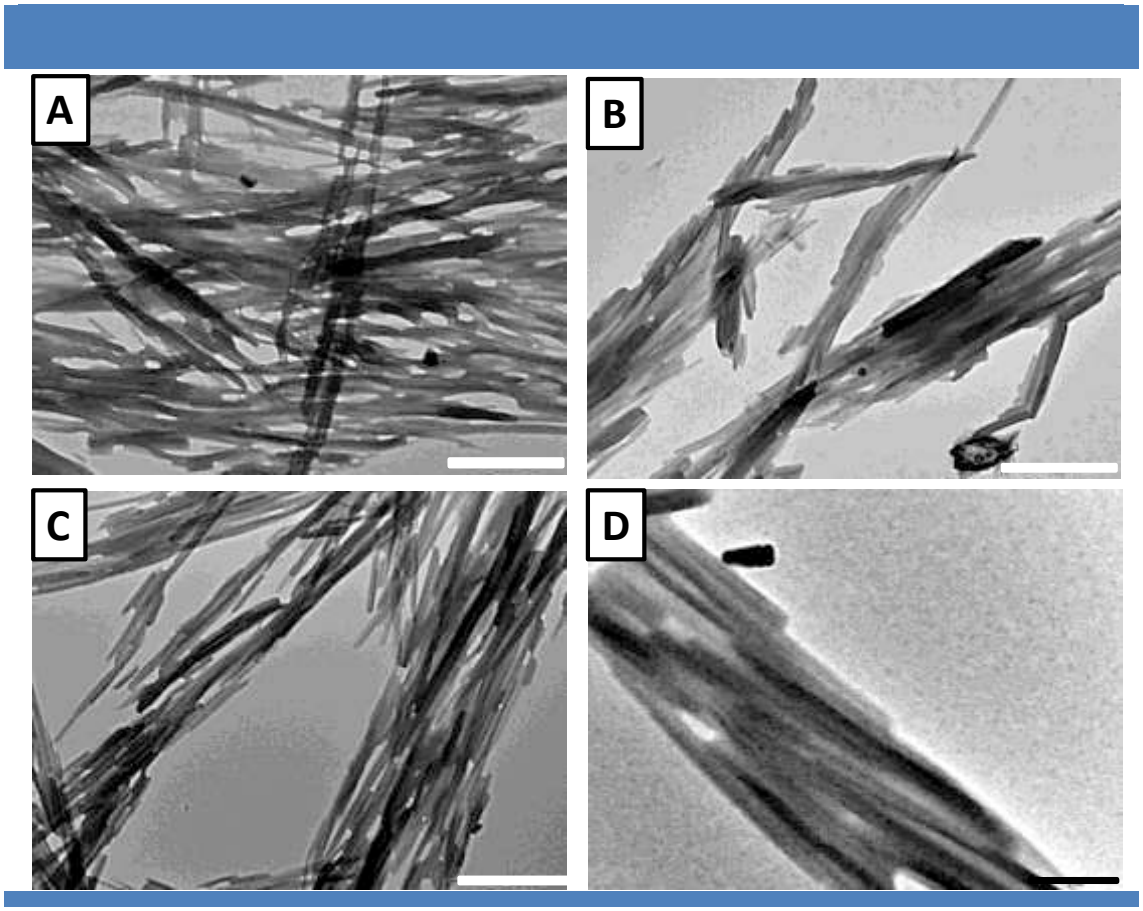

Figure 61| TEM images of the **TAMT**-melamine complex in toluene at concentrations lower than the gelation concentration: 20 mM (A,B), 10 mM (C,D). (Scale bar: A-C: 1µm; D: 200 nm)

Bundles of rigid nanofibers with a micrometric length and a width of around 40 nm were observed. However, it is difficult to correlate the structures observed by SEM and TEM with the current information available. Further experiments such as AFM, SANS or SAXS and cryo-TEM on the gel will have to be performed in order to elucidate the molecular arrangement of the **TAMT**/melamine complex within this fibrillar aggregates.

d. Discussion

In this section, we have shown that the triarylamine-thymine conjugate can be used to form a ternary complex with melamine thanks to a triple ADA-DAD hydrogen bonding array. This complex was found to be stable in various organic solvents such as acetone, chloroform and toluene. We further demonstrated that the complex retains the light-induced self-assembling properties of the triarylamine core, which give rise to the formation of well-defined micrometric fibers. By playing with solvent polarity, we have also demonstrated

that the complex can give rise to different macroscopic structures such as unusual millimetric spherical aggregates in chloroform/methanol mixtures or self-supporting gels in toluene. Interestingly, preliminary information obtained on these structures suggest that on one case the self-assembly is driven by the triarylamine core while in the other one, the thymine/melamine complex is at the origin of the self-assembled structures. Further experiments such as AFM and scattering experiments will have to confirm these first observations by providing information on the molecular arrangement of the **TAMT**-melamine complex within these hierachical self-assemblies. To the best of our knowledge, this work represents the first example of supramolecular polymers build from melamine in organic solvents.

3. Mercury-templated self-assembly of TAMT

We have seen in chapter 4 that molecules with a thymine or uracil residue can be used to detect mercury. Indeed, this heavy metal ion was shown to form specific Hg^{II}-mediated T-T base pair, which have been characterized by means of various physico-chemical analyses such as ^{15}N NMR, Raman, IR and optical spectroscopies along with crystallographic studies.[119] Most of the studies reported so far in the literature deal with the complexation of mercury in aqueous solution. Thus, we were wondering if our monotriarylamine-thymine conjugate could be used to monitor the presence of mercury in organic solvents. We designed a series of spectroscopic experiments which aim at understanding the binding of mercury ions to **TAMT** either in its molecularly dissolved state or in its aggregated state, i.e. in chloroform before and after light irradiation.

a. Spectroscopic characterizations

In order to understand whether the addition of mercury as $HgCl_2$ salt affect the triarylamine structure, we initially perform ^1H NMR experiments in chloroform on either a molecularly dissolved TAMT solution or a self-assembled TAMT solution in the presence or in the absence of mercury (**Figure 62**). The addition of 0.5 equivalent of $HgCl_2$ on a 8.4 mM solution of **TAMT** in $CDCl_3$ lead to drastic changes in the ^1H NMR spectrum (black and red bottom spectra on **Figure 62**). We observed a broadening of the peaks corresponding to the triarylamine core (H5-H8), to the benzylic protons (H4), to the methylene protons close to the amide moiety (H10) and to the amide moiety (H9). Furthermore, we could also observe a downfield shift of the signal corresponding to the imide moiety of the thymine residue. These

observations suggest that mercury binds to this imide proton but it also have a strong influence on the triarylamine core, which will have to be elucidated.

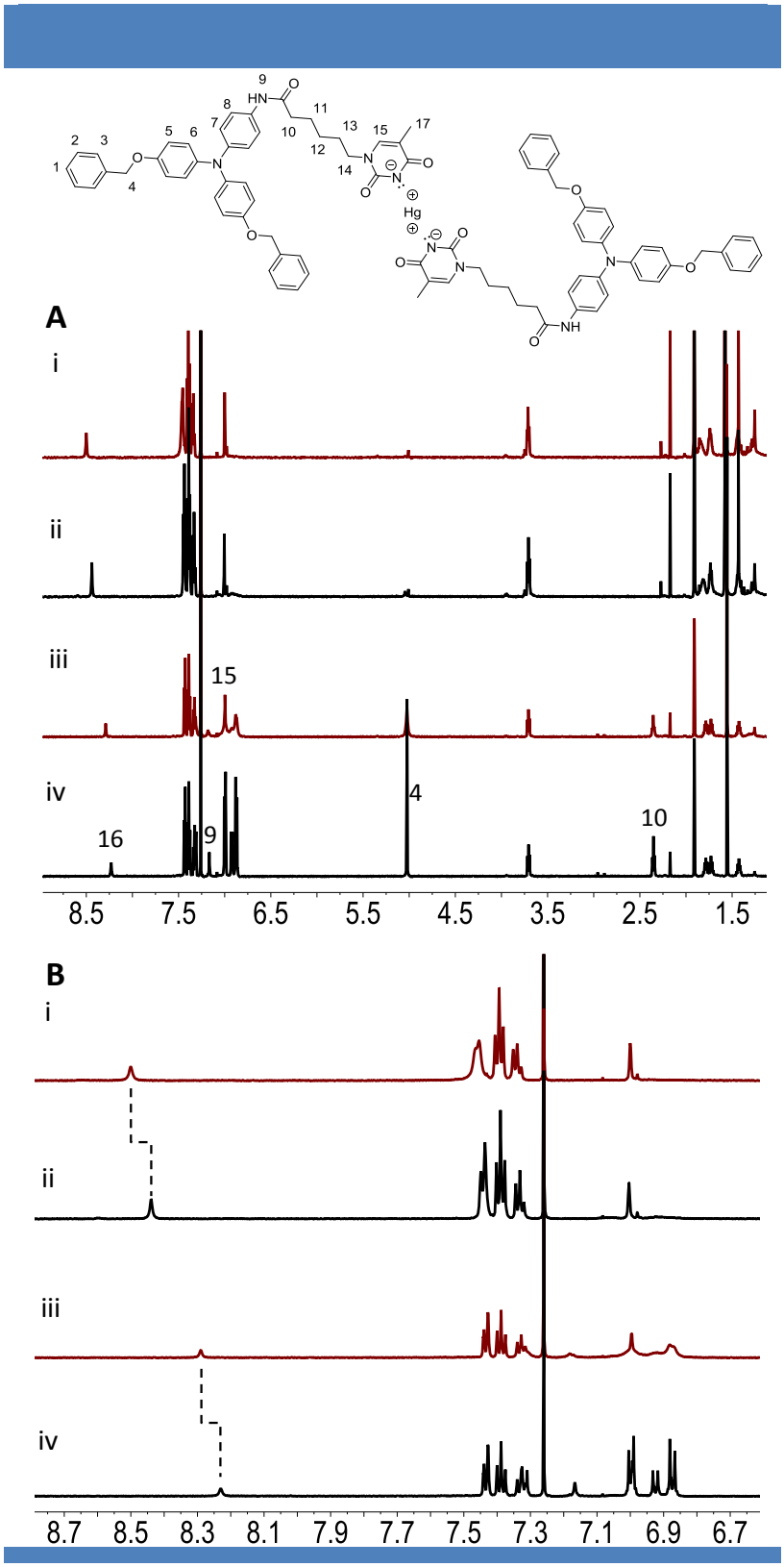

Figure 62| A. ^{1}H NMR spectra of $CDCl_3$ solutions of (i) **TAMT** + 0.5 equiv. of $HgCl_2$ after light irradiation for 1 hour, (ii) **TAMT** after light irradiation for 1 hour, (iii) **TAMT** + 0.5 equiv. of $HgCl_2$ before irradiation and (iv) **TAMT** before irradiation. B. Enlarged (8.8-6.6 ppm) ^{1}H NMR spectra from the A panel.

Upon light irradiation of these two solutions for one hour, we observe a complete flattening of the triarylamine signals in both cases while in the presence of mercury, the downfield shift of the imide proton could still be observed, indicating that the light-induced process do not affect the binding affinity of thymine to mercury. To confirm that the binding of mercury induce a downfield shift of the imide proton, we prepared a thymine derivative decorated at its N1 position with a pentyl chain. Upon addition of mercury, we also observe this downfield shift of the imide proton, confirming the ability of **TAMT** to bind mercury ions even after light irradiation. Furthermore, we also studied the influence of the addition of mercury ions to triarylamine molecules without thymine residues (**Figure S8** and **Figure S9**). When mercury was added to compound **10** (nitro-triarylamine derivative), we did not observe any change of its ^{1}H NMR spectrum. However, when mercury was added to the triarylamine acetamide (**BATA**), we observed the disappearance of all signals corresponding to the molecule except the ones of the benzyl groups. These control experiments confirm that mercury has an influence on the triarylamine core provided that the structure incorporates an amide moiety.

We then investigated chloroform solutions of **TAMT** in the presence and in the absence of mercury by DOSY NMR in order to confirm the formation of a dimeric structure in the presence of the salt (**Table 3**). Surprisingly, a similar hydrodynamic radius was recorded for both solutions. Compared to the hydrodynamic radii recorded for the **TAMT**/melamine complex (~8.8 Å), we believe that sizes recorded for pure **TAMT** and the **TMAT-Hg** complex evidence the formation of dimeric structures in both cases, as thymine is known to form homodimers by double hydrogen bonding interactions (see chapter 3).

Table 3| DOSY results of **TAMT** and **TAMT-Hg** in chloroform without irradiation

	T (K)	D (m^2/s)	Visq (Pa.s)	Gamma	R_H (m)	V molecule (Å^3)
TAMT-Hg	298	5.20E-10	5.390E-4	1.47E-08	7.78E-10	1976
TAMT	298	5.14E-10	5.390E-4	1.48E-08	7.87E-10	2046

Importantly, we also tried to monitor the binding of mercury to the different imide and amide moieties of **TAMT** by using ^{15}N NMR experiments. However, although this technique was used to probe the association of mercury with thymine, all experiments did not allow us to confirm any binding at any position. As FT/IR has been reported as a technique commonly used to record thymine-mercury binding, we studied the influence of the addition of mercury on **TAMT**, **BATA** and thymine-C_5 (compound **20**). These experiments were performed on

powders obtained after concentration of the corresponding solution in chloroform, and by using the ATR mode (**Figure 63**). In the absence of mercury, these experiments show that the imide (I) C=O stretching band corresponds to the broad band at around 1675 cm^{-1}, which overlaps with the amide (I) C=O stretching band of the triarylamine moiety which is located at around 1660 cm^{-1} (**Figure 63B,C**).

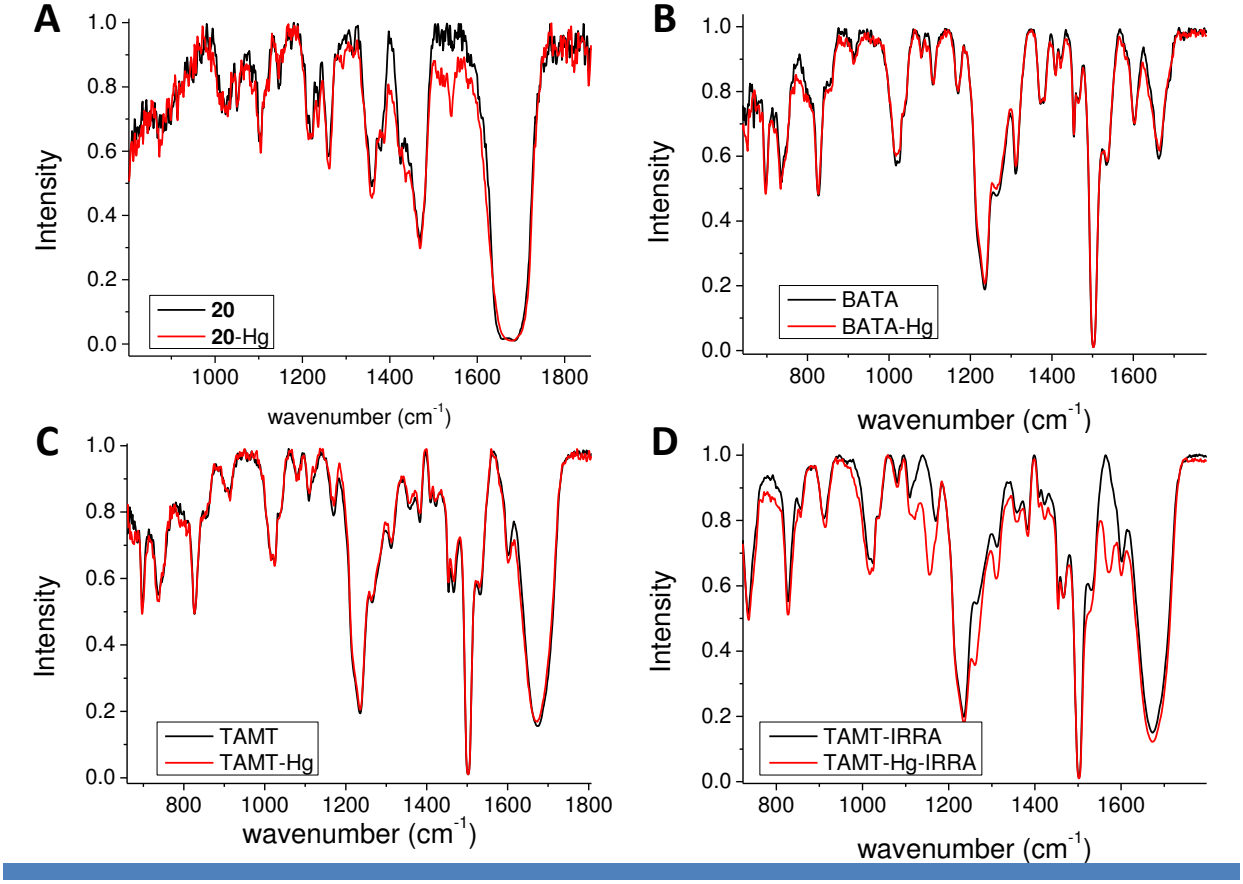

Figure 63| FT-IR spectra of **20** (thyming-C5) (A), **BATA** (B) and **TAMT** (C.before irradiation; D.after irradiation) in the presence or the absence of mercury and recorded on powders using the ATR mode.

Unfortunately, when FT-IR spectra were recorded on powders containing a 2:1 mixture of **TAMT**, **BATA** and thymine-C_5 and $HgCl_2$, we could not observe any major difference. Careful analysis of these data might suggests that the imide (I) C=O band is slightly shifted and broaden upon addition of mercury, but this variation is not strinking.

We then turned to UV-vis-NIR experiments to monitor if the addition of mercury has an influence of the spectroscopic behavior of TAMT. First, we compared the light-induced UV-Vis-NIR response of 0.1 mM chloroform solutions of **TAMT** and **TAMT-Hg(II)** complex (**Figure 64**). As shown on **Figure 64B**, a new absorption band at 782 nm appeared for the **TAMT-Hg(II)** complex upon light irradiation, which indicates the production of localized triarylammonium radical cations. Interestingly, compared to pure **TAMT**, this band is

hypsochromically shifted by around 23 nm. The intensity of these bands increased with irradiation time until reaching a maximum after irradiating for 40 minutes. This maximum absorption after 40 minutes irradiation was found to be associated with a maximum of absorption of the band at 382 nm, which is related to the self-assembly of triarylamine molecules. Further increased irradiation times led to a decrease of the 805 nm band, while the band at 382 nm remained quite stable.

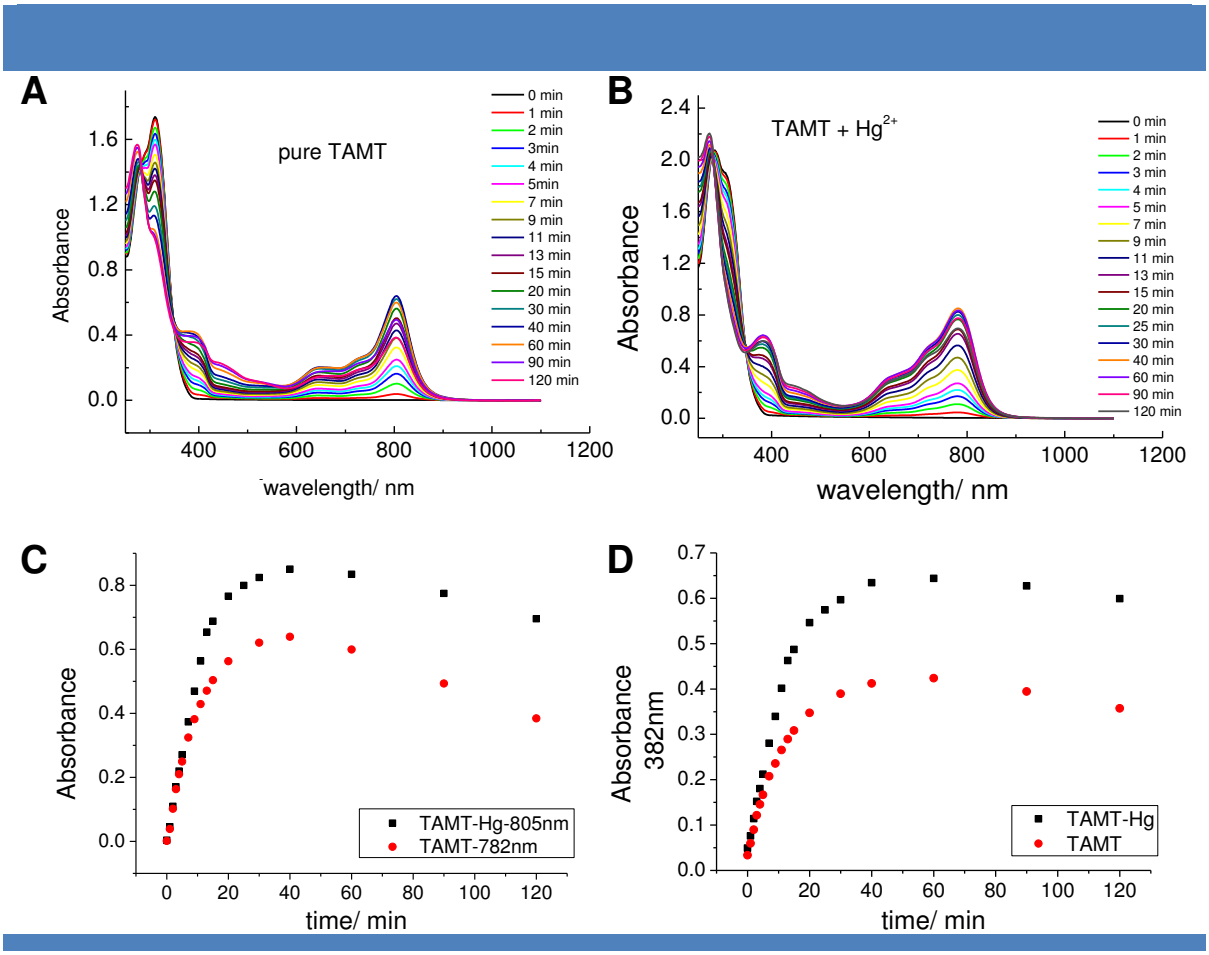

Figure 64| A. UV-vis-NIR spectra of **TAMT** for increasing irradiation times. B. UV-vis-NIR spectra of **TAMT-Hg(II)** complex for increasing irradiation times. C-D. Evolution of the absorbance at C. 782 nm for **TAMT-Hg(II)** complex (black) and 805 nm for **TAMT** (red) and D. at 382 nm for **TAMT-Hg(II)** complex (black) and **TAMT** (red) as a function of irradiation time (c = 0.1 mM in chloroform).

It is important to note that the kinetic of the self-assembly is not affected by the presence of mercury as kinetic plots of these UV-Vis-NIR data are almost identical except that the absorbance intensity is higher for the **TAMT-Hg(II)** complex, suggesting that the complex does not affect the propensity of the triarylamine moiety to self-assemble (**Figure 64C-D**). As the amide moiety is a prerequisite to observe such optical behavior upon light irradiation, these experiments suggest that mercury does not bind to the amide moiety of the triarylamine core. As control experiment, we also monitored the behavior of BATA, which does not incorporate the thymine residue, in the presence and the absence of mercury upon light

irradiation (**Figure 65**).

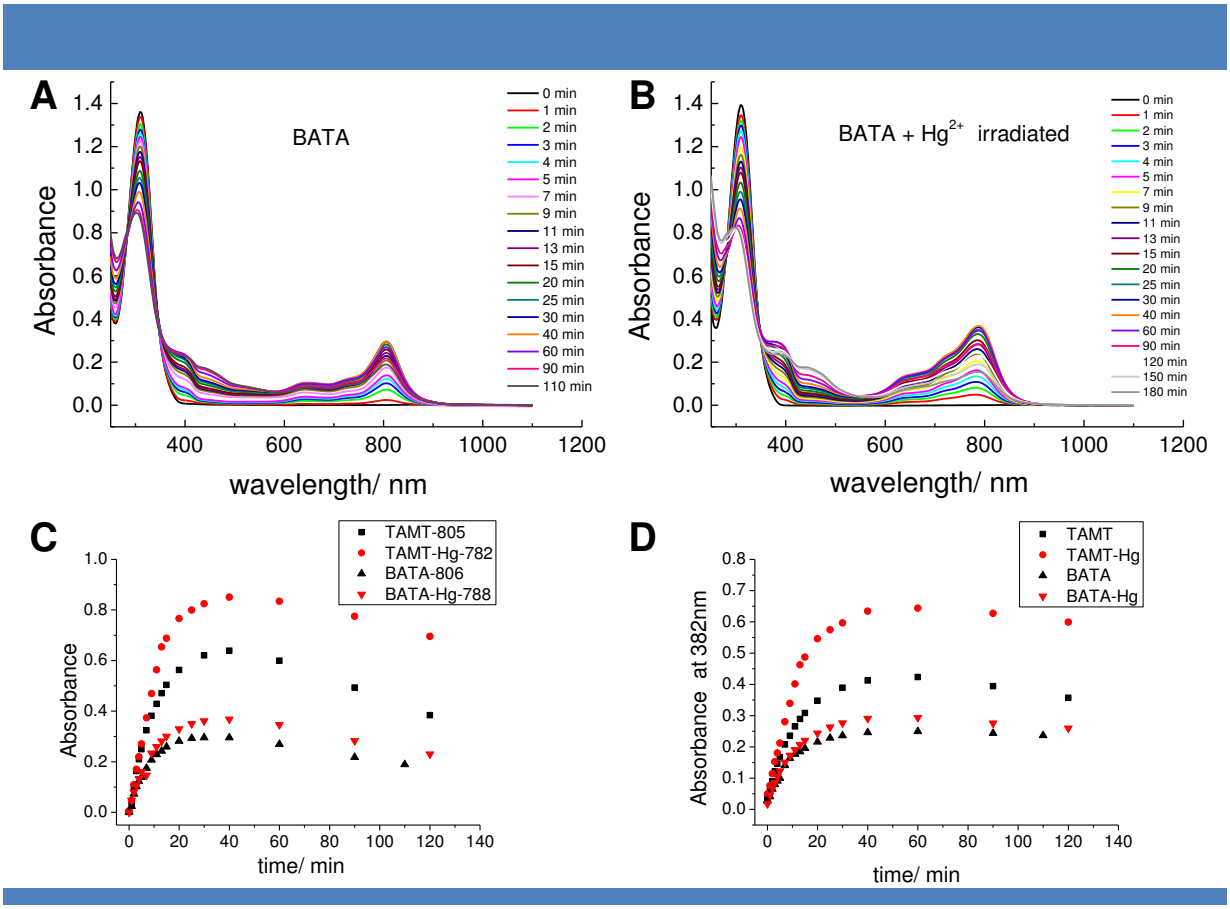

Figure 65| A. UV-vis-NIR spectra of **BATA** for increasing irradiation times. B. UV-vis-NIR spectra of **BATA-Hg(II)** mixture for increasing irradiation times. C-D. Evolution of the absorbance at C. 782 nm for **TAMT-Hg(II)** complex (red dots), 788 nm for **BATA-Hg(II)** mixture (red triangle) and 782 nm for **TAMT** (black square) and for **BATA** (black triangle) and D. at 382 nm nm for **TAMT-Hg(II)** complex (red dots), **BATA-Hg(II)** mixture (red triangle), **TAMT** (black square) and **BATA** (black triangle) as a function of irradiation time (c = 0.1 mM in chloroform).

Similarly to **TAMT**, the band at 806 nm corresponding to **BATA** triarylammonium radical cations is hypsochromically shifted by around 22 nm in the presence of mercury. However, the addition has no influence on the kinetics of the self-assembly process, nor on the absorbance intensity. Furthermore, we also probed the kinetics of self-assembly in the presence of metals ions such as zinc(II), iron (III) and magnesium (II), which are not known to bind to the thymine residue (**Figure S10**). For these three metal ions, no hypsochromic shift was observed for the band corresponding to the triarylammonium radical cation and the kinetic upon light irradiation was almost identical to the one recorded for pure **TAMT**. Currently, we do not have an explanation for the hypsochromic shift observed in the presence of mercury although we believe it is related to its binding to the triarylamine moiety.

We then probed the influence of adding increasing amounts of mercury on a 0.1 mM solution of **TAMT** in chloroform which has been light irradiated for 20 minutes (**Figure 66**).

Upon adding mercury, the absorbance band at 805 nm was shifted to a lower wavelength for increasing amounts of mercury until reaching a stable value after the addition of 0.5 equivalents (**Figure 66A**). We also observed a) a slight decrease of the absorbance at 805 nm, b) a gradually increase of the absorption bands located between 650 nm to 750 nm and c) almost no change of the absorbance at 400 nm, which is characteristic of the self-assembly of the triarylamine molecules. Surprisingly, a similar behavior was also recorded for **BATA** under identical conditions

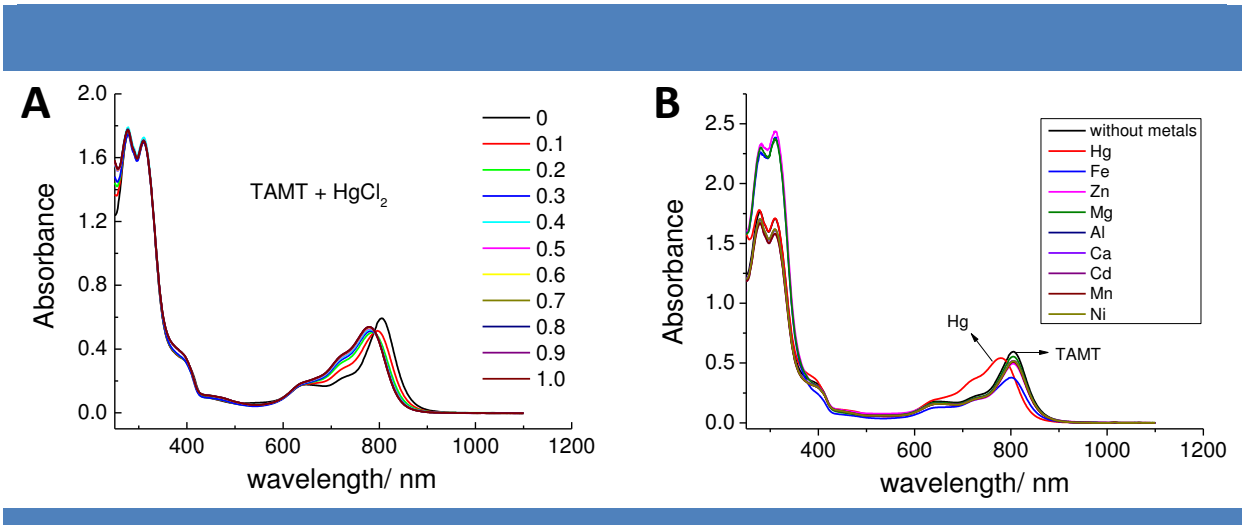

Figure 66| A. UV-vis-NIR absorbance spectra of a light-irradiated solution of **TAMT** upon the addition of mercury (0-1 eq.). B. UV-vis-NIR absorbance spectra of pure **TAMT** and **TAMT** mixed with different metals (0.5 equivalent) (c = 0.1 mM in chloroform).

We also studied the influence of the addition different metals ions (0.5 equivalent) on light-irradiated solutions of **TAMT** (**Figure 66B**). Although a slight decrease of the absorbance intensity was observed for iron ions, no hypsochromic shift of the band corresponding to the triarylammonium radical cation was recorded for any of the metals, confirming that **TAMT** has a selective affinity for mercury.

b. Discussion

Overall, using ^{1}H and DOSY NMR spectroscopy, we have demonstrated that mercury is able to bind to the thymine residue present on the triarylamine-thymine molecule, thus leading to the formation of a dimeric structure. We then probe the light-induced properties of this complex using UV-Vis-NIR experiments and demonstrated that **TAMT** is selective for mercury and that the mercury complex retain the ability to self-assemble in chlorinated solvents upon light irradiation. This observation indicates that mercury does not bind to the amide moiety of the triarylamine core necessary for the self-assembly process. However, we still need to understand why a triarylamine molecule without any thymine residue (**BATA**)

displays a similar spectroscopic behavior to **TAMT**. We believe that imaging of the supramolecular polymers in the presence or the absence of mercury would be very informative but, so far, we did not manage to observe any structure. Finally, we would like to mention that some X-ray scattering experiments are currently on going in order to determine whether differences might be observed on the molecular scale for **TAMT** and **TAMT-Hg(II)** complex.

4. Potassium-templated G-quartet formation

The self-assembly of **TAMG** in absence of salt has already been investigated in chapter 5. Hereafter, we report the study of the formation of **TAMG**-quartet after addition of KI or KPF_6 to TAMG in various solvents (**Figure 67**). Since **TAMG** self-associates into hydrogen-bonded structures in apolar solvents without salts, we will study the transformation of these nanostructures in to **TAMG-K$^+$** complex, as well as the templated self-assembly in presence of potassium salts.

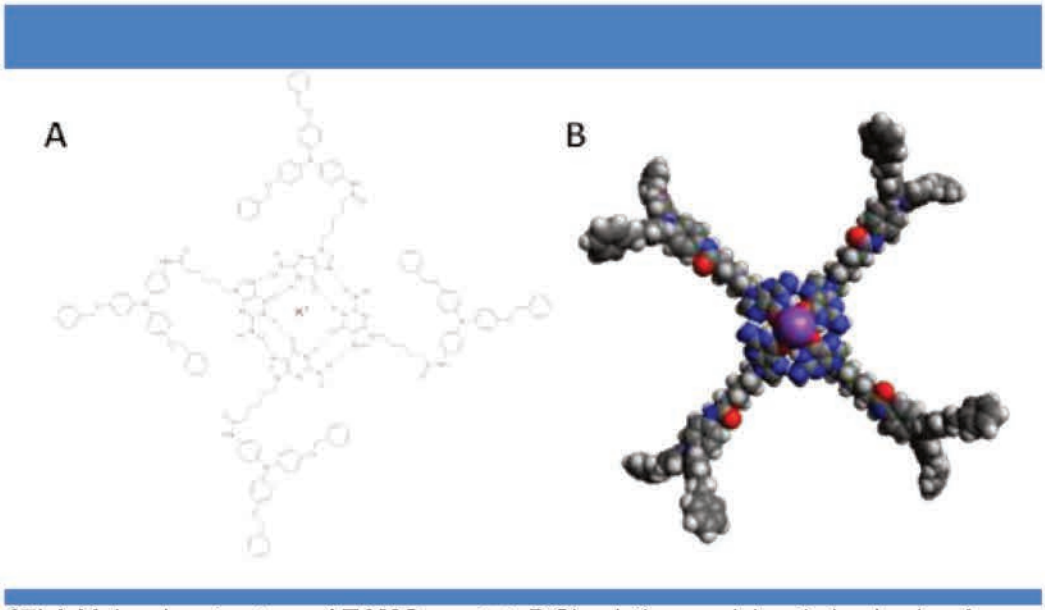

Figure 67| A.Molecular structure of **TAMG**-quartet; B.Simulation model optimized using Avogadro with MMFF94 force field.

a. Characterization

The association of **TAMG** in several apolar solvents (THF, Toluene) was evidenced by ^{1}H NMR spectroscopy as nearly no signals or only several broad peaks were observed in these solvents. To investigate the structural nature and thermodynamic characteristics of guanine self-assemblies, variable-temperature NMR was used in order to dissociate the complex. The NMR spectra of **TAMG** solution in toluene was recorded both in absence of and in presence of KPF_6 (0.25 eq.) from room temperature to 100 °C (**Figure S12**). At room temperature, the

molecules in both solutions are associated into conjugated systems as most ^{1}H NMR signals are flat and broad. We suppose that guanine derivatives are associated with each other through hydrogen bonding to form G-ribbon or other structures. When the temperature was increased to 40°C, the ^{1}H NMR signal corresponding to the benzylic group of pure **TAMG** became sharp and the aromatic peaks between 6.5 – 7.5 ppm were discernible although not clear enough (**Figure 68**). With increasing temperature, the presence of more intense and sharper signals confirmed that the flattening of the spectra at room temperature is caused by the hydrogen-bonded self-assembly.

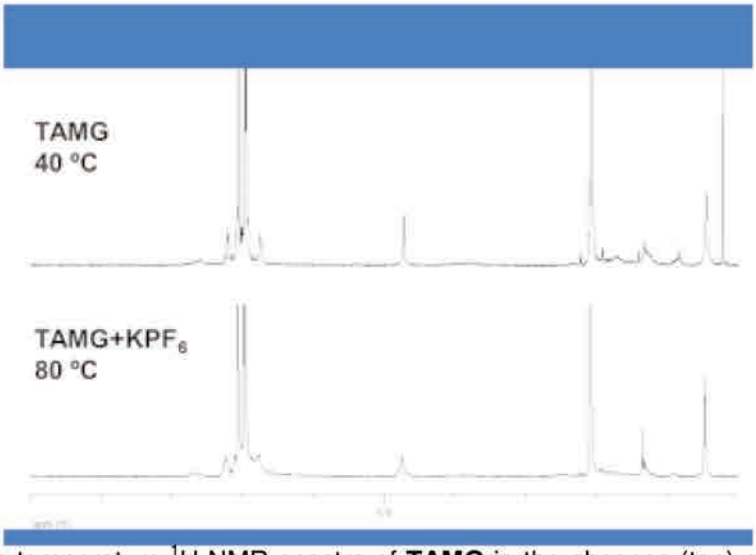

Figure 68| Variable-temperature ^{1}H NMR spectra of **TAMG** in the absence (top) and in the presence (bottom) of KPF_6 (4 mM solution in toluene).

When **TAMG** was mixed with KPF_6 and stirred overnight at room temperature, significant differences were observed, suggesting that the self-assembled structure stabilized by potassium is stable even at high temperatures (**Figure 68** bottom). Comparison of the ^{1}H NMR spectra of **TAMG-K** complex and **TAMG** indicates that the complex is less disassociated at 80 °C than pure **TAMG** at 40 °C. Even at 100 °C, all ^{1}H NMR signals corresponding to the alkyl chain between the guanine and the triarylamine core could not be detected on the spectra of **TAMG**-KPF_6 complex. Therefore, we can conclude that the complex constructed with the potassium salt, which is assumed to be a G-quartet, is much more stable at high temperature than the self-associated system without salt as template.

The formation of G-quartet was further confirmed by ^{1}H NMR spectroscopy in THF solution. It has already been reported that the polarity of solvents had considerable effects on guanine self-association.[188] We thus believe that ^{1}H NMR exepriments in a more polar solvent such as tetrahydrofuran (THF) should reveal more information on the molecular

[188] González-Rodríguez, D. et al. Persistent, well-defined, monodisperse, π-conjugated organic nanoparticles via G-quadruplex self-assembly. J. Am. Chem. Soc. **132,** 4710–4719 (2009).

structure.

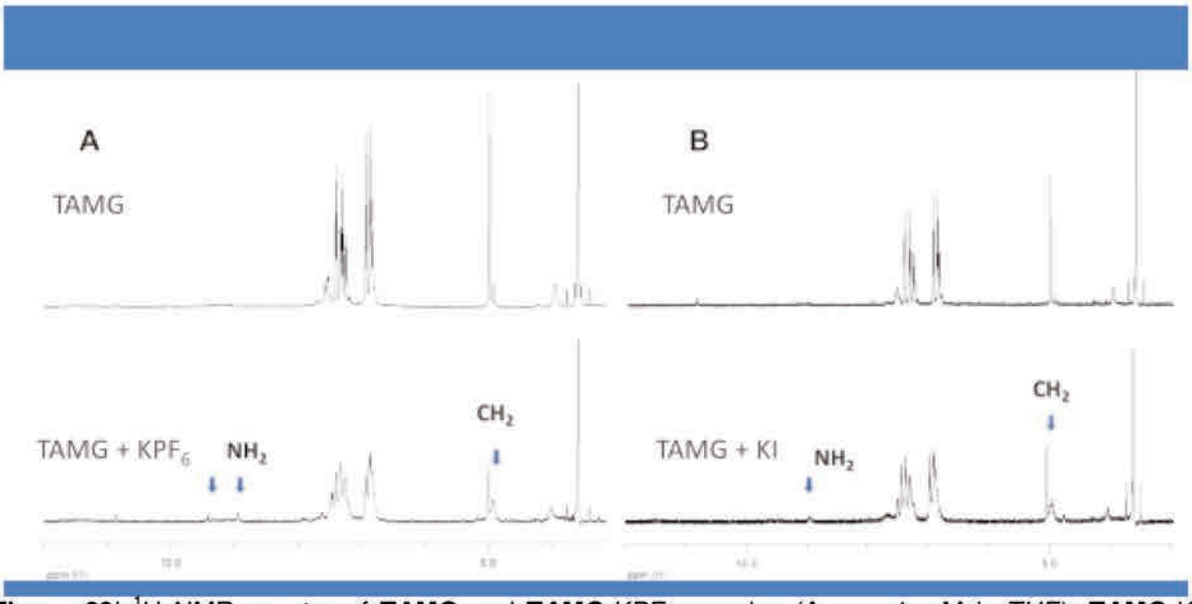

Figure 69| ^{1}H NMR spectra of **TAMG** and **TAMG**-KPF_6 complex (A, c = 4 mM in THF); **TAMG**-KI complex (B, c = 2.8 mM in THF) at room temperature.

As shown in **Figure 69**, after the addition of potassium salts at room temperature, the appearance of amine signals, a broadening of most peaks and the splitting of methyl protons of the benzyl group confirmed complexation. It is well documented that the proton signals of amine cannot sometimes be detected by ^{1}H NMR spectrum, but become discernible when aggregated as complex since hydrogen bonding interactions slower the exchange on the NMR time-scale.[100,140,189,190] In **Figure 69A**, one extra proton signal at 9.41 ppm can be observed, which was reported to be the NH resonance in more complicated columnar G-quadruplex,[144,191] such as a dodecamer consisting of 12 guanines or an octamer made of 8 guanines.

Focusing on informative signals, high-temperature ^{1}H NMR spectra of the **TAMG**-KPF_6 complex were also recorded in THF, as shown in **Figure 70** for the 11-8 ppm and 5.2-4.6 ppm ranges. Interestingly, the amine peak at 8.98 ppm gradually split into two sets of signals when the sample was heated. This observation can be explained by the fact that the reduced intensity of the main peak allows the appearance of the other overlapped weaker peaks: one corresponding to the proton involved in G-quartet by H-bonds and the other one attributed to the free amino proton. As expected, the three kinds of amide protons displayed similar features, i.e. up-field shift and signal broadening, which is due to the partial dissociation of

[189] Arnal-Hérault, C. et al. Functional G-Quartet Macroscopic Membrane Films. Angew. Chemie Int. Ed. **46,** 8409–8413 (2007).
[190] Graziano, C., Masiero, S., Pieraccini, S., Lucarini, M. & Spada, G. P. A Cation-Directed Switch of Intermolecular Spin−Spin Interaction of Guanosine Derivatives Functionalized with Open-Shell Units. Org. Lett. **10,** 1739–1742 (2008).
[191] Kaucher, M. S., Lam, Y.-F., Pieraccini, S., Gottarelli, G. & Davis, J. T. Using Diffusion NMR To Characterize Guanosine Self-Association: Insights into Structure and Mechanism. Chem. - A Eur. J. **11,** 164–173 (2005).

hydrogen bonding interactions at high temperature. In the 5.2 – 4.6 ppm range, the CH_2 proton of the benzyl group obviously performed different chemical shifts due to different kinds of complexation as the temperature increased. The signal splitting might attributed to the fact that the signal corresponding to the G-quartet become less perceptible with increasing temperature and thus the resonance of **TAMG** monomer showed up.

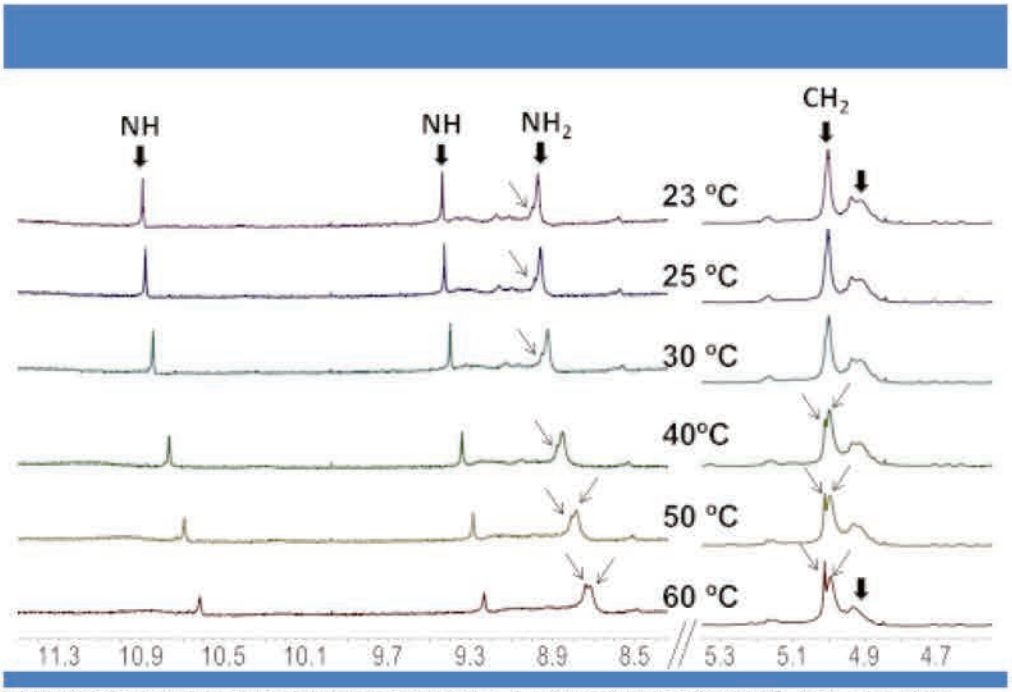

Figure 70| Variable-temperature NMR spectra of a 4 mM solution of **TAMG**-KPF_6 in THF.

We then devised four experiments of complementary small angle X-ray scattering (SAXS), middle angle X-ray scattering (MAXS), wide angle X-ray scattering (WAXS) spectroscopy in order to shed more light on the structural transformation and arrangement patterns occruing during the self-association of guanine as well as for the triarylamine moiety.

Two sets of samples were prepared: **TAMG** in the absence and in the presence of KI, and either without light irradiation or after light irradiation for 1 h. All scattering spectra were recorded at room temperature on powders obtained after evaporation of solvents under vacuum, which resulted in the absence of fluctuation at scattering angles below 0.1 $Å^{-1}$ due to numerous air-solid interfaces. The powder scattering pattern of pure **TAMG** without irradiation reveals the diffraction peaks in the ratio of $1:1/\sqrt{3}:1/2:1/\sqrt{7}$ for d spacing, characteristic for two dimensional hexagonal columnar self-assembly (**Figure 71**, red curve).[72,102, 192 , 193] Interestingly, after mixing **TAMG** with the potassium salt, a new fluctuation appeared leading to a phase transfer since the new d-spacing ratio of

[192] Rosen, B. M. et al. Dendron-Mediated Self-Assembly, Disassembly, and Self-Organization of Complex Systems. Chem. Rev. **109,** 6275–6540 (2009)

[193] Pieraccini, S. et al. Columnar lyomesophases formed in hydrocarbon solvents by chiral lipophilic guanosine-alkali metal complexes. Chirality **13,** 7–12 (2001).

1:1/√2:1/√3:1/2 is indicative of the two-dimensional square packing of body-centered tetragonal phase (**Figure 71**, blue curve).[105,194] In the wide-angle region, the diffraction peak at 1.99 $Å^{-1}$, corresponding to a distance of 0.32 nm, was observed for G-quadruplex, which is the characteristic π-π stacking distance between two planar G-quartets (**Figure 71B**).[189,195] WAXS did not display any sharp reflections for pure **TAMG** powder, thus indicating a lack of crystallinity in the short distances. These results suggest that without the stabilization by salt, **TAMG** molecules self-assembled with molecular-range order and short-range disorder while, for the G-quartet formed in the presence of potassium salt, molecules are arranged into more confined packing. The increase in short-range crystallinity is revealed by the appearance of diffraction peaks on the WAXS spectrum, which dramatically transform the hexagonal molecular arrangement into a tetragonal pattern.

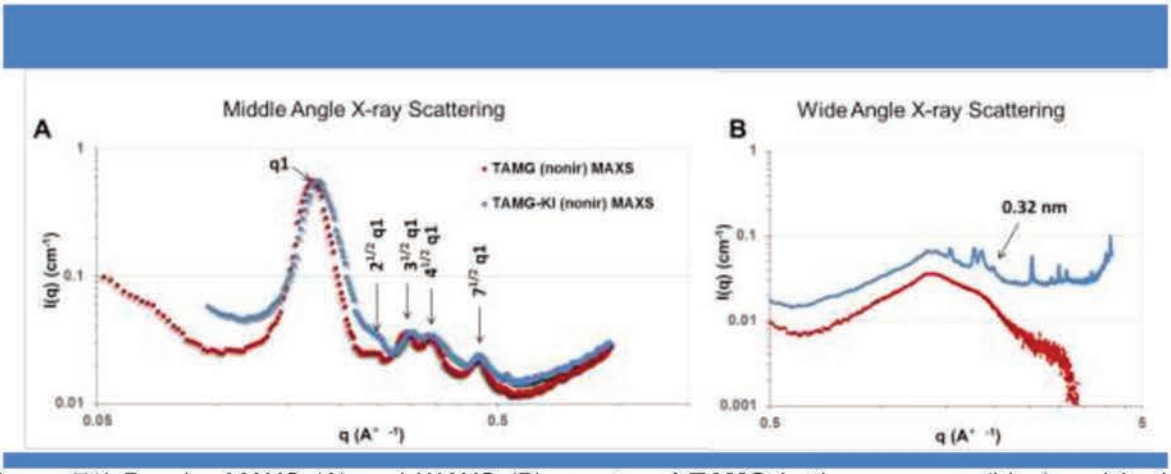

Figure 71| Powder MAXS (A) and WAXS (B) spectra of **TAMG** in the presence (blue) and in the absence (red) of KI.

Further investigations on the morphologies of the light-triggered self-assembly of triarylamine in the presence of G-quartet were carried out and the corresponding SAXS, MAXS and WAXS spectra are displayed in **Figure 72**. After irradiation with white light for 1 hour, the scattering intensity increased indicating a higher electron density, which could be due to the presence of larger aggregates. Besides, the first reflection of high intensity shifted revealing an expansion of the interplanar spacing, from 3.56 nm to 3.84 nm, which might be related to a geometry flattening of the triaryalmine core due to the formation of radicals followed by a nucleation-elongation growth of the triarylamine polymers. In the middle range, another phase transition was observed, indicating that the molecular arrangement turned to a hexagonal lattice with a different size of the cell unit after self-assembly of the triarylamine. It

[194] GOTTARELLI, G. et al. A new lyotropic liquid crystalline phase formed in hydrocarbon solvents by a deoxyguanosine derivative through extensive hydrogen bonding. Liq. Cryst. **26,** 965–971 (1999).

[195] Houbenov, N. et al. Fibrillar Constructs from Multilevel Hierarchical Self - Assembly of Discotic and Calamitic Supramolecular Motifs. Adv. Funct. Mater. **18,** 2041–2047 (2008).

is noteworthy that the existence of G-quartet after irradiation can be rationally supported by the WAXS spectra since the highly short-range ordering nearly remained identical, as evidenced by the sharp diffraction peaks. Another intriguing observation concern the scattering peak corresponding to the π-stacking distance, whose intensity increased a lot after irradiation, indicating that more similar stacking are integrated. Therefore, one could reach the conclusion that the templated G-quartet complex will self-assemble upon white light irradiation and lead to a rearrangement of the packing patterns.

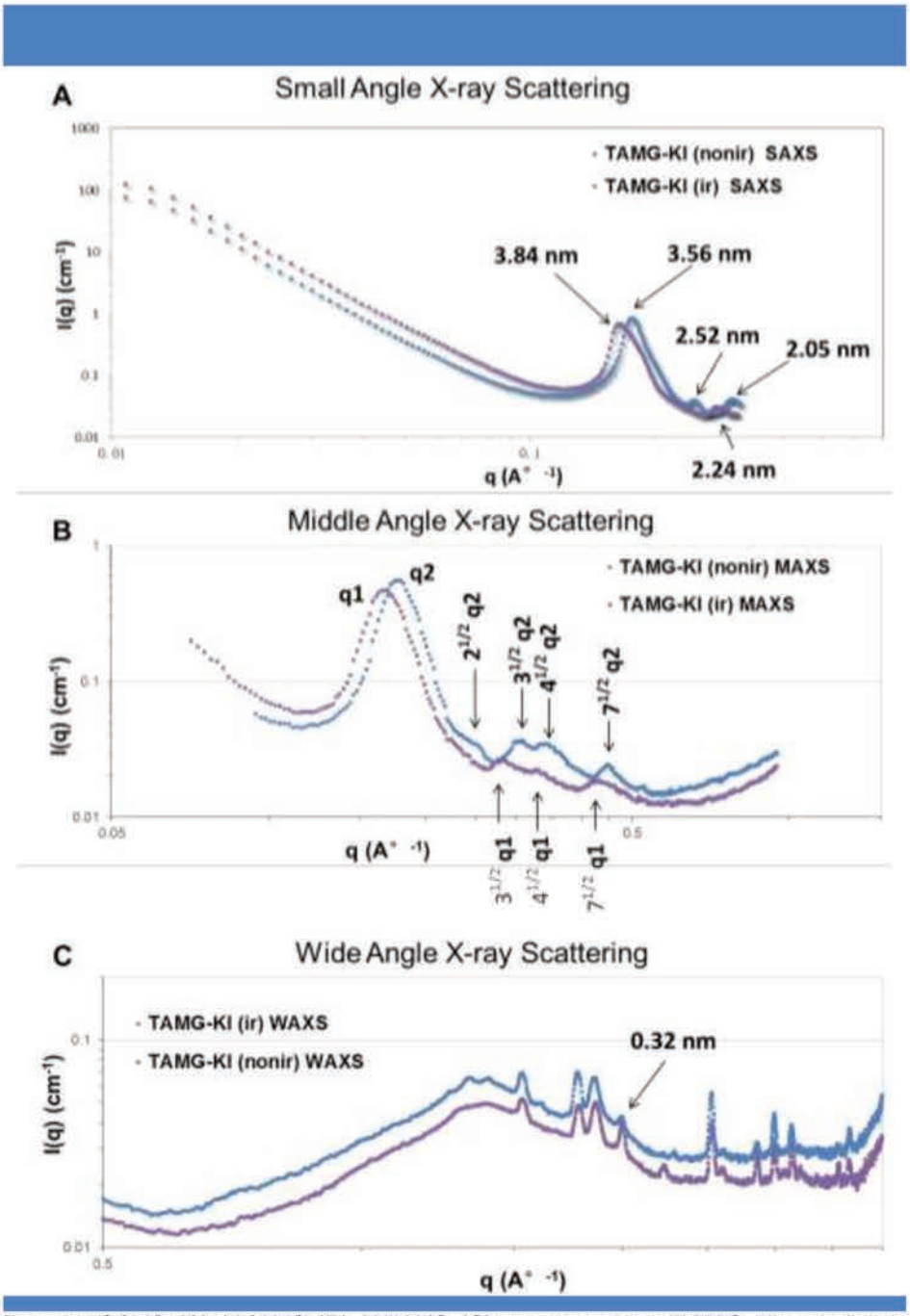

Figure 72| Powder SAXS (A) / MAXS (B) / WAXS (C) spectra of the **TAMG**-KI complex before (blue) and after (purple) irradiaiton with white light.

In order to compare the self-assembly of pure **TAMG** with the templated self-assembly of G-quartet, their scattering reflection curve were compared (**Figure 73**). Obviously, a decrease of the peak width can be observed at the small angle range. It is considered as an evidence of an increase of the aggregated columnar length and decrease of defects in structured aggregation. Besides, the periodical d-spacing peaks set could not be detected for pure **TAMG** after irradiation, suggesting a decreased ordering at the molecular range compared to the potassium templated self-assembled G-quartet but also to **TAMG** ribbons before irradiation. Thus, while triarylamine fibers are usually 1D fibers without much orientation, the fibers became more ordered using potassium as templating ion.

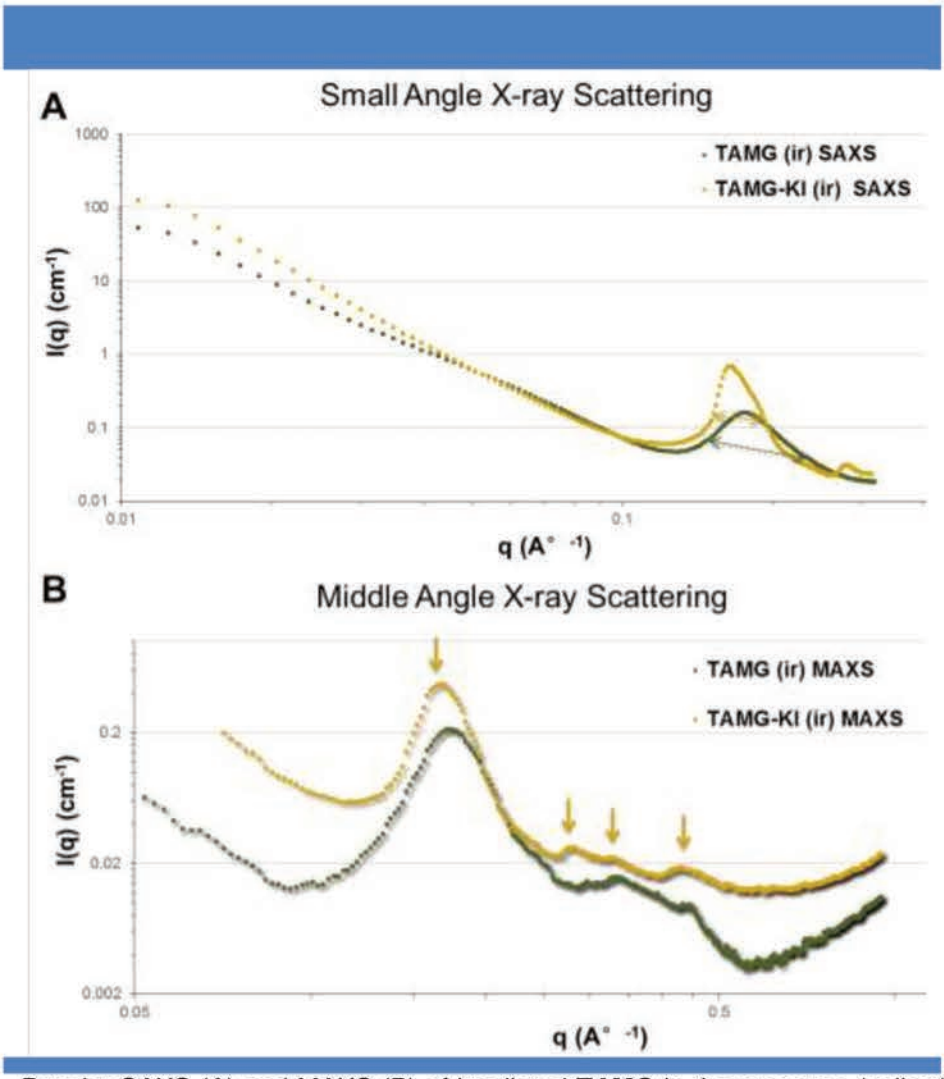

Figure 73| Powder SAXS (A) and MAXS (B) of irradiated **TAMG** in the presence (yellow) and in the absence (green) of KI.

The KPF_6-templated **TAMG**-quartet self-assembly was then kinetically monitored by UV-vis-NIR absorbance experiments. We already discussed about the self-assembly behavior of **TAMG** in chapter 5, and here the spectra of pure **TAMG** and **TAMG**-KPF_6 were compared (**Figure 74**). No absorption wavelength shift from **TAMG** to **TAMG**-K complex

and even the blue shift of the radical band observed for **TAMG** during the irradiation process are observed. However, the absorbance intensities corresponding to the radical cations and to the self-assembly of the triarylamine molecules decreased significantly and their raising trends were also totally different (**Figure 74C-D**). Although there is no direct evidence of the geometry transformation during the irradiation process from UV spectroscopy, one could still propose that triarylamine radicals are more difficult to form in the G-quartet complex as suggested by the delayed appearance of the absorption peaks and their lower intensities. This might be because it is not easy for the molecules which are trapped in the quartet cell to move and twist, i.e. for flattening the triarylamine core, in order to produce triarylamine radicals and stack the triarylamines together.

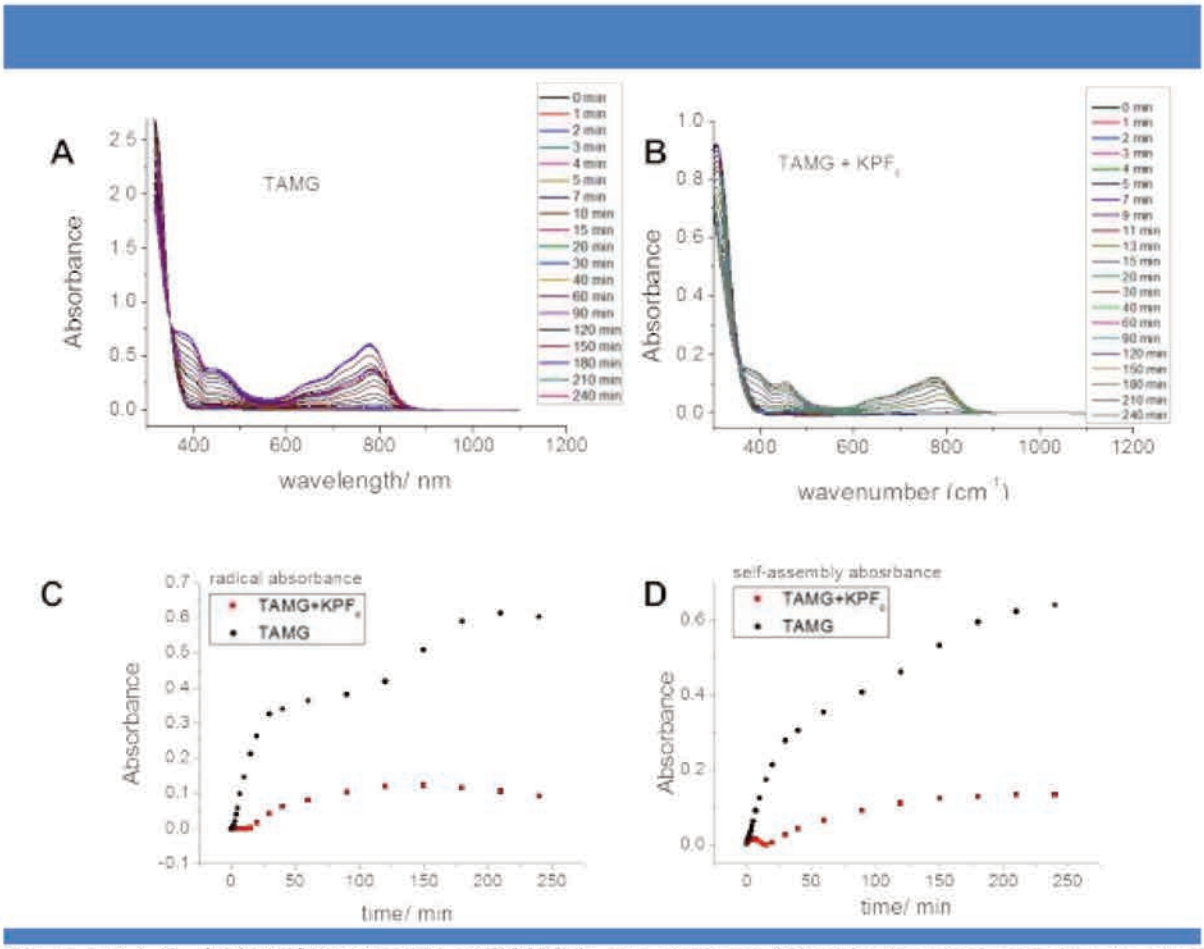

Figure 74| A-B . UV-vis-NIR spectra of **TAMG** in the absence (A) or in the presence of potassium salt (B) for increasing irradiation times. C-D. Evolution of the radical absorbance (C) and the self-assembly absorbance (D) for **TAMG** and **TAMG**-KPF_6 as a function of irradiation time (c = 0.1 mM in chloroform).

In order to get information of the nanostructure morphology, TEM experiments were performed by dropping 6 mM solutions in THF (**Figure 75**) and toluene (**Figure 76**) on grids.

One could definitely distinguish different morphologies for the two solutions made of **TAMG** in THF before and after the addition of KPF_6 (**Figure 75 A** and **B**, respectively). For

pure **TAMG,** many long fibers with a width of 50-100 nm are observed, which might be due to the presence of G-ribbons. After fabrication of the G-quartet stabilized by KPF_6, large quantity of spots appeared as well as relatively uniform fibers (around 100 nm width). The isolated spots which are well distributed over the whole image (**Figure 75B**) are assumed to be nanoparticles composed of **TAMG**-quartets and quadruplexes, with a diameter of around 50-100 nm, while fibers are made of nano-columns resulting from larger aggregation of **TAMG**-quadruplexes which originated from the long-range stacking of **TAMG**-quartets.

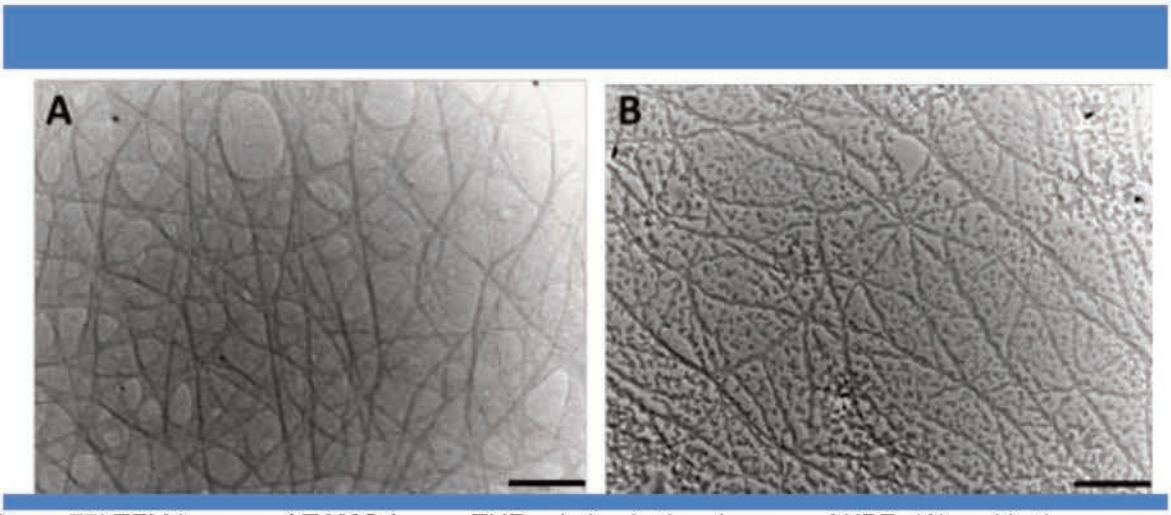

Figure 75| TEM images of **TAMG** from a THF solution in the absence of KPF_6 (A) and in the presence of KPF_6 (B). (Scale bar: 1µm)

Rather different morphologies were observed for **TAMG** solutions in toluene (**Figure 76**). The pure **TAMG** exhibited as thin and long fibers, leading to the formation of networks. However, the **TAMG**-quartet in presence of potassium salt aggregated into much thicker columnar aggregates such as bundles of nanowires, with a diameter of 400 nm. No separated spots could be detected in toluene and the large area of 2D network observed in **Figure 76A** also disappeared upon the addition of potassium salt (**Figure 76B**).

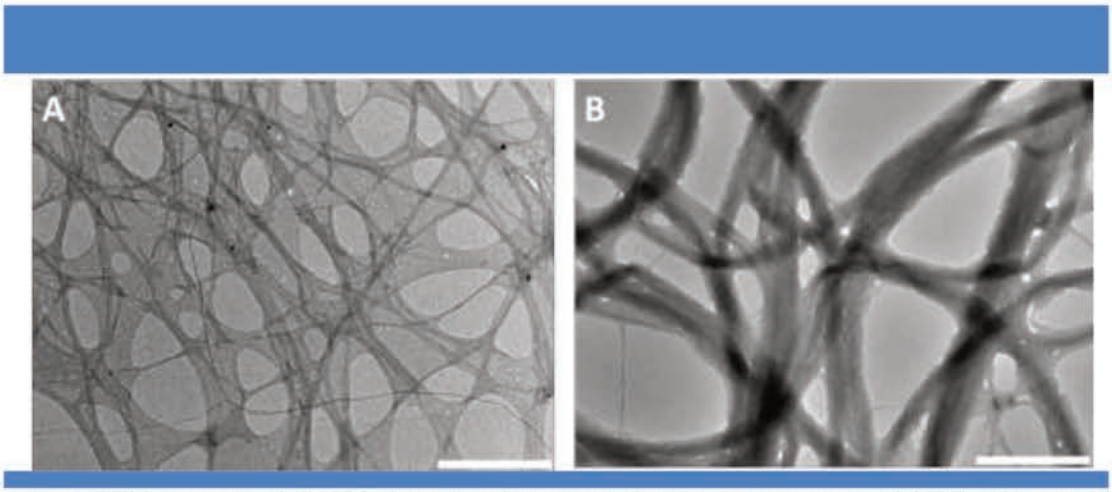

Figure 76| TEM images of **TAMG** from a toluene solution in the absence of KPF_6 (A) and in the presence of KPF_6 (B). (Scale bar: 1µm)

b. Discussion

The formation of G-quartet based on compounds which consist of a guanine (guanosine) residue and another relatively large π conjugated moiety is attractive, but generally studies focused on the molecular arrangement and no obvious evidence for the formation of hierarchical supramolecular polymer was shown.[100,188,196] In this work, we designed a potassium templated self-assembly of triarylamine-guanine conjugates, with the goals to produce bundles of well-ordered triarylamine nanofibers as well as to understand the interactions that govern the different aggregations of **TAMG** and **TAMG**-K-quartet.

TAMG self-association without potassium salt is observed by ^{1}H NMR, TEM microscopy and X-ray scattering. Without light irradiation, **TAMG** self-associates in a hexagonal columnar phase, displaying as a long-range order and short-range disorder in chloroform solution. However, when the **TAMG** was irradiated with white light, no significant well-ordered phase could be detected by X-ray scattering experiments, which suggested that the guanine self-association has to be transferred or broken in order to allow the stacking of the triarylamine units.

When **TAMG** was complexed with potassium salts, G-quartet formation was confirmed by ^{1}H NMR, and X-ray experiments demonstrated that they further associate as square lattice. After irradiation with white light, dramatic difference were recorded by UV-vis-NIR spectroscopy, which showed a much lower quantity of radical cations. Since the generation of triarylamine radicals requires a flattening of the triarylamine geometry, and as these radicals are only stable within the triarylamine fibrils, it becomes more difficult for the **TAMG**-K^+ complex with a rigid arrangement to produce the same quantity of radicals as **TAMG**. However, according to our previous work, only a very little amount of radicals are necessary for the self-assembly of triarylamines and the **TAMG**-K^+ complex is supposed to be self-assembled thanks to the alignment of the triarylamine core as rationally supported by the structural transition after irradiation. X-ray scattering experiments denote the formation of a hexagonal columnar phase with a different lattice parameter, which might due to the flattening of the triarylamine core at the four edges of the complex thus enlarging the periodical distance. Besides, the diffraction peak assigned to π-π stacking increased in intensity without shifting,

[196] (a) Graziano, C., Masiero, S., Pieraccini, S., Lucarini, M. & Spada, G. P. A Cation-Directed Switch of Intermolecular Spin−Spin Interaction of Guanosine Derivatives Functionalized with Open-Shell Units. Org. Lett. **10,** 1739–1742 (2008). (b) Wu, Y.-L., Brown, K. E. & Wasielewski, M. R. Extending Photoinduced Charge Separation Lifetimes by Using Supramolecular Design: Guanine–Perylenediimide G-Quadruplex. J. Am. Chem. Soc. **135,** 13322–13325 (2013). (c) Masiero, S., Gottarelli, G. & Pieraccini, S. G-quartets as a self-assembled scaffold for circular porphyrin arrays. Chem. Commun. **92,** 1995–1996 (2000). (d) Okamoto, A., Inasaki, T. & Saito, I. Nitroxide-labeled guanine as an ESR spin probe for structural study of DNA. Bioorganic Med. Chem. Lett. **14,** 3415–3418 (2004). (e) Martić, S., Liu, X., Wang, S. & Wu, G. Self-Assembly of N2-Modified Guanosine Derivatives: Formation of Discrete G-Octamers. Chem. - A Eur. J. **14,** 1196–1204 (2008).

indicating the fibril growth associated with the self-assembly of the triarylamines followed the same pattern as the G-quartet. The distance of 0.32 nm was even shorter than the original triarylamine stacking distance (0.36 - 0.37 nm),[70] thus suggesting a potentially higher electric conductivity resulting from the denser packing.

Therefore, the ion templated self-assembly of **TAMG** is characterized by a well-ordered arrangement in both long-range and short-range, which can be obviously noticed by comparing SAXS and WAXS datas obtained in the presence and in the absence of potassium salt. The phase transformation induced by a second self-assembly process is a rather novel and peculiar phenomenon for the triarylamine family. Although we only reported preliminary results on this topic, more systematic investigation remain to be performed, but the potassium templated self-assembly of **TAMG** offers potentially new directions for the self-assembly of triarylamine molecules.

Overall, in this chapter, we have reported the templated self-assembly of monotriarylamine-thymine and monotriarylamine-guanine derivatives using either ions or small molecules. We have shown that triarylamine molecules retain their self-assembling properties even in the presence of an external chemical probe, as soon as it does not affect the non-covalent interactions necessary for the self-assembly of the triarylamine core. The use of external stimuli other than light (solvent, chemical) was shown to give rise to new morphologies such as millimetric spherical aggregates. Overall, this work proposes new approaches for the self-assembly of triarylamine molecules, although they are not all driven by the self-assembly of the triarylamine core.

General Conclusion

In this manuscript, I described the results of my PhD work on the self-assembly of well-designed triarylamine molecules, which was pioneered by our group.

In terms of synthetic achievements, we successfully synthesized ten novel triarylamine-nucleobase molecules based either on a mono-amide or a tris-amide triarylamine scaffold in a highly convergent manner. While the syntheses of the monoamide triarylamine-nucleobase molecules (**TAMT**, **TAMG**, **TAMC**, **TAMaC**, **TAUPy**, **4PEGTAMT**) were straightforward from a common brominated intermediate and proceed with reasonable yields, the syntheses of the trisamide triarylamine-nucleobase molecules were complicated by their poor solubility in most organic solvents and water.

We then studied the self-assemblies of these triarylamine monomers in chlorinated solvent upon light irradiation. The corresponding supramolecular polymers were characterized following a systematic approach combining ^{1}H NMR, UV-Vis, and fluorescence spectroscopies. However, so far, it proved difficult to elucidate the molecular arrangement and supramolecular morphologies of the aggregates by scattering and microscopy experiments. For the trisamide triarylamine-thymine molecule, spectroscopic data suggest a molecular arrangement of the triarylamine units in double columnar aggregates as already observed only for monotriarylamine compounds. One important result of this chapter is related to the molecular design of triarylamine molecules in order to keep the self-assembling properties. We suggest avoiding the presence of primary amines which cannot be embedded in hydrogen bonding arrays, as they prohibit the formation of self-assembled structures.

After the fundamental research of the light-triggered self-assemblies of triarylamine-nucleobases conjugates, we also studied the ion- and small molecule-templated self-assemblies of monoamide triarylamine-nucleobase molecules. Using a wide variety of physico-chemical techniques going from optical spectroscopies to X-ray scattering and microscopies, we demonstrated that these chemical stimuli do not hinder the self-assembly process of the triarylamine core. Compared to previous works related to the templated self-assembly of small molecules decorated with nucleobases, we have shown that such templated strategies are not limited to aqueous solutions but can also be performed in organic solvents of various polarities. For instance, we have reported the first example of supramolecular polymers build from melamine in organic solvents. Besides, the hybrid supramolecular polymers with different morphologies of triarylamine-monoguanine conjugate

in absence and in presence of potassium salts were also obtained due to the co-self-assembly of triarylamine core and guanine. However, a deeper interpretation of the different data, in particular for the ion-templated approaches, remains to be perform in order to fully understand the role of the templating ions in the self-assembly process.

Overall, the impact of this work is three-fold: a) it leads to a better understanding of the self-assembly behavior of triarylamine conjugates, b) it influences the design of self-assembling triarylamine structures and c) it offers new approaches for the self-assembly of triarylamine molecules.

Experimental part

1. General procedures

a. Solvents and chemical reagents

All reagents and solvents were purchased at the highest commercial quality and used without further purification unless otherwise noted. Dry solvents were obtained using a double column SolvTech purification system. Water was deionized by using a milli-gradient system (Millipore, Molsheim, France). Microwave reactions were carried out with a single mode cavity Discover SP Microwave Synthesizer (CEM Corporation, NC, USA), producing continuous irradiation at 2455 MHz and equipped with simultaneous external air-cooling system. Yields refer to spectroscopically purified (^{1}H NMR) homogeneous materials.

b. Chromatographic methods

Thin Layer Chromatographies were performed using silica on TLC aluminium foils (silica gel matrix with fluorescent indicator 254 nm, thickness: 500 μm, Sigma-Aldrich). In most cases, irradiation using a Bioblock VL-4C UV-Lamp (6W, 254 nm and/or 365 nm) as well as p-anisaldehyde, phosphomolybdic acid and Cerium ammonium molybdate stainings were used for visualization. Ultra Performance Liquid Chromatographies coupled to Mass Spectroscopy (UPLC-MS) were carried out on a Waters Acquity UPLC-SQD apparatus equipped with a PDA detector (190-500 nm, 80 Hz), using a reverse phase column (Water, BEH C_{18} 1.7 μm, 2.1×50 mm), the MassLynx 4.1 - XP software and a gradient (water-acetonitrile + 0.1% TFA) as eluent. Preparative Adsorption Flash Column Chromatographies were performed using silica gel (60 Å, 230 – 400 mesh, 40 – 63 μm, Sigma-Aldrich) or aluminium oxide 90 (standardized activity Π, 70 – 230 mesh, Merck). Preparative High Performance Liquid Chromatographies coupled to Mass Spectroscopy (HPLC-MS) were performed using a Waters AutoPurify system equipped with a UV detector set at 300 nm, a 3100 mass spectrometer, reverse phase columns (Waters, Sun Fire Prep C_{18} 5.0 μm, 19 × 150 mm; Waters, XBridge Prep C_{18} 5.0 μm, 19 × 150 mm) running with a water/methanol gradient as eluent (with 0.1% formic acid for the Sun Fire Prep C_{18}, or 0.05% ammonia for the XBridge Prep C_{18}) and the MassLynx 4.1 – XP software.

c. Analytical methods and instruments

i. Nuclear Magnetic Resonance (NMR)

^{1}H NMR spectra were recorded on a Bruker Avance 400 spectrometer at 400 MHz and ^{13}C spectra at 100 MHz. The spectra were internally referenced to the residual proton solvent signal

($CDCl_3$: 7.26 ppm, CD_3OD: 3.31 ppm, DMSO-d_6: 2.50 ppm, DMF-d_7: 8.03, 2.92 and 2.75 ppm, Toluene-d_8: 7.09, 7.01, 6.97 and 2.08 ppm and CD_3COCD_3: 2.05 ppm for ^1H spectrum, and $CDCl_3$: 77.16 ppm, CD_3OD: 49.00 ppm, DMSO-d_6: 39.52 ppm, Toluene-d_8: 137.48, 128.87, 127.96, 125.13 and 20.43 ppm and CD_3COCD_3: 206.26 and 29.84 ppm for ^{13}C spectrum). For ^1H NMR assignments, the chemical shifts are given in ppm. Coupling constants J are given in Hz. Peaks are described as singlet (s), doublet (d), triplet (t), multiplet (m), broad (br), and broad singlet (brs).

Diffusion Order Spectroscopy (DOSY) NMR[197] was recorded on a Bruker Avance I spectrometer at 500 MHz at the Service de Résonance Magnétique Nucléaire at the Faculté de Chimie.

The hydrodynamic radius R_H, also called as the Stokes radius is calculated from the measured diffusion coefficient D by the Stokes-Einstein equation:

$$R_H = kT/6\pi\eta D \quad \textbf{(1)}$$

with R_H: radius of molecule; η: dynamic viscosity; D: diffusion coefficient.

If the molecule (aggregate) in solution is assumed as spherical, R_H can be obtained from:

$$R_H = \sqrt[3]{\frac{3M\upsilon}{4\pi N}} \quad \textbf{(2)}$$

with υ partial specific volume and M molecular weight of the molecule.

From equations **(1)** and **(2)**, under identical conditions, the relationship between the diffusion coefficients of two different aggregates (or macromolecules) and their molecular weight can be described as:

$$\frac{D_1}{D_2} = \sqrt[3]{\frac{M_2}{M_1}} \quad \textbf{(3)}$$

ii. Mass spectrometry

ESI-MS mass spectra were recorded in a SQD apparatus from Waters

iii. UV-vis-NIR spectroscopy

UV-Vis-NIR spectra were recorded on a UV-Vis-NIR spectrophotometer Perkin Elmer – Lambda 25, with a 0.1 mM solution in quartz glass cuvette with 1.0 cm optical path.

Solutions of non-self-assembled triarylamine molecules in chlorinated solvents (chloroform, dichloromethane) or in a toluene/methanol mixture containing 5-10 vol% of chloroform were

[197] Schalley, C. A. Analytical Methods in Supramolecular Chemistry: Vol. 1. (John Wiley & Sons, 2012).

generally prepared at 0.1 mM. The first scan was recorded before irradiation and then each solution was irradiated for specific time intervals using a standard 20 W halogen lamp.

iv. Fluorescence spectroscopy

Fluorescence emission spectra were recorded on a FluoroMax-4 (Horiba JobinYvon) spectrofluorometer with the following settings: slit width = 5 nm, increment = 1 nm, integration time = 0.1 s in quartz glass cuvette with a 1.0 cm optical path.

Solutions of non-self-assembled triarylamine molecules in chlorinated solvents (chloroform, dichloromethane) or in a toluene/methanol mixture containing 5-10 vol% of chloroform were generally prepared at 0.1 mM. The first scan was recorded before irradiation and then each solution was irradiated for specific time intervals using a standard 20 W halogen lamp.

v. Fourier transform infrared (FT/IR) spectroscopy

InfraRed (IR) spectra were recorded on a Fourier transform infrared spectrometer VERTEX 70 (Bruker) by drop-casting a solution on an ATR (attenuated total reflection) diamond probe, unless otherwise noted.

vi. Dynamic Light Scattering

DLS experiments were performed using a ZetaSizer Nano ZS (Malvern Instruments, Worcestershire, U.K.). All samples were filtered with a 0.45 µm PTFE filter before measurements.

vii. Transmission Electron Microscopy (TEM)

TEM experiments were performed using a CM12 Philips microscope equipped with a MVIII (SoftImaging System) CCD camera. Samples were analyzed in Bright Field Mode with a LaB_6 cathode and 120 kV tension. Image treatments were performed by using analySIS (Soft Imaging System) software. For sample preparation, a solution containing the compound of interest was dropped (~5 µL) onto a carbon-coated (glow discharged for aqueous samples) copper grid placed on a Whatman filter paper. The grid was then left to dry at air before analysis.

viii. Scanning Electron Microscopy (SEM)

Scanning electron microscopy (SEM) experiments were performed using a Hitachi S-4500 microscope (0.5-30 kV).

ix. X-ray scattering

Small angle/Middle angle/Wide angel X-ray scattering (SAXS/MAXS/WAXS) experiments were performed at the Institut Charles Sadron by using a diffractometer developed by Molecular Metrology (Elexience in France), and a Nanostar diffractometer from Bruker-Anton Paar. Both instruments operate with a pinhole collimation of the X-ray beam and a two-dimensional gas-filled multiwire detector. For the Elexience diffractometer, a monochromatic (λ = 1.54 Å with Dl/l < 4 %) and focused X-ray beam is obtained through a multilayer optic designed and fabricated by Osmic. For the Nanostar, a monochromatic and almost parallel X-ray beam (divergence better than 0.03°) is obtained through a confocal mirror with advanced W/Si multilayer coating from Xenocs. The size of the incident beam on the sample was close to 600 and 300 µm for the Elexience and Nanostar diffractometers, respectively. The sample to detector distance was set at 0.70 m for the Elexience diffractometer and 0.20 m for the Nanostar one, allowing to explore scattering vectors ranging from q = 0.01 $Å^{-1}$ to 0.9 $Å^{-1}$, with $q = 4\pi\sin(\theta/2)/\lambda$, where λ and θ are the wavelength of the incident beam and the scattering angle, respectively. The q-resolution related to the beam size on the sample and the beam divergence was close to 0.005 $Å^{-1}$. Cells of 1 mm thickness and calibrated Mica windows were used as sample holders. Measurements were performed at room temperature. All data were treated according to standard procedures for isotropic small angle X-ray scattering. After radial averaging, the spectra were corrected from electronic noise of the detector, empty cell, absorption and sample thickness. A ^{55}Ir source was used for the corrections of geometrical factors and detector cells efficiency as well as a Silver Behenate sample, for the q-calibration. After all these data treatments, the scattered intensities were corrected from the scattering of the solvent. According to such a procedure, the scattered intensity I(q) containing all the structural information is obtained for each solution.

The Bragg diffraction equation commonly employed for data analysis is:

$$d = \frac{2\sin\theta}{n\lambda} = \frac{2\pi}{q} \quad \textbf{(4)}$$

with d lattice space; θ angle of incident light; λ wavelength of the X-ray beam and q scattering vector.

x. Small angle neutron scattering (SANS)

SANS experiments were performed on the PACE spectrometer at the Laboratoire Leon Brillouin (LLB, CEA Saclay). Typically, three configurations were used: the first was set with a

distance sample to detector of 4.7 m, a wavelength of 13 Å and a collimation distance of 5.00 m, the second at 3 m and 4.6 Å and the last at 1 m and 4.6 Å with a collimation distance of 2.5 m, providing a large accessible q-range from 3×10^{-3} to 0.3 $Å^{-1}$. PACE is a small angle neutron scattering spectrometer dedicated to the study of isotropic scattering. It is equipped with a position sensitive multi-detector made of 30 concentric rings centered around the beam. The monochromator is provided by Dornier Embh, and has the particularity of being very compact that allows retracting it without substantial handling.

xi. Sample preparation of the TAMT-melamine complex

A solution of TAMT (10.0 mg, 14.4 mmol) and melamine (1.82 mg, 14.4 mmol) in acetone (1.0 mL) was heated in the microwave at 90 ºC for 1 h. After the reaction finished, the solution was filtered and then used for further investigation.

A solution of TAMT (20.0 mg, 28.8 mmol) and melamine (1.21 mg, 9.60 mmol) in acetone (2.0 mL) was heated in the microwave at 90 ºC for 1 h. After the reaction finished, the solution was filtered and then used for further investigation.

xii. Sample preparation of the TAMT-mercury complex

Mercury (II) chloride (5.43 mg, 0.02 mmol) was dissolved in chloroform (5.0 mL) and stirred for aoround 24 hours, resulting in a 4 mM $HgCl_2$ solution.

TAMT (5.56 mg, 8 mmol), BATA (4.12 mg, 8 mmol), compound **10** (4.02 mg, 8 mmol) or compound **20** (1.57 mg, 8 mmol) were dissolved by the mercury solution (1.0 mL, 4 mmol). The resulting solution was used as such for spectroscopic measurements.

For UV-Vis-NIR measurement, a mercury solution (2.5 µL, 0.01 µmol) was added sequentially into either a TAMT or a BATA solution (0.1 mM, 1 mL).

xiii. Sample preparation of the G-quartet

Sample preparation for G-quartet follows procedures similar to those reported in the literature[140,144,188]. KI (16.6 mg, 0.10 mmol) or KPF_6 (18.4 mg, 0.10 mmol) were first dissolved in acetone (10.0 mL) as a 10 mM solution. An accurate quantity of one of these salt solutions (100 µL) was evaporated under reduced pressure. Then compound **12** (2.88 mg, 4.00 µmol) and tetrahydrofuran or toluene (1.00 mL) were added directly onto the dry salt and the resulting solution was stirred overnight at room temperature, before being used for characterizations.

2. Synthesis and characterizations of compounds

N, N-bis(4-nitrophenyl)benzene-1,4-diamine **(1)**

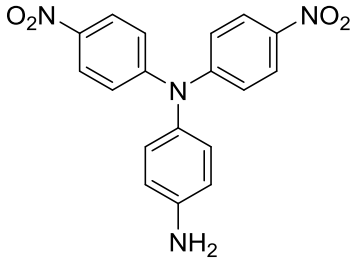

1

Potassium carbonate (2.78 g, 20.0 mmol) was added to a solution of p-phenylenediamine (0.54 g, 5.00 mmol) and 4-fluoronitrobenzene (1.10 mL, 10.0 mmol) in dimethyl sulfoxide (15.0 mL). and the mixture was stirred at 90 °C for three days under an argon atmosphere. The solution was then allowed to cool down to room temperature and the reaction mixture was poured into distilled water (200 mL). The resulting dark red solid was filtered and washed several times with water (3 * 200 mL). This crude compound was finally purified by column chromatography (SiO_2, dichloromethane → dichloromethane/cyclohexane: 3/1) to afford compound **1** (1.52 g, 87 %) as a dark orange solid.

R_f = 0.4 (dichloromethane/cyclohexane: 3/1)

^{1}H NMR ($CDCl_3$, 400 MHz, 25 °C): δ = 8.12 (d, J = 9.2 Hz, 4H), 7.13 (d, J = 9.2 Hz, 4H), 6.98 (d, J = 8.6 Hz, 2H), 6.79 (d, J = 8.6 Hz, 2H), 4.52 (brs, 2H).

^{13}C NMR ($CDCl_3$, 101 MHz, 25 °C): δ = 152.2, 146.1, 142.4, 135.2, 129.1, 125.6, 121.6, 116.6.

MS (ESI+): m/z calcd. for $C_{18}H_{14}N_4O_4$: 351.11 $[M+H]^+$, found: 351.33.

N, N-bis(4-aminophenyl)benzene-1,4-diamine **(2)**

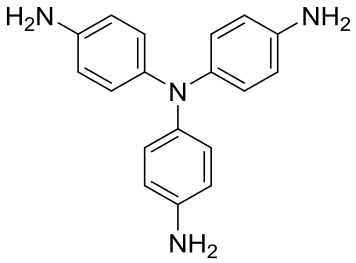

2

A solution of compound **1** (490.5 mg, 1.40 mmol) and tin dichloride (354 mg, 15.7 mmol) in a mixture of acetonitrile (23.0 mL) and ethanol (19.0 mL) was stirred overnight under reflux (80 °C). After that time, the solution was cooled down to room temperature and diluted with dichloromethane (100 mL). The organic phase was washed with Na_2CO_3 (2 × 100 mL) and

brine (100 mL), dried over Na_2SO_4 and concentrated under reduced pressure to provide compound **2** (402 mg, 1.40 mmol) as a dark green solid which was clean enough to be used as such in the next step.

^{1}H NMR (CD_3COCD_3, 400 MHz, 25 °C): δ = 6.71 (d, J = 8.8 Hz, 6H), 6.55 (d, J = 8.8 Hz, 6H), 4.29 (brs, 6H).

^{13}C NMR (CD_3COCD_3, 101 MHz, 25 °C): δ = 143.9, 140.7, 125.3, 116.0.

MS (ESI+): m/z calcd. for $C_{18}H_{18}N_4$: 290.16 $[M]^+$, found: 290.45.

N-{4-{bis[4-(6-bromohexanamido)phenyl]amino}phenyl)-6-bromohexanamide **(3)**

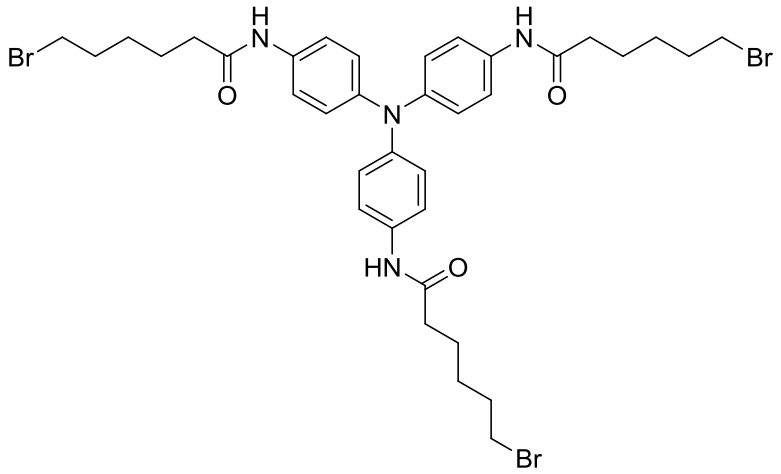

3

A solution of compound **2** (406.5 mg, 1.40 mmol) and triethylamine (0.19 mL, 7.00 mmol) in dichloromethane (30.0 mL) was added dropwise to a solution of 6-bromohexanoyl chloride (0.65 mL, 4.20 mmol) in dichloromethane (10.0 mL) cooled down to 0 °C under an argon atmosphere. The reaction mixture was heated up slowly to room temperature overnight. The resulting precipitate was then filtered and washed by dichloromethane (3 * 50 mL). After drying under vacuum, compound **3** (586.5 mg, 51 %) was obtained as a white solid, pure enough for the next reaction.

^{1}H NMR (d_6-DMSO, 400 MHz, 25 °C): δ = 9.81 (s, 3H), 7.49 (d, J = 8.9 Hz, 6H), 6.89 (d, J = 8.9 Hz, 6H), 3.54 (t, J = 6.7 Hz, 6H), 2.29 (t, J = 7.3 Hz, 6H), 1.81 (tt, J = 7.2, 7.2 Hz, 6H), 1.59 (tt, J = 7.5, 7.5 Hz, 6H), 1.46-1.39 (m, 6H).

^{13}C NMR (d_6-DMSO, 101 MHz, 25 °C): δ = 170.7, 142.7, 134.2, 123.5, 120.3, 36.1, 35.0, 32.0, 27.2, 24.3.

MS (ESI+): m/z calcd. for $C_{36}H_{45}N_4O_3Br_3$: 820.10 $[M]^+$, found: 820.43.

TATG-1 **(4)**

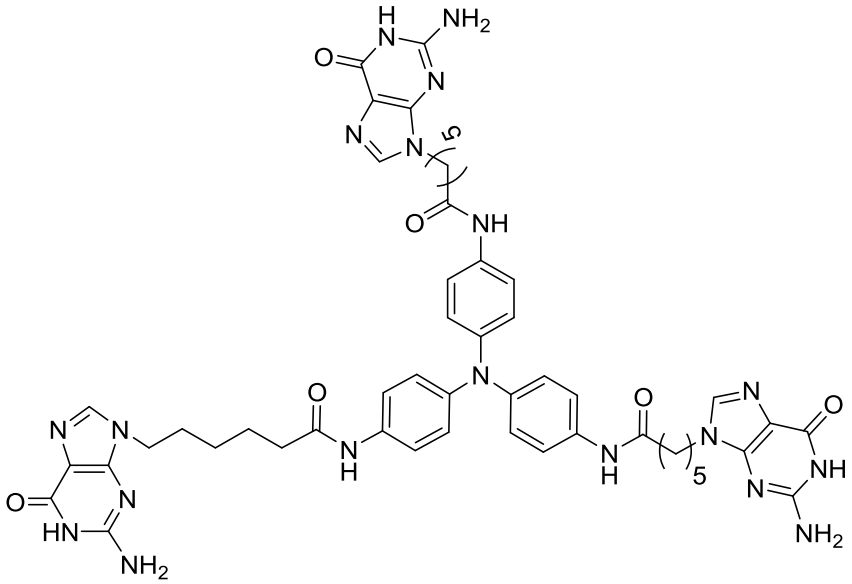

4

To a cold solution of 2-amino-6-chloropurine (510 mg, 3.04 mmol) in dimethylformamide (10.0 mL) was added NaH (60% dispersed, 121.7 mg, 3.04 mmol). The mixture was stirred at 0 °C until complete homogenization. Then, a solution of compound **3** (500 mg, 0.61 mmol) in dimethylformamide (12.0 mL) was added dropwise slowly and the reaction mixture was allowed to warm to room temperature overnight. After concentration under reduced pressure and addition of water (100 mL), a dark brown solid precipitated, was collected by filtration, and then washed with water (5 * 100 mL). This crude residue was directly dissolved in a 3:1 mixture of trifluoroacetic acid/H_2O (8.00 mL) and the resulting solution was stirred at room temperature for 2 days. Solvents were then evaporated and the crude residue was washed several times with diethyl ether (3 * 100 mL) to afford crude compound **4** as a dark green solid. Further purification by reverse phase preparative HPLC-MS (Column: SunFire Prep C18) provided compound **4** (60 mg, 11 %) as a brown solid.

^{1}H NMR (d_7-DMF, 400 MHz, 25 °C): δ = 9.87 (s, 3H), 7.74 (s, 3H), 7.62 (d, J = 8.9 Hz, 6H), 6.96 (d, J = 8.9 Hz, 6H), 6.64 (s, 6H), 4.03 (t, J = 7.1 Hz, 6H), 2.38 (t, J = 7.3 Hz, 6H), 1.84 (tt, J = 7.4, 7.4 Hz, 6H), 1.71 (tt, J = 7.5, 7.5 Hz, 6H), 1.42 - 1.32 (m, 6H).

^{13}C NMR (d_6-DMSO, 101 MHz, 25 °C): δ = 170.7, 162.3, 156.5, 153.6, 151.0, 142.7, 137.4, 134.2, 123.6, 120.3, 42.7, 36.1, 29.2, 25.6, 24.6

MS (ESI+): m/z calcd. for $C_{51}H_{57}N_{19}O_6$: 1032.48 $[M+H]^+$, found: 1032.45.

N-{4-{bis[4-(2-bromoacetamido)phenyl]amino}phenyl)-2-bromoacetamide **(5)**

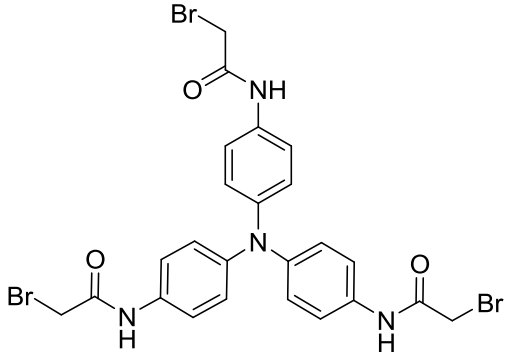

5

A solution of compound **2** (400 mg, 1.40 mmol) and triethylamine (0.63 mL, 4.60 mmol) in dichloromethane (30.0 mL) was added dropwise to a cooled solution of bromoacetyl chloride (340 µL, 4.13 mmol) in dichloromethane (40.0 mL) at 0 °C. The reaction mixture was heated up slowly to room temperature overnight. After that time, a slightly yellow solid precipitated, which was diluted with diethyl ether (100 mL). The organic phase was washed with HCl (2 × 100 mL) and brine (100 mL), dried over Na_2SO_4 and concentrated under reduced pressure. Further purification by column chromatography (SiO_2, dichloromethane → dichloromethane/ethyl acetate: 1/1) provided compound **5** (649 mg, 72%) as a white solid.

R_f = 0.2 (dichloromethane/ethyl acetate: 1/1)

^{1}H NMR (d_6-DMSO, 400 MHz, 25 °C): δ = 10.30 (s, 3H), 7.51 (d, J = 8.9 Hz, 6H), 6.95 (d, J = 8.9 Hz, 6H), 4.23 (s, 6H).

^{13}C NMR (d_6-DMSO, 101 MHz, 25 °C): δ = 164.3, 143.2, 133.5, 123.9, 120.7, 43.5.

MS (ESI+): m/z calcd. for $C_{24}H_{21}N_4O_3Br_3$: 651.92 $[M+H]^+$, found: 651.93.

TATG-2 **(6)**

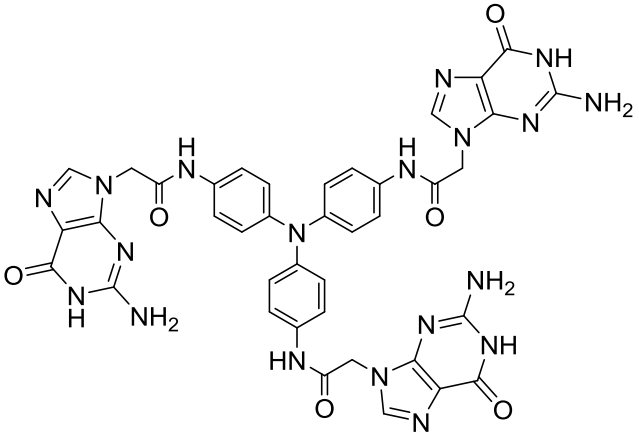

6

To a cold solution of 2-amino-6-chloropurine (649 mg, 3.83 mmol) in dimethylformamide (20.0 mL) was added NaH (60% dispersed, 153.1 mg, 3.83 mmol). The mixture was stirred at

0 °C until complete homogenization. Then, a solution of compound **5** (500 mg, 0.77 mmol) in dimethylformamide (10.0 mL) was added dropwise slowly and the reaction mixture was allowed to warm to room temperature overnight. After concentration under reduced pressure and addition of water (100 mL), a dark brown solid precipitated, was collected by filtration, and then washed with water (5 * 100 mL). This crude residue was directly dissolved in a 3:1 mixture of trifluoroacetic acid/H_2O (8.00 mL) and the resulting solution was stirred at room temperature for 2 days. Solvents were then evaporated and the crude residue was washed several times with diethyl ether (3 * 100 mL) to afford crude compound **6** as a dark green solid. Further purification by reverse phase preparative HPLC-MS (Column: SunFire Prep C18) provided compound **6** (22.0 mg, 2 %) as a brown solid.

^{1}H NMR (d_6-DMSO, 400 MHz, 25 °C): δ = 10.32 (s, 3H), 7.87 (s, 3H), 7.47 (d, J = 8.9 Hz, 6H), 6.91 (d, J = 8.9 Hz, 6H), 6.47 (brs, 6H), 4.83 (s, 6H).

^{13}C NMR (d_6-DMSO, 101 MHz, 25 °C): δ = 164.9, 156.8, 153.6, 151.6, 143.0, 138.4, 133.6, 123.8, 120.5, 116.2, 45.4.

MS (ESI+): m/z calcd. for $C_{39}H_{33}N_{19}O_6$: 864.30 $[M+H]^+$, found: 864.66

TATT **(7)**

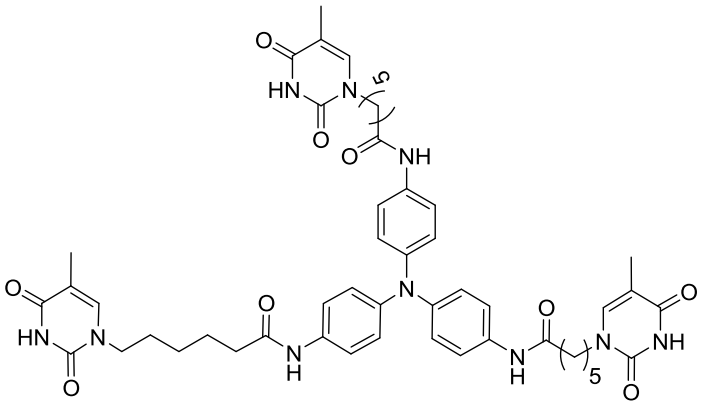

7

A solution of thymine (460.6 mg, 3.65 mmol), potassium carbonate (504.7 mg, 3.65 mmol) and compound **3** (250 mg, 0.30 mmol) in dimethylformamide (6.00 mL) was stirred at 60 °C overnight. After that time, the solution was concentrated under reduced pressure and then, distilled water (50 mL) was added. The resulting white solid was filtered, washed several times with water (5 * 50 mL) and further purified by reverse-phase preparative HPLC-MS (Column: XBridge Prep C18) to afford compound **7** (17.0 mg, 4 %) as a white powder.

^{1}H NMR (CD_3OD, 400 MHz, 25 °C): δ = 7.44 – 7.39 (m, 9H), 6.96 (d, J=8.8 Hz, 6H), 3.73 (t, J = 7.2 Hz, 6H), 2.37 (t, J = 7.3 Hz, 6H), 1.85 (d, J = 1.0 Hz, 9H), 1.78 -1.68 (m, 12H), 1.45 - 1.37 (m, 6H).

^{13}C NMR (d_8-toluene/CD_3OD 5:3, 101 MHz, 25 °C): δ = 173.3, 166.1, 152.3, 145.0, 142.0, 134.7, 125.0, 122.0, 110.8, 37.3, 29.2, 26.5, 25.8, 25.8, 12.3.

MS (ESI+): m/z calcd. for $C_{51}H_{60}N_{10}O_9$: 957.46 $[M+H]^+$, found: 957.79.

TATC **(8)**

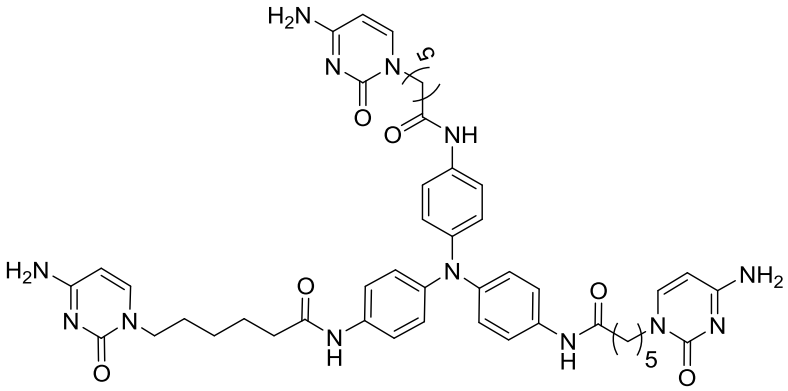

8

A solution of acetylcytosine (335.6 mg, 2.20 mmol), potassium carbonate (302.8 mg, 2.20 mmol) and compound **3** (200 mg, 0.24 mmol) in dimethylformamide (14.0 mL) was stirred at 60 °C overnight. After that time, the solution was concentrated under reduced pressure and then, distilled water (100 mL) was added. The resulting crude residue was filtered and washed several times with water (5 * 100 mL). A suspension of this crude residue (200 mg, 0.19 mmol) and potassium carbonate (239.6 mg, 1.70 mmol) was stirred in methanol (20 mL) at room temperature. The reaction was monitored by UPLC-MS and stopped after 18 hours by concentration under reduced pressure. The crude residue was washed by water (5 * 100 mL) and further purified by reverse-phase preparative HPLC-MS (Column: XBridge Prep C18) to afford compound **8** (14.5 mg, 8 %) as a white powder.

^{1}H NMR (CD_3OD, 400 MHz, 25 °C): δ = 8.51 (brs, 3H), 7.56 (d, J = 7.2 Hz, 3H), 7.41 (d, J = 8.9 Hz, 6H), 6.96 (d, J = 8.9 Hz, 6H), 5.82 (d, J = 7.2 Hz, 3H), 3.78 (t, J = 7.2 Hz, 6H), 2.36 (t, J = 7.3 Hz, 6H), 1.74 (tt, J = 7.5, 7.5 Hz, 12H), 1.45 - 1.36 (m, 6H).

^{13}C NMR (d_6-DMSO, 101 MHz, 25 °C): δ = 170.7, 165.8, 155.7, 146.0, 142.6, 134.2, 123.5, 120.3, 92.9, 48.4, 36.1, 28.5, 25.5, 24.8.

MS (ESI+): m/z calcd. for $C_{48}H_{57}N_{16}O_3$: 912.46 $[M+H]^+$, found: 912.60.

1-(benzyloxy)-4-iodobenzene **(9)**

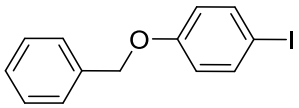

9

Potassium carbonate (8.30 g, 60.0 mmol) was added to a solution of 4-iodophenol (2.64 g, 12.0 mmol) in acetone (66.0 mL) and then, benzyl bromide (1.19 mL, 10.0 mmol) was added dropwise under an argon atmosphere. The reaction mixture was then heated up to reflux overnight. After concentration under reduced pressure, the crude residue was dissolved in ethyl acetate (100 mL) and the organic phase was washed with water (50.0 mL), NaOH 1M solution (2 × 100 mL) and brine (50.0 mL) and dried over Na_2SO_4. Further concentration under reduced pressure afforded compound **9** (3.05 g, 98 %) as a white solid.

^{1}H NMR ($CDCl_3$, 400 MHz, 25 °C): δ = 7.56 (d, J = 8.8 Hz, 2H), 7.45 – 7.30 (m, 5H), 6.76 (d, J = 8.8 Hz, 2H), 5.04 (s, 2H).

^{13}C NMR ($CDCl_3$, 101 MHz, 25 °C): δ = 158.8, 138.4, 136.7, 128.8, 128.3, 127.6, 117.4, 83.2, 70.2.

4-(benzyloxy)-N-[4-(benzyloxy)phenyl]-N-(4-nitrophenyl)aniline **(10)**

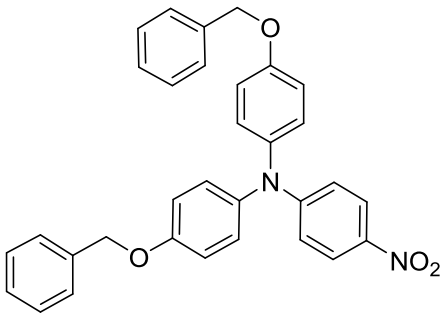

10

In one flask under argon, 4-nitroaniline (1.11 g, 8.06 mmol) and compound **9** (10.0 g, 32.2 mmol) were dissolved in dimethylformamide (30.0 mL). The solution was then added dropwise to a mixture of copper iodide (0.614 g, 3.20 mmol), potassium carbonate (8.91 g, 64.5 mmol) and L-Proline (0.743 g, 6.45 mmol) in a 100 mL Schlenck and the reaction mixture was stirred vigorously at 125 °C. The reaction was followed by UPLC-MS and stopped after 12 days. The mixture was cooled down to room temperature and ethyl acetate (50.0 mL) was then added. The solution was passed through a pad of silica gel and washed with ethyl acetate (600 mL) to remove all copper salts. The resulting organic phase was concentrated under reduced pressure. Further purification by column chromatography (SiO_2, pentane → pentane/diethyl ether: 5/1) afforded compound **10** (220 mg, 69 %) as a dark red solid.

R_f = 0.2 (pentane/diethyl ether: 5/1)

^{1}H NMR ($CDCl_3$, 400 MHz, 25 °C): δ = 8.00 (d, J = 9.4 Hz, 2H), 7.47 - 7.32 (m, 10H), 7.13 (d, J = 9.0 Hz, 4H), 6.98 (d, J = 9.0 Hz, 4H), 6.76 (d, J = 9.4 Hz, 2H), 5.07 (s, 4H).

^{13}C NMR ($CDCl_3$, 101 MHz, 25 °C): δ = 156.8, 154.1, 137.8, 137.7, 136.9, 128.6, 128.5, 127.9, 127.7, 125.7, 116.2, 114.5, 69.5.

MS (ESI+): m/z calcd. for $C_{32}H_{26}N_2O_4$: 503.20 $[M+H]^+$, found: 503.43.

N-{4-{bis[4-(benzyloxy)phenyl]amino}phenyl)-6-bromohexanamide **(11)**

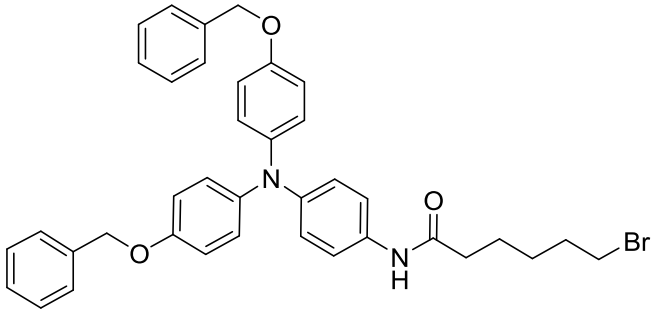

11

A solution of compound **10** (200 mg, 0.40 mmol) and tin dichloride (1016 mg, 4.46 mmol) in a mixture of acetonitrile (6.50 mL) and ethanol (5.50 mL) was stirred overnight under reflux. After that time, the solution was cooled down to room temperature and diluted with dichloromethane (100 mL). The organic phase was washed by Na_2CO_3 sat. (2 x 100 mL) and brine (100 mL), dried over Na_2SO_4 and concentrated under reduced pressure. The resulting product of N,N-bis[4-(benzyloxy)phenyl]benzene-1,4-diamine was clean enough to be used as such in the next step. This crude aromatic amine (188 mg, 0.40 mmol) and triethylamine (0.06 mL, 0.44 mmol) were added dropwise to a cooled solution of 6-bromohexanoyl chloride (0.06 mL, 0.40 mmol) in dichloromethane (10.0 mL) under an argon atmosphere and the reaction mixture was stirred overnight at room temperature. The reaction was then diluted with dichloromethane (50 mL) and the organic phase was washed with NH_4Cl (2 × 50.0 mL) and brine (50.0 mL), and then dried over Na_2SO_4. Further concentration under reduced pressure and purification by column chromatography (SiO_2, cyclohexane → cyclohexane/ethyl acetate: 3/1) afforded compound **11** (232 mg, 90 % over 2 steps) as a light yellow solid.

R_f = 0.3 (cyclohexane/ethyl acetate: 3/1)

^{1}H NMR (d_6-DMSO, 400 MHz, 25 °C): δ = 9.75 (s, 1H), 7.47-7.30 (m, 12H), 6.95 (d, J = 9.2 Hz, 4H), 6.91 (d, J = 9.1 Hz, 4H), 6.81 (d, J = 8.9 Hz, 2H), 5.05 (s, 4H), 3.54 (t, J = 6.7 Hz, 2H), 2.27 (t, J = 7.3 Hz, 2H), 1.82 (tt, J = 7.1, 7.1 Hz, 2H), 1.59 (tt, J = 7.4, 7.4 Hz, 2H), 1.45 - 1.36 (m, 2H).

^{13}C NMR (d_6-DMSO, 101 MHz, 25 °C): δ = 170.6, 154.1, 143.4, 141.0, 137.2, 133.4, 128.4, 127.8, 127.7, 125.1, 122.1, 120.3, 115.7, 69.5, 36.1, 35.0, 32.0, 27.2, 24.3.

MS (ESI+): m/z calcd. for $C_{38}H_{37}N_2O_3Br$: 648.20 $[M]^+$, found: 648.54.

TAMG **(12)**

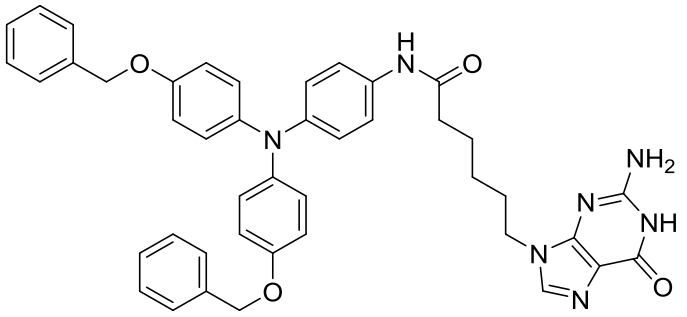

12

To a cold solution of 2-amino-6-chloropurine (195.8 mg, 1.16 mmol) in dimethylformamide (8.0 mL) was added NaH (60% dispersed, 46.2 mg, 1.16 mmol). The mixture was stirred at 0 °C until complete homogenization. Then, a solution of compound **11** (500 mg, 0.77 mmol) in dimethylformamide (16.0 mL) was added dropwise slowly and the reaction mixture was allowed to warm to room temperature overnight. After concentration under reduced pressure and addition of water (100 mL), a solid precipitated, was collected by filtration, and then washed with water (5 * 100 mL). This crude residue was directly dissolved in a 3:1 mixture of trifluoroacetic acid/H_2O (6.5 mL) and the resulting solution was stirred at room temperature for 2 days. Solvents were then evaporated and the crude residue was washed several times with diethyl ether (100 mL) to afford crude compound **12**. Further purification by column chromatography (from dichloromethane → dichloromethane/methanol: 10/1) provided compound **12** (90 mg, 20 %) as a grey solid.

R_f **=** 0.2 (dichloromethane/methanol: 10/1)

^{1}H NMR (d_6-DMSO, 400 MHz, 25 °C): δ = 10.50 (s, 1H), 9.75 (s, 1H), 7.68 (s, 1H), 7.45 - 7.31 (m, 12H), 6.95 (d, J = 9.6 Hz, 4H), 6.91 (d, J = 9.2 Hz, 4H), 6.80 (d, J = 9.0 Hz, 2H) 6.42 (s, 2H), 5.05 (s, 4H), 3.92 (t, J = 7.1 Hz, 2H), 2.24 (t, J = 7.3 Hz, 2H), 1.80 - 1.70 (m, 2H), 1.63 - 1.54 (m, 2H), 1.29 - 1.19 (m, 2H).

^{13}C NMR (d_6-DMSO, 101 MHz, 25 °C): δ = 170.8, 156.9, 154.2, 153.5, 151.5, 151.2, 143.5, 141.1, 139.2, 137.2, 133.3, 128.5, 127.9, 127.7, 125.2, 124.9, 122.1, 120.4, 115.8, 69.6, 34.4, 30.5, 29.3, 24.7, 21.1.

MS (ESI+): m/z calcd. for $C_{43}H_{41}N_7O_4$: 720.33 $[M+H]^+$, found: 720.66

TAMT **(13)**

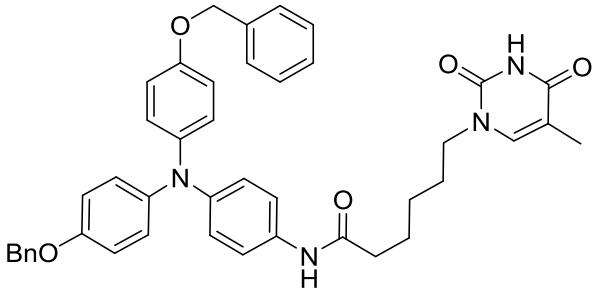

13

A solution of thymine (116.5 mg, 0.92 mmol), potassium carbonate (127.6 mg, 0.92 mmol) and compound **11** (200 mg, 0.31 mmol) in dimethylformamide (20.0 mL) was stirred at 60 °C overnight. After that time, the solution was concentrated under reduced pressure and then, distilled water (100 mL) was added. The resulting white solid was filtered, washed several times with water (5 * 100 mL) and further purified by column chromatography (SiO_2, toluene → toluene/ethyl acetate: 1/4) to afford compound **13** (120 mg, 56 %) as a grey solid.

R_f **=** 0.3 (toluene/ethyl acetate: 1/4)

^{1}H NMR ($CDCl_3$, 400 MHz, 25 °C): δ = 8.28 (s, 1H), 7.45-7.30 (m, 12H), 7.19 (s, 1H), 7.00 (d, J = 9.2 Hz, 4H), 6.92 (d, J = 8.9 Hz, 2H), 6.87 (d, J = 9.0 Hz, 4H), 5.02 (s, 4H), 3.71 (t, J = 7.3 Hz, 2H), 2.35 (t, J = 7.2 Hz, 2H), 1.91 (d, J = 1.1 Hz, 3H), 1.80-1.69 (m, 4H), 1.46 - 1.39 (m, 2H).

^{13}C NMR ($CDCl_3$, 101 MHz, 25 °C): δ = 170.6, 163.9, 154.9, 150.9, 145.5, 141.6, 140.6, 137.2, 131.6, 128.7, 128.1, 127.7, 125.9, 122.5, 121.2, 115.7, 110.9, 70.5, 31.1, 29.8, 28.8, 25.8, 24.7, 12.5.

MS (ESI+): m/z calcd. for $C_{43}H_{42}N_4O_5$: 695.32 $[M+H]^+$, found: 695.60.

TAMaC **(14)**

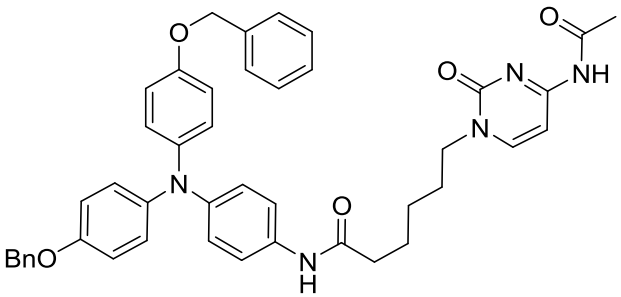

14

A solution of acetylcytosine (63.8 mg, 0.46 mmol), potassium carbonate (70.7 mg, 0.46 mmol) and compound **11** (100 mg, 0.15 mmol) in dimethylformamide (10.0 mL) was stirred at 60 °C

overnight. After that time, the solution was concentrated under reduced pressure and then, distilled water (100 mL) was added. The resulting crude residue was filtered and washed several times with water (5 * 100 mL). Further purification by column chromatography (SiO_2, cyclohexane → cyclohexane/ethyl acetate: 1/2) afforded compound **14** (60 mg, 54 %) as a white solid.

R_f = 0.4 (cyclohexane/ethyl acetate: 1/2)

^{1}H NMR ($CDCl_3$, 400 MHz, 25 °C): δ = 8.38 (d, J = 5.6 Hz, 1H), 7.98 (s, 1H), 7.75 (d, J = 5.5 Hz, 1H), 7.45 - 7.29 (m, 12H), 7.12 (s, 1H), 7.00 (d, J = 8.8 Hz, 4H), 6.92 (d, J = 9.1 Hz, 2H), 6.87 (d, J = 8.7 Hz, 4H), 5.03 (s, 4H), 4.34 (t, J = 6.5 Hz, 2H), 2.36 (t, J = 8.3 Hz, 2H), 2.20 (s, 3H), 1.88 - 1.76 (m, 4H), 1.54 - 1.44 (m, 2H).

^{13}C NMR (CD_3COCD_3, 101 MHz, 25 °C): δ = 171.6, 170.8, 166.0, 161.2, 160.7, 155.8, 145.2, 142.7, 138.6, 134.7, 129.4, 128.7, 128.5, 126.4, 123.4, 121.3, 116.6, 104.2, 70.9, 67.6, 37.7, 26.5, 26.2, 24.6, 24.5.

MS (ESI+): m/z calcd. for $C_{44}H_{43}N_5O_5$: 722.33 $[M+H]^+$, found: 722.60.

TAMC **(15)**

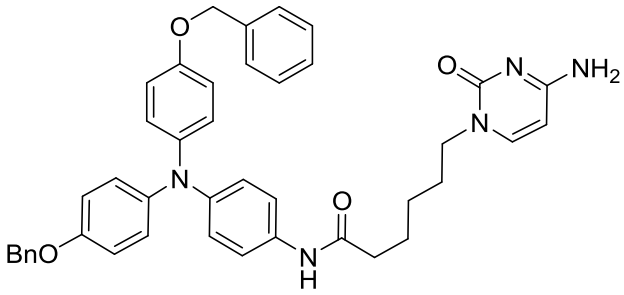

15

A suspension of compound **14** (500 mg, 0.69 mmol) and potassium carbonate (574.4 mg, 4.16 mmol) was stirred in methanol (55.6 mL) at room temperature. The reaction was monitored by UPLC-MS and stopped after 6 hours by concentration under vacuum. The crude residue was washed with water (7 * 100 mL) and further purified by reverse-phase preparative HPLC-MS (Column: XBridge Prep C18) to afford compound **15** (120 mg, 25 %) as a white solid.

^{1}H NMR (CD_3OD, 400 MHz, 25 °C): δ = 7.55 (d, J = 7.2 Hz, 1H), 7.43 - 7.30 (m, 12H), 6.95 (d, J = 9.1 Hz, 4H), 6.90 (d, J = 9.2 Hz, 4H), 6.85 (d, J = 8.9 Hz, 2H), 5.82 (d, J = 7.2 Hz, 1H), 5.04 (s, 4H), 3.77 (t, J = 7.3 Hz, 2H), 2.35 (t, J = 7.4 Hz, 2H), 1.77 - 1.69 (m, 4H), 1.44 - 1.36 (m, 2H).

^{13}C NMR (CD_3OD, 101 MHz, 25 °C): δ = 174.1, 167.9, 159.1, 156.2, 147.5, 146.5, 142.9, 138.8, 133.4, 129.5, 128.8, 128.6, 126.9, 123.1, 122.6, 116.9, 95.6, 71.4, 37.5, 30.7, 29.8, 27.0, 26.4.

MS (ESI+): m/z calcd. for $C_{42}H_{41}N_5O_4$: 680.32 $[M+H]^+$, found: 680.54.

TAMUpy **(16)**

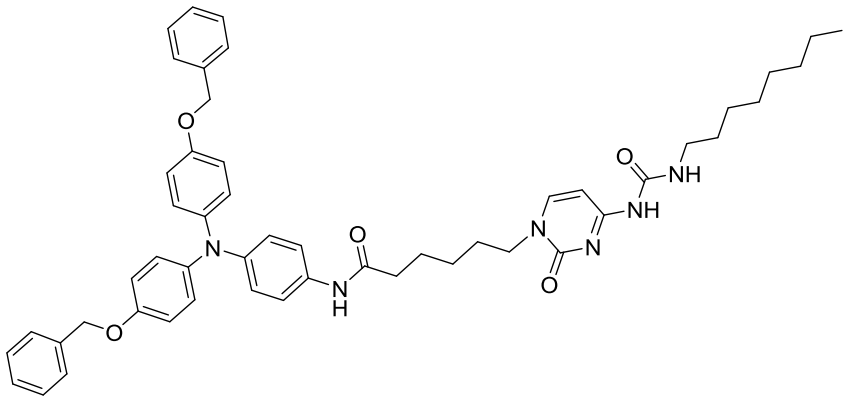

16

A solution of compound **15** (11.0 mg, 0.016 mmol) and octyl isocyanate (5.71 µL, 0.032 mmol) in dry pyridine (0.5 mL) was heated to 90.0 °C and stirred overnight. After that time, the solvent was evaporated under reduced pressure and the residue was purified by column chromatography (SiO_2, ethyl acetate → ethyl acetate/methanol: 10/1) to afford compound **16** (5.00 mg, 37 %) as a white solid.

R_f = 0.6 (ethyl acetate/methanol: 10/1)

^{1}H NMR ($CDCl_3$, 400 MHz, 25 °C): δ = 10.90 (brs, 1H), 8.92 (brs, 1H), 7.44-7.30 (m, 14H), 6.99 (d, J = 9.0 Hz, 4H), 6.92 (d, J = 8.9 Hz, 2H), 6.87 (d, J = 9.0 Hz, 4H), 5.02 (s, 4H), 3.82 (t, J = 7.1 Hz, 2H), 3.27 - 3.20 (m, 2H), 2.33 (t, J = 7.2 Hz, 2H), 1.82 - 1.72 (m, 4H), 1.59 - 1.50 (m, 2H), 1.45 - 1.37 (m, 2H), 1.33 - 1.20 (m, 10H), 0.86 (t, J = 6.9 Hz, 3H).

^{13}C NMR ($CDCl_3$, 101 MHz, 25 °C): δ = 154.9, 154.4, 146.9, 146.3, 145.4, 144.5, 141.6, 137.3, 131.5, 128.7, 128.1, 127.7, 125.9, 122.4, 121.2, 115.8, 70.5, 50.6, 40.3, 32.0, 29.8, 29.7, 29.5, 29.4, 29.1, 27.2, 26.0, 25.0, 22.8, 14.3 (2 carbons missing in the aromatic region).

MS (ESI+): m/z calcd. for $C_{51}H_{58}N_6O_5$: 835.45 $[M+H]^+$, found: 835.16

TAMT-Boc **(17)**

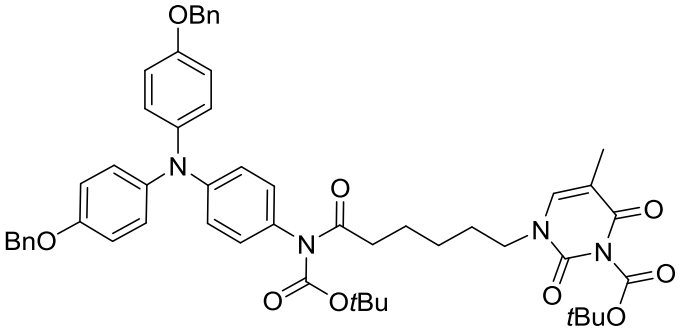

17

Compound **13** (186 mg, 0.267 mmol) was added to a solution of 4-dimethylaminopyridine (130.8 mg, 1.07 mmol) and di-tert-butyl dicarbonate (0.286 mL, 1.34 mmol) into dry tetrahydrofuran (9.3 mL) at 0 °C. The solution was then allowed to be heated slowly to room temperature and stirred overnight. Then the reaction mixture was concentrated under reduced pressure and the resulting residue was dissolved in ethyl acetate (50.0 mL). The organic phase was washed with brine (3 × 50.0 mL), dried over anhydrous Na_2SO_4 and further concentrated under reduced pressure. Further purification by column chromatography (SiO_2, toluene → toluene/ethyl acetate: 4/1) afforded compound **17** (210.0 mg, 88 %) as a white solid.

R_f **=** 0.25 (toluene/ethyl acetate: 4/1)

^{1}H NMR (CD_3OD, 400 MHz, 25 °C): δ = 7.47 - 7.30 (m, 11H), 7.01 (d, J = 9.0 Hz, 4H), 6.93 (d, J = 9.0 Hz, 4H), 6.86 (s, 4H), 5.05 (s, 4H), 3.73 (t, J = 7.3 Hz, 2H), 2.85 (t, J = 7.2 Hz, 2H), 1.87 (t, J = 1.0 Hz, 3H), 1.73 - 1.66 (m, 4H), 1.56 (s, 9H), 1.41 (s, 11H).

^{13}C NMR (CD_3OD, 101 MHz, 25 °C): δ = 177.7, 163.6, 156.8, 154.2, 150.5, 149.8, 142.3, 138.8, 132.7, 129.9, 129.5, 128.9, 128.6, 127.8, 121.6, 117.0, 111.1, 87.7, 84.2, 71.4, 38.5, 30.9, 29.6, 28.1, 28.1, 27.7, 26.9, 25.6, 12.2.

MS (ESI+): m/z calcd. for $C_{53}H_{58}N_4O_9$: 894.43 $[M]^+$, found: 894.07.

Compound **18**

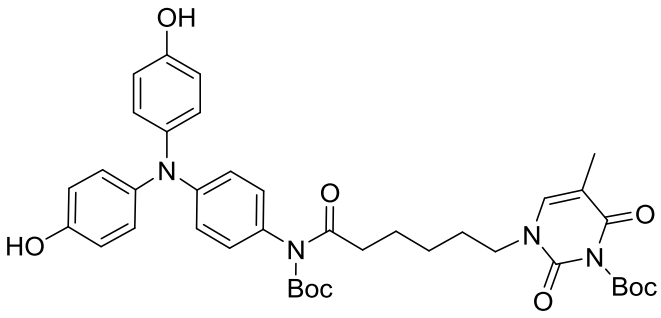

18

Compound **17** (210 mg, 0.235 mmol) was dissolved in ethyl acetate (4.7 mL) to form a 50.0 mM solution. A H-Cube continuous flow reactor was used for the hydrogenation. The flow rate was set with the HPLC pump to 0.10 mL/min. The hydrogen pressure was set to full H_2 mode, the temperature to 70°C and a cartridge containing 10% Pd/C was used. After the reaction, the sample was collected and evaporated to give product **18** (150.9 mg, 90 %) as a white solid.

^{1}H NMR (CD_3COCD_3, 400 MHz, 25 °C): δ = 8.24 (s, 2H), 7.54 (d, J = 1.2 Hz, 1H), 6.98 (d, J = 8.9 Hz, 4H), 6.88 (d, J = 9.0 Hz, 2H), 6.82 (d, J = 8.9 Hz, 4H), 6.78 (d, J = 9.0 Hz, 2H), 3.77 (t, J = 7.3 Hz, 2H), 2.91 (t, J = 7.2 Hz, 2H), 1.84 (d, J = 1.2 Hz, 3H), 1.76 - 1.66 (m, 4H), 1.56 (s, 9H), 1.47 - 1.41 (m, 2H), 1.40 (s, 9H).

^{13}C NMR (d_6-DMSO, 101 MHz, 25 °C): δ = 175.0, 161.2, 154.2, 152.6, 151.5, 148.1 , 139.3, 138.5, 130.1, 128.7, 127.3, 125.0, 117.7, 116.3, 108.1, 85.9, 82.4, 47.8, 34.4, 30.4, 27.4, 27.0, 21.0, 11.8.

MS (ESI+): m/z calcd. for $C_{39}H_{46}N_4O_9$: 715.34 $[M+H]^+$, found: 715.38.

PEG4-TAMT **19**

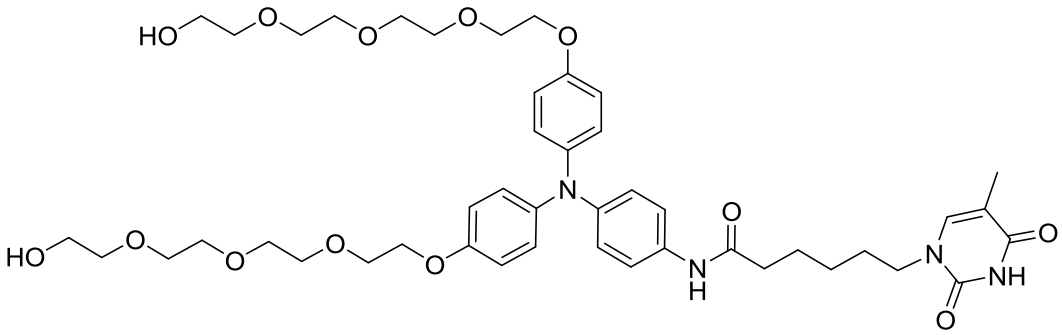

19

Diisopropyl azodicarboxylate in tetrahydrofuran (2.0 mL) was added dropwise to a solution of compound **18** (170 mg, 0.238 mmol), tetraethylene glycol (99.0 µL, 0.571 mmol) and triphenylphosphine (156 mg, 0.595 mmol) in tetrahydrofuran (8.00 mL) at 0 °C. The whole solution was allowed to warm to room temperature, then heated to 60.0 °C slowly and stirred overnight. After that time, the solvent was removed in vacuum and the residue was purified by column chromatography (SiO_2, ethyl acetate/methanol: 50/1) to provide Boc-protected compound **19** (140 mg, 55 %). Trifluoroacetic acid (20.0 mL) was then added dropwise to this compound (110.0 mg, 0.10 mmol) in ethyl acetate (20.0 mL). After stirring overnight at room temperature, the reaction mixture was concentrated under reduced pressure and further purification by reverse-phase preparative HPLC-MS (Column: XBridge Prep C18) afforded compound **19** (21.0 mg, 23 %) as a white solid.

^{1}H NMR (CD_3OD, 400 MHz, 25 °C): δ = 7.42 (d, J = 1.2 Hz, 1H), 7.33 (d, J = 9.0 Hz, 2H), 6.95 (d, J = 9.0 Hz, 4H), 6.86 (d, J = 9.0 Hz, 4H), 6.84 (d, J = 9.0 Hz, 2H), 4.11 - 4.08 (m, 4H), 3.84 - 3.81 (m, 4H), 3.75 - 3.61 (m, 22H), 3.56 - 3.54 (m, 4H), 2.35 (t, J = 7.3 Hz, 2H), 1.84 (d, J = 1.1 Hz, 3H), 1.77 - 1.68 (m, 4H), 1.46 - 1.35 (m, 2H).

^{13}C NMR (CD_3OD, 101 MHz, 25 °C): δ = 174.1, 166.9, 156.3, 153.0, 146.6, 143.2, 142.9, 133.3, 126.9, 123.0, 122.6, 116.6, 111.1, 73.7, 71.7, 71.7, 71.6, 71.4, 70.9, 69.0, 62.3, 37.5, 29.7, 26.9, 26.4, 12.2. (One peak overlaps with the solvent peak).

MS (ESI+): m/z calcd. for $C_{45}H_{62}N_4O_{13}$: 867.44 $[M+H]^+$, found: 867.16.

5-methyl-1-pentylpyrimidine-2,4(1H,3H)-dione **(20)**

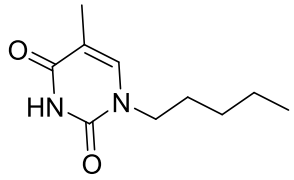

20

A solution of 1-bromohexane (100 µL, 0.709 mmol), thymine (268 mg, 2.13 mmol) and potassium carbonate (294 mg, 2.13 mmol) in dimethylformamide (20.0 mL) was gently heated to 60 °C overnight. After evaporation of the solvent under reduced pressure, the residue was dissolved in ethyl acetate (50 mL) and the organic phase was washed with brine (5 * 50 mL) and dried over anhydrous Na_2SO_4. After concentration under reduced pressure, the crude residue was further purified by reverse-phase preparative HPLC-MS (Column: SunFire Prep C18) to afford compound **20** (65 mg, 44%) as a white solid.

^{1}H NMR (CD_3COCD_3, 400MHz, 25 °C): δ = 9.89 (brs, 1H), 7.41 (d, J = 1.1 Hz, 1H), 3.70 (t, J = 7.4 Hz, 2H), 1.81 (d, J = 1.1 Hz, 3H), 1.70 - 1.62 (m, 2H), 1.36 - 1.28 (m, 4H), 0.88 (t, J = 6.8 Hz, 3H).

^{13}C NMR (CD_3COCD_3, 101 MHz, 25 °C): δ = 164.9, 151.9, 141.9, 110.0, 48.6, 32.3, 26.9, 23.3, 14.4, 12.4.

MS (ESI+): m/z calcd. for $C_{11}H_{18}N_2O_2$: 211.15 $[M+H]^+$, found: 211.44.

Annexes

Annexes for Chapter 5.

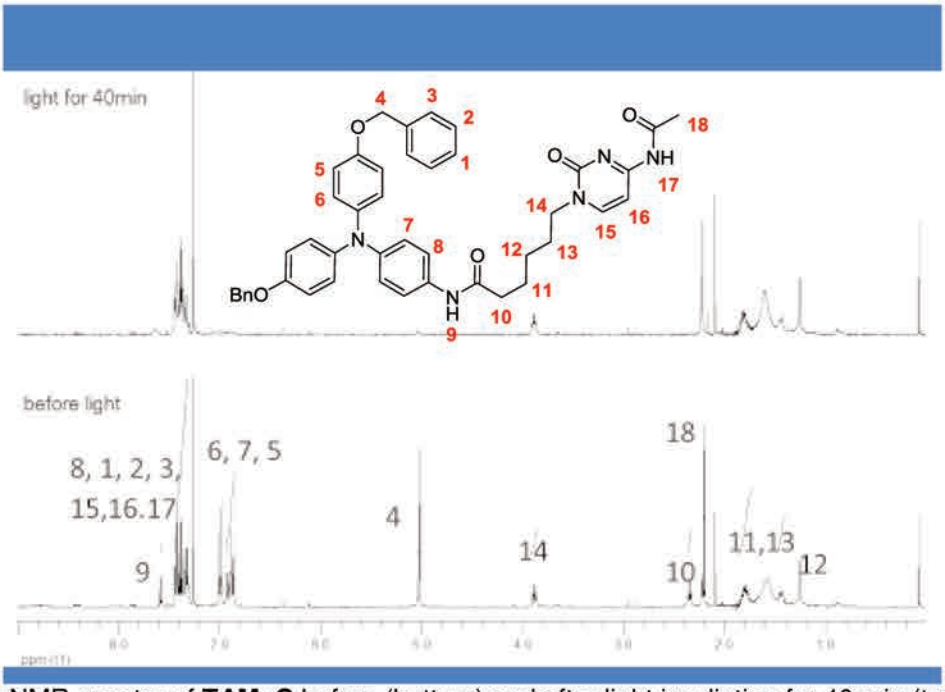

Figure S1 | NMR spectra of **TAMaC** before (bottom) and after light irradiation for 40 min (top).

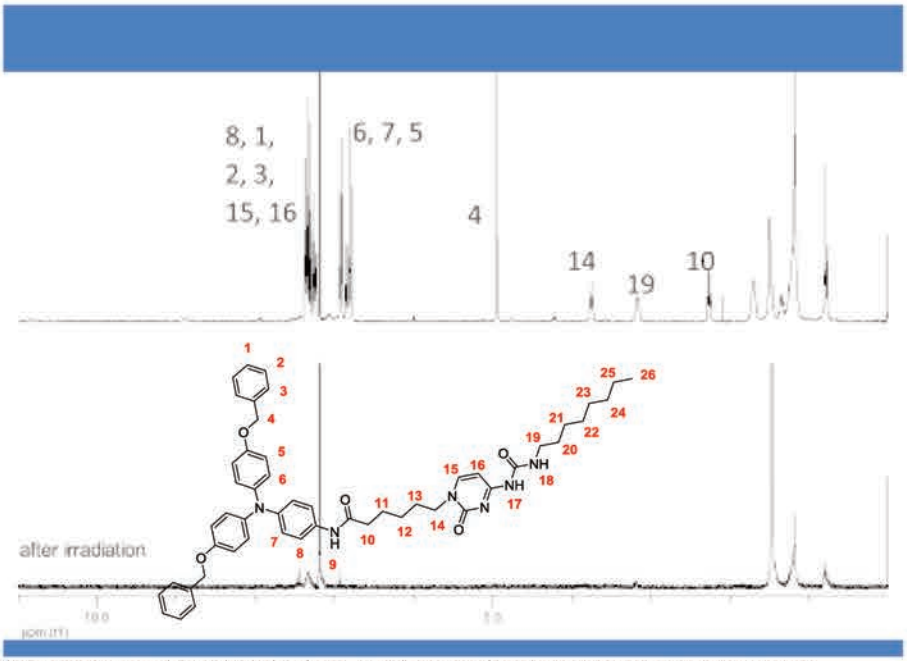

Figure S2| NMR spectra of **TAUPy** before (top) and after light irradiation (bottom).

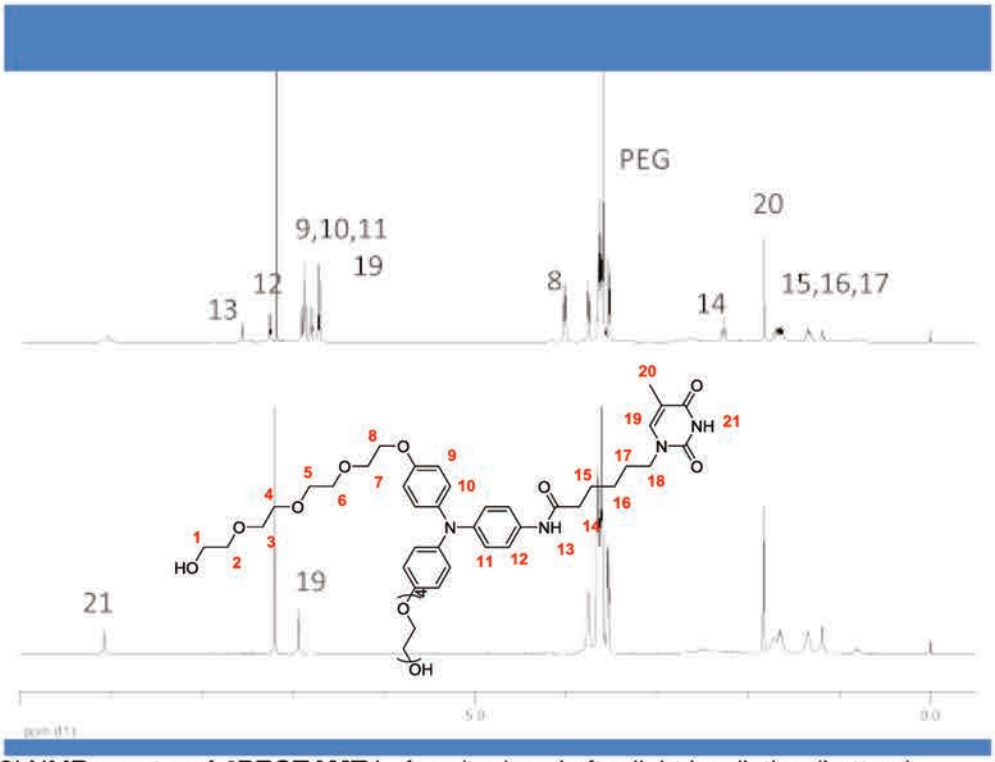

Figure S3| NMR spectra of **4PEGTAMT** before (top) and after light irradiation (bottom).

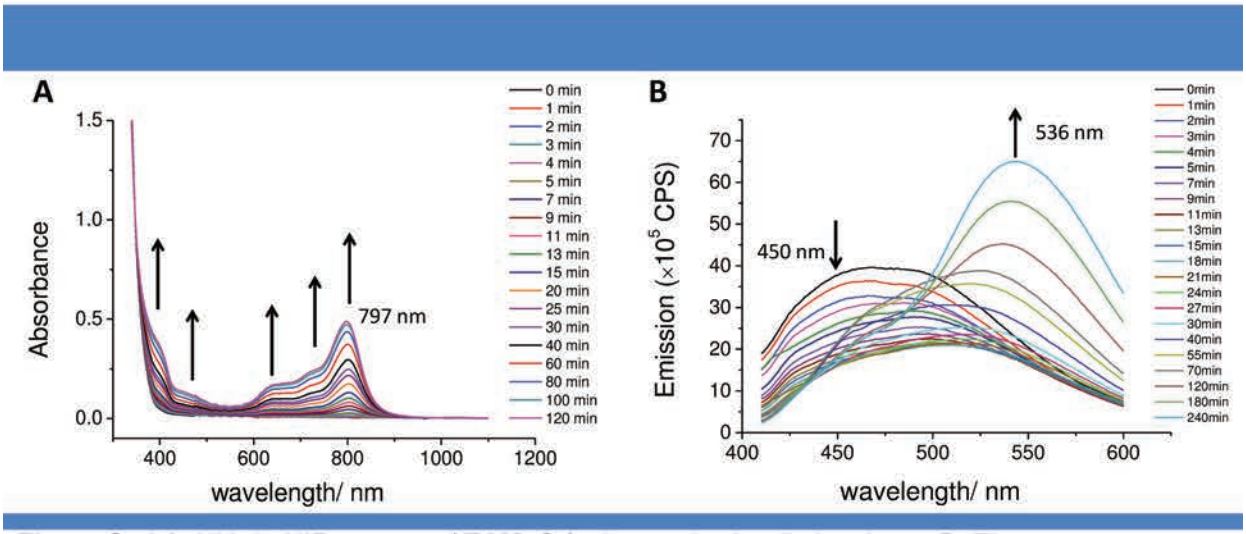

Figure S4 | A. UV-vis-NIR spectra of **TAMaC** for increasing irradiation times. B. Fluorescence spectra of **TAMaC** for increasing irradiation times ($\lambda_{exc.}$ = 400 nm) (c = 0.1 mM in chloroform).

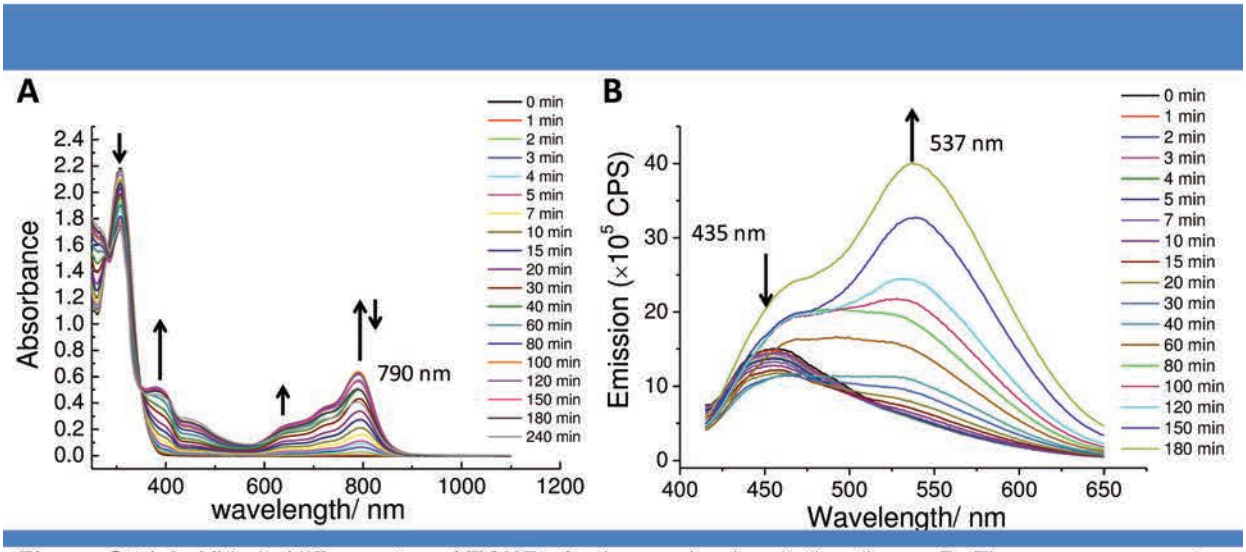

Figure S5 | A. UV-vis-NIR spectra of **TAUPy** for increasing irradiation times. B. Fluorescence spectra of **TAUPy** for increasing irradiation times ($\lambda_{exc.}$ = 400 nm) (c = 0.1 mM in chloroform).

Annexes for Chapter 6.

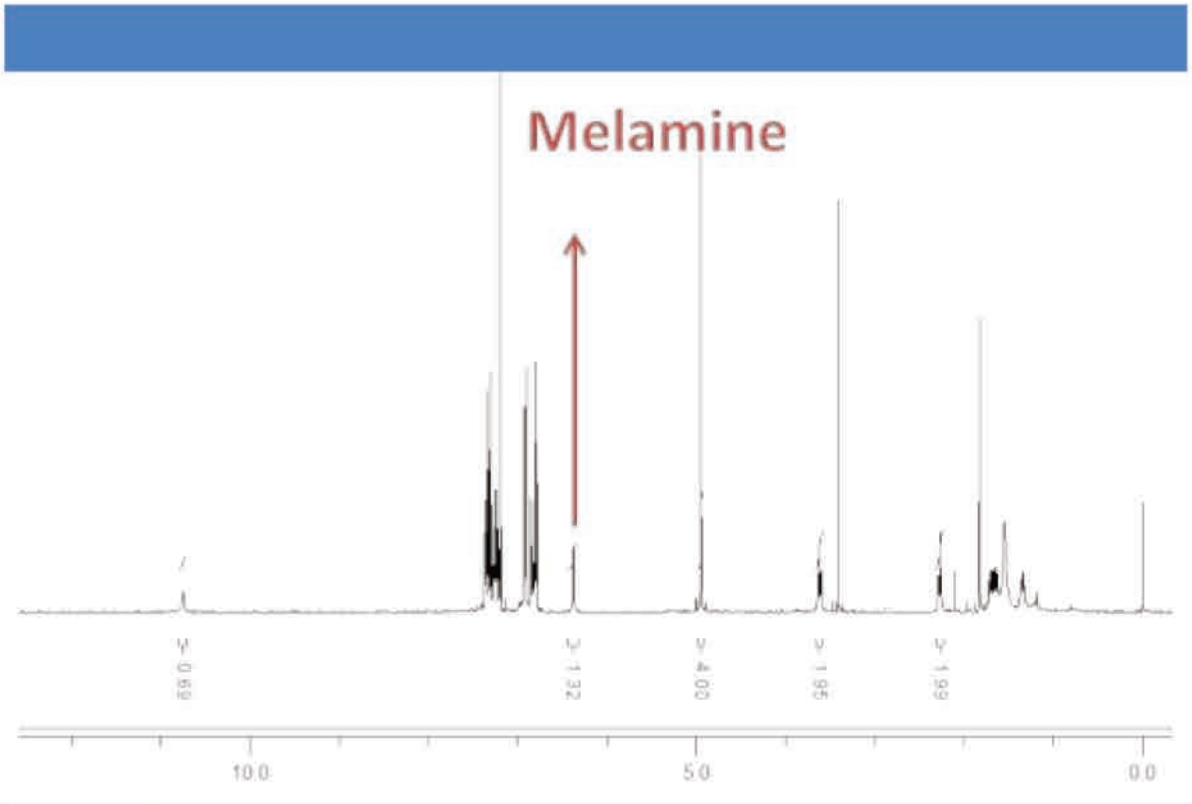

Figure S6 | ^{1}H NMR spectra of TAMT-melamine complex formed in acetone and dissolved after concentration under reduced pressure in chloroform.

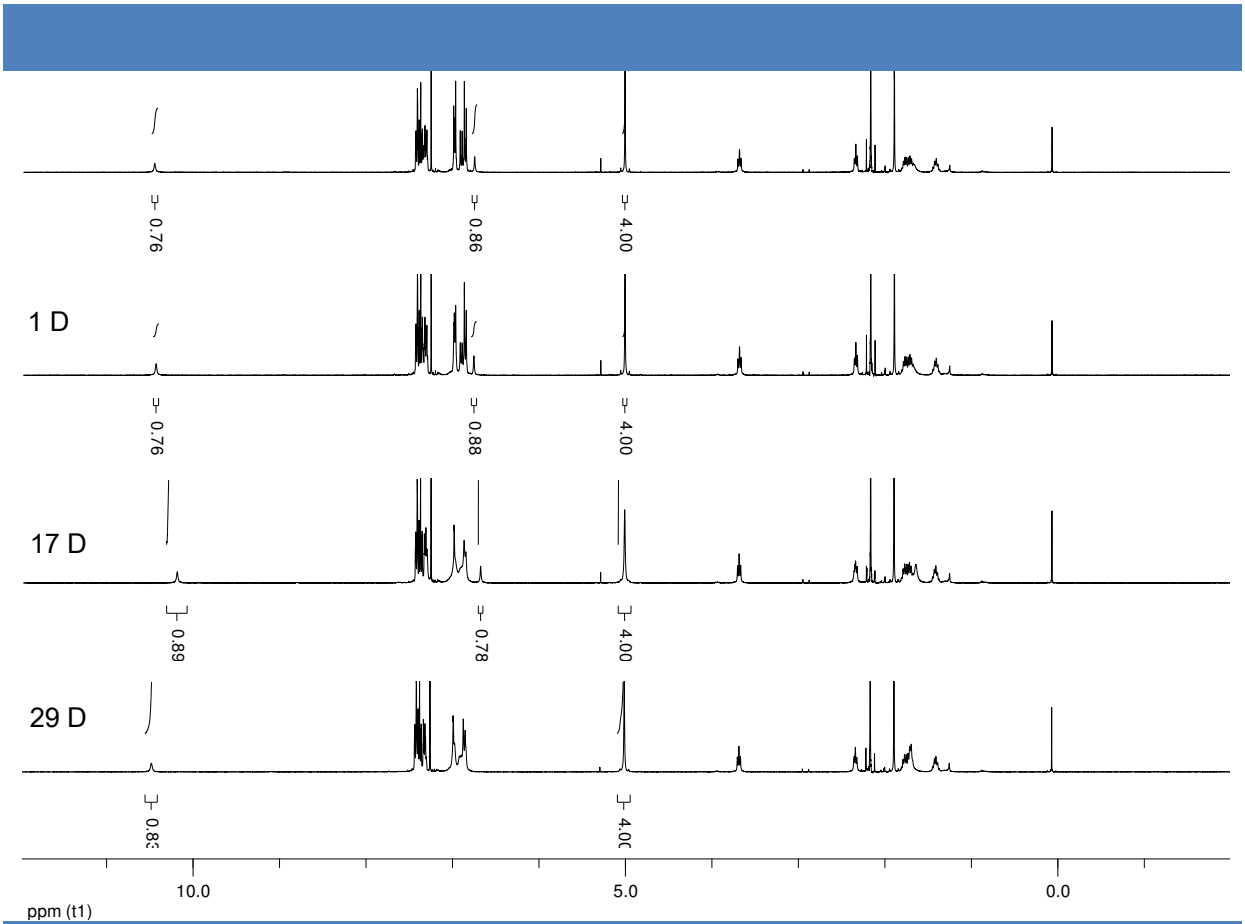

Figure S7 | 1H NMR spectrs of the **TAMT**-melamine complex in chloroform recorded just after dissolution; after 1 day and after 17 and 29 days.

Table S1 | NMR kinetics results for the formation of TAMT-Melamine complex at 60 °C

Heating time (h)	16H chemical shift	Melamine chemical shift	Inte 16H	Inte mel	Inte 5H,6H	Inte 7H	Inte 4H	Inte 14H	Inte 10H
0	9.731	--	0.54	--	7.98	1.98	4	1.95	1.99
2	10.803	6.209	0.45	0.64	7.99	2.00	4	1.95	2.02
4	10.821	6.226	0.48	0.72	7.98	2.00	4	1.94	1.97
4	10.791	6.205	0.51	0.76	7.96	1.98	4	1.94	1.98
4	10.786	6.201	0.51	0.77	7.93	1.99	4	1.96	2.00
4	10.812	6.224	0.57	0.8	7.99	2.00	4	1.94	2.00
8	10.929	6.252	0.57	0.92	7.90	1.97	4	1.95	2.01
8	10.896	6.231	0.56	0.94	7.92	1.97	4	1.96	2.00
12	10.885	6.245	0.55	0.96	7.99	1.97	4	1.97	2.00
15.5	10.89	6.31	0.63	0.91	8.01	1.99	4	1.95	2.00
15.5	10.889	6.313	0.60	0.97	7.92	1.98	4	1.96	2.01
15.5	10.939	6.37	0.66	1.01	7.91	1.97	4	1.96	2.00
15.5	10.905	6.349	0.67	1.01	7.94	1.96	4	1.95	2.00
15.5	10.925	6.388	0.64	1.03	7.92	1.96	4	1.95	2.01

Table S2| NMR kinetics results for the formation of TAMT-Melamine complex at 90 °C

Heating time (min)	16H chemical shift	Melamine chemical shift	Integration 16H	Integration melamine
0	9.731	5.932	0.54	0
10	11.184	6.147	0.49	1.22
20	11.245	6.16	0.51	1.34
30	11.33	6.166	0.56	1.49
50	11.306	6.198	0.57	1.48
70	11.275	6.236	0.59	1.45
130	11.258	6.279	0.59	1.39
190	11.183	6.321	0.63	1.26
910	11.006	6.376	0.54	0.9

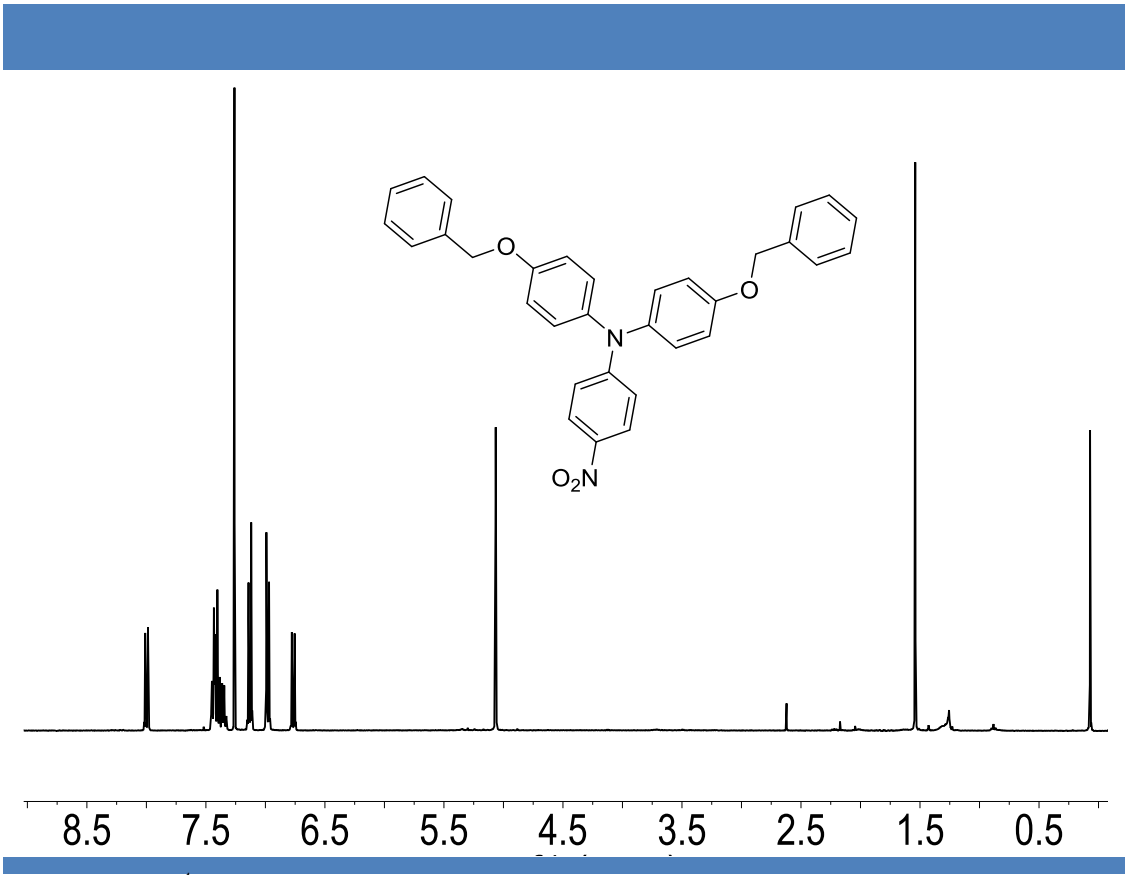

Figure S8 | ^{1}H NMR spectrum of compound **10** after the addition of $HgCl_2$ in chloroform.

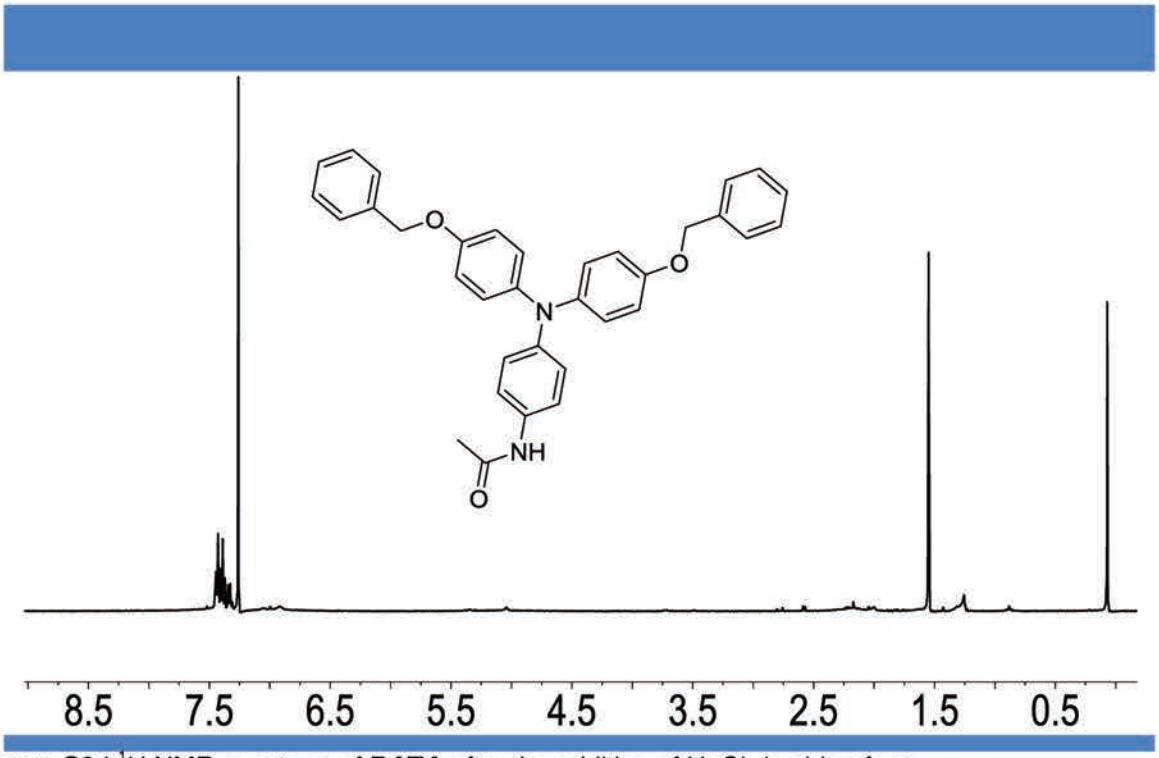

Figure S9 | ^{1}H NMR spectrum of **BATA** after the addition of $HgCl_2$ in chloroform.

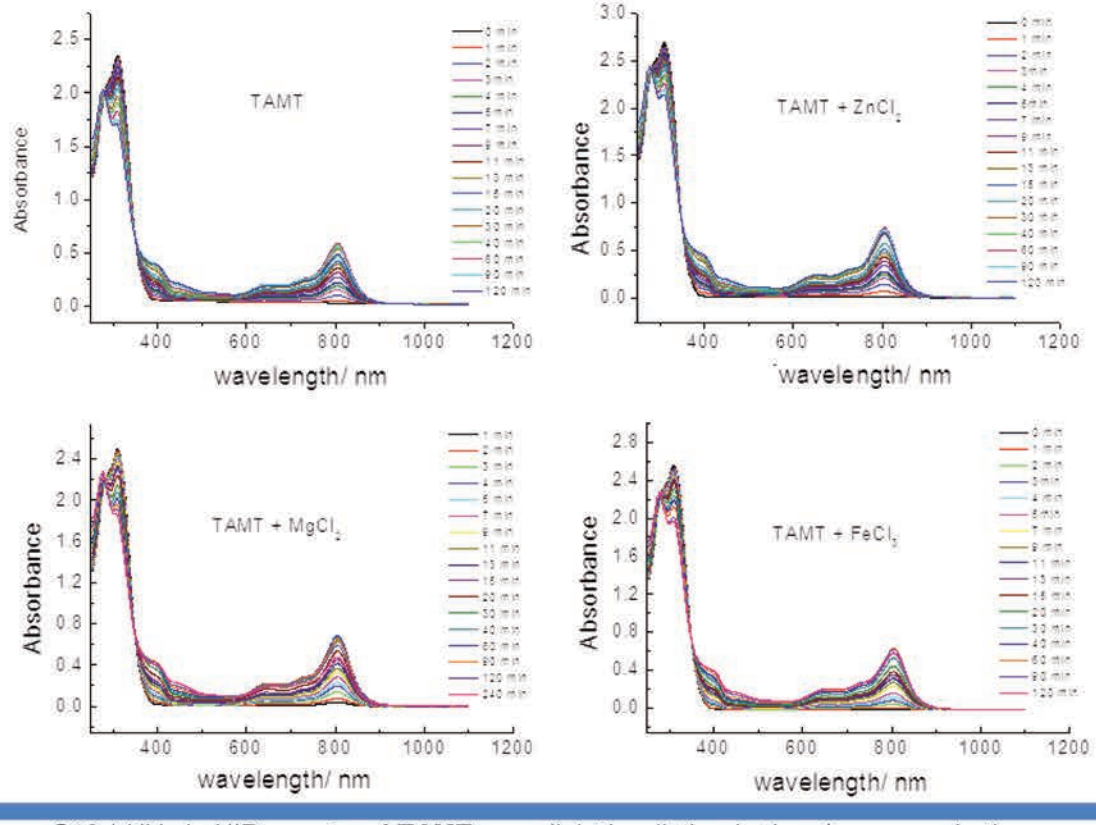

Figure S10 | UV-vis-NIR spectra of **TAMT** upon light irradiation in the absence or in the presence of different metal ions.

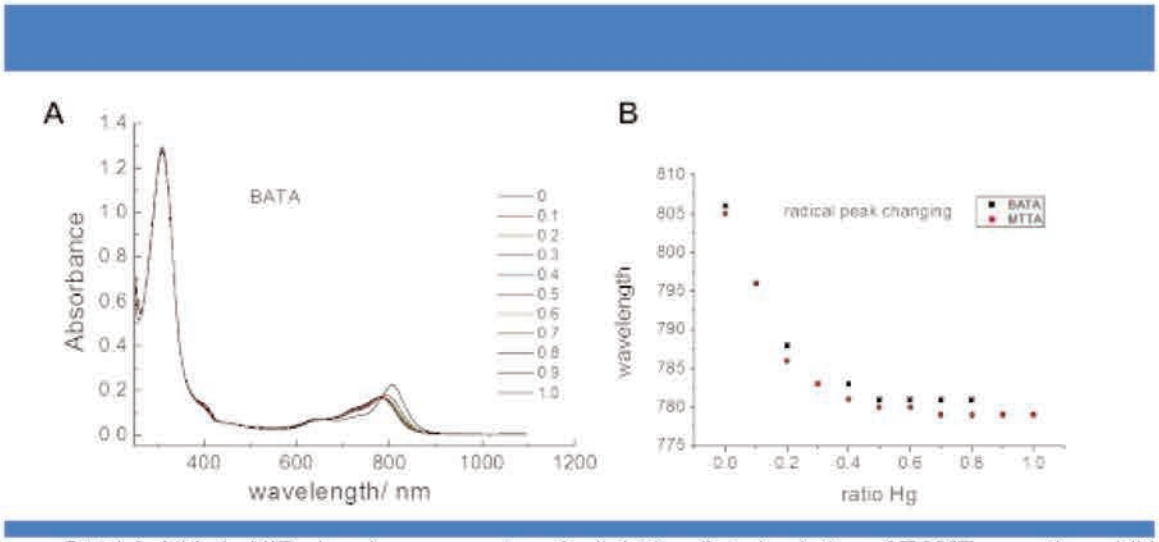

Figure S11 | A. UV-vis-NIR absorbance spectra of a light-irradiated solution of **TAMT** upon the addition of mercury (0-1 eq.). B. Plots of the evolution of the wavelength corresponding to the triarylammonium radicals for **TAMT** and **BATA** as a function of the mercury ratio (c = 0.1 mM in chloroform).

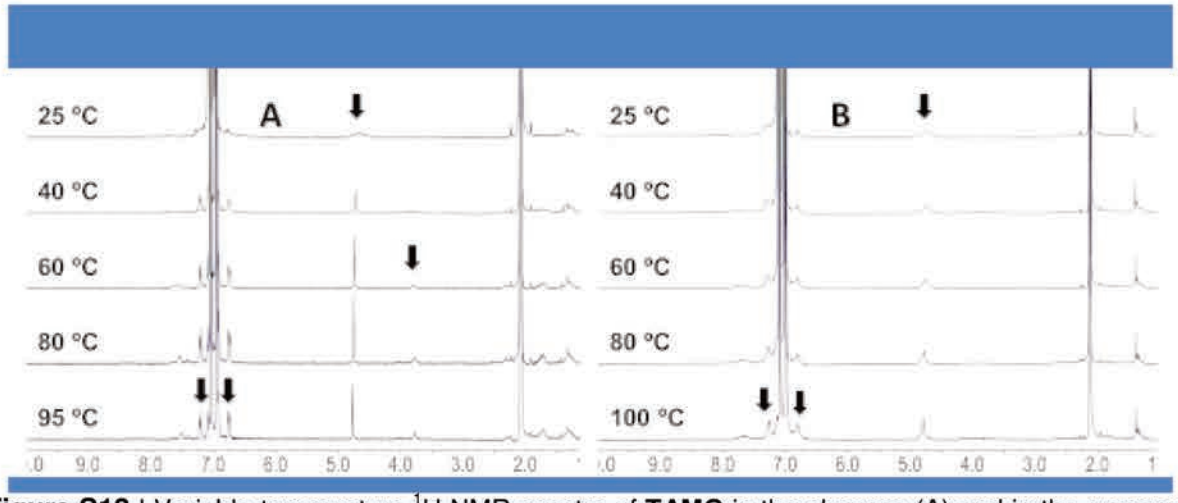

Figure S12 | Variable-temperature ^{1}H NMR spectra of **TAMG** in the absence (A) and in the presence (B) of KPF_6 (4 mM solution in toluene).

RESUME

1) Introduction

La construction d'architectures nanoscopiques complexes à partir de molécules d'ADN est aujourd'hui bien contrôlée, permettant d'espérer la miniaturisation des dispositifs électroniques.[1] Alors que de nombreuses études ont établi la conductivité limitée des doubles brins d'ADN, diverses approches telles que la métallisation des brins d'ADN ou la synthèse de polymères covalents conjugués sur un gabarit d'ADN ont été proposées comme alternatives.[2,3] Cependant, toutes ces méthodes manquent de sélectivité vis-à-vis des diverses séquences d'ADN potentiellement présentes sur un simple brin d'ADN. En effet, les propriétés de reconnaissance des diverses bases nucléiques permettent d'adresser spécifiquement une molécule (ou polymère) incorporant une (des) base(s) nucléique(s) sur une séquence particulière d'ADN.[4,5]

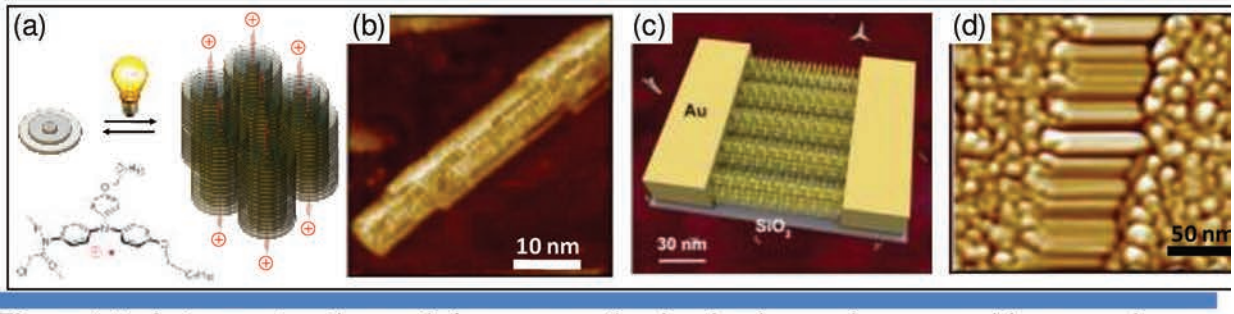

Figure 77. Auto-construction activée par un stimulus lumineux de nano-cables organiques supramoléculaires. (a) Nucléation des fibres sous l'influence de la lumière par associations supramoléculaires entre triarylamines chimiquement modifiées; (b) Image AFM d'un fagot de fibres auto-assemblées; (c) Croissance et insertion dirigées par un champ électrique de fibres de 100 nm de long entre des électrodes métalliques; et (d) image AFM correspondante des nano-cables présentant des propriétés de conductivité élevée.

Récemment, notre groupe a mise en évidence les propriétés d'auto-assemblages particulières du motif triarylamine (TAA). Ces molécules précisément modifiées peuvent s'auto-assembler dans des solvants chlorés en fagots de fibres très denses, qui présentent des propriétés de conduction similaires aux métaux grâce à un processus de polymérisation non-covalente (Figure 1a-b).[6-9] Au cours des dernières années, notre groupe a démontré que des modifications chimiques des chaines latérales présentent sur ce synthon TAA n'inhibaient pas leurs propriétés d'auto-organisation et pouvaient conduire à l'obtention de morphologies diverses principalement dans des solvants apolaires.[10-13]

L'objectif de mon travail de thèse était donc d'étudier si des triarylamines modifiées par des bases nucléiques conservaient leurs propriétés d'auto-assemblages et, de façon ultime, de construire des systèmes hybrides ADN-TAA conducteurs en tirant partie des propriétés de reconnaissance exceptionnelles des acides nucléiques présent aussi bien sur les brins d'ADN que sur les molécules de triarylamines, connues pour s'auto-assembler en nano-cables supramoléculaires hautement conducteurs.

2) Résultats et discussions

Au sein du laboratoire, notre équipe a mis en évidence que les composés TAAs mono- et tris-substitués pouvaient conduire à l'obtention de structures auto-assemblées respectivement multi- et mono-colonnaires de par la coopérativité de diverses interactions non-covalentes (liaisons hydrogènes,

interactions π-π, phénomène de transfert de charge).[6,9] Ainsi, nous avons envisagé la synthèse de dérivés TAAs mono- et tris-substitués par des bases nucléiques telles que la guanine (G), la thymine (T), la cytosine (C) ou l'acetylcytosine (aC), situées en bout de chaines latérales (Figure 2).

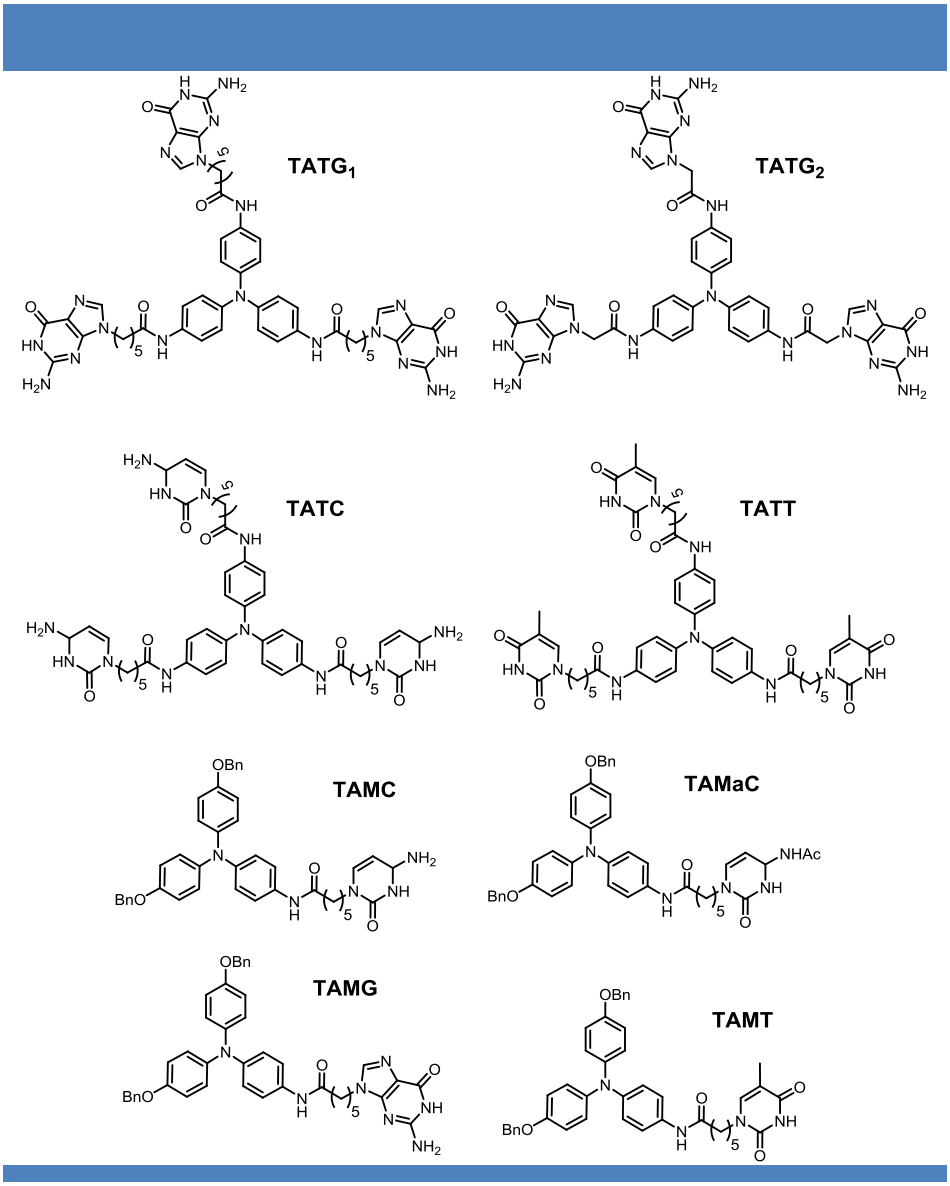

Figure 2. Structures de triarylamines mono- et tri-substituées synthétisées au cours de ce travail de thèse.

La voie de synthèse que nous avons développée pour obtenir ces molécules est hautement convergente puisqu'un seul intermédiaire bromé,

obtenus en trois étapes et avec un excellent rendement, est utilisé pour accéder à tous les dérivés d'une même famille (Schéma 1 avec le composé **TAMBr** comme intermédiaire commun pour obtenir toutes les TAAs monosubstituées). Les différents composés **TAMaC**, **TAMG**, **TAMT** et **TAMC** ont ensuite été obtenus en une ou deux étapes (substitution nucléophile et déprotection) à partir du dérivé bromé. Une approche synthétiques similaire a également été développée pour accéder aux triarylamines décorées par trois bases nucléiques identiques (**TATG$_1$**, **TATG$_2$**, **TATC**, **TATT**) mais ne peut être détaillée compte tenu de la taille de ce résumé (Schéma 2).

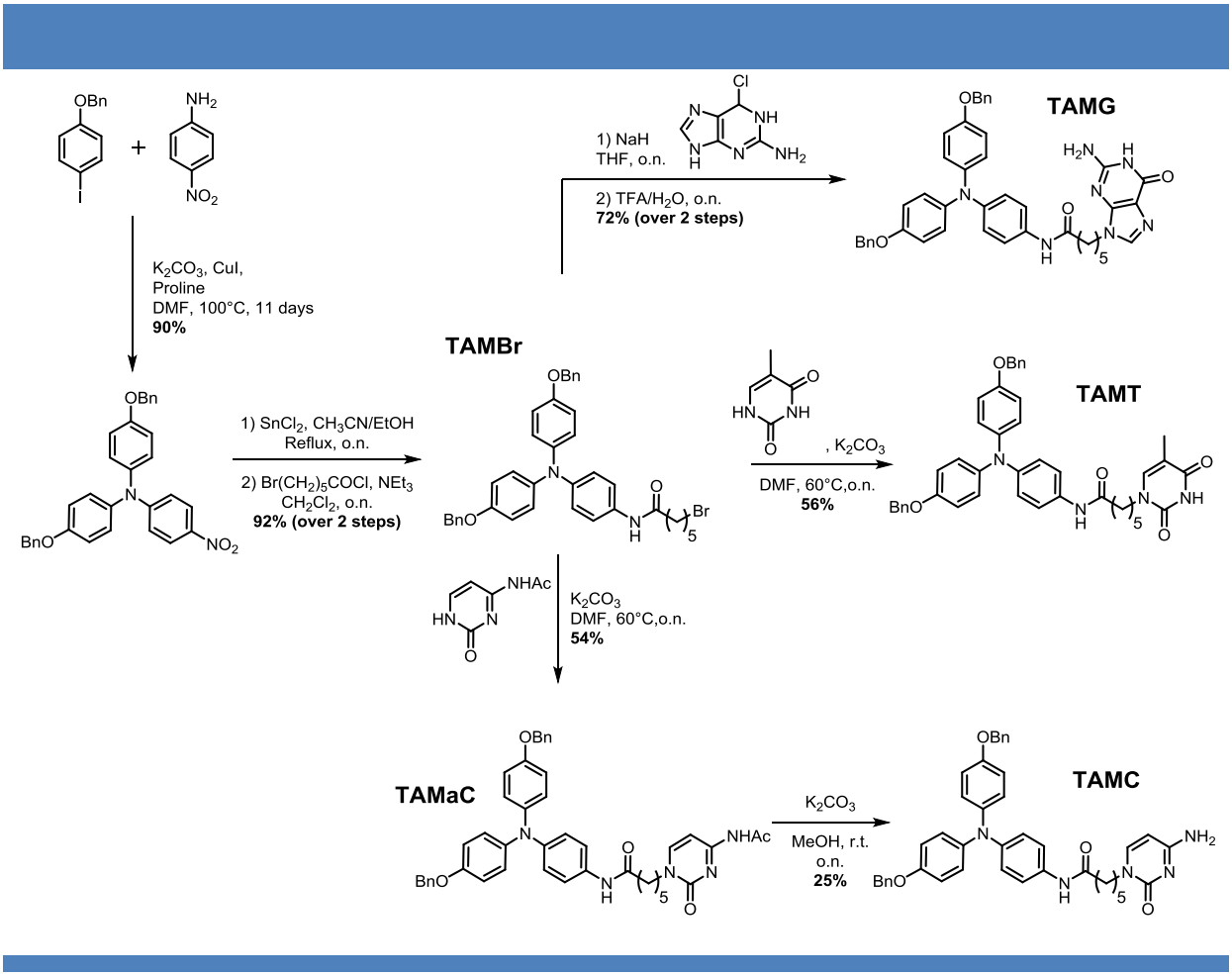

Schéma 1. Voies de synthèse développées pour accéder aux triarylamines modifiées par une base nucléique sur la chaine latérale.

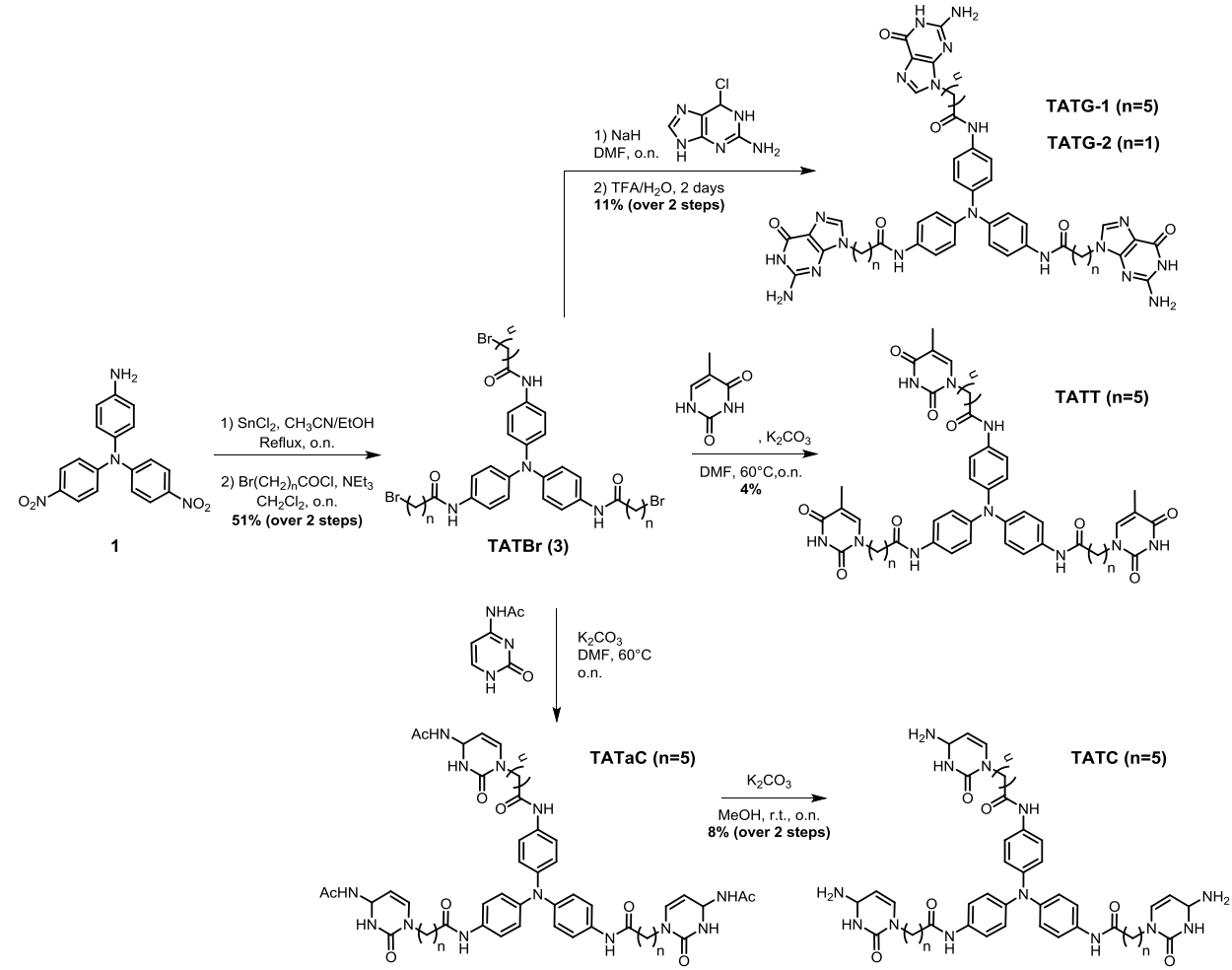

Schéma 2. Voies de synthèse développées pour accéder aux triarylamines modifiées par trois bases nucléique sur la chaine latérale.

Nous avons ensuite étudié l'auto-assemblage de ces molécules dans les solvants chlorés par diverses expériences de spectrocopie (RMN, UV-Vis-NIR et fluorescence), qui sont les techniques couramment utilisées pour démontrer l'auto-assemblage des dérivés TAAs.[6,9] Parmi les huit molécules décrites en Figure 2, quatre composés (**TATT**, **TAMG**, **TAMT**, **TAMaC**) ont démontré les caractéristiques typiques de la formation d'un auto-assemblage: a) disparition des signaux de RMN ^{1}H correspondant au cœur TAA après irradiation lumineuse,

b) augmentation de l'intensité des bandes d'absorption UV-Vis-NIR à 800 et 400 nm sous irradiation lumineuse et qui correspondent respectivement à la présence de radicaux triarylammonium cations et à la formation d'un auto-assemblage, et c) phénomène d'émission induite par l'agrégation (AIE) observé par fluorescence après excitation à 400 nm (excepté pour le composé **TAMG**). Un résumé de ces analyses est présenté en Figure 3 pour le composé **TAMT** monosubstitué par une thymine. Ces études démontrent que la présence de bases nucléiques telles que la thymine ou l'acétylcytosine sur le synthon TAA n'inhibe pas leurs propriétés d'auto-assemblages dans les solvants chlorés. Cependant, il apparait que la présence de bases nucléiques telles que la guanine ou la cytosine, qui incorporent des amines primaires, inhibe ce processus. Cette observation est en accord avec des expériences précédemment réalisées au laboratoire sur d'autres dérivés TAAs (résultats non publiés).

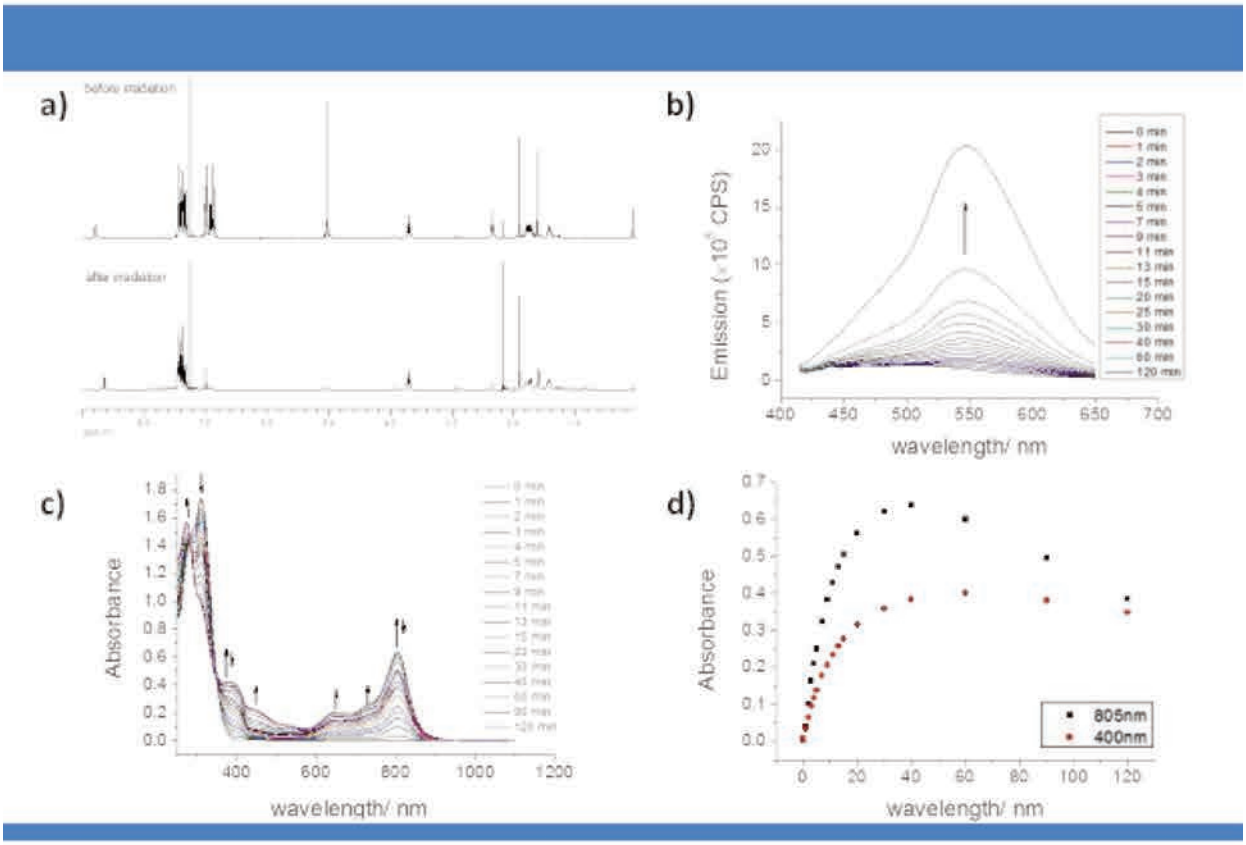

Figure 3. Phénomène d'auto-assemblage induit par l'irradiation lumineuse pour le compose **TAMT** mis en évidence par a) RMN ^{1}H dans le chloroforme deutérié ([**TAMT**] ~ 1 mM), b) spectrocopie de fluorescence (0.1 mM dans $CDCl_3$, excitation à 400 nm) et c-d) spectroscopie UV-Vis-NIR (0.1 mM dans $CDCl_3$). Le graphique reporté en d) indique l'évolution de l'absorbance à 805 et 400 nm pour des temps d'irradiation croissant.

Parallèlement à l'étude de l'auto-assemblage des molécules uniques sous irradiation lumineuse, nous nous sommes également intéressés à la possibilité d'utiliser les bases nucléiques telles que la thymine et la guanine comme unité de reconnaissance pour des métaux, des cations ou des petites molécules. En effet, la thymine est un motif à liaison hydrogène, qui est connu pour former des espèces dimériques avec le mercure,[14-16] mais aussi des complexes ternaires avec la mélamine *via* un réseau de liaisons hydrogène.[17-19] Par ailleurs, les dérivés incorporant des guanines sont reconnus pour conduire à la formation de G-quartet en présence d'ions potassium.[20-24] Ainsi, au cours de

cette thèse, nous avons étudié le comportement de la molécule **TAMT** en présence de mercure ou de mélamine et celui de la molécule **TAMG** en présence d'ions potassium en utilisant une combinaison de techniques spectroscopiques, microscopiques et de diffusion du rayonnement. Compte tenu de la taille de ce résumé, nous ne détaillerons que les résultats obtenus pour la molécule **TAMT** en présence de mercure. Cependant, nous avons pu observer que la triarylamine **TAMT** en présence de mélamine conduit à la formation d'un complexe ternaire (3 **TAMT** pour une molécule de mélamine), qui s'assemble en longues fibres rigides de plusieurs micromètres de long et d'environ 30 nanomètres de diamètre (Figure 4a). Par ailleurs, en ce qui concerne la molécule **TAMG**, des expériences de RMN du proton ont mis en évidence la formation d'un G-quartet lorsque cette molécules est mélangée avec le sel KPF_6 dans le toluène. Des études de microscopie électronique démontrent la formation d'objets fibrillaires flexibles enchevêtrés avec des longueurs de plusieurs dizaines de micromètres (Figure 4b).

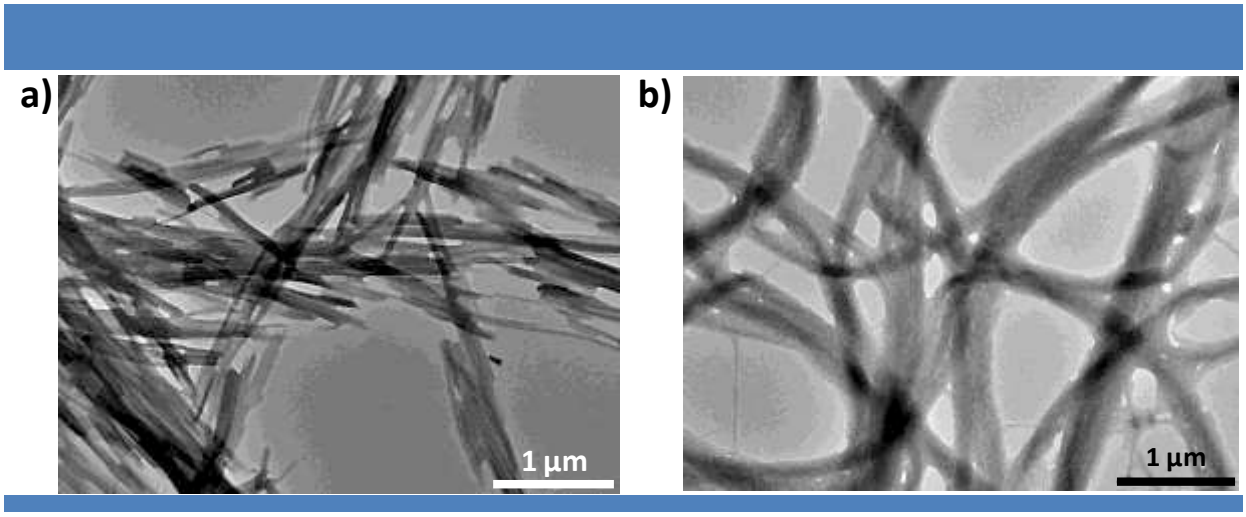

Figure 4. Images TEM de l'auto-assemblage des molécules a) **TAMT** en présence de mélamine dans le toluène et b) **TAMG** en présence de KPF_6 dans le toluène.

La capacité de la molécule **TAMT** à interagir avec le mercure a principalement été analysée par spectroscopie d'absorption UV-Vis-NIR (Figure 5). Nous avons tout d'abord titré une solution à 0.1 mM de TAMT dans le chloroforme avec des quantités croissantes de dichlorure de mercure et observé une augmentation de l'absorption à 280 nm, qui peut être considérée pour une signature de l'association entre l'atome de mercure et la fonction imide du dérivé thymine. Nous avons ensuite étudié le processus d'auto-assemblage induit par la lumière sur un mélange **TAMT**/$HgCl_2$ (2:1) dans le chloroforme. Les bandes d'absorption caractéristiques de l'auto-assemblage des triarylamines et de la présence de radicaux triarylammonium cations respectivement à environ 400 et 782 nm ont pu être observées, indiquant que la capacité d'auto-assemblage de **TAMT** n'est pas affectée par la présence de mercure. Par ailleurs, nous avons observé un déplacement hypsochrome de la bande d'absorption située dans le proche infrarouge (805 → 782 nm) et une augmentation de l'intensité de la bande à 280 nm lorsqu'une solution préalablement irradiée a été titrée avec des quantités croissantes de $HgCl_2$. Cette série d'expérience suggère que le mercure ne se lie pas uniquement au résidu thymine mais affecte également l'empilement des radicaux triarylammonium dans l'auto-assemblage. D'autres expériences sont en cours pour mieux comprendre ce phénomène.

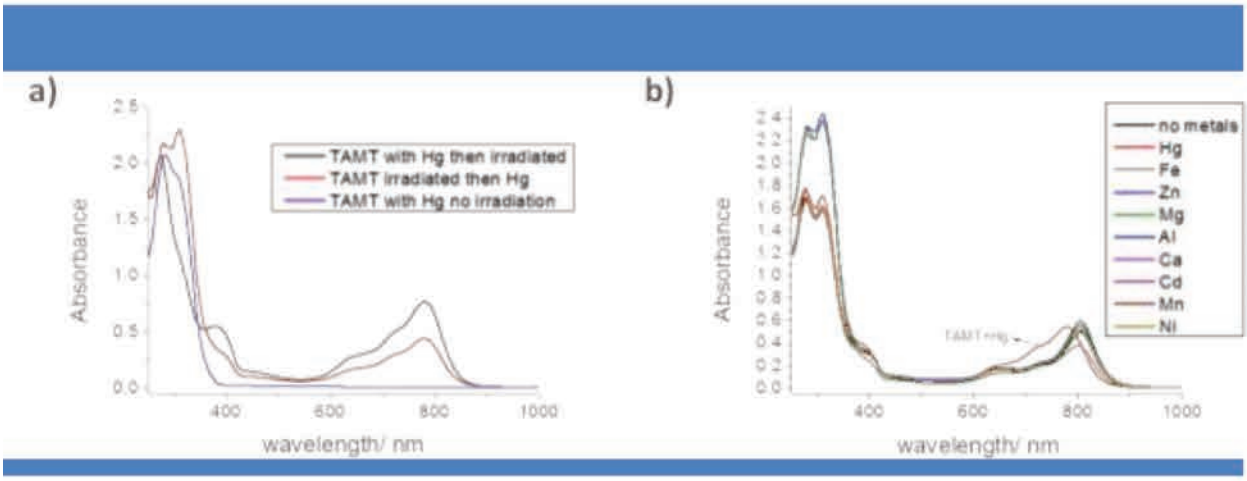

Figure 5. a) Spectres d'absorbance UV-vis-NIR obtenus pour le composé **TAMT** dans diverses conditions (avec/sans $HgCl_2$ et/ou avec/sans irradiation lumineuse, 0.1 mM dans le chloroforme); b) Spectres d'absorbance UV-vis-NIR obtenus pour une solution irradiée du composé **TAMT** (0.1 mM dans le chloroforme, irradiation durant 20 min) après addition de 0.8 équivalents de différents ions métalliques.

Enfin, nous avons également étudié la sélectivité de la molécule **TAMT** pour le mercure en titrant une solution préalablement irradiée par différents ions métalliques (Figure 5b). Les expériences d'absorption UV-Vis-NIR démontrent l'absence de déplacement hypsochrome de la bande à 802 nm pour tous les ions métalliques excepté le mercure et indiquent donc la forte sélectivité de notre système pour le mercure. A notre connaissance, ce travail représente le premier exemple de détection de mercure en un milieu organique.

En complément de ces études d'auto-assemblage, nous avons également réalisé de premières expériences d'hybridation entre les dérivés TAAs incorporant les résidus thymine ou guanine et des simples brins d'ADN. Ainsi, des solutions de **$TATG_1$**, **$TATG_2$**, **TATT** ou **TAMT** dans le THF ou dans un mélange THF/DMSO ont été ajoutées à des solutions d'ADN simple brin préparées dans

un tampon TE (pH 7.4, 10 mM tampon Tris buffer et 1 mM EDTA) et le processus de reconnaissance a été caractérisé par des techniques spectroscopiques telles que l'absorption UV-Vis et le dichroïsme circulaire. Cependant, aucun changement significatif n'a pu être observé pour ces différentes solutions. Nous pensons que la faible solubilité de nos dérivés dans les solvants polaires tels que l'eau interdit toute association avec des brins d'ADN mais aussi d'APN (acides peptido-nucléiques).

Afin de palier à ces problèmes de solubilité en milieux aqueux ou fortement polaires, nous avons envisagé la synthèse d'une nouvelle molécule TAA-thymine, qui présente des chaines latérales de type oligo(éthylène glycol) en remplacement des groupements benzyles (**4PEGTAMT**, Schéma 2). La synthèse de cette molécule a été réalisé en quatre étapes à partir de la molécule **TAMT** selon la voie décrite sur le schéma 3.

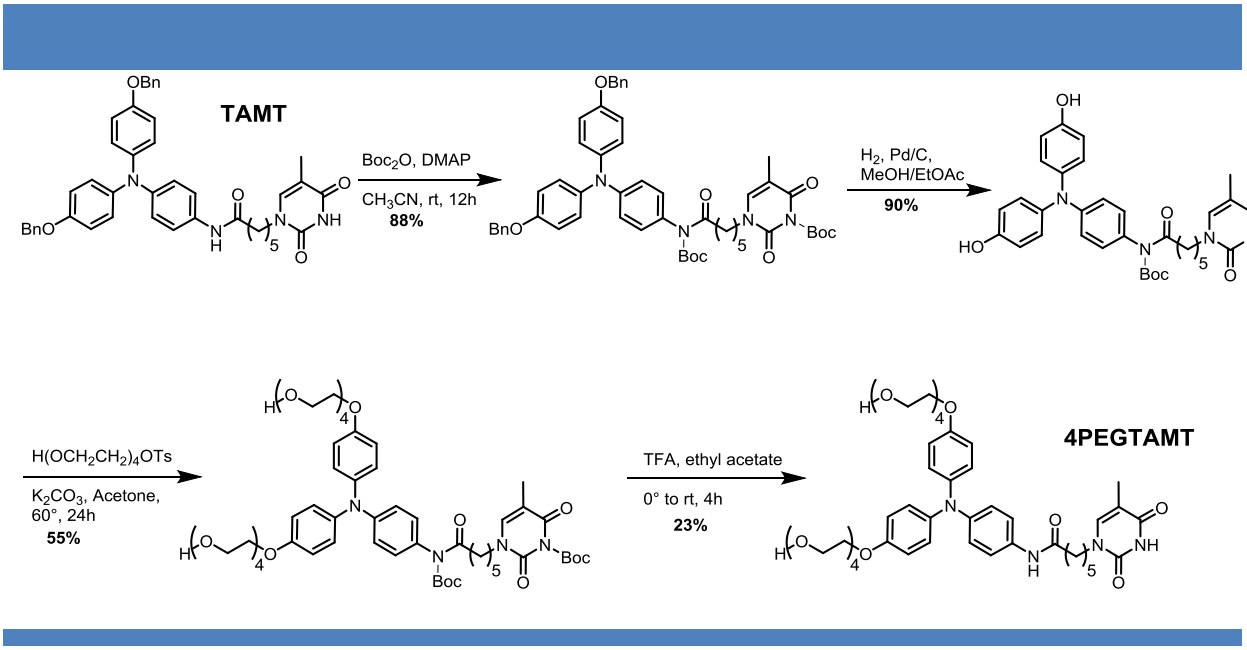

Schéma 3. Voie de synthèse permettant l'obtention de la molécule **4PEGTAMT**.

Après protection de la fonction imide sur le résidu thymine, les fonctions

phénols ont été déprotégées par hydrogènolyse des groupements benzyles. L'alkylation des unités phénols ainsi libérées par le composé tétra(éthylène glycol) *p*-toluènesulfonate disponible commercialement suivie de la déprotection de la fonction imide avec l'acide trifluoroacétique a permis l'obtention du composé **4PEGTAMT** après purification par HPLC préparative en phase inverse. Les premières études sur cette molécule ont démontré sa solubilité accrue dans les solvants polaires (par rapport à **TAMT**) et mis en évidence que les chaines tétra(éthylène glycol) n'inhibent pas la formation d'auto-assemblage dans les solvants chlorés.

3) Conclusion générale

Au cours de ce travail, nous avons synthétisé deux séries de molécules hybrides triarylamine-base(s) nucléique(s) avec l'objectif de produire des nanostructures d'ADN conducteur par une nouvelle approche purement supramoléculaire. Cet objectif très ambitieux n'a, pour l'instant, pas été atteint mais nous espérons que les expériences encore en cours seront couronnées de succès. Par ailleurs, nous avons démontré que ces molécules hybrides triarylamine-base(s) nucléique(s) peuvent être utilisées pour produire de nouvelles structures auto-assemblées avec des propriétés fonctionnelles intéressantes. En utilisant une combinaison de techniques physico-chimiques, nous avons démontré la capacité de ces molécules à produire des dispositifs fonctionnels tels que les senseurs mais également à conduire à des

morphologies nouvelles telles que des sphères micrométriques faites de nano-rubans entrelacés. Ce travail confirme l'importance du motif triarylamine comme nouvelle unité de structure en chimie supramoléculaire et sa capacité à produire des nanomatériaux fonctionnels.[25]

4) Références

[1] Seeman, N. C., *Annu. Rev. Biochem.* **2010**, *79*, 65-87.

[2] Wind, S. J. *et al. J. Self-Ass. Mol. Elec.* **2013**, *1*, 177–194.

[3] Watson, S. M. D.; Pike, A. R.; Pate, J.; Houlton, A.; Horrocks, B. R. *Nanoscale* **2014**, *6*, 4027-4037.

[4] Ruiz-Carretero, A.; Janssen, P. G. A.; Kaeser, A.; Schenning, A. P. H. J. *Chem. Commun.* **2011**, *47*, 4340-4347.

[5] Janssen, P. G. A.; Vandenbergh, J.; van Dongen, J. L. J.; Meijer, E. W.; Schenning, A. P. H. J. *J. Am. Chem. Soc.* **2007**, *129*, 6078-6079.

[6] Moulin, E.; Niess, F.; Maaloum, M.; Buhler, E.; Nyrkova, I.; Giuseppone, N. *Angew. Chem. Int. Ed.*, **2010**, *49*, 6974-6978.

[7] Faramarzi, V.; Niess, F.; Moulin, E.; Maaloum, M.; Dayen, J.-F.; Beaufrand, J.-B.; Zanettini, S.; Doudin, B.; Giuseppone, N. *Nature Chem.*, **2012**, *4*, 485-490.

[8] Moulin, E.; Cid, J.-J.; Giuseppone, N., *Adv. Mater.* **2013**, *25*, 477-487.

[9] Armao, J. J.; Maaloum, M.; Ellis, T.; Fuks, G.; Rawiso, M.; Moulin, E.; Giuseppone, N., *J. Am. Chem. Soc.* **2014**, *136*, 11382-11388.

[10] Moulin, E.; Niess, F.; Fuks, G.; Jouault, N.; Buhler, E.; Giuseppone, N. *Nanoscale* **2012**, *4*, 6748-6751.

[11] Busseron, E.; Cid, J.-J.; Wolf, A.; Du, G.; Moulin, E.; Fuks, G.; Maaloum, M.; Polavarapu, P.; Ruff, A.; Saur, A.-K.; Ludwigs, S.; Giuseppone, N. *ACS Nano* **2015**, *9*, 2760-2772.

[12] Domoto, Y.; Busseron, E.; Maaloum, M.; Moulin, E.; Giuseppone, N. *Chem. Eur. J.* **2015**, *21*, 1938-1948.

[13] Armao, J. J.; Rabu, P.; Moulin, E.; Giuseppone, N. *Nano. Lett.* **2016**, *16*, 2800-2805.

[14] Tanaka, Y.; Kondo, J.; Sychrovský, V.; Šebera, J.; Dairaku, T.; Saneyoshi, H.; Urata, H.; Torigoe, H.; Ono, A., *Chem. Commun.* **2015**, *51*, 17343-17360.

[15] Ono, A.; Togashi, H., *Angew. Chem. Int. Ed.,* **2004**, *43*, 4300-4302.

[16] Miyake, Y.; Togashi, H.; Tashiro, M.; Yamaguchi, H.; Oda, S.; Kudo, M.; Tanaka, Y.; Kondo, Y.; Sawa, R.; Fujimoto, T.; Machinami, T.; Ono, A., *J. Am. Chem. Soc.,* **2006,** *128*, 2172-2173.

[17] Qi, W. J.; Wu, D.; Ling, J.; Huang, C. Z., *Chem. Commun.,* **2010**, *46*, 4893.

[18] Sanji, T.; Nakamura, M.; Kawamata, S.; Tanaka, M.; Itagaki, S.; Gunji, T., *Chem. Eur. J.*, **2012**, *18*, 15254-15257.

[19] Zeng, Y.; Pratumyot, Y.; Piao, X.; Bong, D., *J. Am. Chem. Soc,.* **2012**, *134* , 832-835.

[20] Davis, J. T., *Angew. Chem. Int. Ed.*, **2004**, *43*, 668-698.

[21] González-Rodríguez, D.; van Dongen, J. L. J.; Lutz, M.; Spek, A. L.; Schenning, A. P. H. J.; Meijer, E. W., *Nature Chem.,* **2009**, *1*, 151-155.

[22] González-Rodríguez, D.; Janssen, P. G.; Martín-Rapún, R.; Cat, I. D.; Feyter, S. D.; Schenning, A. P.; Meijer, E., *J. Am. Chem. Soc.,* **2009**, *132*, 4710-4719.

[23] Arnal-Hérault, C.; Pasc, A.; Michau, M.; Cot, D.; Petit, E.; Barboiu, M., *Angew. Chem. Int. Ed.,* **2007**, *46* , 8409-8413.

[24] Spada, G. P., *J. Chem. Soc., Chem. Commun.*, **1995**, *24*, 2555-2557.

[25] Busseron, E., Ruff, Y., Moulin, E., Giuseppone, N., *Nanoscale*, **2013**, *5*, 7098-7140.

LISTE DES PRESENTATIONS

Communication par affiche

Q. Cao, E. Moulin and N. Giuseppone
Synthesis and Self-assembly of Triarylamine-Nucleobase Conjugates
2016 INDO-FRENCH CONFERENCE "Functional polymers and self-assembled systems", 23-25 May 2016, Strasbourg, France

---

Qing CAO

Synthesis and self-assembly of triarylamines modified with nucleobases

Résumé

Les triarylamines sont de petites molécules largement utilisées comme porteurs de charges dans le domaine de l'électronique organique, car elles présentent des mobilités de transport de trous élevées. En 2010, notre groupe a démontré pour la première fois que les molécules de triarylamine décorées avec des groupements amide subissent une polymérisation supramoléculaire. D'autre part, les propriétés de reconnaissance des résidus de nucléobases ont été largement utilisées au cours des 25 dernières années pour déclencher des processus d'auto-assemblage de polymères ou de petites molécules en polymères supramoléculaires bien définis.

Dans cette thèse, une série de molécules triarylamine décorées avec des amides sur leurs chaînes latérales avec différentes nucléobases comme la guanine, la thymine et la cytosine ont été synthétisées. Nous avons démontré que les monomères de triarylamine conservent leurs propriétés d'auto-assemblage dans les solvants chlorés lors de l'irradiation lumineuse, à condition que le résidu de la nucléobase n'affecte pas les interactions non covalentes nécessaires pour l'auto-assemblage du cœur de triarylamine. En outre, nous avons démontré que la présence d'amines primaires sur le résidu de la nucléobase interdit la formation de structures auto-assemblées dès qu'elles ne sont pas incorporées dans des réseaux de liaisons hydrogène. Dans un deuxième chapitre, nous avons ensuite étudié les auto-assemblages de nos molécules triarylamine-nucléobase dans des solvants organiques en utilisant des ions ou de petites molécules comme matrice. Tout d'abord, la polymérisation supramoléculaire de la triarylamine-monothymine à l'aide de mélamine dans divers solvants a été étudiée. Par ailleurs, l'influence sélective des ions de mercure sur les propriétés sensibles légères de triarylamine-monothymine a été soigneusement analysé. Enfin, les polymères supramoléculaires hybrides de triarylamine-monoguanine conjugué en absence et en présence d'ions potassium ont été obtenus. En particulier, nous avons décrit le premier exemple de polymères supramoléculaires construits à partir de mélamine dans des solvants organiques.

Dans l'ensemble, l'impact de ce travail est triple: a) il conduit à une meilleure compréhension du comportement d'auto-assemblage des conjugués de triarylamine, b) il influence la conception des structures de triarylamine auto-assemblées et c) il offre de nouvelles approches pour l'auto-assemblage des molécules de triarylamine.

Résumé en anglais

Triarylamines are small molecules widely used as charge carriers in the field of organic electronics as they display high hole-transport mobilities. In 2010, our group demonstrated for the first time that chemically-tailored triarylamine amide molecules undergo supramolecular polymerization. On the other hand, the recognition properties of nucleobase residues have been widely used in the last 25 years to trigger self-assembling processes of polymers or small molecules into well-defined supramolecular polymers.

In this thesis, a series of triarylamine amide molecules decorated on their side chains with various nucleobases such as guanine, thymine and cytosine have been synthesized. We have demonstrated that the triarylamine monomers retain their self-assembling properties in chlorinated solvent upon light irradiation, provided that the nucleobase residue does not affect the non-covalent interactions necessary for the self-assembly of the triarylamine core. In addition, we have demonstrated that the presence of primary amines on the nucleobase residue prohibit the formation of self-assembled structures, as soon as they are not embedded in hydrogen bonding arrays. In a second chapter, the templated self-assemblies of our triarylamine-nucleobase molecules in organic solvents were studied. Firstly, templated supramolecular polymerization of triarylamine-monothymine using melamine in various solvents was investigated. Besides, selective influence of mercury ion on the light responsive properties of triarylamine-monothymine was analyzed carefully. At last, hybrid supramolecular polymers of triarylamine-monoguanine conjugate in absence and in presence of potassium ion were obtained. In particular, we have described the first example of supramolecular polymers build from melamine in organic solvents.

Overall, the impact of this work is three-fold: a) it leads to a better understanding of the self-assembly behavior of triarylamine conjugates, b) it influences the design of self-assembling triarylamine structures and c) it offers new approaches for the self-assembly of triarylamine molecules.